Improving Seasonal Rainfall and Streamflow Forecasting in the Sahel Region via Better Predictor Selection, Uncertainty Quantification and Forecast Economic Value Assessment

by

Ketvara Sittichok

Thesis submitted to the
Faculty of Graduate and Postdoctoral Studies
in partial fulfillment of the requirements
for the Doctorate in Philosophy degree in
Environmental Engineering

Department of Civil Engineering
Faculty of Engineering
University of Ottawa

Dr. Ousmane Seidou

DIRECTEUR (DIRECTRICE) DE LA THÈSE / THESIS SUPERVISOR

EXAMINATEURS (EXAMINATRICES) DE LA THÈSE / THESIS EXAMINERS

Dr. Ioan Nistor (University of Ottawa)

Dr. Abdolmajid Mohammadian (University of Ottawa)

Dr. Abhijit Sarkar (Carleton University)

Dr. Khalidou Bâ (Universidad Autónoma del Estado de México)

Friday, December 18, 2015

DATE DE LA SOUTENANCE / DATE OF ORAL DEFENCE

Thesis committee (from left to right): Dr. Ioan Nistor, Dr.Ousmance Seidou, Ketvara Sittichok, Dr. Khalidou Bâ, Dr. Abdolmajid Mohammadian, Dr. Abhijit Sarkar and Dr. Jean-Philippe Leblond (Committee chair)
[Photo courtesy: Soheil Ghareh Aghaji Zare]

Abstract

The Sahel region located in Western Africa is well known for its high rainfall variability. Severe and recurring droughts have plagued the region during the last three decades of the 20^{th} century, while heavy precipitation events (with return periods of up to 1,200 years) were reported between 2007 and 2014. Vulnerability to extreme events is partly due to the fact that people are not prepared to cope with them. It would be of great benefit to farmers if information about the magnitudes of precipitation and streamflow in the upcoming rainy season were available a few months before; they could then switch to more adapted crops and farm management systems if required. Such information would also be useful for other sectors of the economy, such as hydropower production, domestic/industrial water consumption, fishing and navigation.

A logical solution to the above problem would be seasonal rainfall and streamflow forecasting, which would allow to generate knowledge about the upcoming rainy season based on information available before it's beginning. The research in this thesis sought to improve seasonal rainfall and streamflow forecasting in the Sahel by developing statistical rainfall and streamflow seasonal forecasting models. Sea surface temperature (SST) were used as pools of predictor. The developed method allowed for a systematic search of the best period to calculate the predictor before it was used to predict average rainfall or streamflow over the upcoming rainy season.

Eight statistical models consisted of various statistical methods including linear and polynomial regressions were developed in this study. Two main approaches for seasonal streamflow forecasting were developed here: 1) A two steps streamflow forecasting approach (called the indirect method) which first linked the average SST over a period prior to the date of forecast to average rainfall amount in the upcoming rainy season using the eight statistical models, then linked the rainfall amount to streamflow using a rainfall-runoff model (Soil and Water Assessment Tool (SWAT)). In this approach, the forecasted rainfall was disaggregated to daily time step using a simple approach (the fragment method) before being fed into SWAT. 2) A one step streamflow forecasting approach (called as the direct method) which linked the average SST over a period prior to the date of forecast to the average streamflow in the upcoming rainy season using the eight statistical models.

To decrease the uncertainty due to model selection, Bayesian Model Averaging (BMA) was also applied. This method is able to explore the possibility of combining all available potential predictors (instead of selecting one based on an arbitrary criterion). The BMA

is also capability to produce the probability density of the forecast which allows end-users to visualize the density of expected value and assess the level of uncertainty of the generated forecast. Finally, the economic value of forecast system was estimated using a simple economic approach (the cost/loss ratio method).

Each developed method was evaluated using three well known model efficiency criteria: the Nash-Sutcliffe coefficient (E_f), the coefficient of determination (R^2) and the Hit score (H). The proposed models showed equivalent or better rainfall forecasting skills than most research conducted in the Sahel region. The linear model driven by the Pacific SST produced the best rainfall forecasts ($E_f = 0.82$, $R^2 = 0.83$, and $H = 82\%$) at a lead time of up to 12 months. The rainfall forecasting model based on polynomial regression and forced by the Atlantic ocean SST can be used using a lead time of up to 5 months and had a slightly lower performance ($E_f = 0.80$, $R^2 = 0.81$, and $H = 82\%$). Despite the fact that the natural relationship between rainfall and SST is nonlinear, this study found that good results can be achieved using linear models.

For streamflow forecasting, the direct method using polynomial regression performed slightly better than the indirect method ($E_f = 0.74$, $R^2 = 0.76$, and $H = 84\%$ for the direct method; $E_f = 0.70$, $R^2 = 0.69$, and $H = 77\%$ for the indirect method). The direct method was driven by the Pacific SST and had five months lead time. The indirect method was driven by the Atlantic SST and had six months lead time. No significant difference was found in terms of performance between BMA and the linear regression models based on a single perdictor for streamflow forecasting. However, BMA was able to provide a probabilistic forecast that accounts for model selection uncertainty, while the linear regression model had a longer lead time.

The economic value of forecasts developed using the direct and indirect methods were estimated using the cost/loss ratio method. It was found that the direct method had a better value than the indirect method. The value of the forecast declined with higher return periods for all methods. Results also showed that for the particular watershed under investigation, the direct method provided a better information for flood protection.

This research has demonstrated the possibility of decent seasonal streamflow forecasting in the Sirba watershed, using the tropical Pacific and Atlantic SSTs as predictors. The findings of this study can be used to improve the performance of seasonal streamflow forecasting in the Sahel. A package implementing the statistical models developed in this study was developed so that end users can apply them for seasonal rainfall or streamflow forecasting in any region they are interested in, and using any predictor they may want to try.

Acknowledgements

I would like to express my sincere appreciation to my thesis supervisor, Dr. Ousmane Seidou for his guidance and encouragement over the years of my PhD study at the University of Ottawa. During that period, Dr. Seidou contributed many discussions and provided experimental assistance that helped to shape this dissertation into its final format. Due to his various expertise, I was able to cover successfully all of the aims and objectives addressed for this research.

I would also like to express my gratitude to the committee members, Dr. Ioan Nistor, Dr. Abdolmajid Mohammadian, Dr. Abhijit Sarkar and Dr. Khalidou Bâ for their thoughtful feedback and helpful suggestions. With the same grateful attitude, I would like to thank Dr. Jean-Philippe Leblond who served as the chairman of the defense. To all of you, I appreciate your time and your interest in my research.

In parallel to that, I would like to thank the Royal Thai Government for their scholarship that covered all the period of my PhD study. Without their financial support, this work would not have been possible. My sincere appreciation also goes to Dr.Surat Bualert, my Master's thesis supervisor. With his guidance during my master study until now, I can successfully complete this research.

I would also like to thank all my friends and colleagues at the University of Ottawa for their encouragement and support, particularly thanks to Dr. Antoun El Khoury and Dr. Gado Djibo Abdouramane for their valuable discussions and assistance in all aspects. To all my friends in Ottawa, particularly Kagi's family, Ms. Nattawadee Panikom and her family, Mr. Parinya Phasook, Ms. Rumplu Buddachai and Ms. Pranee Attasansathit for their support and help to overcome challenges and difficulties that I faced during my study.

At last but not least, warm gratitude goes to my family, particularly to my mother, my father, my sisters as well as to all my friends in Thailand for their support, encouragement and understanding. Without them, it would not have been possible for me to pursue my PhD degree.

Contents

List of Tables

List of Figures

List of Abbreviations and Symbols

ACMD	African Center Meteorological Application and Development
AEJ	African Easterly Jet
AO	Arctic Oscillation
AGCMs	Atmospheric General Circulation Models
AMO	Atlantic Multidecadal Oscillation
ARC	Agrhymet Regional Center
BMA	Bayesian Model Averaging
BASINS	Better Assessment Science Integrating Point and Nonpoint Sources
CCA	Canonical Correlation Analysis
CGCMs	Coupled General Circulation Models
CPT	Climate Predictability Tool
DEM	Digital Elevation Map
ENSO	El-Nino-Southern Oscillation
EOF	Empirical Orthogonal Function
GCM	General Circulation Model
GDP	Gross Domestic Product
GLUE	Generalize Likelihood Uncertainty Estimation
GUI	Graphical User Interface
HRU	Hydrological Response Unit
ITCZ	Intertropical Convergence Zone
JAS	July-August-September
LEPS	Linear Error in Probability Space
LHS	Latin Hypercube Sampling
MCMC	Markov Chain Monte Carlo
MSE	Mean Square Error
MSLP	Mean Sea Level Pressure
MSR	Mean Square Regression
NAO	North Atlantic Oscillation
NOAA	National Oceanic and Atmospheric Administration
OGCMs	Oceanic General Circulation Models

ParaSol	Parameter Solution
PC	Principal Component
PCA	Principal Component Analysis
PET	Potential Evapotranspiration
PIP	Posterior inclusion probability
PMP	Posterior model probability
PRESAO	Prevision Saisonniere en Afrique de l'Ouest
PSO	Particle Swarm Optimization
SLP	Sea Level Pressure
SOI	Southern Oscillation Index
SST	Sea Surface Temperature
SUFI2	Sequential Uncertainty Fitting
SWAT	Soil and Water Assessment Tool
SWAT-CUP	SWAT Calibration and Uncertainty Program
USDA	United States Department of Agriculture
USEPA	United States Environmental Protection Agency
WAM	West African Monsoon
WeMO	Western Mediterranean Oscillation
B	Regression coefficient
$BLAI$	Potential maximum leaf area index for the plant
C	Cost from taking protective actions
$CANMX$	Maximum canopy storage
CH_K2	Effective hydraulic conductivity
$CN2$	Moisture condition II curve number
E_0	Potential evaporation rate in depth
E'_0	Potential evapotranspiration modified for evaporation of free water in the canopy
E_a	Amount of evapotranspiration
E_{always}	Cost of always taking protective actions
E_{can}	Amount of water that evaporated from the canopy
$E_{climate}$	Expense based on climatology
E_f	Nash-Sutcliffe coeffcient
$E_{forecast}$	Expense based on forecasting data
E_{never}	Amount of loss for each adverse event

$E_{perfect}$	Expense for taking protective actions for a stationary assumption
E_s	Maximum amount of evaporation from soil
E_{soil}	Evaporative demand between the different layers of the soil
E_t	Maximum transpiration
$ESCO$	Soil evaporation compensation coefficient
F	Monthly historic flow
F_{inf}	Cumulative amount of water entering to the soil
F^*	Simulated annual flow
F^{**}	Simulated monthly flow
FC_{ly}	Water volume content at field capacity of the layer
G	Soil heat flux density
$GWQMN$	Threshold water level in shallow aquifer for base flow
H	Hit Score
H_0	Null hypothesis
H_1	Alternative hypothesis
H_{net}	Net radiation
I_a	Innitial abstraction before a runoff even
K_e	Green&Ampt effective hydraulic conductivity
K_{sat}	Saturated hydraulic conductivity
L	Amount of loss from taking no protective actions regarding an extreme event
LAI	Index of leaf area
N_{max}	Maximum number of SST time series
Q_{gw}	Amount of return flow
Q_{surf}	Surface runoff
R	Correlation coefficient
R^2	Coefficient of determination
R_{day}	Amount of precipitation
R_{int}	Initial amount of water held in the vegetation
$REVAPMN$	Threshold depth of water in the shallow aquifer for revap to occur
S	Retention parameter
SAT_{ly}	Water content when the soil is saturated
SD	Standard deviation of historic data
SOL_{AWC}	Available water capacity of the soil layer
SOL_Z	Depth from soil surface to bottom of layer

$SURLAG$	Surface runoff lag coefficient
SW	Water content in the soil
$\bar{T}_{av}$	Average temperature
T_{mx}	Maximum temperature
T_{mn}	Minimum temperature
TT_{perc}	Travel time of percolation
V	Economic value of forecasting system
W	Monthly fragment flow
$W_{crk,btm}$	Bypass flow at the bottom of the soil
W_{seep}	Amount of water exiting the bottom of the soil profile
$W_{perc,ly}$	Total of the water quantity coming out from the soil layer
$W_{perc,ly=n}$	Total of the water quantity coming out from the lowest layer
WP_{ly}	Total water content at the wilting point
Y	The year the forecast issue
c_p	Specific of air at constant pressure
cov_{soil}	Index of soil cover in the area
crk	Formation of crakes in the soil
$crk_{ly,i}$	Initial crack volume
$crk_{ly,d-1}$	Volume of crack of the previous day
$crk_{max,ly}$	Maximum crack volume
crk_{max}	Potential crack volume
cv	Biomass and residue on the ground
$depth_{ly}$	Depth of the soil layer
e	Least error
e'	Eigenvector
e_z^0	Saturation vapor pressure
e_z	Ambient water vapor pressure
f_{int}	infiltration rate
h_{wtbl}	Height of water table
l_{crk}	lag factor of crack
L_{gw}	Distance from the main stream to the border of the groundwater system
m_c	Particle density
r_a	Aerodynamic resistance

r_c	Canopy resistance to water vapor transfer
r_c^2	Canonical correlation
$z_{l,ly}$	Depth from the surface to the bottom of the soil layer
λ	Latent heat flux density
λ'	Eigenvalue
γ	Psychrometric constant
α	Significant level
Ψ_{wf}	Wetting front matrix potential
Δ	Slope of the curve between the saturation vapor pressure and the air temperature
$\Delta\Theta_v$	Change in the amount of water across the wetting front area
$\oslash_{soil}$	Soil permeability
ρ_{air}	Air density
ρ_b	Bulk density

Chapter 1

Introduction

1.1 Problem statement

The Sahel region is a semi-arid area located along the southern edge of the Sahara desert extending from the Atlantic coast of Africa to Ethiopia. The area is well-known for high climate variability, which makes it difficult to employ water allocation management in advance. High inter-annual rainfall variability and an increase in aridity in the region over the last three decades were reported by several authors (Brooks, 2004; Lu and Delworth, 2005). Lu and Delworth (2005) reported rainfall decreases of 20 to 50% in the region between 1950 and 2000. However, Samimi et al. (2012) found exceptionally heavy precipitation, with return periods up to 1,200 years, during the 2007 rainy season in one Sahelian watershed. Extreme precipitation events in the region gained international media attention from 2007 to 2014. In addition, in August 2013 rice fields along the Niger River, and more than 7,000 other farms, were flooded due to the heavy precipitation (IRIN, 2013). Recurring extreme events of both low and high precipitations have damaged several sectors of the local economy. The sector most often impacted is rainfed agriculture, as productivity drops in years with below normal rainfall, and can also be devastated by flooding.

The damages mentioned above occurred largely because the amount of rainfall or the peak water level in a given area was either too high or low for the crops being cultivated. If rainfall information was available a few months before a rainy season, farmers could switch to a crop or a farm management scheme that would be most appropriate for the upcoming rainy season. Any technique that can predict an upcoming rainy season a few months in advance, could improve agricultural yields by increasing stakeholders' degree

of preparedness. The forecasts would be useful to other water users as well, including hydropower producers and municipalities relying on surface water for domestic and/or industrial consumption. Seasonal forecasting is defined as the best available prediction of what the climate will be like in the next few months. It can be accomplished through dynamical or statistical approaches. Dynamical models are based on relatively accurate simulations of the physical processes that drive interactions between the atmosphere, land and ocean, and they can account for nonlinearities and feedback loops in these interactions. In contrast, statistical models rely on stationary relationships between predictors and predictands (Schepen et al., 2012). Although, dynamical models are theoretically more likely to provide skillful forecasts (Marengo et al., 2003; Palmer, 1986), they are computationally intensive. As well, seasonal forecasting with dynamical models specifically for precipitation often has outputs with low temporal and/or spatial resolutions, and require an additional downscaling step for local impact studies (Busuioc et al., 2008; Wetterhall et al., 2011). Raje and Mujumdar (2011), who studied three downscaling methods for daily precipitation in the Panjab region of India, declared that the output resolution of some types of general circulation models (GCMs) was inadequate for runoff simulation. Thus, statistical models play a prominent role in applications requiring higher temporal and spatial scales.

Seasonal forecasts in the Sahel region are presently issued by two institutions: the African Center of Meteorological Application and Development (ACMAD) and the Agrhymet Regional Center (ARC). They both use a Climate Predictability Tool (CPT) to link sea surface temperature (SST) to monthly or seasonal rainfall (ACMD and ARC) or streamflow (ARC) data. CPT uses multiple linear regressions to link a grid predictor to a predictand. These forecasts were compared to those developed by international climate centers at an annual meeting of PRESAO (Prevision Saisonniere en Afrique de l'Ouest), and the consensus forecast was issued categorically; that is, probability of above normal, normal, and below normal precipitation or streamflow. Though this application has been applied for more than a decade, droughts and floods still regularly affect the local economy, and usually surprise the authorities. The low predictive skill of PRESAO was confirmed by Konte (2011), who used the rank probability skill score and relative operating characteristic to evaluate its performance in Senegal from 1998 to 2010. He found that the forecast reliability varied according to geographical location in the region, but overall, the forecasts were better than the climatology only 54 % of the time. This highlights the need for increased effort to develop better forecasting approaches, and for a forecast format that will be more straightforward and end-users friendly.

1.2 Thesis objectives

1.2.1 Main objective

The main objective of this research study is to develop a scientifically sound, seasonal streamflow forecasting approach that can help decision makers assess the effects of rainfall/streamflow variability on a number of key sectors proactively. The approach would significantly improve the quality and usefulness of forecast outputs, by systematically searching for the best lead time and averaging period to select the best predictor for a given watershed. It would also accommodate both linear and non-linear relationships between predictors and predictands (precipitation/streamflow), and extend seasonal precipitation forecasting to streamflows using a rainfall runoff model. In addition, a framework for assessing the economic value of the forecast systems will be developed.

A case study was conducted on the Sirba Watershed, and guidelines and algorithms are provided for users to apply the application to other watersheds in the region.

1.2.2 Secondary objectives

The study has the following secondary objectives:

1. Evaluate existing precipitation forecasting methods in the Sahel region.
2. Introduce new statistical models for seasonal precipitation and streamflow forecasting, and compare their performances to the approaches already in use.
3. Implement and test a temporal disaggregation method to produce forecasts for use as a rainfall-runoff model.
4. Implement and calibrate a rainfall-runoff model.
5. Generate hydrological forecasts, using temporally disaggregated rainfall forecasts and the hydrological model developed in secondary objective 4.
6. Assess the quality of the hydrological forecasts, and compare them to current practices.
7. Develop a framework to evaluate the benefit of the forecast systems and optimize their usage.

1.3 Novelty

- So far, only linear models and an arbitrary selection of aggregate predictors are currently used by local organizations to forecast rainfall or streamflow events in the Sahel region, with limited success. The approaches developed in this study will allow for a systematic search of the optimal region, in order to select the predictor, the optimal lead time and a non-linear mapping function between the predictors and the predictands.

- The seasonal forecasts presently issued to end users in the Sahel region are difficult to use. The seasonal precipitation forecasts issued by the African Centre of Meteorological Applications for Development (ACMAD) are typically probabilities of the occurrence of three categorical events (i.e. below normal, normal, and above normal precipitation). An example of the forecast is presented in Figure 1.1 such forecasts are of little value to end users as, a) they apply to large areas and disregards local conditions; b) they are not quantitative and c) they do not produce time series of precipitation that could be used with an impact model. The end result of this thesis will be a probabilistic set of hydrographs that can be used to provide inundation risk management.

- The case study using the cost/lost ratio method to estimate forecast value is one of the first to demonstrate how a set of probabilistic seasonal forecasts can be used to optimize water resources management in the Sahel region.

1.4 Scope of work

Seasonal rainfall and streamflow forecasting, temporal disaggregation and rainfall-runoff transformation can be performed using many predictors, techniques and models. The scope of this study is limited to the following.

- Though the approaches are general and can be applied anywhere, they were specifically conducted on the Sirba watershed, located between the countries of Niger and Burkina Faso.

- Only sea surface temperature (SST) was employed as a predictor to forecast rainfall/streamflow in the study area.

- The temporal disaggregation method used in this study was the fragment method. However, various implementations of the fragment method were tested.

1.5 Study area

The area used to represent the Sahel in this study was the Sirba watershed. This basin is located in Niger and Burkina Faso, and has an area of approximately 37,000 km^2. The reasons for selecting this watershed are as follows:

- Water from the Sirba watershed is the main cause of flooding during the rainy season in Niamey, the capital of Niger. Being able to predict exceptionally high flows from the Sirba will be beneficial for flood protection in Niamey.
- The Sirba basin is located near the center of the Sahel region. Consequently, the climate characteristics of both the northern Sahel (the Sahara desert) and the southern Sahel (the Sudanian Savanna) can be found in the basin. The basin is therefore representative of many medium size watersheds in the Sahel.
- A number of climate stations inside and around the basin collect climate data at the daily time scale. Additionally, long series of historical precipitation data were available for use.
- A relatively long time series of streamflow observations at the outlet (i.e. the GarbeKorou station) was available for the study.

The details of the study site and the observed data are discussed further in Chapter 4.

1.6 Organization of the thesis

The thesis is organized in eight chapters, the focus of which is stated below:

Chapter 1: This chapter includes the problem statement, the objectives and scope of the research, and a brief description of study area.

Chapter 2 :This chapter provides a comprehensive literature review. Teleconnections, statistical approaches used for seasonal forecasting, particulary in Sahel, are discussed. Hydrological models used for streamflow forecasting, specifically the Soil and Water Assessment Tool (SWAT) are presented as well.

Chapter 3: The theory behind specific statistical methods, including principal component analysis, canonical correlation analysis, stepwise regression, simple/multiple linear regression, polynomial regression are presented. The concepts of rainfall-runoff transformation (with a focus on the SWAT model) are presented. The cost/loss ratio method used to estimate economic value of the forecast systems, are also described in this chapter.

Chapter 4: This chapter investigates the climate and geographic information of the Sahel region, including social and economic factors. The characteristics of the Sirba basin are also presented.

Chapter 5: The proposed methodologies for seasonal precipitation and streamflow forecasting are explained in this chapter. The implementation and calibration of the SWAT model of the Sirba basin are presented. A description of all the data sets used or generated in this study, using either statistical or the rainfall-runoff model, is provided. Finally, the methods used to estimate the model uncertainty and the use of the cost/loss ratio method for economic value estimation of streamflow forecasts is described.

Chapter 6: An evaluation of the performance of the proposed models is conducted in this chapter. Their relative performances are discussed and compared to that of existing models. The economic values of streamflow forecasts using each method are presented and discussed.

Chapter 7: The MATLAB package implementing the proposed statistical models is described. A step by step user guide is also provided.

Chapter 8: The findings of the study as well as suggestions for future research are presented.

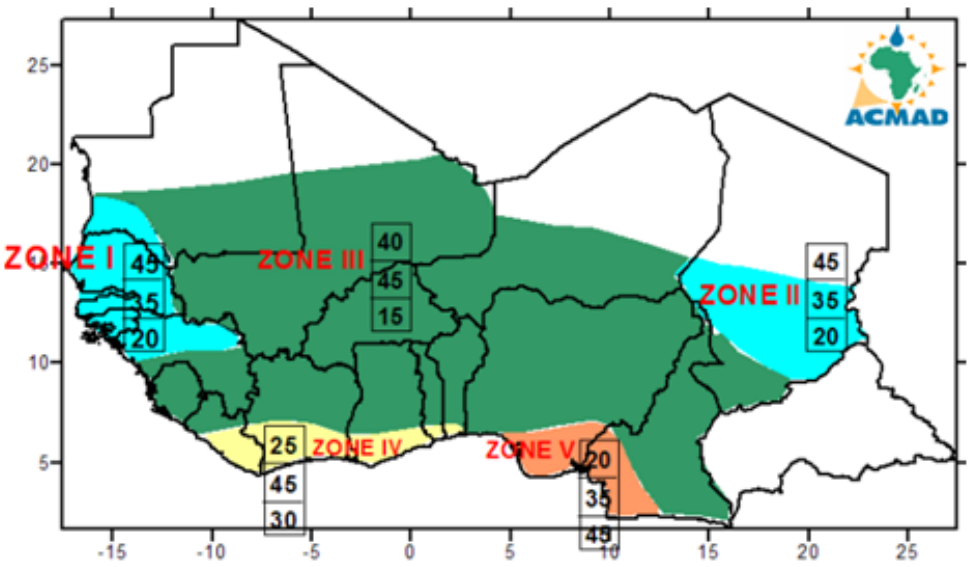

Figure 1.1: Example of seasonal precipitation forecast issued by the African Center for Meteorological Applications for Development (ACMAD) in 2010

Chapter 2

Literature review

2.1 Teleconnections

An understanding of teleconnection has played an important role in climatological and hydrological studies for more than several decades. Teleconnection is the linkage of climate variables between two different areas which may be next to each other or a great distance apart (Hatzaki et al, 2007; Kwon et al., 2009; Liu and Alexander, 2007). The term 'teleconnection' generally refers to the atmospheric circulation on larger than continental scales which affects climate in other areas on local or larger scales. Rowell (2001), and Sheridan and Lee (2012) determined that an understanding of teleconnection mechanisms in an individual region can extend the knowledge of frequency changes in circulation and weather patterns. It can also increase understanding of surface condition patterns which could help predict seasonal weather on a local scale. Chase et al. (2005) summarized that teleconnections can be due to two mechanisms: the variability of circulation in time and space between atmosphere and oceans (e.g. the Hadley cell, subtropical jet streams and monsoons); and the disturbance of inherent circulations might cause prolonged changes in general atmospheric circulations that could affect other regions in different ways.

Examples of well-known large scale circulation patterns are presented in the next section, and the relationships with local climate and hydrologic variables in different regions are clarified. Finally, the effects of sea surface temperature (SST) on Sahel precipitation and other hydrologic variables are revealed.

2.1.1 Large-scale atmospheric and oceanic indices

The interactions between atmospheric and oceanic circulations that affect local climate and hydrologic variables have been of interest in several areas for the last decade. Atmospheric and oceanic patterns, such as SST, the El-Nino-Southern Oscillation (ENSO) and the North Atlantic Oscillation (NAO), and their relationships to local variables have been investigated extensively. Their specific patterns could lead to the occurrence of extreme events in particular locations. As this current study focuses on precipitation and streamflow forecasting, only teleconnection indices that influence these variables are reviewed. The climatic and oceanic indices commonly used in various studies are as follows:

2.1.1.1 Sea surface temperature

SST is the ocean water temperature at the surface. A variety of techniques are used to measure this such as temperature recording devices on shorelines, ships and buoys. These measurements deliver SST data at different levels of detail, depending on the location of the device or if the data is collected by different ships. The limitation of this method is the difficulty of obtaining SST data at a global scale. However, almost all SST measurements of the world's oceans can be accessed when weather satellites are available. The satellite sensors can measure the difference in wavelength amplitudes, which vary with ocean temperature.

SSTs at global and regional scales are useful to link to variables at a local scale. Maity and Kumar (2007) investigated Indian summer rainfalls during monsoon seasons regarding correlations to SST, land surface temperature and ocean-land temperature contrast. Their results showed that SST influenced the occurrence of rainfall more than the other indices, particularly the SST of the tropical eastern Pacific Ocean. Srivastava et al. (2002) also researched the relationships between large scale atmospheric and oceanic patterns and the Indian summer rainfall monsoon. They used outgoing long wave radiation and the SST over the North Atlantic Oceans as indices, and found that the Indian summer rainfalls were associated with these two variables. Diro et al. (2011) focused on the teleconnections between SSTs and the summer rainfall variability in Ethiopia in eastern Africa. They found associations between the equatorial Pacific SST and rainfall over northeast and western Ethiopia; the warm phase of the SST led to rainfall reduction and vice versa. The Atlantic SST near the Gulf of Guinea also corresponded to rainfalls, with its warm phase leading to rainfall decrease in northern and central Ethiopia. The

precipitation variability over southern Africa was also examined and showed association with the variation of SST over the Pacific Ocean (Mirsa, 2003). Keener et al. (2010) linked SST to precipitation, streamflow and nitrate concentration in the Little River Watershed in Georgia USA. They reported that the decrease of ocean temperature was noticeable from El Nino (1997 to 1998) to La Nina (1998 to 1999). Their results seemingly revealed that ENSO affected precipitation and streamflow and caused a change of nitrate load in the river.

2.1.1.2 El Nino Southern Oscillation

The El Nino Southern Oscillation (ENSO) is an ocean-atmosphere phenomenon that occurs mainly in the tropical Pacific Ocean. ENSO refers to a fluctuation of the ocean temperature that is higher than average, known as El Nino. The El Nino event has a connection to the Southern Oscillation Index (SOI) which indicates the difference in sea level pressure between Tahiti and Darwin. The mean sea level pressure at Tahiti is less than at Darwin (around -8), which corresponds to the El Nino. This phenomenon is recognized as a major force that causes variations in climate patterns in many areas of the globe.

ENSO events are frequently analyzed to indicate variations in regional climate patterns. The winter severity indices in the Great Lake basin, which were simply characterized as warm, normal and cold winters were investigated for the relationships to ENSO by Rodionov and Assel (2000). They found that a higher frequency of warm winters corresponded to positive ENSO events; cold winters were more complicated and required integration of more than two atmospheric indices to define their patterns. Shaman and Tziperman (2011) identified the association of ENSO with precipitation in southwestern Europe, and found that ENSO events were responsible for the precipitation decrease during the wet season (September to December). ENSO also played a dominant role in precipitation in eastern and southern Africa, while the tropical Atlantic SST was highly correlated to western and west equatorial Africa rainfalls. The results of multiple regression models driven by the two climate indices (ENSO and the tropical Atlantic SST) explained the relationships between the indices and Sahel and Guinea rainfalls (Camberlin et al., 2001). Chiew and McMahon (2002) found that streamflow in Africa showed a moderate relationship to ENSO. Low flows in northern and southeast Africa were associated with ENSO.

2.1.1.3 North Atlantic Oscillation

The North Atlantic Oscillation (NAO) is the variations in low pressure around Iceland and high pressure near the Azores (a region of Portugal). High intensity of this pressure pattern between the two locations is termed a positive phase, and weakening of the pattern a negative phase. The NAO patterns were found to be related to regional climate in global areas, such as U.S., Europe and Africa.

Linderholm et al. (2009) linked droughts in Europe to the summer NAO. The positive phase of the summer NAO was responsible for dry and wet episodes in northern and southern Europe respectively. Lopez-Bustins et al. (2008) searched for correlations between Iberian winter precipitation trends and three teleconnection indices: the Arctic Oscillation (AO), NAO, and the Western Mediterranean Oscillation (WeMO). They found positive agreements between the precipitation and AO and NAO, and a negative trend with WeMO. Krichak et al. (2014) investigated relationships between five large-scale circulation patterns and extreme precipitation events in the Euro-Mediterranean region. The NAO and AO indices had negative relationships to extreme precipitation in the western Mediterranean, while positive relationships were found between ENSO and the Scandinavian and eastern Atlantic/western Russian patterns. The eastern Mediterranean was also positively related to the eastern Atlantic/western Russian patterns.

Numerous studies have investigated the relationships between local climatic and hydrologic variables, and the large scale patterns of atmosphere and oceans. However, the physical mechanisms and dynamic aspects of those relationships have not yet been fully explained (Chase et al., 2005; Srivastava et al., 2002).

2.1.2 Teleconnections between SST and the Sahel rainfall

Over the past ten years, many studies have attempted to determine the impact of large-scale climate/ocean indices on rainfall variability in the Sahel region. SSTs are considered one of the most prominent climate/ocean patterns linked to Sahel rainfall. An increase in SSTs could cause a high rate of evaporation corresponding to wet episodes in some regions, as well as higher sea levels in some ocean areas (Singh, 2001).

2.1.2.1 Physical mechanisms between tropical SSTs and the Sahel rainfall

Variations of Sahel rainfall are chiefly associated with temperatures of the ocean surfaces and the movement of warm and cold SST in the oceans. SST anomalies influence the changes of atmospheric circulation patterns on both local and regional scales. An area of atmospheric subsidence improves rainfall reduction, while atmospheric convection results in increased rainfall. Mohino et al. (2011) and Palmer (1986) found that the tropical circulation related to the variation of both Pacific and Atlantic SSTs accounted for seasonal rainfall variability over western Africa. Rowell (2001) also determined that the Sahel rainfall fluctuation was substantially regulated by various SST patterns around the globe. However, this research only focuses on using Pacific and Atlantic ocean SSTs for seasonal forecasting, and thus describes only the physical mechanisms between the SSTs and Sahel rainfall.

A movement of warm SST, particularly in the tropical Pacific region, strongly influences changes in location of anomalous subsidence over western Africa responding to wet and dry episodes in the area (Rowell, 2001). Movement of warm SST from the tropical region to the easternmost central Pacific and western Indian Oceans, leads to an increase in high convective heating (convergence at low level and divergence at high level) over the two areas (Mohino et al., 2011). This enhances large atmospheric subsidence over the northeastern equatorial Atlantic, the Sahel region, the South of Sahara and the Middle East. The atmospheric subsidence causes instability in convective heating and increases mean sea level pressure, resulting in decreased moisture from the oceans to the Sahel region influenced rainfall reduction (Palmer, 1986). The warmest SST temporarily remains at the eastern central Pacific for a while, then the movement of warm SST from the eastern Pacific Ocean, combined with cooler in tropical Atlantic and maritime continent (Indonesia, New Guinea and Malaysia) SSTs and warmer Indian Ocean SST, are associated with anomalous subsidence decreases, resulting in rainfall increases in the Sahel (Rodriguez-Fonseca et al., 2011). These mechanisms correspond to the study of Rowell (2001) depicted in Figure 2.1, which shows the combination of the change of SST, location and the direction of the Kelvin and Rossby waves influencing to the Sahel rainfall variability. Strong ENSO, which is warmest SST in the eastern Pacific, combined with warm SST in the Indian Ocean, causes dry conditions (narrow convective clouds) in the Sahel (shown in Figure 2-1 (a)), while anomalous SST in western Pacific (shown in Figure 2-1 (c)) is associated with rainfall increase over western Africa. More details of the impact of the Rossby and Kelvin waves can be found in Rowell (2001).

While the tropical Pacific SST is associated with large scale atmospheric circulation across the Pacific Ocean to western Africa, the Atlantic SST anomalies influence nearby Sahel precipitation through changes of sea level pressure gradient. Zheng et al. (1999) showed the interaction between a warm spring Atlantic SST (April to June) and western African rainfall. They concluded that positive SST anomalies in the spring caused African rainfall reductions in the same season, but led to rainfall increases in the following summer and autumn seasons. Rowell (2001) also indicated that the Sahel drought was associated with a warm phase of the Atlantic SST. The physical mechanism behind this phenomenon was explained by Zheng et al. (1999), who showed that positive SST anomalies in spring caused immediate warming air currents over the ocean, leading to a decrease of density gradient between ocean and land that resulted in a reduction of monsoon strength in the spring. Following this, precipitation over land increased in summer (when the strength of the positive SST anomaly was reduced) due to the influence of advection by the large scale circulation increase. This enhanced moisture over land was also affected by an increase in greenhouse trapping, which raises the air temperature over land and induces a strong monsoon signal. Biasutti et al. (2004) investigated how changes in the tropical Atlantic SST affected the Sahel rainfall. Their simulations showed that movement of the Intertropical Convergence Zone (ITCZ) was related to changes of SST at a seasonal scale. The ITCZ naturally locates over the warmest area of the ocean, and is the main factor driving the Western African Monsoon (WAM). SST variability responds to a change of the boundary layer of the atmosphere, specifically the advection of temperature anomalies from the northern Atlantic over the Sahara, and the advection of moisture from the Gulf of Guinea and equatorial Africa to the Sahel (Biasutti et al., 2004). Rodriguez-Fonseca et al. (2011) concluded that the mechanisms of changes of SSTs corresponded to rainfall variability in the Sahel. This is clearly illustrated in Figure 2.2 , which shows that SST variations in all tropical regions, combined with other factors such as Rossby wave (high latitude air circulation moving westward) and Kelvin wave, cause fluctuation in rainfall over the Sahel.

2.1.2.2 Relationships between SST and rainfall in the Sahel

Folland et al. (1986) investigated changes in wet and dry periods in the Sahel region that were driven by worldwide SSTs, and found that SST patterns accounted for shifts of tropical atmospheric circulation related to rainfall variability in the Sahel. Giannini et al. (2003) found correlations between the SST of all oceans in a tropical region and Sahel rainfall. This conclusion is similar to Ward's (1992) who stated that the variation

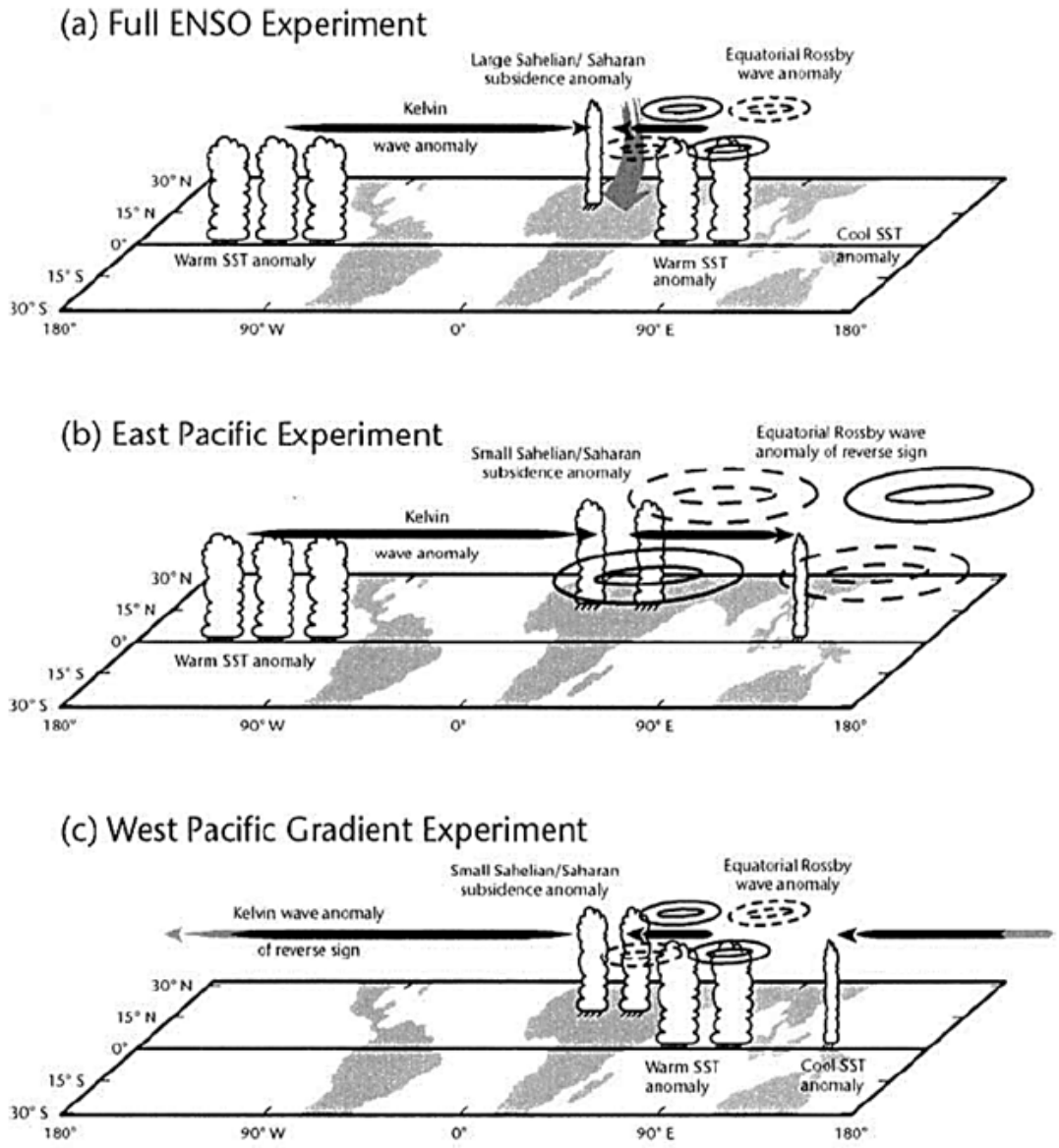

Figure 2.1: Schematic of SST anomalies, Rossby wave and Kevin wave impact on rainfall variability over the Sahel (Rowell, 2001)

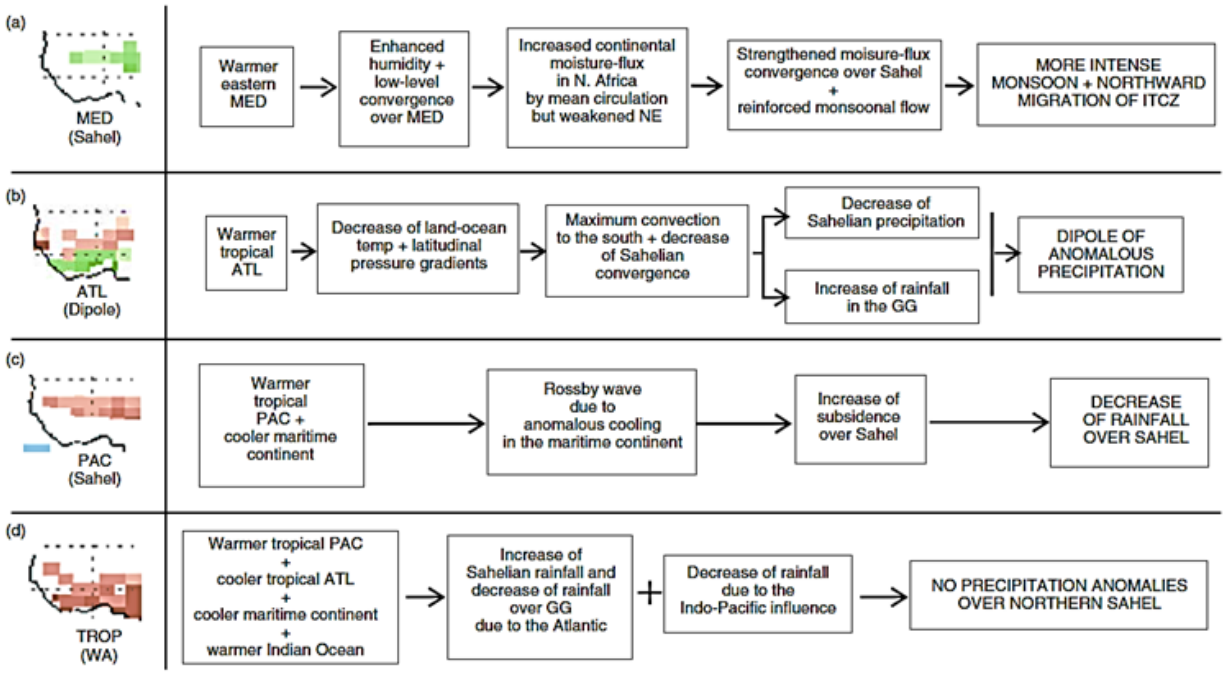

Figure 2.2: Diagrams of the mechanism between the West African Monsoon and SST: a) Mediterranean b) tropical Atlantic c) tropical Pacific and d) global tropical SST forcing (Rodriguez-Fonseca et al., 2011)

in Sahel rainfall was due to the tropical Atlantic and other oceans.

Hunt (2000) studied the correlation between prolonged rainfall in the Sahel as reproduced by a couple atmospheric-oceanic CSRIO model and the Pacific SST, and found a negative correlation of -0.39 between the Sahel rainfall and the low latitude Pacific SST. Rowell (2001) confirmed the teleconnection between summer rainfall over the Sahel and the tropical Pacific SST, and found associations of the local rainfall to the temperatures of the western Pacific and the eastern Indian oceans. The impact of changes in Pacific and Indian SSTs on dry conditions over the Sahel was also verified by Mohino et al. (2011). Increasing SST in these oceans was the cause of a dry season in Sahel. Palmer (1986) explained that rainfall reduction over the western Sahel was influenced by the Pacific and Atlantic Oceans, while the Indian Ocean was responsible for rainfall decreases in the eastern Sahel. Biasutti et al. (2008) concluded that the Sahel rainfall had a negative correlation with the tropical Indo-Pacific SSTs, but a positive correlation with the tropical Atlantic meridional SST gradient. Janicot et al. (2001) linked the inter-annual variability of the 1954 to 1973, July-August Sahel rainfall (during a wet period and transitions to a dry period) to the tropical Atlantic and western equatorial Indian Ocean SSTs. The dry season showed positive correlations with both SSTs, while the wet rainy season had negative correlations. Furthermore, rainfall events from 1970 to 1989 (the dry period) negatively correlated with the eastern equatorial and tropical Pacific SSTs (ENSO event). Lu and Delworth (2005) used a climate model to investigate teleconnections between the tropical oceans with Sahel droughts. Though all tropics were associated with Sahel dry periods, the greatest impact on drought was due to changing SSTs in the Indian and Pacific oceans, rather than the Atlantic. Fontaine and Janicot (1996) concluded that negative and positive SSTs in the northern and southern Atlantic Ocean respectively were important to addressing drought seasons in the Sahel. Rowell (2003) found that the Sahel rainfall variability was related to the changes in the Mediterranean SST. Increasing the SST was responsible for high rainfall amounts, and vice versa. High moisture content at low atmosphere levels naturally results in higher rainfall. Studies of atmospheric modeling and analysis of observational climate data since the 1980s confirm that rainfall variability in Sahel is naturally governed by SSTs (Held et al., 2005).

Table 2.1 and 2.2 summarized the teleconnections between SSTs and Sahel rainfall. It is worth noting that the dominant role of SST on rainfall varies in the aforementioned studies, due to the differences in time periods, data sources, specific SST area and methodologies. However, all the studies found robust scientific evidence support-

ing the use of SSTs for seasonal rainfall forecasting in the Sahel. Further details of the teleconnections between SSTs and Sahel rainfall can be found in Biasutti and Giannini (2006), Caminade and Terray (2010), Folland et al. (1991), Lough (1986), Xue and Shukla (1998).

2.1.3 Teleconnections between other variables and the Sahel rainfall

Other well-known, large scale atmospheric patterns connected with local rainfalls in the Sahel region include sea level pressure (SLP), the North Atlantic Oscillation (NAO), the El Nino Southern Oscillation (ENSO). Raicich et al. (2003) studied the connection between SLP and Sahel rainfall and concluded that the rainfall was apparently influenced by the SLP of the Mediterranean and the Etesian wind strength. Ward (1992) found that the low SLP in the tropical Pacific near New Guinea accounted for wet seasons in the Sahel. Haarsma et al. (2005) explained the physical mechanisms between mean sea level pressure (MSLP) and rainfall in the Sahel. Decreasing MSLP over the Sahara resulted in increasing surface air temperature, which led to higher rainfall in the Sahel. Linderholm et al. (2009) explored the relationship between wet and dry seasons in the Sahel, and summer NAO. Though, they found that dryness was associated with the positive summer NAO, the physical mechanism behind this relationship was undetermined. Wolter (1989) found that the Southern Oscillation was connected to Sahel rainfall especially in the Pacific and Indian oceans. In addition, the Atlantic Multidecadal Oscillation (AMO) also induced droughts in the Sahel (Knight et al., 2006).

2.2 Seasonal forecasting

Seasonal forecasting is a prediction of changes in average weather or hydrologic conditions over the subsequent few months (Udall and Hoerling, 2005). It can be achieved various ways, which are generally divided into three groups: dynamic models, statistical models and dynamic and statistical model combinations. Dynamic models consist of algorithms representing the interactions between atmosphere, ocean and land conditions. Statistical models account for the trends and statistical parameters of variables to be investigated. The combination of dynamic and statistical models initially develops variables using dynamic models, then applies statistical analysis to determine interactions with local conditions. Seasonal forecasting is of great benefit to decision-makers in various sectors,

Table 2.1: Teleconnections between SSTs and the Sahel rainfall as published by various studies

SST location	**Correlation to the Sahel rainfall**	**Reference**
the tropical Pacific Ocean	negative correlation	Caminade and Terray (2010); Hunt (2000);Janicot et al. (2001; Mohino et al. (2011)
the south-east tropical Pacific Ocean	negative correlation	Rowell (2001)
the eastern equatorial Pacific	negative correlation	Janicot et al. (2001)
the tropical Indo-Pacific	negative correlation	Biasutti et al. (2008)
the tropical Atlantic Ocean	negative correlation	Janicot et al. (2001);Rowell (2001)
the tropical Atlantic Ocean	positive correlation	Biasutti et al. (2008); Janicot et al. (2001)
the north of Atlantic Ocean	negative correlation	Fontain and Janicot (1996)
the south of Atlantic Ocean	negative correlation	Rowell (2001)
the the south of Atlantic Ocean	positive correlation	Fontain and Janicot (1996)

Table 2.2: Teleconnections between SSTs and the Sahel rainfall as published by various studies (con't)

SST location	**Correlation to the Sahel rainfall**	**Reference**
the Indian Ocean	negative correlation	Mohino et al. (2011); Rowell (2001)
the western equatorial Indian Ocean	positive correlation	Janicot et al. (2001)
the south of Atlantic Ocean	negative correlation	Fontain and Janicot (1996)
the Mediterranean	positive correlation	Rowell (2003)
the eastern Mediterranean	positive correlation	Rowell (2001)
the southern Hemisphere SST	negative correlation	Folland et al (1991)
the Gulf of Guinea	positive correlation	Caminade and Terray (2010)

including agriculture, water resource management and disaster mitigation. Garric et al (2002) indicated that seasonal rainfall forecasting was important for northern Africa because rainfall generally occurs in monsoon season, which varies strongly at interannual scales.

2.2.1 Seasonal precipitation forecasting

Seasonal precipitation forecasting can be achieved using dynamic or statistical models. A general circulation model (GCM), a dynamic model, is widely known but has limitations including computational access and the use of forecasted outputs at a local scale when the model is implemented. Consequently, statistical models are preferable for seasonal forecasting, particularly when studying local impacts. The following section discusses researching seasonal precipitation using both approaches.

2.2.1.1 Seasonal precipitation forecasting using dynamic models

GCMs are large, and complex applications based on physical laws, such as Newton's law of motion and the laws of thermodynamics. They are typically divided into three groups: atmospheric general circulation models (AGCMs), oceanic general circulation models (OGCMs) and coupled general circulation models (CGCMs). AGCMs consider atmospheric processes, including dynamical, physical and chemical activities, and OGCMs consider oceanic circulation. CGCMs integrate the interaction between atmospheric and oceanic processes to simulate an atmospheric-oceanic circulation system.

GCMs have been widely used to forecast seasonal precipitation in various regions, including the Sahel. The most common variable forced into these models is SST. Marengo et al. (2003) studied regional rainfall predictability in various areas, including central Australia, India and eastern Africa, at a seasonal time scale using AGCM (CPTEC/COLA) driven by SST. Though, reliable forecasts were achieved in most areas, some required the El Nino and La Nina conditions. Giannini et al. (2003) used AGCM forced by observed SSTs from 1930 to 2000 to estimate oceanic influence on Sahel July-August-September (JAS) precipitation variability. The correlation coefficient (R) between the forecasted and observed rainfalls was approximately 0.6. Ndiaye et al. (2011) forecasted the seasonal Sahel rainfall using several AGCMs and CGCMs. Results revealed that the forecasting skill of AGCMs driven by observed SSTs for seasonal rainfall prediction was low. However, the skill improved at one month lead times when statistical post-processing and the predicted low-level wind field over the tropical Atlantic and West

Africa were applied; the R value between predicted and observed rainfall increasing to 0.6. Ndiaye et al. (2009) predicted the JAS Sahel rainfall using a GCM forced by SST combined with a model output statistic, and obtained a correlation skill of approximately 0.55 with a one month lead time. Garric et al. (2002) compared the performances of a dynamic atmospheric model known as ARPEGE and a simple regression model for precipitation prediction during a monsoon season. They found that the ARPEGE was less capable than the statistical model for forecasting, but more successful at generating the variability of large scale monsoon circulation. July-September Sahel rainfall were forecasted using GCM forced by worldwide SST patterns (Rowell et al., 1992). The R value between simulation and observed precipitation was 0.87 at one month lead time, and gradually decreased with longer time lags.

As mentioned, the main limitations of dynamical models are their high computational costs, and the volume of resources require to issue the forecasts. Furthermore, because their outputs have low spatial resolution, additional steps are required to complete the analysis. Raje and Mujumdar (2011) found that the resolution of variables provided by GCMs was inadequate for generating runoff in most study areas. GCM predicted fields are available at low spatial scales of approximately 2.5 x 2.5 degrees. Thus, downscaling approaches are required to forecast precipitation and streamflow at a practical spatial scale (Sankarasubramanian et al., 2008).

2.2.1.2 Seasonal precipitation forecasting using statistical models

Due to the high variability of rainfall, statistical models also play an important role in seasonal rainfall simulations (Chow et al, 1988). The models use historical observations as predictands, and climate or oceanic indices as predictors. Both linear and non-linear regressions have been applied to describe the connections between predictors and predictands (Collins et al, 2004; Rajeevan et al., 2005; Chambers, 2003).

Statistic methods have been used in various regions to predict local climate and hydrologic variables. For example, Ward and Folland (1991) forecasted rainfall in the North Nordeste of Brazil using multiple linear regression and linear discriminant analysis. The models were driven by the tropical Atlantic and Pacific SSTs, and they revealed that 50% rainfall variance or more could be forecasted with the statistical techniques. Gissila et al. (2004) conducted cluster analysis for rainfall forecasting in Ethiopia, a location with high spatial rainfall variability. They also used linear regression forced by the SST of the tropical western Indian Ocean and Nino index one season before the target rainy season for each section, and found that applying the cluster method was

a key to successful rainfall forecasting in this area. Mason (1998) employed quadratic discriminant analysis to forecast rainfall in South Africa three and six months in advance, using the SSTs in the Indian, South Atlantic and Pacific oceans. High forecasting skills were also achieved in many countries in South Africa. Mutai et al. (1998) tested the abilities of linear discriminant analysis and multiple linear regression for seasonal rainfall forecasting in eastern Africa using the tropical SST patterns of the Pacific, Indian and Atlantic oceans specifically. They found that rainfall prediction with zero lead time was possible with these methods. Wang et al (2012) employed Bayesian model averaging (BMA) to merge forecasts from multiple statistical models for rainfall forecasting, and found that merged forecasts developed forecasting skills more effectively, and were reliable to represent uncertainty spread. Luo et al. (2007) used BMA for seasonal forecasts of SST over the equatorial Pacific and precipitation over the Ohio River basin, and showed that BMA successfully generated forecasts with smaller root mean square error and rank probability score compared to climate models. Since statistical seasonal forecasting in the Sahel is the focus of this study, more details of the research conducted in the region are presented in the following section.

Most seasonal rainfall forecasting studies conducted in the Sahel region frequently used SST as a predictor. Abedokun (1979) used lag correlation analysis to forecast rainfall, by initially searching for the relationship of rainfall data sets obtained from climate stations. He divided the Sahel into three zones, and found that the best correlation (R) with two month lag was 0.8 at the Lago station in southern Sahel and the inland Sahel stations. Folland et al. (1991) applied two statistical models, stepwise linear regression and stepwise linear discriminant analysis, to forecast the Sahel rainfall using global SSTs, and generated a best forecast R of 0.72. Barnston et al. (1996) used canonical correlation analysis (CCA) to forecast precipitation in Africa at lead times of up to 13 months, using four consecutive three month periods of global SSTs. They found the ability of the model to forecast rainfall over Sahel with one month lead time was a relatively moderate R of 0.33. The Sahel precipitation was also forecasted using SSTs in the equatorial Atlantic, equatorial Indian, eastern equatorial Pacific, southern tropical Indian oceans as well as rainfall averaged over the Guinea Coast as predictors (Garric et al., 2002). They applied linear and multiple linear regressions, and obtained a best generated forecast using rainfall averaged of the previous monsoon (12 month lead time) with R of 0.67. Mo and Thiaw (2002) used an ensemble canonical correlation method with SSTs to predict rainfall in the Sahel, and stream functions at one month lead time as predictors. Their best output was achieved using the ensemble mean between SST and stream function,

with an R of 0.40. Badr et al. (2014) tested ten statistical methods with various large scale variables in different areas, using principal component analysis (PCA) to combine all-purpose predictors. Artificial Neural Network was the best method, with an R of 0.71. Table 2.3 and 2.4 summarized the statistical methods used for seasonal rainfall forecasting in the Sahel and their forecasting performance.

2.2.2 Seasonal streamflow forecasting

Seasonal streamflow forecasts provide valuable information for water allocation and flood protection. Two main methods are widely used to simulate river flows: physically based hydrological models and statistical models. Hydrological models are capable of simulating streamflows based on relevant physical processes in the real world, and they probably generate more accurate forecasts than statistical models. However, they need to be forced with numerous related parameters and climate variables from either observations or climate model generation, and these prerequisites often make it difficult for users to get reliable forecasts. The forecasting skill of seasonal hydrological models could be improved with more effective climate predictions or initial condition estimates (Yossef et al., 2013).

Statistical models are the other option for seasonal streamflow forecasting. They generate statistical relationships between significant variables that are available prior to forecasted date. Statistical models require far less information than physical based hydrological models, but their simulations are more sensitive and they only analyze data characteristics, no physical processes are considered. However, statistical models can simulate acceptable outputs several months in advance, unlike hydrological models which usually can only provided acceptable forecasts with shorter lead times (one to three months) (McCuen et al., 1979; Shukla and Lettenmaier, 2011).

There is a distinct need for more research on seasonal streamflow forecasting in the Sahel region. Investigating current works with statistical and hydrological models developed in other regions would improve understanding of the methodologies and the models' capabilities. Both linear and non-linear regression can be found in seasonal streamflow forecasting when statistical approaches are applied.

Table 2.3: Performances of statistical seasonal models in the Sahel region as published in various studies

Author (s)	**Statistical methods**[1/]	**Predictor (s)**	**Predictand**	**Results**[2/]	**Lead time**
Abedokun (1979)	Linear regression model	Rainfalls of the South of Sahel;	Rainfall	$R \backsim 0.8$	2 months
Folland et al. (1991)	Empirical orthogonal function (EOF)/ Stepwise linear regression / Stepwise linear discrimination	Worldwide SSTs	Rainfall	R=0.72	1 months
Barnston et al. (1996)	EOF/CCA	Global SST	Rainfall	R=0.33	1 months
Garric et al. (2002)	Simple/ multiple linear regression	SSTs/ Rainfall	Rainfall	R=0.67	12 months
Mo and Thiaw (2002)	Ensemble canonical correlation	SSTs/ Streamfunction	Rainfall	R=0.4	1 months

Remark: [1/]: All statistical methods were tested in each study.
[2/]: Best result generated from each study.

Table 2.4: Performances of statistical seasonal models in the Sahel region as published in various studies (con't)

Author (s)	**Statistical methods**[1/]	**Predictor (s)**	**Predictand**	**Results**[2/]	**Lead time**
Badr et al. (2014)	-Full-covariate generalized linear model -Selected generalized linear model based on stepwise selection -Full-covariate generalized additive model -Selected generalized additive model based on penalized terms -Multivariate adaptive regression spline -Classification and regression trees model -Bagged classification and regression trees model -Bayesian additive regression trees model -Random forest model -Artificial neural network	-Surface air temperature -SST -Sea level pressure -SOI -ENSO -AMO -NAO -Hurricane main development -Northern Pacific Pattern -Pacific decadal Oscillation	Rainfall	$R = 0.71$	0 months

Remark: [1/]: All statistical methods were tested in each study.
[2/]: Best result generated from each study.

2.2.2.1 Hydrologic models

One of the conceptual rainfall-runoff models regularly used for hydrologic estimation and forecasting is the Soil and Water Assessment Tool (SWAT). SWAT devised by the USDA Agriculture Research Service, and has been continuously developed and enhance for almost 30 years. Gassman et al. (2007) indicated that SWAT is a watershed modeling tool that strongly outperforms others in hydrologic schemes. SWAT has been adopted as a part of the United States Environmental Protection Agency (USEPA) Better Assessment Science Integrating Point and Nonpoint Sources (BASINS) software package, and it is being used by various U.S. federal and state agencies. Trambauer et al. (2013) attempted to find suitable models for hydrological drought forecasting in Africa at different temporal and spatial scales. Of the 16 well-known hydrological models, SWAT was one of the five of deemed suitable for African hydrological drought forecasting; the other did not consider significant hydrological processes in arid regions, such as transmission losses along the channel, re-infiltration and evaporation of surface runoff. SWAT has been applied in many African hydrologic research studies, including climate change scenarios (Amadou et al., 2014; Lubini and Adamowski, 2013; Sood et al., 2013), calibration and sensitivity analysis applications (Mulungu and Munishi, 2007; Schuol and Abbaspour, 2006) and land use effects (Baker and Miller, 2013; Bossa et al., 2012; Mango et al., 2011).

SWAT has rarely been used for streamflow forecasting in the Sahel, but it has been applied in various other regions. Akiner and Akkoyunlu (2012) employed SWAT for river flow forecasting in the Melen watershed in Turkey, achieving acceptable river flow simulations using daily precipitation forecasts as the key input data. In addition, they showed that the model's reliability was dependent on an operation in the calibration process. Jajarmizadeh et al. (2014) used the SWAT model for monthly streamflow prediction in southern Iran. They compared SWAT performance to that of a support vector machine model, and both showed satisfactory monthly flow predictions with only minor differences. However, both models were unable to capture high flow periods. Alansi et al. (2009) confirmed the efficiency of SWAT for flow forecasting in humid tropical condition, when they used it to study the effects of land use change on flow in the Upper Bernam River Basin, Malaysia.

Other rainfall-runoff models used for streamflow forecasting are discussed here. The MWB and the SIMHYD models were employed to simulate streamflows in eastern Australia (Wang et al., 2011). The SIMHYD, the most common model used in Australia,

needs up to ten parameters, while the MWB requires only four parameters. They used monthly rainfall and potential evaporation before the forecasted year at various time scales (eg. one year and five years) and initial soil moisture and groundwater storage conditions to simulate streamflows. The accuracy of their results varied each month. Tuteja et al. (2011) used three rainfall-runoff models for streamflow forecasting in eight catchments in Australia. Sacramento, SIMHYD and SMAR models were driven by rainfall forecast combinations of one month and three months lead time, and the potential evapotranspiration data. SMAR was relatively outperformed by the other two models. Shukla and Lettenmaier (2011) simulated seasonal hydrologic forecasts in the U.S. using a macro scale hydrological model known as the Variable Infiltration Capacity. They forced the model with the initial hydrologic conditions and climate forecasts, and concluded that better climate forecast and initial condition skills can potentially improve the forecasting skill.

2.2.2.2 Statistical models

Eldaw et al. (2003) applied multiple linear regression and PCA to forecast the seasonal river flow in the Nile River during flood season (July to October). They used the Pacific, Atlantic and Indian ocean SSTs and Guinea precipitation, with every consecutive four month period up to one year as predictors. Their best prediction for validation phase indicated a coefficient of determination (R^2) of 0.68, using the most suitable period between August and November from the previous year as the predictor. The Pacific and Atlantic SSTs were also employed to forecast streamflow in the continental United States with 12 month lead times by Tootle et al. (2007), using partial least squared regression. They applied the LEPS score to estimate their simulations, and as it was greater than 10% the forecasting skills were acceptable. Wang et al. (2009) used Bayesian joint probability for seasonal streamflow forecasting in southeast Australia with ENSO indices and antecedent streamflows as predictors. They obtained an acceptable LEPS skill score (30% or higher) with one month lead time, which showed better forecasting skills than previous studies in the same region. Piechota et al. (1998) forecasted every three-month streamflows average for an entire year in ten eastern Australian catchments, with the Pacific SST and SOI as predictors. They used linear discrimination and linear combination as tools, and estimated their results by categorizing the flows into three classes. If forecast probabilities are similar to climatology no new information will be obtained. The performance of models was better than the climatology in many stations and various seasons. Landman et al. (2001) simulated streamflow forecasts over southern Africa, using SSTs at one and

three month lead times to force the GCM to simulate geopotential height and relative humidity at the first step. These results were then downscaled and statistical approaches were applied to examine the relationship with local streamflows. Sankarasubramanian et al. (2008) forecasted streamflows five months in advance for a reservoir system in the Philippines, using both climate and statistical models. They first forced the ECHAM 4.5 GCM with SSTs and generated synthetic precipitation, then linked the precipitation to monthly streamflows using principal component regression. The results showed that monthly streamflows during October to February were correlated with the simulated precipitation data that was generated via SSTs five months ahead.

Large scale atmospheric-oceanic patterns are not the only predictors of streamflow forecasting, the initial states of land surface variables are also employed for the seasonal forecasting. Initial conditions, such as streamflow or rainfall available up to three months before forecasted date, are also suitable for characterizing the initial conditions of a basin (Robertson and Wang 2012). McCuen et al. (1979) used base flow and snow water equivalencies to forecast streamflow in south Utah. They developed various models with multiple linear regression, stepwise regression and PCA, and got good results with various lead times up to 12 months, with an R of 0.8 to 0.9. Maurer and Lettenmaier (2003) attempted to improve the forecasting skills of runoff in the Mississippi River, USA, by applying both climatic indices (i.e. SOI and AO) with soil moisture and snow water equivalents as predictors, using multiple linear regression. Their results showed that adding land surface variables significantly improved the model's ability in many areas. Applying Bayesian approach, (Kwon et al., 2009) used upland snow cover and global SSTs as predictors of seasonal streamflow forecasting in the Yangtze River basin China. Seasonal and peak flows were forecasted one season prior to the issued forecasts, and the correlation coefficients between observations and forecasts were approximately 0.7 to 0.8 respectively. Other research studies of seasonal streamflow forecasting using statistical models include Souza Filho and Lall (2003), Robertson et al. (2013), Abudu et al. (2010), Berri and Flamenco (1999), Hamlet and Lettenmaier (1999) and Piechota and Dracup (1999).

2.3 Model calibration and validation

One of the main aspects of rainfall-runoff applications is identifying optimum values for model parameters. Conceptual models such as SWAT typically have a large number of parameters. Streamflow simulation, for example, consists of various factors (e.g. surface runoff, return flow, evapotranspiration and channel transmission losses) which are comprised of several parameters that cannot be measured in the field. Therefore, searching for suitable parameter values is done by repetitively adjusting the significant parameters until simulated outputs correspond to observations. An approach is the calibration process, and the criteria employed to measure how consistent data sets are with each other are called calibration criteria or objective functions (Duan et al, 1994). The input parameters lastly determined by the calibration are used to produce simulations in a validation process (Moriasi et al., 2007). Yang et al. (2008) found that the uncertainties in model structure, parameters and input data make this a challenging task in watershed model calibration. Inadequate calibration is one of various reasons (e.g. short periods of streamflow observation and lack of rainfall spatial variability in the watershed) for poor hydrologic prediction using SWAT (Arnold et al., 2012).

2.3.1 The calibration of SWAT model

Since SWAT has a large number of parameters, a prior process known as sensitivity analysis is applied to identify the significant parameters for a particular basin, and for a variable of the interest. Sensitivity analysis determines the rate of change in the simulation corresponding to the adjustment of parameter values (Arnold et al., 2012; Moriasi et al., 2007). There are two methods of sensitivity analysis: local and global. The local method changes parameter values one parameter at a time, and the global method adjusts all parameters simultaneously. While using global sensitivity analysis requires a large number of simulations, the local method leads to difficulty defining the correct values for fixed parameters (Arnold et al., 2012). Sensitivity analysis ultimately defines a set of significant parameters, and the values of these will then be adjusted in the calibration process; which can be done using the auto calibration tools in SWAT or by applying SWAT-CUP (SWAT calibration and uncertainty programs). SWAT-CUP has been used to calibrate SWAT models in many research works (e.g. Jajarmizadeh et al., 2013; Masih et al., 2001; Wang et al., 2014).

Model parameterization can be accomplished using one of these five approaches available in SWAT-CUP: sequential uncertainty fitting (SUFI2), particle swarm optimization

(PSO), generalize likelihood uncertainty estimation (GLUE), parameter solution (ParaSol) and Markov chain Monte Carlo (MCMC). These techniques have differences in perspective, and in objective functions they use for estimation; consequently, it is impossible to clearly compare their calibration performance (Yang et al., 2008). Yang et al. (2008) compared the performance of SUFI2, GLUE, Parasol and MCMC in terms of their parameter distribution, simulation performance, uncertainty of model prediction and difficulty of implementation, as well as the computational effort required. They concluded that GLUE, SUFI2 and ParaSol were computationally inexpensive compared to MCMC, and that SUFI2 and GLUE were liable for all uncertainties (e.g. structural, input and parameter) while Parasol was only responsible for parameter uncertainty. In addition, GLUE, SUFI2 and MCMC had similar uncertainty prediction bands. Setegn et al. (2008) employed SWAT for streamflow prediction in the Lake Tana Basin in Ethiopia. They used SUFI2, GLUE and Parasol algorithms for the model calibration, and concluded that all three approaches could minimize the differences between flow simulations and observations. They also found that SUFI2 was an efficient algorithm, though it required more iterative and manually alteration the range of significant parameters. Mamo and Jain (2013) compared the efficiency of SUFI2 to Parasol, and concluded that SUFI2 was superior for changing the objective estimation functions and modifying the parameter ranges.

The performance of SUFI2 and GLUE were also compared by Luo et al. (2011) and Nkonge et al. (2014). Luo et al. (2011) simulated discharge in a Japanese river catchment, and applied SUFI2 and GLUE in the calibration step. Their results showed that GLUE had insignificantly better performance than SUFI2, but SUFI2 was better for simulations with the smallest sample size. Nkonge et al. (2014) used SUFI2 and GLUE to calibrate the model for streamflow simulation in the upper Tana sub-watershed in Kenya, and determined that SUFI2 was generally more efficienct than GLUE, with lower computational cost. And similar to Ma et al.(2014), also found that SUFI2 had higher performance than the other SWAT-CUP algorithms, and that it was widely used for calibrating streamflow simulation, sediment yield and water quality.

SUFI2 applied a sampling method known as Latin Hypercube Sampling (LHS) to define the values of specific parameters for a calibration period. LHS splits each parameter equally into n intervals (where n is the number of defined simulations), and selects one sample from each interval according to the density of the interval (Wyss and Jorgensen, 1998). The SUFI2 algorithm first determines the objective functions to be used as estimation criteria, then defines the ranges of significant parameters for the first

run of LHS; the ranges can be equal or smaller than the absolute ranges determined in SWAT-CUP. Then n simulations with parameter combinations are run using LHS, with n specified by the user. Following this, the sensitivity matrix known as the Jacobian matrix, which is the ratio between the value of defined objective function and parameters, is constructed. A Hessian matrix resulting from the multiplication of the Jacobian matrix and its transpose is calculated, the parameter covariance matrix is computed, and the 95% confidence interval of the parameter is generated. Finally, the range of parameter is updated, resulting in a smaller range. The details of the SUFI2 algorithm can be found in Abbaspour (2012).

2.3.2 Model evaluation

There is no comprehensive information to completely explain the methods or criteria for evaluating model accuracy (Moriasi et al., 2007). Moriasi et al. (2007) demonstrated three quantitative statistics used to evaluate watershed simulations: standard regression, dimensionless index and error index. Standard regression techniques can determine the strength of the linear relationship between observations and simulations, while dimensionless indices define relative model evaluation, and error indices resulted in the deviation of simulated and observed data (graphical techniques can also be used for visual comparison of the two data sets). The statistical criteria used extensively for estimation in the calibration process are R^2 and the Nash-Sutcliffe coefficient (E_f) (Arnold et al., 2012). The criteria can be seen in numerous research works related to rainfall-runoff model simulations, for example Fiseha et al. (2013), Kushwaha and Jain (2013), Ridwansyah et al. (2014), Saha et al. (2014), Setegn et al. (2014). R^2 is a standard regression statistic that indicates the proportion of observation variance described by the model. R^2 ranges from 0 to 1, with 0 representing no correlation, and values close to 1 representing high variance correlation. E_f is used to estimate the relative magnitude of the variance of the residual compared to the variance of observation (Nash and Sutcliffe, 1970 cited in Moriasi et al., 2007). E_f values range from ∞ to 1, with 1 being perfect simulation. Negative values of E_f refer to the use of average observations for predictions, rather than simulated values.

Currently, there is no absolute value for each criterion to identify how well a model can establish simulations (Arnold et al., 2012). Moriasi et al (2007) concluded that R^2 values higher than 0.5 most often signify acceptable simulation, and presented recommended E_f value from various studies, as shown in Table 2.5. In comparisons of monthly and

daily simulations, E_f values resulting from daily data seem to be higher than those from monthly data, due to the increase in sampling size. The performance ratings of monthly simulation reported by Moriasi et al. (2007) are illustrated in Table 2.6

2.4 Temporal disaggregation

Temporal resolution of input variables higher than monthly scale is usually required to force in rainfall-runoff applications for hydrologic simulation and prediction (e.g. surface runoff, streamflow and sediment yield). However, significant limitations of rainfall measurements using rain gauges at high temporal scale are experienced globally, so reliable data mostly are typically presented at a monthly or lower time step (Guenni and Bardossy, 2002). Thus, temporal disaggregation methods are normally required to transform data, in order to acquire the data in high temporal resolution.

The method of fragments, the basic temporal disaggregation approach, was first proposed by Harms and Campbell (1967), and it has been continuously developed since. The main challenge of this method is to find a suitable way to calculate the fragment series used to multiply with the variable of interest. The fragment series are generated using historic data (Maheepala and Perera, 1996). Mcmahon and Mein (1986) employed this method to disaggregate annual flow forecasts to monthly flows by applying equations to compute simulated monthly flows using monthly fragment series. These equations are shown in Equation 2.1 and 2.2

$$W_{ij} = \frac{F_{ij}}{\sum_{i=1}^{12} F_{ij}} \tag{2.1}$$

$$F_{ij}^{**} = F_j^{*} * W_{ij} \tag{2.2}$$

where W_{ij} is the monthly fragment flow of month i and year j, F_{ij} is the monthly historic data of month i and year j, and F_j^* and F_{ij}^{**} are the simulated annual flow from a model of year i and the simulated monthly flow of month i and year j respectively. Though, the method of fragments initially selects fragment series randomly, this random selection does not provide satisfactory outputs related to the significant statistics (Wey, 2006). Mcmahon and Mein (1986) presented the key site approach to select the set of fragment series. This method selects the set of fragments by considering the monthly historic data with the closest magnitude to the generated annual flow.

Table 2.5: Performance rating of daily simulations for E_f (Moriasi et al., 2007)

Model	**Value**	**Performance rating**	**Modeling phase**	**Reference**
HSPE	>0.8	Satisfactory	Calibration-validation	Donigian et al. (1983)
APEX	>0.40	Satisfactory	Calibration-validation	Ramanarayanan et al. (1997)
SAC-SMA	<0.70	Poor	Autocalibration	Gupta et al. (1999)
SAC-SMA	>0.80	Efficient	Autocalibration	Gupta et al. (1999)
DHM	>0.75	Good	Calibration-validation	Motovilov et al. (1999)[a]
DHM	>0.36 to 0.75	Satisfactory	Calibration-validation	Motovilov et al. (1999)[a]
DHM	<0.36	Unsatisfactory	Calibration-validation	Motovilov et al. (1999)[a]
SWAT	>0.65	Very good	Calibration-validation	Saleh et al. (2000)
SWAT	0.54 to 0.65	Adequate	Calibration-validation	Saleh et al. (2000)
SWAT	>0.50	Satisfactory	Calibration-validation	Santhi et al. (2001); adapted by Bracmort et al. (2006)
SWAT	>0.65	Satisfactory	Calibration-validation	Saleh et al. (2004); adapted by Narasimhan et al. (2005)

[a] Adapted by Van Liew et al. (2003) and Fernandez et al. (2005)

Table 2.6: Performance rating of monthly simulations for E_f (Moriasi et al., 2007)

Performance rating	E_f **value**
Very good	$0.75<E_f\leq1.00$
Good	$0.65<E_f\leq0.75$
Satisfactory	$0.50<E_f\leq0.65$
Unsatisfactory	$E_f \leq0.50$

Srikanthan et al. (2002) used the method of fragments and the nonparametric model to acquire monthly rainfall data throughout Australia, and concluded that both models were equally capable of maintaining monthly rainfall characteristics. Wojcik and Buishand (2003) combined a nearest-neighbour resampling approach and the method of fragments to disaggregate daily precipitation and temperature for Maastricht, Netherlands to 6-hourly data, and found that the two methods could preserve a number of second order statistics of both rainfall and temperature. The performance of the fragment method was also compared to the Random Multiplicative Cascades and Randomized Bartlett Lewis models for rainfall disaggregation from daily to hourly scale (Pui et al, 2009). The results revealed that the method of fragments outperformed the other two models in terms of reproducing statistic parameters closest to the observed data. However, this method will only provide satisfactory outputs when a long record of historical rainfall data is available.

Porter and Pink (1991) developed another method of fragments, which they dubbed 'the method of synthetic fragments'. As the method of fragments generates a monthly fragment series which might have only a weak relationship to the original data set and cause repetitive cyclic patterns (Wey, 2006; Maheepala and Perera, 1996), the method of synthetic fragments was developed to address this type of problem. Similar to the method of fragments, this approach produced the simulated annual data using applicable models. The fragment series are generated by creating the synthetic data from various methods (e.g. k-nearest neighbour), rather than using historic data as in the method of fragments (Wey, 2006). The annual data computed from the monthly fragments that closely conforms to the simulated data are selected to be used for disaggregation. After computing the synthetic monthly fragments by the appropriate approaches, the monthly series to be applied to the disaggregated simulated annual data are selected by Equation

2.3

$$\propto_j = \sum_{i=1}^{n} ((F_{ik}^{*} - W_{ij})/(SD_x^i))^2 \tag{2.3}$$

where $\propto_j$ is the parameter for computing the minimum difference of the simulated annual data using the models of year k and site i (F_{ik}^{*}) with the annual data generated by calculating the monthly fragments of year j and site i (W_{ij}) and SD_x^i is the standard deviation of the historic data (Maheepala and Perera, 1996). Although, this method can preserve the statistical properties of monthly data, it cannot maintain the correlation between the last month of the past year and the first month of the following year. To avoid this, data should be from the month with the minimum serial correlation in starting year (Srikanthan and McMahon, 2001).

2.5 Conclusion and discussion of the literature review

As indicated by diverse past works, there are teleconnections between large scale atmospheric - oceanic patterns, and climatic and hydrologic variables at regional or local scale. This is one of keys to successful development of hydrological seasonal forecasting in specific areas. The mechanisms of ENSO related to SST are responsible for rainfall variations in West Africa, and many studies have strongly confirmed the predictability of Sahel rainfall using the equatorial Pacific and Atlantic SSTs as predictors. Some researchers investigated the capability of the Indian Ocean and the Mediterranean SSTs for seasonal rainfall forecasting, but the teleconnection signals of the both indices are apparently not as strong as the Pacific and Atlantic SSTs. Positive and negative correlations of these SSTs to the Sahel rainfall depended on various factors and limitations of these studies, including rainfall data, time period, the location of SST. More work related to directly links of climate indices to streamflows in the Sahel is required, as only the relationships between rainfalls and large-scale circulation patterns has been regularly investigated in this region.

Seasonal rainfall forecasting in the Sahel was typically done using both dynamical and statistical models. GCMs were widely used in the region, and they resulted in acceptable to high forecasting skills using the correlation coefficient. However, the limitations of GCMs in terms of high computation costs and low spatial resolution made seasonal

rainfall forecasting difficult, so statistical models played a pivotal role. Various statistical methods were employed to forecast the Sahel rainfall, and the results ranged from moderate to high forecasting skills using the correlation coefficient as an estimator. Most research produced rainfall forecasts at zero to one month lead times, although one study had outputs up to 12 months lead time, with moderate forecasting skill. All this work confirms the potential of using statistical models driven by various indices such as SST, ENSO and antecedent rainfalls, for seasonal rainfall forecasting. However, most forecasting studies in the Sahel were completed without considering streamflow forecasting, which is highly important to the preparation for and alleviation of adverse events such as droughts and flooding.

Seasonal streamflow forecasting can be accomplished using two main methods: hydrological models and statistical models. To forecast streamflow in advance, hydrological models should be forced with forecasted rainfall and other climate variables. Here, SWAT was selected as the tool to forecast streamflow on a monthly scale. SWAT is a physically based model, commonly used for hydrologic variable simulations, such as streamflow, sediment yield and nutrient loading. This study examined SWAT performance to forecast streamflow in the Sahel. To obtain highly accurate streamflow forecasts using SWAT, the calibration needs to be initially done. Various studies have tested and compared calibration methods. There are five approaches available to users for SWAT model calibration in the SWAT-CUP application, and each has its own advantages and disadvantages (e.g. GLUE, SUFI2 and Parasol applications with less computation costs); SUFI2 and GLUE are responsible for all uncertainty sources. Calibrated model performance is estimated using various criteria, R^2, E_f and mean square error, for example.

Statistical methods have been used as tools to directly link streamflow to climatic-oceanic indices in other regions, but few were conducted in Sahel. Outputs in the other areas confirmed the possibility of predicting streamflow using large-scale circulation indices, which is why direct linkages between SST to streamflow in the Sahel are examined in this study. The method of fragments used to increase temporal scales is reviewed here. The efficiency of this fragment method has been successful in many studies. Since using this method to find appropriate fragment series to generate new higher temporal scale data set is challenging, this work attempts to determine the most suitable way to acquire the most accurate disaggregated data.

Chapter 3

Theory

This section presents all theories relating to this study. Though there are various statistical methods widely used for seasonal forecasting, only the four main approaches of principal component analysis (PCA), canonical correlation analysis (CCA), simple/multiple linear regressions and polynomial regression are described in details in this chapter. All the concepts of hydrologic regime used to calculate streamflow based on the Soil and Water Assessment Tool (SWAT) model are examined in the following section. Then the techniques employed to evaluate the model's performance, and the details of the cost/loss ratio method used to estimate the economic value of the forecasting system are explained.

3.1 Statistical techniques for seasonal forecasting

One of main objectives of this study is to apply statistical techniques to develop more accurate forecasts on seasonal time scale. Statistical seasonal forecasting generally deals with large scale atmospheric and oceanic patterns as independent variables. These data are usually constructed as a grid of information consisting of a large number of data sets. Thus appropriate methods for data reduction are necessary to decrease the data sets that will be used in the regression analysis.

3.1.1 Principal component analysis

PCA, sometimes known as empirical orthogonal function is possibly the most extensively used analysis in multivariate statistical techniques (Wilks, 1995). McCuen et al. (1979) and Tootle et al. (2007) indicated that PCA can overcome multicollinearlity in predictor data. It is regularly used to reduce large volumes of data; decreasing data redundancy and generating fewer data sets that account for variance and maintain general information of original data set (Wilks, 1995). PCA applies mathematical concepts of general statistics and linear algebra, such as covariance, standard deviation, eigenvectors and eigenvalues. Step-by-step is used to produce the new data sets called principal components (PCs), which are described in the following section.

Given that a data set called X is of interest. X contains K variables, and each element consists of n observations. PCs are usually calculated from anomalies of the original data, particularly if the data set consists of variables indicating different scales or units. The method used to compute anomalies is simple subtraction of all values from the sample mean, as shown in Equation 3.1.

$$X' = \begin{bmatrix} X_{11} & X_{12} & ... & X_{1k} \\ X_{21} & X_{22} & ... & X_{2k} \\ & \cdot & & \\ & \cdot & & \\ & \cdot & & \\ X_{n1} & X_{n2} & ... & X_{nk} \end{bmatrix}, \begin{bmatrix} X'_{11} \\ X'_{21} \\ \cdot \\ \cdot \\ \cdot \\ X'_{n1} \end{bmatrix} = \begin{bmatrix} X_{11} \\ X_{21} \\ \cdot \\ \cdot \\ \cdot \\ X_{n1} \end{bmatrix} - \bar{X}_1, X' = \begin{bmatrix} X'_{11} & X'_{12} & ... & X'_{1K} \\ X'_{21} & X'_{22} & ... & X'_{2K} \\ & \cdot & & \\ & \cdot & & \\ & \cdot & & \\ X'_{n1} & X'_{n2} & ... & X'_{nK} \end{bmatrix} \tag{3.1}$$

All anomalies of K variables and n observations are computed using the same process. Finally, the original X data set is changed to the form of anomalies (X') with the mean values are zero; the physical dimensions, variances and inter-correlations remain the same as the original data sets.

Then a variance-covariance matrix [S] of the X' data set (Equation 3.2) is generated by calculating the variance of each K variable and the covariance between the variables, with all variables in X' (K variables) paired to each other. The number of generated variance and covariance data in the matrix [S] depends on the number of K. Equations 3.3 and 3.4 are used for variance and covariance calculations respectively. For example, $S_{1,1}$ in Equation 3.3 refers to the variance of the first variable ($K1$) and $S_{1,2}$ in Equation 3.4 is the covariance of the pairwise relationship between the first ($K1$) and second ($K2$) variables.

$$S = \begin{bmatrix} S_{1,1} & S_{1,2} & S_{1,K} \\ S_{2,1} & S_{2,2} & S_{2,K} \\ & \cdot & \\ & \cdot & \\ & \cdot & \\ S_{K,1} & S_{K,2} & S_{K,K} \end{bmatrix} \tag{3.2}$$

$$Var(S_{1,1}) = [\sum_{i=1}^{n}(x_i^{'} - \bar{x}^{'})^2]/(n-1) \tag{3.3}$$

$$Cov(S_{1,2}) = [\sum_{i=1}^{n}(x_{i,k1}^{'} - \bar{x}_{k1}^{'})(x_{i,k2}^{'} - \bar{x}_{k2}^{'})]/(n-1) \tag{3.4}$$

Eigenvector (e') and eigenvalue (λ') were then generated based on the variance-covariance matrix [S]. The relationships between these three variables (i.e. [S], e' and λ') are expressed in Equation 3.5 and 3.6. Each pair of eigenvectors and eigenvalues must meet this function, and a simple linear algebra calculation helps to compute the two variables. M pairs of eigenvector-eigenvalues are then generated, where $M = K$. Wilks (1995) explained that the first pair of eigenvalue-eigenvectors can be defined by considering the greatest number of eigenvalues, and the first eigenvector geometrically responds to the largest variability of the given data [S].

$$[S]e' = \lambda e' \tag{3.5}$$

$$([S] - \lambda'[I])e' = 0 \tag{3.6}$$

Principal components (PCs) are then computed using Equation 3.7, where u_m represents the principal component (PC) (i.e u_1 is the PC1). The first PC is the summation of the multiplication of each element in the first eigenvector by the corresponding K variable. The new axis is defined based on the first eigenvector, which is responsible for the maximum joint variability of the data (Wilks, 1995). The second axis is perpendicular to the first, and so on, as in Figure 3.1. The highest explained variance is found in the first PC, and it decreases in the following PCs. Wilks (2011) compared anomalies of the original data and the newly constructed data with PC1, as illustrated in Figure 3.2. It is clear that the difference in anomalies between the raw data and the new data sets generated by PC1 is insignificant.

$$u_m = e_m^{'T} X^{'} = \sum_{k=1}^{K} e^{'}_{k,m} x^{'}_{k,m=1,2,3...m} (3.7)$$

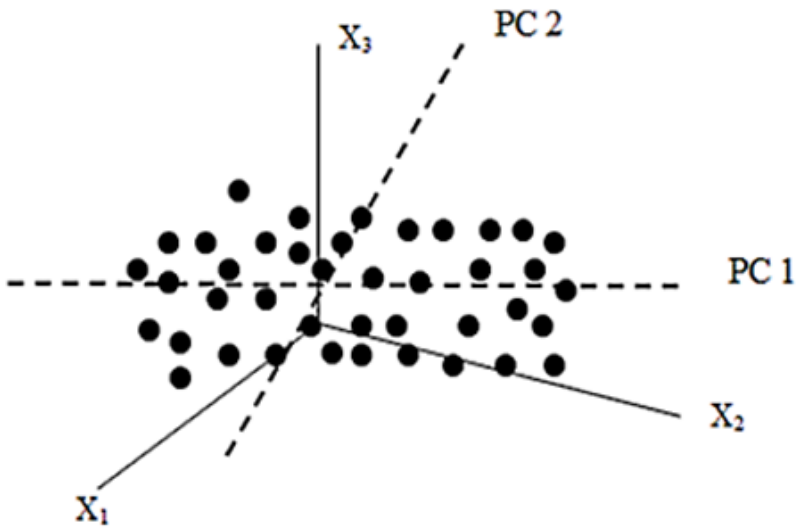

Figure 3.1: Examples of PC1 and PC2 in three variables (Wilks, 1995)

3.1.2 Canonical correlation analysis

Applying PCA to construct new data sets only accounts for the variability of independent variables, while CCA, developed by Hotelling (1936), allows users to search for interrelationships in linear form between multiple independent and dependent variables. The typical form of CCA is shown in Equation 3.8.

$$Y_1 + Y_2 + Y_3 + ... + Y_n = X_1 + X_2 + X_3 + ... + X_n \quad (3.8)$$

To calculate canonical variables, both original data sets (i.e. independent and dependent variables) are converted to anomalies as showing in Equation 3.1, thereby constructing a matrix of $X^{'}$ (IxJ) (for dependent variables) and $Y^{'}$ (IxK) (for independent variables). Note that the number of observations of both X and Y must be equal, though they can have a different number of variables. A covariance matrix of X and Y variables $[S_c\ ]$ $(J+K, J+K)$ is then generated, as showing in Equation 3.9. $[S_{(x,x)}]$ and $[S_{(y,y)}]$

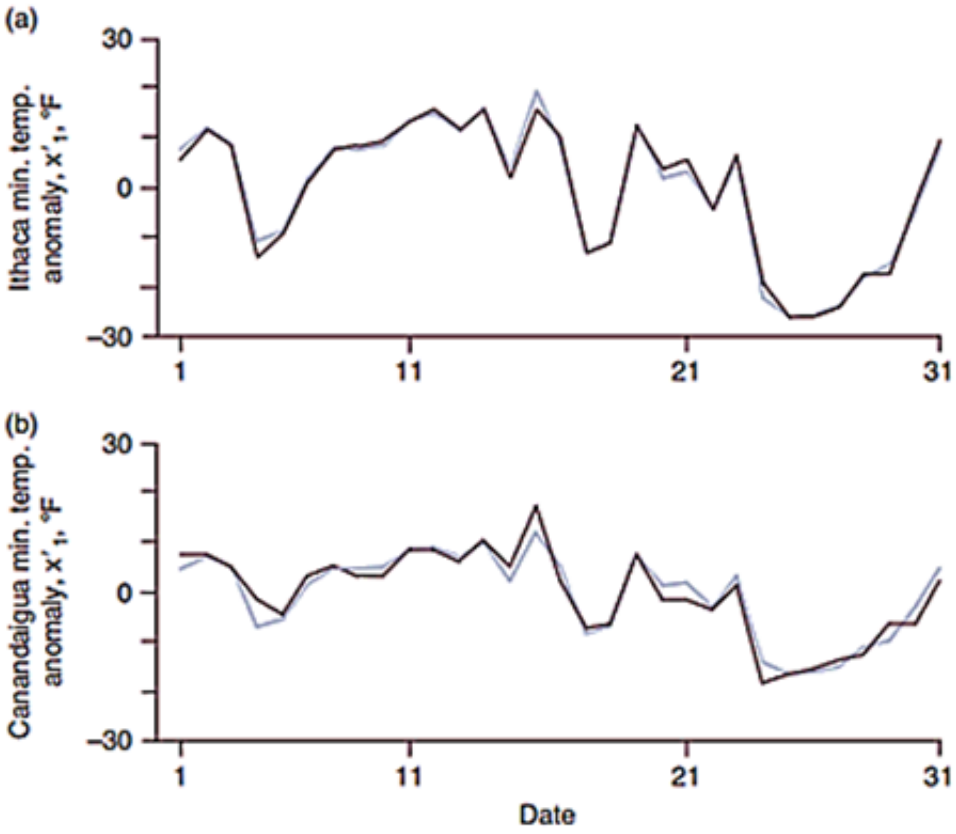

Figure 3.2: Anomalies of temperature data in two cities (black line) and their new series constructed using PC1 (gray line) (Wilks, 2011)

are the matrix of intercorrelation of variables in X and Y respectively, $[S_(x,y)\ ]$ is the matrix of interrelationships between X and Y and $[S_(y,x)]$ is the transpose of $[S_(x,y)]$.

$$\left[S_c\right] = \begin{bmatrix} \begin{bmatrix} S_{x,x} \\ S_{y,x} \end{bmatrix} & \begin{bmatrix} S_{x,y} \\ S_{y,y} \end{bmatrix} \end{bmatrix} \tag{3.9}$$

Next, eigenvectors (e') and eigenvalues (λ') of the matrices $[M_x]$ (JxJ) and $[M_y]$ (KxK) are calculated, as shown in Equation 3.10 and 3.11 respectively. A number of eigenvalues are related to the minimum values of J and K (min (J,K)), and the remaining eigenvalues of the matrix with higher variables will be equal zero (Wilks, 1995).

$$\left[M_x\right] = \left[S_{xx}\right]^{-1}\left[S_{xy}\right]\left[S_{yy}\right]^{-1}\left[S_{yx}\right] \tag{3.10}$$

$$\left[M_y\right] = \left[S_{yy}\right]^{-1}\left[S_{yx}\right]\left[S_{xx}\right]^{-1}\left[S_{xy}\right] \tag{3.11}$$

The square root of an eigenvalue is called the canonical correlation (r_c^2), and the respective eigenvectors of the two matrices $[M_x]$ and $[M_y\ ]$ are known as canonical vectors (a_m) and (b_m), respectively. Eigenvalues allow users to measure the strength of relationship between each pair of canonical variants, and canonical correlation can be used to estimate the degree of shared variance between them.

Equations 3.12 and 3.13 show the relationship between canonical correlation and the canonical vector of the two matrices (Wilks, 1995). The dimensions of a_m and b_m correspond to the minimum ranks of matrices M_x and M_y respectively.

$$\left[M_x\right] a_m = r_{c,m}^2 a_m.m = 1,2,3,...M \tag{3.12}$$

$$\left[M_y\right] b_m = r_{c,m}^2 b_m.m = 1,2,3,...M \tag{3.13}$$

Finally, new variables (canonical variants) of independent variable set (v_m) and response data set (w_m) are constructed by multiplying their anomalies and canonical vectors (Equations 3.14 and 3.15).

$$v_m = a_m^T x^{'} = \sum_{i=1}^{l} a_{m,i} x_i^{'}, m = 1,2,3...,min(J,K) \tag{3.14}$$

$$w_m = b_m^T y^{'} = \sum_{i=1}^{l} b_{m,i} y_i^{'}, m = 1, 2, 3..., min(J, K) \tag{3.15}$$

3.1.3 Regression analysis

Regression analysis is a well-known statistical tool used to examine relationships between variables of interest. Statistical relationships between dependent and independent variables are explained by an equation constructed using regression analysis. The degree of influence of predictors (independent variables) on predictands (dependent variables) can be defined after completion of the regression.

A hypothesis test is a method used to test a significant relationship between variables. The null hypothesis and the alternative hypothesis will be stated as H_0:β_1=0 and H_1:β_1 $\neq$ 0 respectively, where β_1 is a regression coefficient. If the regression coefficient is zero, there is no relationship between independent and dependent variables. To confirm the significant relationship between the variables for a non-zero of β_1, a significant level (α) must first be determined. The significant level is the probability of rejecting H_0 when it is true. Common significant levels are defined as 0.01, 0.05 and 0.1. If the significant level of 0.05 is specified, 5% of false rejected H_0 will be accepted. A lower number of significant value indicates that there is more confidence to reject the null hypothesis. Then, a P-value which is the strength of the evidence to reject the null hypothesis and support the alternative hypothesis, is calculated. P-value can be calculated using various statistical tests, such as Students t, Snedecors F and Chi-square, and they can be interpreted by comparison with the significant level that is first determined. Hooper (2014) also stated the interpretation of P-value as follows:

"P>0.10: No evidence against the null hypothesis. The data appear to be consistent with the null hypothesis.

0.05<P≤0.10: Weak evidence against the null hypothesis in favor of the alternative.

0.01<P≤0.05: Moderate evidence against the null hypothesis in favor of the alternative.

0.001<P≤0.01: Strong evidence against the null hypothesis in favor of the alternative.

P≤0.001: Very strong evidence against the null hypothesis in favor of the alternative."

3.1.3.1 Simple linear regression

Simple linear regression is widely used in statistical forecasting. This method searches for the relationship between an independent variable (x) and a dependent variable (y). The simple correlation between these two data sets can be shown graphically, as in Figure 3.3. The linear regression line in this figure, which is generated in the cloud of scatter plots between the x and y variables, are produced by considering the least error (e) of prediction y corresponding to observation x. This method is called least squares regression or least squares error, as it determines the specific straight line that minimizing the sum of the squared error for all observations of both data sets.

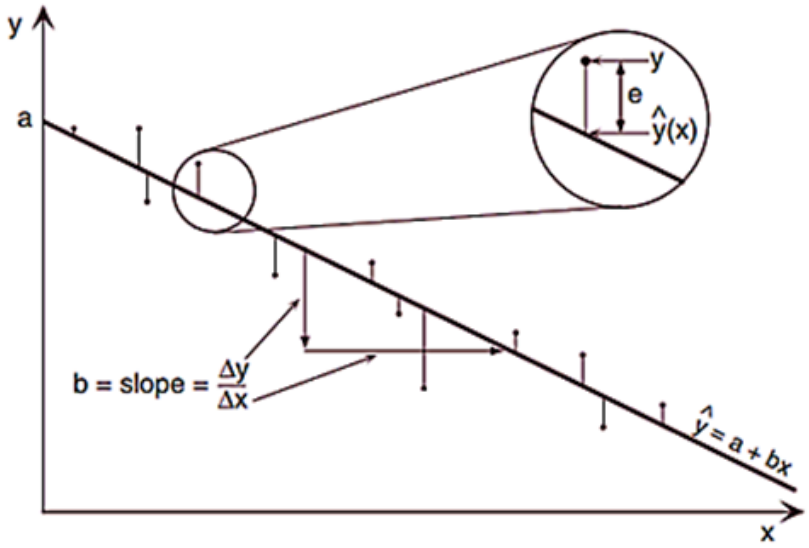

Figure 3.3: Linear regression line (Wilks, 2011).

Equation 3.16 represents the regression line in Figure 3.3. $\hat{y}$ is the predicted value of the dependent data, and a and b are the least squares intercept and slope of the line respectively. The residual of observation y (e_i) can be computed with Equation 3.17. Thus, the response variable y_i can be expressed in the another way (Equation 3.18) by combining Equation 3.16 and 3.17.

$$\hat{y} = a + bx \tag{3.16}$$

$$e_i = y_i - \hat{y}(x_i) \tag{3.17}$$

$$y_i = \hat{y} + e_i = a + bx + e_i \tag{3.18}$$

Though, a computational tool can simply calculate a and b, it is important to identify the equations used to compute these parameters. Wilks (2011) described the steps to obtain the least squares intercept (a) and slope (b) to minimize the sum of square error. The equation for the sum of the square error of residuals (Equation 3.19) is set and solved using the basic calculus. Equation 3.20 and 3.21 are the derivatives of a and b, and Equation 3.22 and 3.23 are the normal form of these derivatives when they are set to zero.

$$\sum_{i=1}^{n}(e_i)^2 = \sum_{i=1}^{n}(y_i - (a + bx_i))^2 \tag{3.19}$$

$$[\partial \sum_{i=1}^{n}(y_i - (a + bx_i))^2]/\partial a = -2\sum_{i=1}^{n}(y_i - a - bx_i)) = 0 \tag{3.20}$$

$$[\partial \sum_{i=1}^{n}(y_i - (a + bx_i))^2]/\partial b = -2\sum_{i=1}^{n} x_i(y_i - a - bx_i)) = 0 \tag{3.21}$$

$$\sum_{i=1}^{n} y_i = na + b\sum_{i=1}^{n} x_i \tag{3.22}$$

$$\sum_{i=1}^{n} x_i y_i = a\sum_{i=1}^{n} x_i + b\sum_{i=1}^{n}(x_i)^2 \tag{3.23}$$

Finally, the simple models for a and b parameters are expressed as in Equations 3.24 and 3.25

$$b = \{\sum_{i=1}^{n}[(x_i - \bar{x})(y_i - \bar{y})]\}/\sum_{i=1}^{n}[(x_i - \bar{x})^2 \tag{3.24}$$

$$a = \bar{y} - b\bar{x} \tag{3.25}$$

3.1.3.2 Multiple linear regression

The mathematics of multiple linear regression are similar to simple linear regression, except multiple linear regression deals with several independent variables with only one set of dependent variable. Therefore, the prediction equation of multiple linear regression consists of various coefficients that correspond to given independent variables and one

parameter for interception, as in Equation 3.26. A potential issue when applying multiple linear regression is intercolineality between more than one predictor, which could produce irrational regression coefficients (McCuen et al., 1979).

$$\hat{y} = a + b_1x_1 + b_2x_2 + b_3x_3.. + b_kx_k \tag{3.26}$$

Similar approaches to search for the a and b parameters and minimize the sum of squares error of the residuals is also required. The difference is the number of coefficients. Thus, matrix algebra is useful for solving these equations. Derivatives of Equation 3.27, which are the example sum of squares error for two independent variables (x_1,x_2), are presented in Equation 3.28 to 3.30. Chen (2014) presented the matrix form for computing a and b for two independent variables, as shown in Equation 3.31.

$$\sum_{i=1}^{n}(e_i)^2 = \sum_{i=1}^{n}(y_i - (a + b_1x_{1(i)} + b_2x_{2(i)}))^2 \tag{3.27}$$

$$[\partial \sum_{i=1}^{n}(y_i - (a + b_1x_{1(i)} + b_2x_{2(i)}))^2]/\partial a = -2\sum_{i=1}^{n}(y_i - a - b_1x_{1(i)} - b_2x_{2(i)}) = 0 \tag{3.28}$$

$$[\partial \sum_{i=1}^{n}(y_i - (a + b_1x_{1(i)} + b_2x_{2(i)}))^2]/\partial b_1 = -2\sum_{i=1}^{n}x_{1(i)}(y_i - a - b_1x_{1(i)} - b_2x_{2(i)}) = 0 \tag{3.29}$$

$$[\partial \sum_{i=1}^{n}(y_i - (a + b_1x_{1(i)} + b_2x_{2(i)}))^2]/\partial b_2 = -2\sum_{i=1}^{n}x_{2(i)}(y_i - a - b_1x_{1(i)} - b_2x_{2(i)}) = 0 \tag{3.30}$$

$$\begin{bmatrix} n & \sum x_1 & \sum x_2 \\ \sum x_1 & \sum x_1^2 & \sum x_1x_2 \\ \sum x_2 & \sum x_1x_2 & \sum x_1^2 \end{bmatrix} \begin{bmatrix} a \\ b_1 \\ b_2 \end{bmatrix} = \begin{bmatrix} \sum y_i \\ \sum x_{1(i)}y_i \\ \sum x_{2(i)}y_i \end{bmatrix} \tag{3.31}$$

3.1.3.3 Polynomial regression

As with the two previous models, polynomial regression also relies on least squares regression. Simple and multiple linear regressions only determine relationships between two or more variables by plotting them in a straight line. However, most relationships, particularly in the climate and hydrological regimes, normally non-linear correlations. The typical form of polynomial regression consists of different powers of independent

variables (x). If the equation has only independent variables with degree powers of 1, it will be multiple linear regression; non-linear regression is generated by degrees higher than one. Equation 3.32 shows the general form of polynomial regression.

$$\hat{y} = a + b_1 x_i + b_2 x_i^2 + b_3 x_i^3 + ... + b_p x_i^p \tag{3.32}$$

Polynomial regression also uses the sum of squares error method to search for the best coefficients of a and b. The processes to solve for coefficients of independent variables and interception are similar to multiple linear regression, expect for the degree powers of independent variables. Chen (2014) provided an example of the matrix of two degree polynomial equations as in Equation 3.33 to 3.37.

$$\sum_{i=1}^{n}(e_i)^2 = \sum_{i=1}^{n}(y_i - (a + b_1 x_i + b_2 x_i^2))^2 \tag{3.33}$$

$$[\partial \sum_{i=1}^{n}(y_i - (a + b_1 x_i + b_2 x_i^2))^2]/\partial a = -2\sum_{i=1}^{n}(y_i - a - b_1 x_i - b_2 x_i^2) = 0 \tag{3.34}$$

$$[\partial \sum_{i=1}^{n}(y_i - (a + b_1 x_i + b_2 x_i^2))^2]/\partial b_1 = -2\sum_{i=1}^{n} x_i(y_i - a - b_1 x_i - b_2 x_i^2) = 0 \tag{3.35}$$

$$[\partial \sum_{i=1}^{n}(y_i - (a + b_1 x_i + b_2 x_i^2))^2]/\partial b_2 = -2\sum_{i=1}^{n} x_i^2(y_i - a - b_1 x_i - b_2 x_i^2) = 0 \tag{3.36}$$

$$\begin{bmatrix} n & \sum x_1 & \sum x_i^2 \\ \sum x_i & \sum x_i^2 & \sum x_i^3 \\ \sum x_i^2 & \sum x_i^3 & \sum x_i^4 \end{bmatrix} \begin{bmatrix} a \\ b_1 \\ b_2 \end{bmatrix} = \begin{bmatrix} \sum y_i \\ \sum x_i y_i \\ \sum x_i^2 y_i \end{bmatrix} \tag{3.37}$$

3.1.3.4 Stepwise regression

Stepwise regression is a statistical method to find suitable candidate independent variables and exclude the unsuitable, so only the set of predictors showing high predictive ability remains. This method is likely the practical for selecting suitable predictors for the simulation (Wang et al., 2009). It can also reduce statistically significant intercorrelation between predictors (McCuen et al., 1979). There are two main types of stepwise regression: forward and backward selections. Forward stepwise regression starts with no

candidate variables in the model, then variable are added individually according to the values of specific criteria. Backward stepwise regression begins with all the predictor variables in the model, then the least significant predictor is discarded for each calculation until only significant variables remain.

a) Forward stepwise regression: No predictor variable is considered when forward stepwise regression is first applied. Thus, the prediction ($\hat{y}$) at the first step is equal to the sample mean of the predictand data set, and only the intercept term is in the equation 3.38.

$$\hat{y} = b_0 \tag{3.38}$$

Each candidate variable is then added in Equation 3.38 one at a time, and if there are K variables, K equations need to be constructed and tested. The predictor, its coefficient and new intercept value showing the highest values of the coefficient of determination (R^2), the smallest mean square error (MSE) and the largest F ratio are applied, as in Equation 3.39. In this equation, x_1 is the predictor which meets those criteria.

$$\hat{y} = b_0 + b_1 x_1 \tag{3.39}$$

The remaining independent variables ($K - 1$) are then added to Equation 3.39 to determine the next best predictor. The same criteria are calculated for each $K - 1$ regression, and the best remaining predictor (x_2) is added in the model, as shown in Equation 3.40.

$$\hat{y} = b_0 + b_1 x_1 + b_2 x_2 \tag{3.40}$$

The next steps follow this pattern until all predictors are tested. One variable is added to the previous equation each time, and all regression coefficients and intercept terms change.

b) Backward stepwise regression: In contrast, backward stepwise regression typically begins with all the independent variables, and every K variable is forced into the model with their coefficients and the intercept terms of the regression. The

independent variables are discarded individually, and the three criteria are calculated. The variable with the smallest R^2 and F ratio and the largest MSE is then removed from the equation, and a new equation is generated with different variable coefficients and the intercept terms. Equation 3.41 is the initial stage of the backward stepwise regression, and Equation 3.42 is the difference after removing one variable.

$$\hat{y} = b_0 + b_1 x_1 + b_2 x_2 + ...b_k x_k \tag{3.41}$$

$$\hat{y} = b_0 + b_1 x_1 + b_2 x_2 + ...b_{k-1} x_{k-1} \tag{3.42}$$

Wilks (2011) suggested that backward stepwise regression might not be practical with regressions containing fewer observations than the number of variables ($n < K$), since the data could include redundant and useless information. The criteria for estimating regression equations generated by stepwise regression are explained in the following section.

c) Criteria for stepwise regression estimation: Three criteria are commonly used to estimate potential predictors in stepwise regression: R^2, mean square error (MSE) and F ratio. This section only discusses the last two, as R^2 is described in the forecast verification section.

- **Mean square error (MSE):** This is the square of the difference between each pair of observations and predictions, as shown Equation 3.43. The square of MSE leads to the possibility of large errors, particularly if the data sets contain outliers. A perfect forecast has an MSE of zero; a higher MSE indicates a model is less efficient.

$$MSE = 1/n \sum_{i=1}^{n} (\hat{y}_i - y_i)^2 \tag{3.43}$$

- **F ratio:** This is the ratio of mean square regression (MSR) and MSE, as shown in Equation 3.44; the ratio can be calculated with Equation 3.45. A higher F ratio refers to better performance of the regression line to explain the variance of observations with small errors between observations and predictions.

$$MSR = SSR/k = [\sum_{i=1}^{n}(\hat{y}_i - \bar{y})]/k \tag{3.44}$$

$$F_{ratio} = MSR/MSE \tag{3.45}$$

If no threshold is defined for stopping the stepwise regression process, both forward and backward stepwise regression will continue (i.e. add and eliminate candidate predictors) until all the predictors have been considered. Therefore, specific values of R^2, F ratio or MSE should be defined.

3.1.4 Bayesian model averaging

Bayesian model averaging (BMA) is a recent statistical method used for ensemble multi-model forecasting. It allows a user to generate the posterior distribution of variables of interest by assigning a weight to individual posterior distributions. The technique is based on the framework of Bayesian data analysis, and can account for uncertainty persistence in model selection by allocating higher weight to better predictions (Liang et al., 2013; Wang et al., 2012). Madigan and Raftery (1994) compared the predictive performance of the model averaging approach to rational selection of a single model, and found higher forecasting skill in the results generated by the model averaging method. Liang et al. (2013) compared the performance of the simple average method and BMA to combine two hydrological models, and concluded that BMA gave better results and provided more accurate simulation for peak flow events. Examples of the success of BMA in the forecast community can be found in Casanova and Ahrens (2009); Duan et al. (2007); Pokhrel et al. (2013) and Raftery et al. (2005).

3.1.4.1 Bayesian data analysis

Bayesian data analysis, based on Bayes' theory of considering the conditional probabilities of an event of interest, allows a user to infer the parameter values given the observed data. A user can also assign different credibility across parameters when there is new information available (Kruschke et al., 2012). Unlike the frequentist approach, Bayesian analysis can develop the posterior distribution of variables calculated from all parameter spaces. Frequentist statistics produce only the point estimation of the maximum likelihood approach, and provide a set of data with no distributional information.

Bayesian data analysis consists of three main keys: the likelihood function, the prior probability and the evidence. The mathematical function of Bayesian theory is shown in Equation 3.46. $p(X|\Theta)$ is the likelihood function referring to the probability of observed data, given a vector of parameter Θ. $p(\Theta)$ is the prior probability of parameter Θ, indicating the current knowledge of parameters. Different credibility regarding the prior knowledge of a user can be quantified to each parameter (Kruschke et al., 2012). Finally, the evidence $p(X)$ is the marginal likelihood that can be computed by an integral over the parameter space; Equation 3.47 is applied to calculate the evidence. If there are a large number of parameters in the parameter space, difficulty of integration over all parameters will arise. Therefore, the Markov chain Monte Carlo (MCMC) approach becomes an important key, as it can generate random samples without integrating all parameters.

$$p(\Theta|X) = p(X|\Theta)p(\Theta)/p(X) \tag{3.46}$$

$$p(X) = \int p(D|\Theta)p(\Theta)d(\Theta) \tag{3.47}$$

3.1.4.2 Bayesian model averaging technique

Bayesian model averaging provides a coherent way combining the predictions of several models based on their credibility. The final output of BMA is an average of the posterior distributions of all models considered weighted by their posterior probability, as shown in Equation 3.48. Equation 3.48 and 3.49 will apply only if all the models have the same structure. In this work the candidate models are linear regression models with different numbers of predictors; in order to have the same structure, the length of parameter vector (θ) will be the size of the pool of potential predictors. When a predictor is not included, the corresponding coefficient in θ is constrained to be zero. $p(\Theta|y, X)$ is the posterior distribution of parameter (Θ) given the observed data set (y) and predictor data X calculated from all models. $p(\Theta|M_k, y, X)$ is the posterior distribution of Θ given the model M_k , the observed data y and the predictor X. M is the model space (M_1, M_2, ..., M_k) which is the combinations of predictors. The posterior model probability, $p(M_k|X, y)$, sometimes called the model weight (wi) is the probability of each model's performance, given the data X and all w_i (i=1,2,,k) add up to a total of 1. A weight average ($p(M_k|X, y)$) can be estimated using Equation 3.49.

$$p(\Theta|y,X) = \sum_{k=1}^{K} p(\Theta|M_k,y,X)p(M_k|X,y) \tag{3.48}$$

$$p(M_k|X,y) = p(y|M_k,X)p(M_k)/p(y|X) = p(y|M_k,X)p(M_k)/\sum_{s=1}^{K} p(y|M_s,X)p(M_s) \tag{3.49}$$

Finally, the posterior mean of the predictand y given X is generated by the summation of all multiplications of the model weight and the expected value of each y_k given observed data and model M_k. The posterior variance is also weighted using the posterior model probability, $p(M_k|X,y)$. Equations 3.50 and 3.51 show the methods used to estimate the mean and variance of posterior probability respectively. The mean value from BMA can be used in the same way as the results of multi-model forecasting, since probabilistic forecasts are developed from several models (Liang et al., 2013).

$$E(y|X) = \sum_{k=0}^{K} y_k p(M_k|X) \tag{3.50}$$

$$Var(y|X) = \sum_{k=0}^{K} (Var(y|X,M_k) + y_k^2)p(M_k|X) - E(y|X)^2 \tag{3.51}$$

3.2 Forecast verification

After all prediction processes are completed, the forecasted outputs are assessed for model performance estimation. Krause et al. (2005) specified the benefits of model evaluation as a) to define a quantitative estimation of model's performance, b) to provide criteria for model improvement by adjusting relevant parameters or modifying the model structure and c) to compare model outputs with those of previous studies. Methods of verification can be categorized by three types of output characteristic: deterministic, categorical and probabilistic data. Regonda et al (2006) identified the important terminologies wildly used for model verification as follows:

"-Accuracy: agreement of forecasts and observations, with few large errors.

-Bias: agreement of the means of observations and forecasts.

-Association: linear relationship between forecasts and observations.

-Skill: forecast accuracy compared to climatology or random chance of observations."

Numerous measurements are used to estimate model performance. The two techniques most widely used to evaluate climate and hydrologic forecasting schemes are R^2 and the Nash-Sutcliffe coefficient (E_f) (Arnold et al., 2012; Krause et al, 2005). Though outputs in this research are deterministic data. Categorical verification is employed to determine variance by dividing forecasted and observed data into three categories; below-normal, normal and above normal.

3.2.1 Coefficient of determination (R^2)

R^2 is traditionally used to measure the fit of a regression equation to observations (O) and model predictions (P). It can determine the proportion of variation of measurement data (O) described or accounted for by the regression. Equation 3.52 shows the general form of R^2.

$$R^2 = [(\sum_{i=1}^{n}(O_i - \bar{O})(P_i - \bar{P}))/(\sqrt{\sum_{i=1}^{n}(O_i - \bar{O})^2})(\sqrt{\sum_{i=1}^{n}(P_i - \bar{P})^2})]^2 \tag{3.52}$$

In a perfect model, R^2 equals one. It is zero for an unsuccessful model, which means there is no variation in the observation that can be explained by the prediction. An example of the difference between successful and unsuccessful models by Wilks (2011) is shown in Figure 3.4. In the figure, y and x are observations and predictions respectively. The scatter is closely aligned with the regression line in Figure 3.4 (a), which represents a good model. However, the scatter in Figure 3.4 (b) is relatively far from the regression line and the line is close to the mean of response variable, which demonstrates the failure of the model to predict y.

The slope and intercepts of regression equations can be considered as the relationships between observations and predictions. The slope represents the relative relationship between (x) and (y), while the intercept indicates the lag between predictions and observations. A slope of one and an intercept of zero define the best model (Moriasi et al., 2007).

Another estimator frequently used to measure the correlation between measured and simulated data based on standard regression is the correlation coefficient (R). This can be calculated by the square root of R^2 , as shown in Equation 3.53. R is used to estimate the degree of linear relationship between two variables, and R^2 indicates the proportion

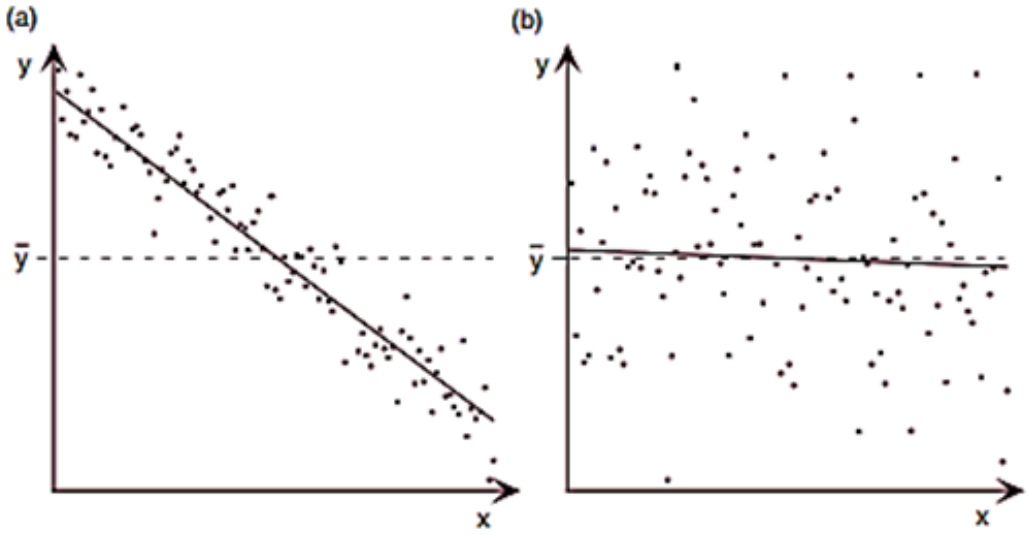

Figure 3.4: A fairly good regression (a) and ineffective model (b) (Wilks, 2011).

of the variance in observation data explained by the model (Moriasi et al., 2007). R ranges from -1 (perfect negative correlation) to 1 (perfect positive correlation).

$$R = \sqrt{R^2} = \sqrt{[(\sum_{i=1}^{n}(O_i - \bar{O})(P_i - \bar{P}))/(\sqrt{\sum_{i=1}^{n}(O_i - \bar{O})^2})(\sqrt{\sum_{i=1}^{n}(P_i - \bar{P})^2})]^2} \quad (3.53)$$

The disadvantages of these two criteria are their sensitivity to outliers, and insensitivity to the proportional difference between observations and predictions respectively. Misleading estimated model performances could occur if the data contains outliers. McCuen et al. (1979) advised against using these two criteria alone. When the total variance is relatively high, errors can be large. This leads to a high value of R even the average error might be large. In addition, these criteria could indicate high agreement even if there are a large proportional difference between simulations and measure data (Moriasi et al, 2007). Wilks (2011) showed an example of completely different scatter plots between x and y, all with the same regression relationship and correlation coefficient in Figure 3.5 .

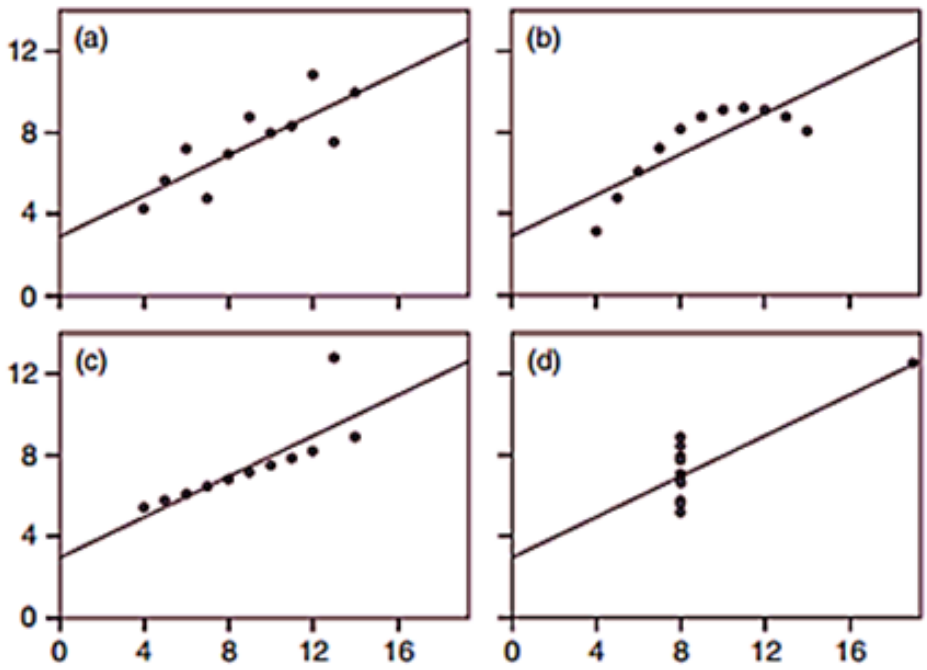

Figure 3.5: Examples of different scatter plots with the same regression line (Wilks, 1995).

3.2.2 The Nash-Sutcliffe coefficient ($\mathbf{E}_f$)

The Nash-Sutcliffe coefficient (E_f), first proposed by Nash and Sutcliffe in 1970, is an alternative method of evaluating model performance. It is used to determine the relative magnitude of the residual variance and the observation variance (Moriasi et al, 2007). E_f can be determined by computing the ratio of the sum of square error of observations and predictions, and variance of the observations. Then, this ratio is subtracted with 1 (Gupta et al, 2009). Equation 3.54 shows the formula to compute E_f. The range of E_f starts from -$\propto$ to 1, with 1 being the perfect model. An E_f equal or less than 0 indicates that the mean of observations should be used, rather than the simulated data (Moriasi et al, 2007). Lian et al. (2007) indicated that a model can be evaluated as satisfactory if the E_f value is 0.36 to 0.75, and evaluated as good if the value is above 0.75.

$$E_f = 1 - [(\sum_{i=1}^{n}(\hat{y}_i - y_i)^2)/(\sum_{i=1}^{n}(y_i - \bar{y})^2)] \tag{3.54}$$

Though, there is little to no difference between R^2 and $E_f$in simple regression models, the difference can be seen with more complex models, such as multiple linear or polynomial regressions. The disadvantage of E_f is related to the variance of the observation data. For example, if two simulated results for two watersheds showing the same systematic errors compared to their observations for an entire period are evaluated using E_f, over- or under- estimation could occur, depending on the variation of the measured data.

To define the acceptable model for calibration, Santhi et al. (2001), Akiner and Akkoyunlu (2012) indicated that E_f and R^2 should be higher than 0.5 and 0.6 respectively.

3.2.3 Hit score (H)

The two previous criteria are suitable for evaluating model performance with continuous data. However, they both have drawbacks, as they rely on the variance of measured data and outliers which could lead to incorrect conclusions of a model's performance. Therefore, this study evaluates model performance with the other option, by converting continuous data to categorical data and using a common statistical tool, the Hit score (H) as an estimator. This is accomplished by considering each individual value of continuous variables that fall into a categorical set of data. Categorical data sets can be displayed in an IXJ contingency table, the simplest being 2X2, which manages four combinations of

events for each pair of forecasted and observed data. If the simulated and measured data are classified by three categories (e.g. normal, below-normal and above-normal), this contingency table will consist of nine combinations of events (Figure 3.6). The letters in the tables represent the value of forecasts and observations in the same category. Thus, the perfect model will zero for b and c in Figure 3.6 (a) and for s, t, u, a and y in Figure 3.6 (b).

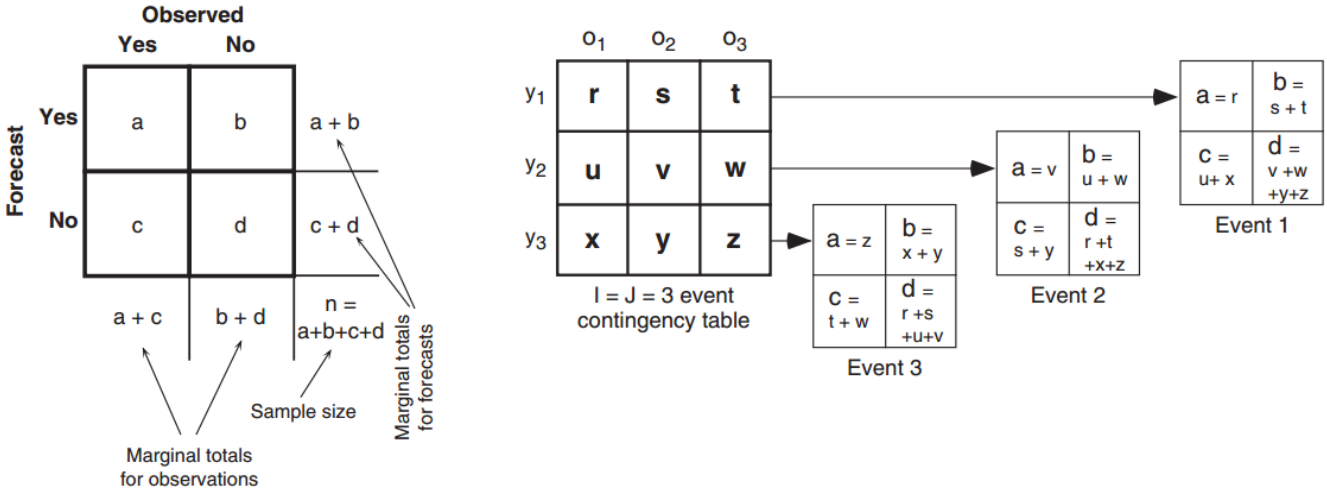

Figure 3.6: 2x2 and 3x3 contingency tables (Wilks,2011).

Equations 3.55 and 3.56 are used to calculate H for 2x2 and 3x3 contingency tables respectively. With this type of measurement, the properties of the prediction and observation data (e.g. mean and variance) are not involved for assessment, as it only measures the number of both data that fall into the same section. If H is a high percentage, it means that the predictions correspond well to the observations, whereas a low value indicates relatively low model performance. H ranges between 0 and 100%.

$$H = [(a + d)/n] * 100 \tag{3.55}$$

$$h = [(r + v + z)/n] * 100 \tag{3.56}$$

3.2.4 Cross validation method

The cross validation method is an approach to arranging data by dividing it into two sections and using both data sets as training and testing data. Using the cross validation method can decrease overestimation in simulations, since the data sets used to generate outputs are removed from those used to construct an empirical equation. There are three main methods for cross validation; the k-fold cross validation, leave-one-out cross validation, and repeated k-fold cross validation. The k-fold cross validation method divides all available data into k sized segments. The data of k-1 sections are used in the training data set, and the remaining sections are used in the testing data set. The process repeats until all sections of data represent both training and testing data sets. Leave-one-out cross validation follows a process similar to k-fold cross validation, but k in this process is equal to the number of observations; Figure 3.7 illustrates the leave-one-out cross validation method. Repeated k-fold cross validation repeats the process of k-fold validation, but reshuffles the data before each new simulation (Refaeilzadeh et al., 2008).

1st	Testing set	Training set	Training set	Training set	Training set
2nd	Training set	Testing set	Training set	Training set	Training set
3rd	Training set	Training set	Testing set	Training set	Training set
4th	Training set	Training set	Training set	Testing set	Training set
5th	Training set	Training set	Training set	Training set	Testing set

Figure 3.7: Leave one out cross validation procedure

3.3 Rainfall-runoff modelling

The limitations of techniques for measuring the significant parameters that are important for understanding hydrological processes in a particular area are the main reason to expand the use of rainfall-runoff modeling for hydrological scheme (Beven, 2012; Seibert, 1999). In addition, some current measurement techniques might provide unsatisfactory results in terms of space and time, particularly in areas without gauge stations. Thus, rainfall-runoff modelling is an effective alternative. It can help predict future events,

thereby allowing decision makers to prepare for hydrologic problems by proactively implementing measures such as, water resource management and flood protection (Beven , 2012).

3.3.1 Definition of rainfall-runoff modelling

Rainfall-runoff modeling is a mathematical model used to convert rainfall amounts into runoff hydrograph, with or without considering the physical processes in a given watershed or drainage area. Several definitions of rainfall-runoff modeling in the literatures were complied by Dzubakova (2010). The simplest definition was defined by Moradkhani and Sorooshian (2009), who stated that rainfall-runoff modeling is a tool to represent the reality of the world system. Wainwright and Mulligan (2004) and Huggett (1980) added more details to complexity of model. They defined that the model should convert the complexity of a system to the simplest way to understand it, and the best model should have minimal parameters. Black et al. (2011) focused on user requirements, and concluded that best practice modeling should meet users' main objectives of by developing and implementing methods for all applications in the model.

3.3.2 Rainfall-runoff model classification

Rainfall-runoff models can be classified into a variety of categories, depending on their characteristics. If models are classified by the complexity of their mechanisms, they can generally be divided into three categories. Or, if models are classified by the type of model mathematics, they can be classified into two classes. Details of the model classification are follow:

3.3.2.1 Model classification by complexity

- **Empirical models:** The simplest type of rainfall-runoff modeling is the empirical model, also known as the black box or metric model (Dzubakova, 2010). This model is based on simple equations typically constructed from observed data, normally applies regression relationships to fit the equations (Vaze et al., 2012). Vaze et al. (2012) also indicated that predictors commonly used for empirical models are rainfall, evapotranspiration, ground water level and observed flows from nearby stations. Empirical models do not consider to physical processes in the catchment, and treat the watershed as single units. Thus, a physically complex watershed

(e.g. slope and soil variations) might not be suitable for this type of model. In addition, empirical equations generated in one watershed should not be applied to other basins with different characteristics, since the equations were constructed from the measured data in a specific area.

- **Conceptual models:** Conceptual rainfall-runoff models generally consider water storage in a catchment, such as ground water, or the water storing in soil and vegetation. These models use mathematical equations governing the storage types, and their complexity ranges from simple mass balance equations to the complex non-linear partial differential equations (Beven, 2012). Most conceptual models consider the basin as a lump area and treat all physical variables the same across the watershed (Vaze et al., 2012). Since these models are physical based, there could be some parameters that cannot be measured, but still necessary. In theses case, the calibration process might be the best way to obtain these parameters. Examples for rainfall-runoff conceptual models are IHACRES and SIMHYD (Whyte et al., 2011; Ye et al., 1997) .

- **Physically based model** This type of rainfall-runoff modeling focuses on understanding all the physical parameters related to a hydrologic cycle. Physically based models divide a catchment into sub-catchments or grid cells. The values of the parameters in the same grid cell are the same for the entire grid, and they are different from others due to the disparities in the physical characteristics of the segments. These models can explain watershed behavior in detail, but they can be difficult to use since a large number of parameters must be forced to the models. Examples of physically based model are the Systeme Hydrologique Europeen: SHE model and the Soil and Water Assessment Tool (SWAT) (Feyen et al., 2000; White et al., 2011).

3.3.2.2 Spatial classification

Each rainfall-runoff model treats the catchment area differently, and they can be divided into two classes; single unit and spatial discretization. The single unit (lumped) model considers the entire catchment as a homogeneous area. All physical characteristics are assumed to be equal for the entire watershed, and the spatial variability of parameters is disregarded. The lumped model can generate river flows only at the outlet of the main basin. The distributed model (the spatial discretization model) partitions a basin into smaller sections according to previously defined criteria, and all variables in the

catchment vary spatially. Each sub-basin or segment has specific inputs, outputs and individual parameter values, all of which are different from other sub-basins.

3.3.2.3 Randomness of the output

Rainfall-runoff models can also be categorized by considering the type of the output. The deterministic type always produce the same outputs whenever the same sets of inputs are forced in the models, because the model algorithms are fixed and no random processes are involved. Stochastic models refer to various sets of output, even if the same data sets are introduced as input layers. This type of model randomly generates relevant parameters in the models.

3.3.3 Soil and Water Assessment Tool (SWAT)

Algorithms, parameters and variables used in the Soil and Water Assessment Tool (SWAT) are briefly discussed here; more details can be found in Neitsch et al. (2011). SWAT was first developed at the USDA Agriculture Research Service. It allows users to simulate physical processes (e.g. water and sediment movement, nutrient cycles, management practices) in complex basins with high variation in soil, land use and geography.

SWAT uses the water balance equation as the governing term as shown in Equation 3.57. Only the main equations of each variable in the water balance equation are considered in the following sections.

$$SW_t = SW_0 + \sum_{i=1}^{n}(R_{day} - Q_{surf} - E_a - W_{seep} - Q_{gw}) \tag{3.57}$$

SW_t and SW_0 are the water content in the soil on the final day t and the initial water content in the soil on day i (mm H_2O). R_{day} is the amount of precipitation on day i (mm H_2O). Q_{surf} is the surface runoff on day i (mm H_2O). E_a is the amount of evapotranspiration on day i (mm H_2O). W_{seep} and Q_{gw} are the amount of water exiting the bottom of the soil profile on day i and the amount of the return flow on day i (mm H_2O).

3.3.3.1 Precipitation

Measured precipitation is a required input for SWAT. Neitsch et al (2011) suggested that measured precipitation in any period is a key to improve stream hydrograph simulation. However, if there is no available precipitation or the input file is incomplete, SWAT can use the WXGEN weather generator to address missing values in the input data. Since precipitation affects relative humidity, solar radiation and temperature, the weather generator initially develops daily precipitation or fills the gaps of missing data. The distribution of generated precipitation is then used to simulate minimum and maximum temperatures, relative humidity and solar radiation.

At the first stage, a wet or dry day is defined using the first-order Markov-chain model, which assesses the probability of rain event on a given day by referring to dry or wet episodes on the previous day. Users provide the probabilities of a wet day occurring after a wet day (P_i (W/W)) and after a dry day (P_i (W/D)) for each month of the year. SWAT then generates a random number between 0.1-1.0 for all days, which is then compared to the probability defined in the preceding step. If the random number of a given day is lower value than the wet-dry probability, that day is considered a rainy day and vice versa. The amount of precipitation on a given wet day is then calculated using either the skewed distribution or the exponential distribution.

3.3.3.2 Surface runoff

Surface runoff occurs when soil has reached its limit of infiltration, and the excess precipitation flows over the surface. SWAT has two options to address surface runoff simulation; the SCS curve number method and the Green & Ampt infiltration method.

- **SCS curve number method:** This method focuses on the amount of runoff according to land use zones and soil types. Three main variables are required for this surface runoff calculation (Q_{surf},(mm H_2O), which are the amount of rainfall (R_{day},(mm H_2O)) on a given day, the initial abstraction before a runoff event (I_a, (mm H_2O)) and the retention parameter (S,(mm H_2O)). Equation 3.58 shows the formula used for runoff calculation.

$$Q_{surf} = [(R_{day} - I_a)^2]/[(R_{day} - I_a + S)] \tag{3.58}$$

  The initial abstraction is usually obtained by multiplying the retention parameter (S) by 0.2. The value of S varies according to the characteristics of the soil, land

use and management practices. The SCS curve number (CN) is defined using the difference of soil hydrologic groups, the antecedent soil moisture condition, land use and land cover. Equation 3.59 shows the method to calculate the retention parameter (in mm).

$$S = ((25,400/CN) - 254) \tag{3.59}$$

The range of CN is 40 to 100. Figure 3.8 illustrates the relationship between the amount of rainfall, runoff and CN. The final equation for runoff calculation after applying 0.2S in the Equation 3.58 is showed in Equation 3.60.

$$Q_{surf} = [(R_{day} - 0.2S)^2]/[(R_{day} + 0.8S)] \tag{3.60}$$

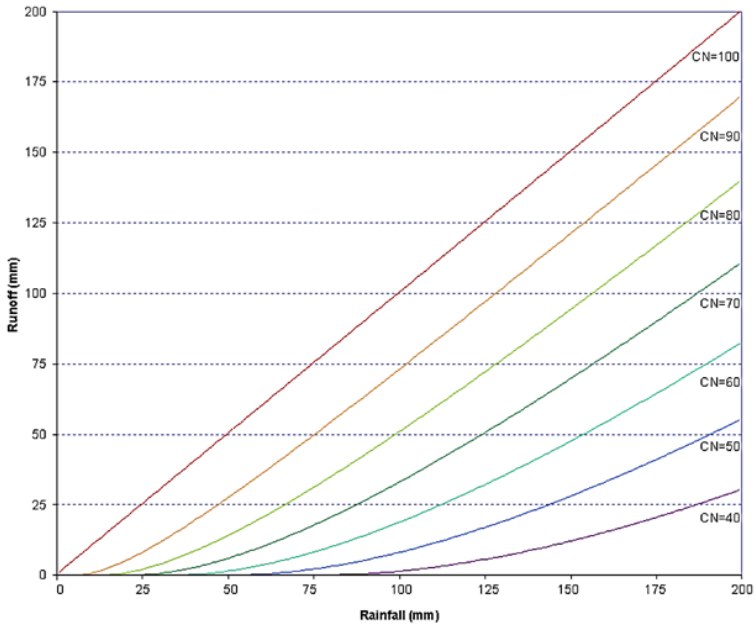

Figure 3.8: Relationship between rainfall, runoff and CN (Neitsch et al. (2011))

- **Green & Ampt infiltration method** The Green & Ampt infiltration method is the other SWAT surface runoff simulation option. It assumes a homogeneous soil profile and uniform antecedent moisture. To apply this method, sub-daily precipitation must be input into SWAT. At each time step, SWAT uses the method

to calculate the water infiltrating the soil and the water excess is considered as surface runoff. The infiltration rate is acquired by Equation 3.61.

$$f_{int,t} = K_e[1 + ((\Psi_{wf}.\Delta\Theta_v)/F_{inf,t})] \tag{3.61}$$

where $f_{int,t}$ is the infiltration rate at time t (mm H_2O). K_e is the Green & Ampt effective hydraulic conductivity (mm/hr), which can be found using the saturated hydraulic conductivity of the soil and the curve number value (Equation 3.62).

$$K_e = [((56.82)K_{sat}^{0.286})/((1 + 0.051)exp(0.062 * CN))] - 2 \tag{3.62}$$

$F_{inf,t}$ is the cumulative amount of water entering to the soil at time t (mm H_2O). It is found by computing the amount of cumulative infiltration prior to time t and the amount of rainfall during the time step ($R_{\Delta t}$) (mm H_2O), as shown in Equation 3.63.

$$F_{inf,t} = F_{inf,t-1} + R_{\Delta t} \tag{3.63}$$

Ψ_{wf} and $\Delta\Theta_v$ is the wetting front matrix potential and the change in the amount of water across the wetting front area respectively. Ψ_{wf} depends on the soil type (i.e. the percentage of clay and sand content, m_c and m_s respectively) and the soil permeability ($\oslash_{soil}$). Equation 3.64 and 3.65 indicate formulae used to compute Ψ_{wf} and $\Delta\Theta_v$.

$$\Psi_{wf} = (10)exp\begin{bmatrix} 6.5309 - 7.32561(\oslash_{soil}) & +0.001583(m_c^2) \\ +3.809479(\oslash_{soil}^2) & +0.000344(m_s)(m_c) \\ -0.049837(m_s)(\oslash_{soil} & +0.001608(m_s^2)(\oslash_{soil}^2) \\ +0.001602(m_c^2)(\oslash_{soil}^2) & -0.0000136(m_s^2)(m_c) \\ -0.003479(m_c^2)(\oslash_{soil}) & -0.000799(m_s^2)(\oslash_{soil} \end{bmatrix} \tag{3.64}$$

$$\Delta\Theta_v = (1 - (SW/FC) * (0.95 * \oslash_{soil})) \tag{3.65}$$

SW is the amount of water in the soil profile subtracted from the soil water at wilting point (mm H_2O). FC is the soil water content in the soil profile at field capacity.

The peak runoff rate and the time of concentration is also determined by SWAT. Information about these two variables can be found in (Neitsch et al (2011)).

3.3.3.3 Evapotranspiration

Evapotranspiration is the process of water evaporation from the ground and vegetation, and it is the main mechanism that removes water from a basin. Neitsch et al (2011) found that approximately 62% of precipitation is removed from the watershed by evapotranspiration. Two main hydrological variables, potential evapotranspiration and actual evapotranspiration, are explained in the following section.

a) Potential evapotranspiration: potential evapotranspiration (PET) is the maximum amount of water that could be removed from the watershed by both evaporation and transpiration processes. SWAT has three options for this: the Penman-Monteith, Priestley-Taylor and Hargreaves methods.

- **The Penman-Monteith method:** this method requires solar radiation, air temperature, relative humidity and wind speed data. It can be partitioned into two main terms: the effect of available radiation and the interaction between surface and atmosphere (Pereira, 2004). Equation 3.66 presents this method.

$$\lambda E = [\Delta.(H_{net} - G) + \rho_{air}.C_p.((e_z^0 - e_z)/r_a)]/\Delta + \gamma.(1 + (r_c/r_a)) \quad (3.66)$$

  where λ is the latent heat flux density (MJ m^{-2} d^{-1}). E is the evaporation rate in depth (mm $d^{-}1$). Δ is the slope of the curve between the saturation vapor pressure and the air temperature (kPa C^{-1}). H_{net} and G are the net radiation and the soil heat flux density respectively (MJ m^{-2} d^{-1}). ρ_{air} is the air density (kg m^{-3}). c_p is the specific of air at constant pressure (MJ kg^{-1} C^{-1}). e_z^0 and e_z are the saturation vapor pressure and the ambient water vapor pressure at height z respectively (kPa). γ is the psychrometric constant (kPa C^{-1}).r$_c$ and r_a are the canopy resistance to water vapor transfer and the aerodynamic resistance respectively (s m^{-1}).

- **The Priestley-Taylor method:** this method is specifically applied when the surface area in the catchment is wet. It defines the coefficient (α_{pet} = 1.28) to multiply with the term of energy component, and does not accounted for changes in low advection conditions. Thus, it could give an error if it is used in an area with a significant advection component. The equation is presented in Equation 3.67, in which λ is the latent heat of vaporization (MJ kg^{-1}) and E_0 is the potential evapotranspiration on a given day (mm d^{-1}).

$$\lambda E_0 = \alpha_{pet}.(\Delta/(\Delta+\gamma)).(H_{net} - G) \tag{3.67}$$

- **The Hargreaves method:** this method requires only maximum and minimum temperatures (T_{mx} and T_{mn},C) as shown in Equation 3.68. Therefore, it is useful for a location lacking other climate variables, such as wind speed and humidity. H_0 is the extraterrestrial radiation (MJ m^{-2} d^{-1}) and $\bar{T}_{av}$ is the average temperature (C).

$$\lambda E_0 = 0.0023.H_0.(T_{mx} - T_{mn})^{0.5}.(\bar{T}_{av} + 17.8) \tag{3.68}$$

b) Actual evapotranspiration: the potential evapotranspiration calculated in the previous step is used to calculate the actual evapotranspiration. SWAT begins by computing the actual evapotranspiration, considering the evaporation intercepted by the vegetation. Then, the amount of water removed by plant transpiration is determined. If there is snow in the catchment, the amount of sublimation is also calculated, otherwise the evaporation from soil is directly computed. This study only focuses on the evaporation from soil.

- **Evaporation of intercept rainfall:** this actual evaporation is calculated from the amount of water held in the vegetation canopy of the watershed. The final amount of water held in the canopy on a given day ($R_{int(f)}$) is computed by subtracting the initial amount of water held in the vegetation ($R_{int(i)}$) from the amount of water that evaporated from the canopy on a given day (E_{can}). The units of these variables are mmH_2O and Equation 3.69 is the equation of intercept rainfall evaporation. The amount of water remaining in the canopy after this evaporation process ($E_0^{'}$) is adjusted by transpiration and sublimation, or evaporation from the soil (Equation 3.70).

$$R_{int(f)} = R_{int(i)} - E_{can} \tag{3.69}$$

$$E_0^{'} = E_0 - E_{can} \tag{3.70}$$

- **Transpiration:** this calculation is used only for The Priestley-Taylor and Hargreaves methods. SWAT combines the transpiration calculation with the Penman-Monteith method (details in Neitsch et al (2011)). The estimation of transpiration is shown in Equation 3.71 and 3.72 where E_t and $E_0^{'}$ are the maximum transpiration on a given day, and the potential evapotranspiration modified for evaporation of free water in the canopy (mmH_2O). LAI is the index of leaf area.

$$E_t = [E_0^{'}(LAI)]/3.0; 0 \leq LAI \leq 3.0 \tag{3.71}$$

$$E_t = E_0^{'}; LAI > 3.0 \tag{3.72}$$

- **Evaporation from soil:** The sublimation and soil evaporation is impacted by the degree of shading in the area. The maximum amount of this evaporation on a given day (E_s, mmH_2O) can be calculated using Equation 3.73, where E_0' is the potential evapotranspiration modified for evaporation of free water in the canopy (mmH_2O) and cov_{sol} (Equation 3.74) is the index of soil cover in the area where cv is the biomass and residue on the ground (kg ha^{-1}).

$$E_s = E_0'.cov_{sol} \tag{3.73}$$

$$cov_{sol} = exp(-5.0x10^{-5}.cv) \tag{3.74}$$

Then, SWAT calculates the evaporative demand between the different layers of the soil ($E_{soil,z}$) using Equation 3.75 where z is the depth from the soil surface.

$$E_{soil,z} = (E_s^{''})[z/(z + exp(2.374 - 0.00713.z))] \tag{3.75}$$

3.3.3.4 The amount of water exiting the bottom of soil profile (W_{seep})

The other process that reduces the amount of water from the hydrologic cycle in the watershed is the movement of water out from the bottom of the soil profile. This reduction is specifically related to the soil characteristics of each area. The amount of water exiting the lowest layer of the soil (W_{seep}) is the total of the water quantity coming out

from the lowest layer ($W_{perc,ly=n}$) and the bypass flow at the bottom of the soil ($W_{crk,btm}$) as shown in Equation 3.76.

$$W_{seep} = W_{perc,ly=n} + W_{crk,btm} \tag{3.76}$$

The amount of water that percolates from the soil layer ($W_{perc,ly}$) relies on the water volume on a given day ($SW_{ly,excess}$) and the travel time of percolation (TT_{perc}). In addition, the time step is on an hourly scale (Δt). Equation 3.77 shows the equation for $W_{perc,ly}$.

$$W_{perc,ly} = (SW_{ly,excess})[1 - exp((-\Delta t)/TT_{perc})] \tag{3.77}$$

The water available to percolate to the next layer is determined when the amount of water in layer (SW_{ly})exceeds the volume of water content at field capacity of the layer (FC_{ly}). Thus, there is no water excess for the next layer if the soil is still capable of holding water, as defined in Equation 3.78 and 3.79.

$$SW_{ly,excess} = SW_{ly} - FC_{ly} \tag{3.78}$$

$$SW_{ly,excess} = 0 \tag{3.79}$$

FC_{ly} can be estimated by the total water content at the wilting point (WP_{ly}), which can be calculated using Equation 3.80 and the available water capacity of the soil layer defined by users.

$$WP_{ly} = (0.40)[(m_c \rho_b)/100] \tag{3.80}$$

Where ρ_b is the bulk density (i.e. the fraction of the solid mass to the total volume of air, water and solids, Mg m^{-3}). m_b is the particle density, which is defined as a constant of 2.65 Mg m^{-3}.

The percolation travel time in Equation 3.77 is estimated using Equation 3.81. SAT_{ly} in this equation is the water content when the soil is saturated (mm H_2O), and K_{sat} is the hydraulic conductivity of the saturated soil (mm h^{-1}).

$$TT_{perc} = (SAT_{ly} - FC_{ly})/K_{sat} \tag{3.81}$$

The bypass flow at the bottom of the soil (W_crk, btm) in Equation 3.76 is estimated using Equation 3.82. This variable relies on the formation of crakes (crk) in the soil,

which can be determined by the total crack volume in the soil profile on a given day, expressed as (mm). The methods to calculate the crack volume depend on the layer of soil profile, and the water content in the soil compared to the soil water at field capacity.

$$W_{crk,btm} = (0.5)(crk)(crk_{ly=nn}/depth_{ly=nn}) \tag{3.82}$$

The initial crack volume (crk_ly, i) (mm) can be calculated using Equation 3.83, and the maximum crack volume $(crk_{max,ly})$ (mm) by using Equation 3.84 with the coefficient of crack flow at 0.10. crk_{max} in Equation 3.84 is the potential crack volume estimated as a fraction of the total volume; this parameter must be prepared by users. $z_{l,ly}$ and $depth_{ly}$ are the depth from the surface to the bottom of the soil layer and the depth of the soil layer (mm) respectively.

$$crk_{ly,i} = (crk_{max,ly})[(coef_{crk}.FC_{iy}.SW_{ly})/(coef_{crk}.FC_{iy})] \tag{3.83}$$

$$crk_{max,ly} = (0.916)crk_{max}.exp[-0.0012.z_{l,ly}].depth_{ly} \tag{3.84}$$

If the water content in the soil layer is higher than 90% of the filed capacity on a given day, Equation 3.83 is applied, while Equation 3.85 is used when the soil water is less than 90% of the field capacity. l_{crk} is the lag factor of crack, which is set in SWAT at 0.99. $crk_{ly,d-1}$ is the volume of crack on the previous day (mm).

$$crk_{ly} = (l_{crk})(crk_{ly,d-1}) + (1.0 - l_{crk})(crk_{ly,i}) \tag{3.85}$$

After surface runoff is calculated, water will penetrate the soil. The amount of rainfall excess on a given day is related to the volume of cracks in the soil profile on that day. The initial accumulated rainfall excess will be greater than zero if the volume of surface runoff is higher than the volume of the total crake volume (crk) on the day. Therefore, the amount of water moving to the soil profile is determined by subtracting of the amount of rainfall after interception calculation on a day from the surface runoff on the same day.

3.3.3.5 Groundwater (Q_{gw})

Groundwater (Q_{gw}) is stored in underground aquifers in the saturated zone, the top of which is called the water table. Groundwater is recharged by precipitation that percolates into the aquifers, and is one of many factors that affect streamflow. The area of stream links to the movement of groundwater can increase or decrease the flow. Figure 3.9 shows the relationships between the level of water table and streamflow. Figure 3.9 (a) indicates that a stream receives groundwater, and Figure 3.9 (d) shows how a river gains and loses groundwater instantaneously. Figure 3.9 (c) and (d) illustrates the loss of groundwater.

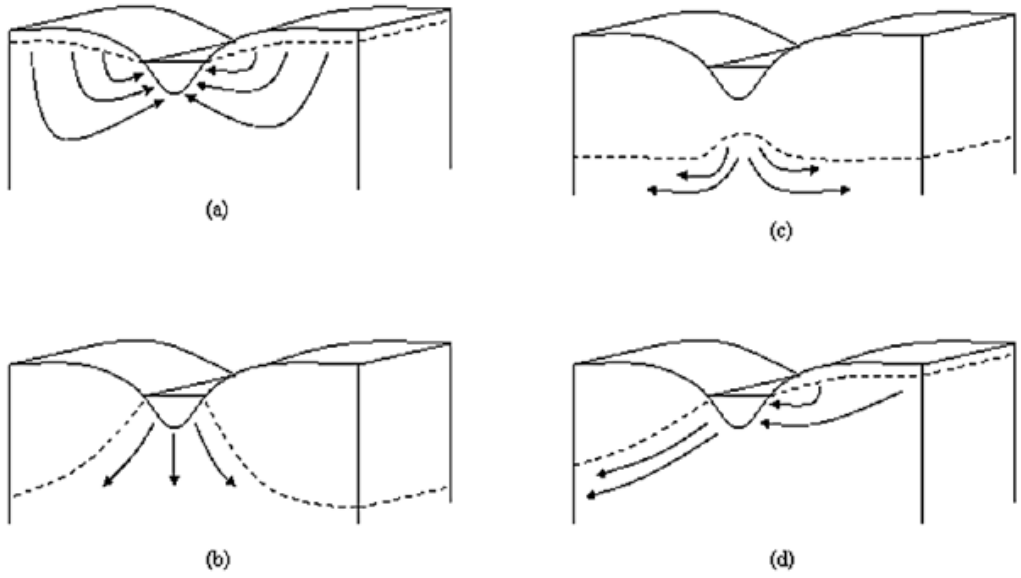

Figure 3.9: The relationships between groundwater and streamflow (Neitsch et al (2011))

Equation 3.86 is used to calculate the groundwater flow. Three variables should be determined first: the hydraulic conductivity of the aquifer (K_{sat}) (mm/day), the height of water table (h_{wtbl}) (m) and the distance from the main stream to the border of the groundwater system (L_{gw}) (m).

$$Q_{gw} = [(8000.K_{sat})/L_{gw}](h_{wtbl}) \tag{3.86}$$

3.4 Economic value of forecasting system

Successful studies of seasonal climate and hydrologic forecasting are common in the forecasting community. However, the research from basic to apply until the potential practical benefits needs to be developed (Meza et al., 2008). In most areas with high climate variability, critical decisions are made by local people and organizations. Seasonal climate predictability combined with local economic information, can increase opportunities for the development of powerful adverse weather risk management strategies, particularly with respect to agriculture. The value of seasonal forecasts includes enhancing farmers' preparedness, and increasing their ability to adapt products for the upcoming season. Forecasting also help decision makers make rational choices to mitigate extreme events, such as flooding or drought. Palmer (2002) stated that the ability to determine climate risks is one of the keys to making reasonable economic decisions. He clarified that decision makers should not only be concerned about abnormal climate, but also the negative social consequences of decreased crop yield, inaccessibility to infrastructure and property damage of extreme weather events.

Forecast value can be defined as the assessment of the state of nature with and without forecasts, combined with other socio-economic information, such as crop price and the cost of preventative and protective actions (Meza et al., 2008). An approach of interest for estimating the potential economic value of forecasts is the cost/lost ratio method, first purposed by Thompson (1952). This simple static method was attractive to hydrologists who want to estimate hydrologic forecasts such as heavy rainfall or flooding events. Lee and Lee (2007) and Murphy (1976) mentioned that the advantage of the cost/lost ratio method was the capability to explain realistic situations, which allows decision makers to generate forecasts with a simple framework.

Palmer (2002) used the cost/loss ratio method to estimate the potential economic value of probabilistic rainfall predictions developed from ensembles of weather and climate prediction systems (EPSs). He showed that increasing both model resolution and ensemble size accounted to forecast values in all cost/loss ratios. Similar to Richardson (2001), he also confirmed that the predictability and frequency of an event was different when the ensemble size of EPSs was changed, which affected the alteration of a user's cost/loss ratio. However, though enhancing forecasting skills was intended to increase overall benefits, this was not always achieved, even when the forecasting skills were more positive (Richardson, 2001). Roulin (2007) also assessed the value of hydrological prediction systems using the framework of cost/loss ratio decision model. He estimated the

value of flood forecasts generated by the IRMB water balance model using the precipitation forecasts, and concluded that the optimum economic value depended on the total cost of actions to prevent damage and the loss amount. Lee and Lee (2007) modified the cost/loss ratio method to profit/loss ratio, by maximizing profit instead of only expenses. They recommended using a decision function and users' subjective reliability for forecasts that affect the continuous level of actions, and the value of profit/loss ratio to calculate the economic value of forecasts. The cost/loss ratio application was also employed to evaluate the economic value of forecast system in Fundel et al. (2013); Murphy (1977); Mylne (2002).

The cost/loss ratio method is based on categorical forecasting focusing on a specific adverse event. In each case, the two simplest approaches are assumed for decision makers: doing nothing or taking action. In addition, the protective action is expected to totally prevent all potential losses. Taking no protective actions regarding an extreme event will cost amount L, while the actions for protection from an event will cost C. The four combinations of events and actions taken, known as the expense matrix, is illustrated in Table 3.1 (Richardson, 2012). If protective actions are taken with or without an adverse event happening, it will cost C. While loss L will only occur if an adverse event takes place without any actions taken.

Table 3.1: Expense matrix of the simple cost/loss decision model (Richardson, 2012)

Action taking	**Event occur YES**	**Event occur NO**
YES	C	C
NO	L	0

Afterward, the assumption of no hydrologic forecasts available for decision makers is set up, and applicable actions taken for each situation are based on the length of the period of occurrence for the events. Only two options are available: always or never taking protective actions (Richardson, 2012). If decision makers chose to always protect, the cost will be C for every event ($E_{always=C}$). The amount of loss from disregarding an adverse event is related to the historical probability of that event occurring. The ratio of how many times an event occurred in the past to all event occurrences is called the climatology base rate (s); the calculation of s is described in the following section. Thus, the amount of loss for each adverse event can be calculated by multiplying the climatology base rate by the loss ($E_{never=sL}$).

In the previous assumption, decision makers only take the length of the long period of observation into account, not the forecasting system. The expense based on climatology ($E_{climate}$) is found by considering the minimum average expense (Equation 3.87).

$$E_{climate} = min(C, sL) \tag{3.87}$$

If a stationary assumption is assumed for the future, the mean expense for taking protective actions can be defined by multiplying C by the climatology base rate ratio ($E_{perfect=sC}$).

Finally, forecast results are assessed by estimating their economic value. The contingency table is required to measure the accuracy of the model to predict hydrologic variables. The extreme event will be defined first, then a number of predictions that are lower and higher than the event are counted and compared to observations. The contingency table is showed in Table 3.2.

Table 3.2: Contingency table for a single extreme event (Richardson, 2012)

Event forecast	**Event observed**		
	Yes	**No**	**Marginal totals**
Yes	a	b	a+b
No	c	d	c+d
Marginal totals	a+c=ns	b+d=n(1-s)	a+b+c+d=n

The base rate of climatology (s) can be computed using Equation 3.88, and the expense based on forecast outputs can be determined by Equation 3.89. Equation 3.90 finds the value of a forecasting system, which is defined by the ratio of the difference of the expense of forecasts and climate, to the difference of the expense of forecast and perfect forecast. If V = 0 the forecasting system has no value, and only climatological information can be used to make decisions. On the other hand, V= 1 refers to a perfect forecast, from which a decision maker can get the most benefit from. Richardson (2001) pointed out that the value of V was not the only influence of the forecasting system, as climatological information and the cost/loss ratio defined by users were also affected.

$$s = (a + c)/n \tag{3.88}$$

$$E_{forecast} = (a/n)C + (b/n)C + (c/n)L \tag{3.89}$$

$$V = (E_{climate} - E_{forecast})/(E_{climate} - E_{perfect}) \tag{3.90}$$

Chapter 4

Study area

The purpose of this chapter is to provide the general characteristics of the Sahel, since seasonal forecasting applications proposed in this study are focus on that area. Information about the Sahel region, such as climate, topography and socio-economy, is discussed in the first section, followed by the behavior of the main watershed in the Sahel, the Niger River basin. Finally, the Sirba basin which was used as the study site to represent the Sahel region, is examined.

4.1 Sahel

The Sahel region is located in the transition zone between the Sahara desert to the north and savannah to the south (14N to 18N). It extends for approximately 5,000 km, from the Atlantic Ocean on the west coast to the Red Sea on the east (Nicholson, 1995). The eight countries located in the Sahel (Figure 4.1); Mauritania, Senegal, Mali, Niger, Chad, the Sudan, Nigeria and Burkina Faso, have a total population of approximately 58 million. The major cities in the region are Dakar and St. Louis in Senegal, Niamey in Niger, Tombouctou in Mali, Ndjamena in Chad, and Khartoum in the Sudan (Nicholson, 1995). The Sahel is known as one of the most vulnerable regions of the world (World Bank, 2013). The main livelihoods of this area are livestock, fishing and agriculture, with millet, sorghum, cowpea, groundnut and cotton being the dominant crops. The optimum farming season is the three to four months with summer rainfall; irrigation is required the rest of the year. Since agriculture is the main livelihood in this region, climate variability can cause problems in terms of both social and economic issues. Kandji et al. (2006) showed that droughts reoccur an average of two every five years, with different levels of

severity. This causes acute uncertainty with respect to agricultural products, and leads to social conflicts over food, security and poverty.

Figure 4.1: The Sahel region (U.N. Office for the Coordination of Humanitarian Affairs, 2013)

4.1.1 Climate characteristics

The Sahel region is a well-known for its significant interannual and interdecadal climate variability, and prolonged periods of sustained drought. The primary climate characteristic is warm and arid most of the year, with a two to four month summer monsoon. There are two general climate zones in the area, arid and semi-arid. From approximately October to June, sub-tropical high pressure and the Harmattan trade winds over northern Africa produce aridity. In contrast, sub-tropical low pressure in the north from July to September, including southern movement of the dry Harmattan trade winds, is strong stimulus for humidity (Nicholson, 1995). Figure 4.2 displays the patterns of wind and pressure over Africa in January and July/August, the dry and wet seasons of the Sahel region respectively.

Brook (2004) contributed more details regarding rainfall incidence in the Sahel. The rainfall gradient of the region is strongly toward the south, and the distribution is approximately 100 to 200 mm in the north and 500 to 600 mm in the south (see Figure 4.3). Local rainfall in the region is mainly due to the West Africa Monsoon (WAM), which

usually occurs from July to September. This WAM inherently consists of two separate monsoons, one week and one strong (UNEP, 2012). Together, these monsoons are capable of producing up to 80 inches of rainfall in western Africa, toward the Ethiopian mountains (Potts et al., 2013). The WAM is generated by interactions between land, oceans and large scale patterns of atmospheric circulation (Messager et al., 2006). The main factor associated with WAM occurrences is the Intertropical Convergence Zone (ITCZ), which is a tropical rain belt resulting from converging tropical airflows from outside the region that generate rising air currents with high moisture content, thereby increasing rainfall events (Folland et al., 1991). Figure 4.4 shows the movement of the ITCZ over the African continent. It moves to 10N around July then shifts southward in January, which causes naturally dry conditions in the Sahel (Nicholson and Grist, 2001; Mohino et al., 2011).

Thiaw and Mo (2005) and Messager et al (2006) suggested that the African easterly jet (AEJ) is another factor driving local rainfall in Sahel. The AEJ consists of low-level flows moving toward southern Africa, while upper-level flows moves easterly. Thiaw and Mo (2005) also indicated that the movement of AEJ to the south is responsible for the dry episodes in the Sahel. Nichoson and Grist (2001) came to the same conclusion in their study, and showed that the location of AEJ could provide information regarding dry or wet seasons in the region. The tropical Atlantic is another source of moisture for the Sahel region. It depends on the convergence of water vapour that evaporated from the southern tropical Atlantic Ocean. However, Klonne (2012) indicated that the most significant moisture source in this area is water flowing across the coast of Guinea.

Even though, the average rainfall in the southern Sahel approaches 600 mm, the loss due to evaporation is still relatively high. Brook (2004) indicated that rainfall of 500 to 600 mm occasionally occurred in the southern Sahel which is approximately similar as the Great Plains of the United States where an agricultural activity is still successful. The rainfall in Sahel is less effective and unreliable because rainfall events are inconsistent. In addition, the soil cannot hold water for plant growth, and the high temperatures most of the year lead to increased evaporation rate. Nicholson (1995) proposed that the high evaporation rate in the area is due to the intensity of incoming solar radiation. Since the Sahel is located in the lower latitudes there is little cloud cover for most of the year, which allows a high degree of solar radiation.

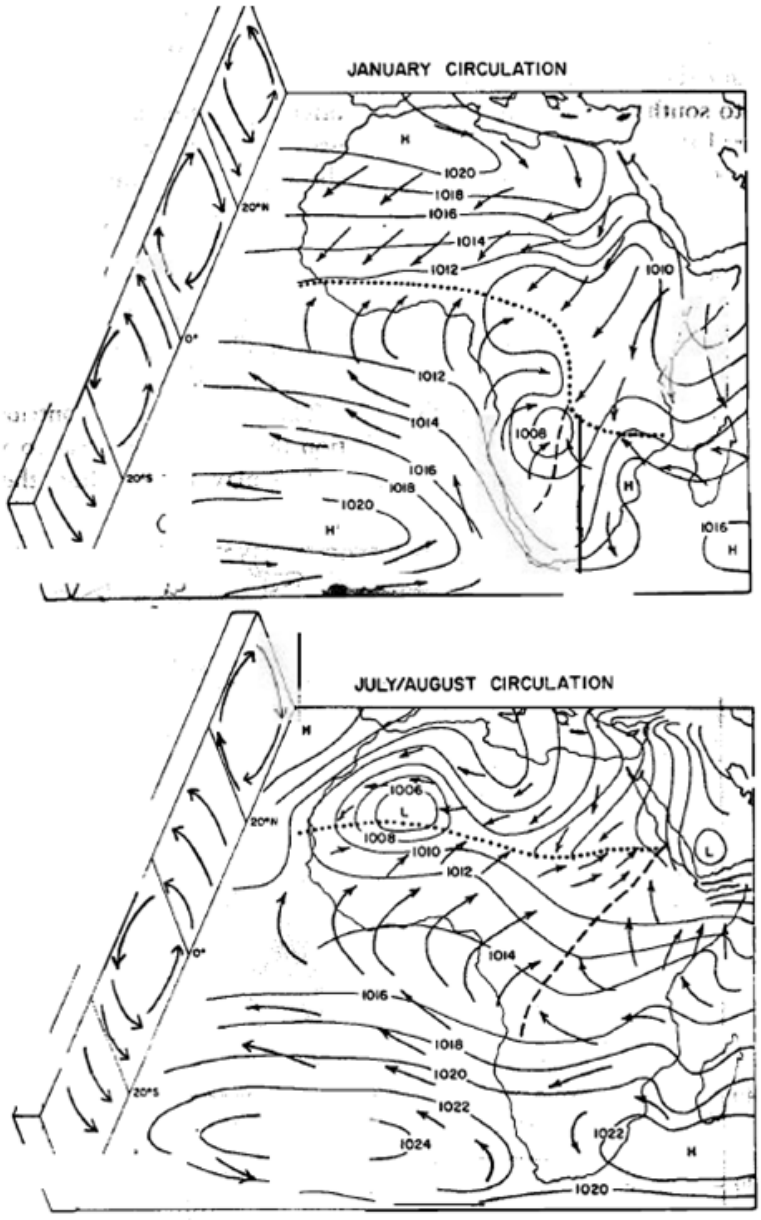

Figure 4.2: Wind circulation and pressure patterns over Africa during January and July/August (Nichoson, 1995)

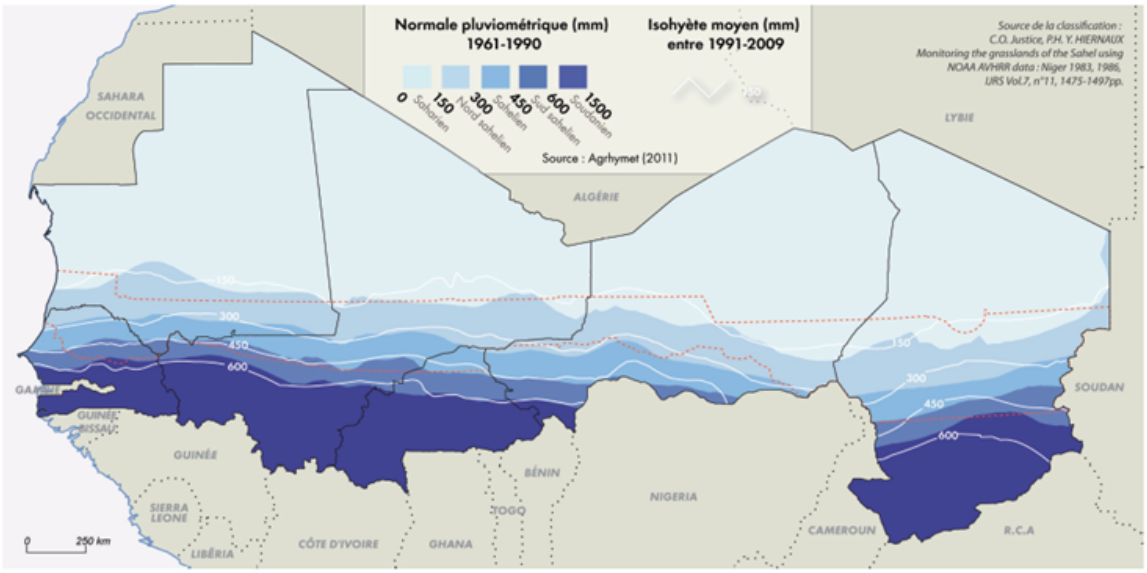

Figure 4.3: Rainfall distribution over the Sahel (Ickowicz et al., 2012)

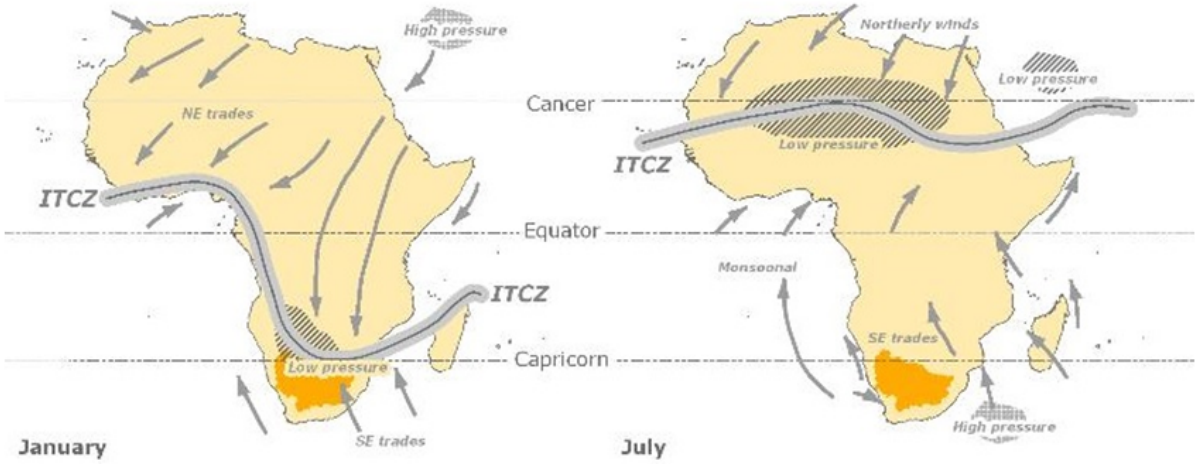

Figure 4.4: ITCZ movement along the Africa continent (Ker et al., 1978)

4.1.2 Landscape and soils

The Sahel is a combination of arid and semi-arid zones. The south is largely flat savannah, and a few scattered plateaus and mountain range toward the north (UNEP, 2012). The area is mostly covered by vegetation in the south, which declines northward due to less rainfall. Grasses cover most of region, and the dominant species are such as, corn, sorghum and wheat. There are various plant species in southern Sahel, Acacia being the most dominant. UNEP (2012) explained that the landscape in central Sahel is parkland ecosystem, which is utilized mostly for agricultural activity. There are elevations of up to 3,400 m in some areas of northern Sahel, including Mali, Niger, Mauritania and Chad. The main Sahel water basins are the Niger and Senegal Rivers, including Lake Chad.

Soil in the Sahel can be divided into three categories: sandy Aeolian soils, which cover approximately 50% of the area, iron-rich soils and lacustrine soils (Nicholson, 1995). The sandy Aeolian soil consists mostly of materials that are transported and deposited by wind. The iron-rich soil is composed of rock and sandstone, with loamy texture soil. The structure of lacustrine soil is made up of sandy soils over a clay bottom layer. Soil in southern Sahel has relatively few nutrients, due to leaching by rainfalls (UNEP, 2012).

4.1.3 Impacts of rainfall variability on social and economic aspects of the Sahel

Potts et al. (2013) reported that approximately 100 million of the world's poorest people live in the Sahel, and population growth in the region is significant, increasing from about 30 million in 1950 to over 100 million in 2010. Figure 4.5 shows projected population growth in the Sahel, which will reach 200 million in the late 2020s. Accelerating population growth is one of the main issues leading to food insecurity in the area. The main livelihoods of Sahelian people depend on agriculture, including cereal production, sorghum, millet and cassava, and livestock. As well, some who live along rivers or by the coast in the western coast live by fishing. Figure 4.6 illustrated the livelihood system in the Sahel. More than 50% of the Sahel gross domestic product (GDP) is from agricultural activities, which are largely rain-fed practices, followed by pastoralism with approximately 40% of the GDP (UNEP, 2011).

The long periods of desiccation and occasional devastating flooding strongly impact the people living in the area, particularly those involved in agriculture. There have been sustained periods of drought from the late of 1960s to the 1990s, most severely in the early 1970s and the early to mid-1980s. There are also periods of heavy rainfall, such as in

2003 which lead to above average rainfall throughout 2004 (Brook, 2004). Hissler (2010) studied the economic relationship between rainfall variability and agricultural products, and found that the rainfall variability is responsible for the sensitivity of agricultural production and growth of the economy. In addition, statistical evidence in his study confirmed that climate variability causes fluctuations in GDP growth. UNEP (2011) also reported that millions of farmers and ranchers were impacted by the severe drought period of 1969 to 1974, and this caused a reduction in agricultural products that led to widespread economic issue, from individual household income thru the national level. World Bank (2013) highlighted the impact of climate variability on social issues and the economy, and reported that the combination of devastating drought, food insecurity and environmental disaggregation affected 17 million people in the Sahel.

With respect to the devastating flooding in the region discussed in the previous section, it occurred mostly central Sahel, specifically in southern Burkina Faso, northern Nigeria and southwestern Niger. Between 1985 and 2009, these countries experienced up to ten severe floods, and up to twelve on the border of Benin and Niger and in some parts of Nigeria (UNEP, 2011). UNEP (2011) also estimated the damage due to flooding in the Sahel in 2010, and found that approximately 180,000 hectares of crops in Nigeria were destroyed, and 140,000 hectares of agricultural land spoiled. Samimi et al. (2012) reported severe flooding in 2007 with a return period of between 1 to 50 year and up, and up to 1200 year in some regions, which caused great economic losses and limited the availability of food.

4.2 The Niger River basin

The Niger River basin (Figure 4.7) located between 10N to 20N and 20W to 10E, is the largest basin in the Sahel (Goulden and Few, 2011). Since most of the basin is in the Sahel, its climate, topography and land characteristics are explained in the previous section. This section focuses on the physical geography and water resources of the Niger River basin, and the hydrologic regime of the Niger River.

The Niger River is the longest river in the western Africa and the third longest river in Africa after the Nile and Congo. The Niger, which flows 4,200 km through Nigeria, Mali, Niger, Algeria, Guinea, Cameroon, Burkina Faso, Benin, Ivory Coast and Chad, has a drainage area of over 2.2 million km^2 (FAO, 1997). The river consists of four main systems: the upper Niger River, the inner delta, the middle Niger River and the lower Niger River. The Sirba basin was chosen as the study site of this study, as it

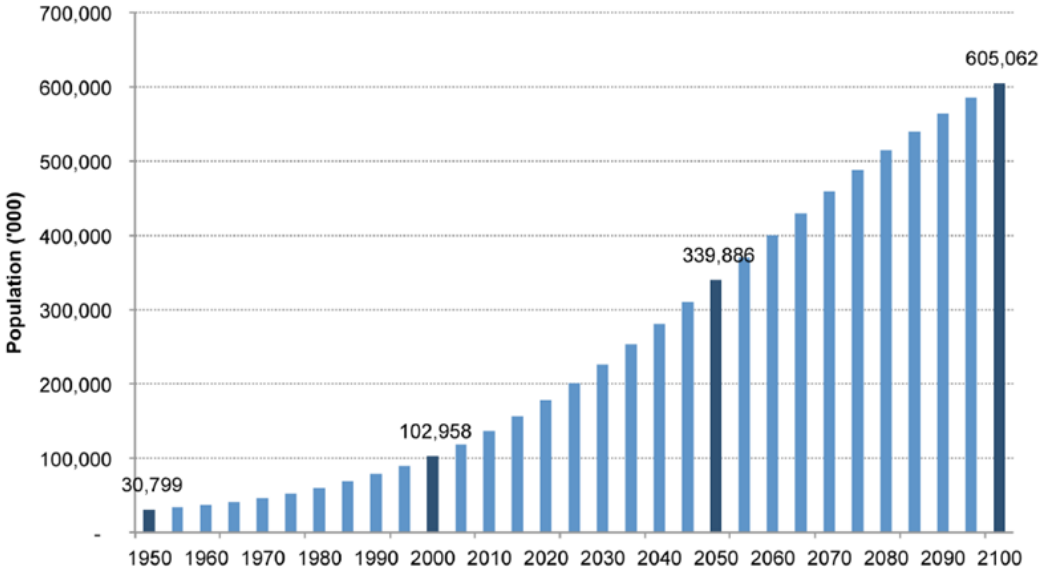

Figure 4.5: Past and projection of population growth in the Sahel during 1950-2100 (Potts et al., 2013)

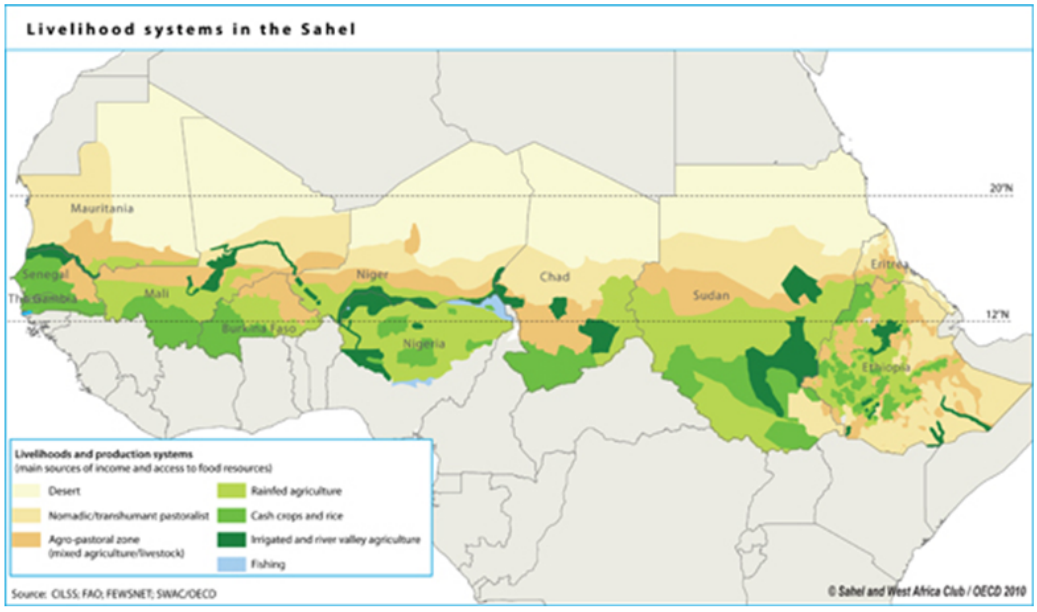

Figure 4.6: Livelihood systems in the Sahel (Sahel and West Africa club, 2015)

is representative of the Sahel region and is located in the centre of the Niger River system. The water of the Niger flows from the inner delta to the country of Niger. The six main tributaries (Gorouol, Dargol, Sirba, Goroubi, Diamangou and Tapoa) in the middle Niger River section that originate in Burkina Faso, and the three tributaries (the Mekrou, Alibori and Sota) that originate in Benin, all discharge water to the Niger River. (FAO, 1997).

The western African economy relies largely on the Niger River to provide water for local consumption, hydropower generation and irrigation (BMZ, 2010). The Niger River is extremely important, as it supports 100 million people living in the basin, particulary in the West Sahel. The country of Niger, in particular, depends on upstreamflows of the river (Goulden and Few, 2011). Dams in the Niger River generates approximately 6,000 gigawatt hours of hydropower for the population, and help store irrigation water for farmers along the river (BMZ, 2010). Though the river is used for irrigation, rain-fed agriculture is still the main livelihood for people growing crops.

The Niger River had an annual average flow approximately 32.5 km^3 from 1970 to 1998 measured at Koulikoro station, Mali (BMZ, 2010). The flow conditions of the river system primary are influenced by topography and climate in the region (Andersen et al., 2005). The main source of water for the river is rainfall, most of which comes from the mountains of Guinea and the West Africa Monsoon that normally occurs from July to September. The consistency between the amount of rainfall and river flow, at Koulikoro in Mali for example, is illustrated in Figure 4.8. There were sustained drought episodes from 1970 to the late 1990s (Conway et al., 2009; Descroix et al., 2009); this agrees with the BMZ report of 2010 (Figure 4.9). In this figure, the annual discharges of three stations, Koulikoro in the Middle Niger, Mopti at the Nantika in the Inner Delta and Niamey in the Middle Niger were compared. The wet period from approximately 1951 to 1970 was followed by the dry episode. The loss of water in this area is largely due to evaporation rate and seepage loss. In addition, Andersen et al. (2005) reported that river flow variability in the Niger River is influenced by groundwater. The variation of groundwater due to the amount of rainfall causes fluctuations of river flow.

Figure 4.7: The Niger River basin (Rosen, 2013)

4.3 The Sirba River basin

The Sirba watershed (Figure 4.10) is a trans-boundary basin located between the countries of Niger and Burkina Faso (latitude 12.2 to 14.5 N and longitude 1.4W to 1.7E). It has an area of approximately 37,000 km^2, most of which is in Burkina Faso. This basin is a sub-basin of the Middle Niger basin, and it has three main tributaries (the Faga, Yeri and Sirba), which originate in Burkina Faso and discharge to the Niger River at Garbe-Kourou in Niger. The Faga River, at 360 km, is the longest tributary in the Sirba basin. Taweye (1995) indicated that the Sirba River is one of the most important tributaries of the Niger River in the integrated area of southwestern Niger, eastern Burkina Faso and northern Mali. Descroix et al. (2009) provided the main hydrological characteristics of the basin, as shown in Table 4.1. The climate of this area is semiarid south or semiarid tropical, and the annual rainfall is approximately 300 to 750 mm (Andersen et al., 2005).

Since the entire Sirba basin is located in the Sahel region, most of its climatic characteristics are similar to those described in the first section. The Sirba basin has two distinct seasons, a wet summer and a dry winter. The wet season influenced by the WAM starts about July, while the dry episode influenced by the Harmattan trade wind is from

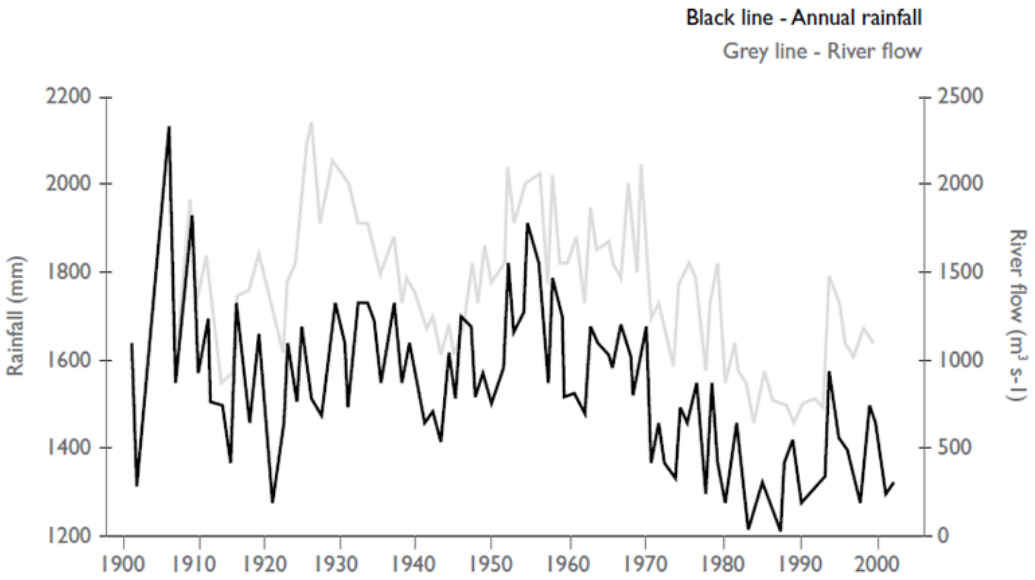

Figure 4.8: The comparison of annual rainfall and river flow of the Niger River (Conway et al., 2009)

October to June. The highest temperature in the basin is approximately 42C in April and the lowest is 17C in January.

The topography of the Sirba basin is low altitude plateau. The major soil types, based on Anderson et al. (2005) and Picouet (1999) are ferralitic and tropical ferruginous soils, both of which have high concentrations of iron and sand (Andersen et al., 2005). Ferralitic soils are highly penetrable, with little capacity to hold water or nutrients (i.e. 1 mm of available water per centimetre of soil). Tropical ferruginous soils are made up of sandy soils at the surface combined with clay, and are also relatively incapable of holding water (Mohamed-Saleem, 1984).

The basin includes eight provinces in Burkina Faso (Ganzourgou, Gnagna, Gourma, Kourittenga, Namentenga, Sanmatenga, Seno and Sourn) and three departments of Niger (Kollo, Say and Tera). All these areas are characterized as a rural, and the main livelihoods rely on agriculture and livestock. Wilby (2008) indicated that Niger is one of the most vulnerable countries in Africa in terms of food security and water scarcity.

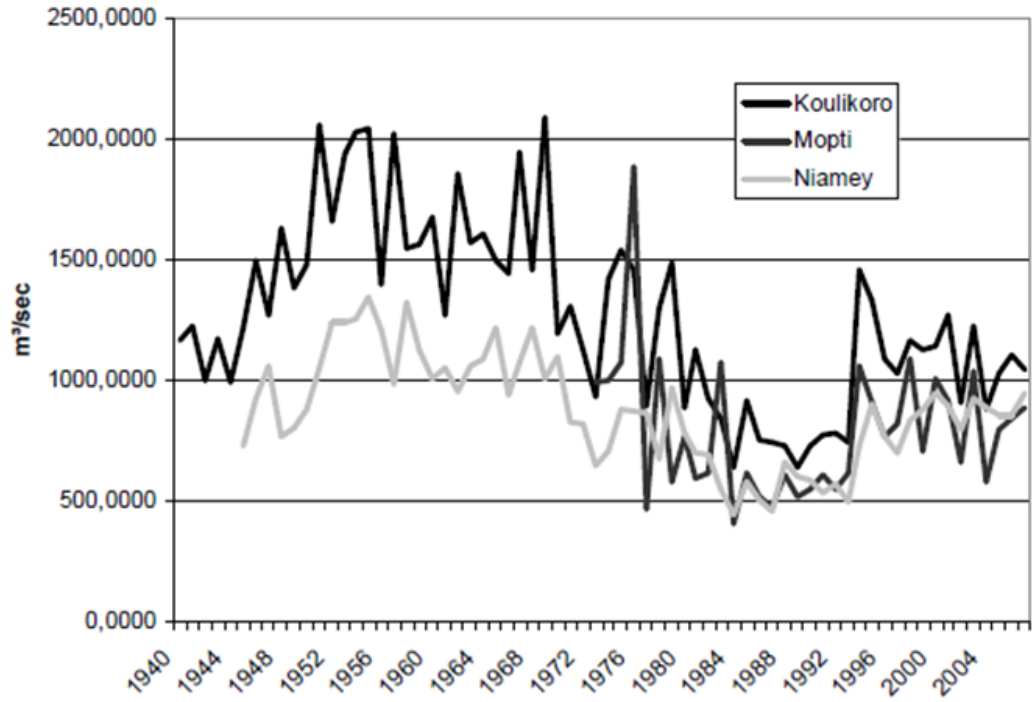

Figure 4.9: Comparison of river discharges of the Niger River at Koulikoro, Mopti and Niamey (BMZ, 2010)

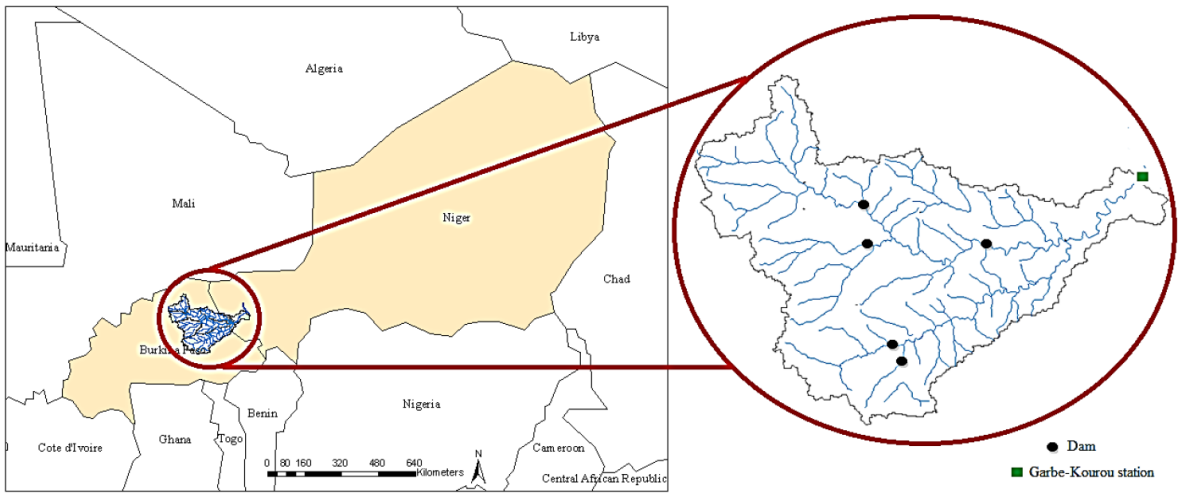

Figure 4.10: The Sirba River watershed

Table 4.1: Main data of the hydrological regime in the Sirba basin at Garbe Kourou (Descroix et al., 2009)

	Data
Mean discharge (m^3s^{-1}) (1950-2007)	24.5
Area (km^2)	38,750
Mean specific discharge (l $s^{-1}km^{-2}$) (1950-2007)	0.63
Mean rainfall depth (mm) (1950-2007)	18.3
Latitude of basin	12.2-14.5N
Longitude of basin	1.4W 1.7E

Chapter 5

Methodology

This chapter details the methodologies and data sets (input, output and intermediate) used to achieve the thesis objectives. The first section provides a general overview of the workflow in the thesis. Then, the characteristics of the input data are examined, followed by a review of the generated data. Research activities are explained in the next section. These are divided into six subsections of 1) statistical methods, 2) SST data preparation 3) indirect methods for streamflow forecasting, 4) direct methods for streamflow forecasting, 5) uncertainty analysis and 6) estimation of economic value of streamflow forecast.

5.1 Overview of methodologies

The research activities and outcomes of the study objectives and sub-objectives are presented in Figure 5.1. The figure provides an overview of all methodologies applied in this research. The links of each research activity to the sub-objectives discussed in Chapter 1 are clearly identified. The blue and green parallelograms represent input data and generated information respectively. The rectangular boxes refer to methodological developments, such as statistical modeling, temporal disaggregation or economic evaluation of the forecasts, or the generation of knowledge about the study area (i.e. development of the SWAT model). This chapter provides relevant information about each type of input data, activities and outcomes, as outlined below:

Input data: The source and quality of the data, the reason for its selection, and its spatial and temporal coverage/resolution are provided.

Generated information: Descriptions of the format of each generated data, and how the data set are used to achieve specific objectives or sub-objectives are presented.

Research activities: This chapter details the techniques used in this study. The means of evaluating the performance of the techniques is also discussed.

5.2 Input data

The details of the input data used for both rainfall and streamflow forecasting are provided in this section. These include data characteristics, data sources and the resolutions of all data sets.

5.2.1 Observed daily precipitation

The daily precipitation data used in this research were obtained from climate stations and prepared by Niger and Burkina Faso Meteorological Services. Though, there are several stations in and around the Sirba basin, only daily rainfall data sets from climate stations presenting missing data less than 10% over the entire observation period were selected for this study. Finally, eleven rainfall time series, spanning 1960 to 2006, were applied as input data in statistical models for rainfall and streamflow forecasting. Figure 5.2 displays the locations of the climate stations chosen for the study, and Table 5.1 shows the details of the stations. Monthly rainfall climatology in the basin, as shown in Figure 5.3, indicated that the highest amount of rainfall usually occurred from July to September (JAS) which was consistent with various other studies relating to rainfall prediction in the Sahel, including Barnston et al. (1996), Garric et al.(2002), Mo & Thiaw (2002), and Raicich et al. (2003); these researchers also used JAS precipitation for a wet period in the Sahel region in their studies.

The highest total rainfall amount was 777 mm in 1964 and the lowest was 370 mm in 1984. The average annual rainfall and standard deviation from 1960 to 2006 was 529 mm and 100 mm respectively. The rainfall anomalies from 1960 to 2006, presented in Figure 5.4, show that there is high rainfall variability in this area, particularly at the end of the 1988 to 2006 period. The major dry episode in the basin was from 1970 to 1987,

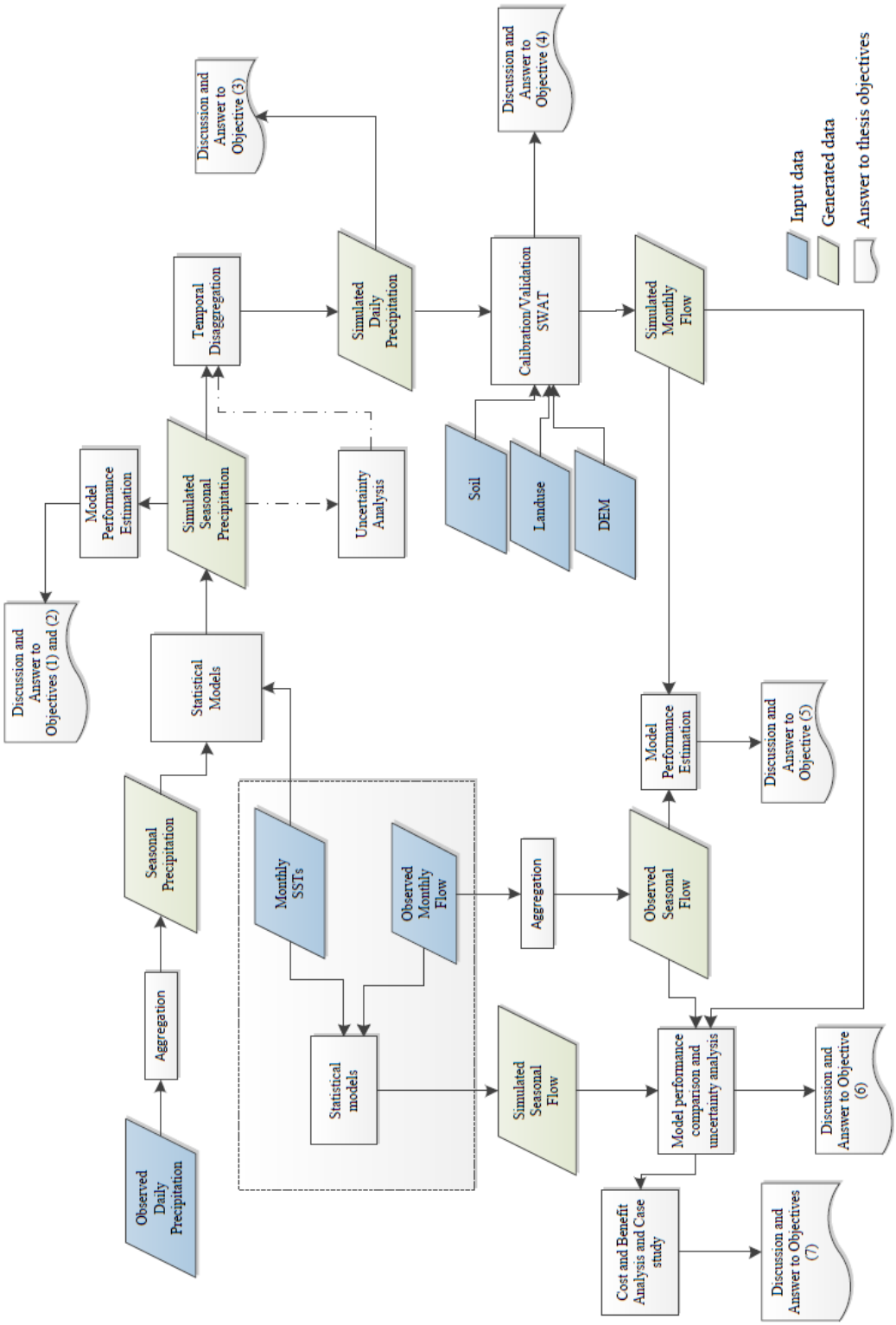

Figure 5.1: Overview of methodologies

which corresponds with the findings of Nicholson and Palao (1993) who reported drought episodes from 1968 to 1990 and Janicot et al. (2001) who referred to the dry conditions of the Sahel beginning in 1970. Thus, the Sirba rainfall data used in this study is clearly consistent with that of other studies conducted in the Sahel.

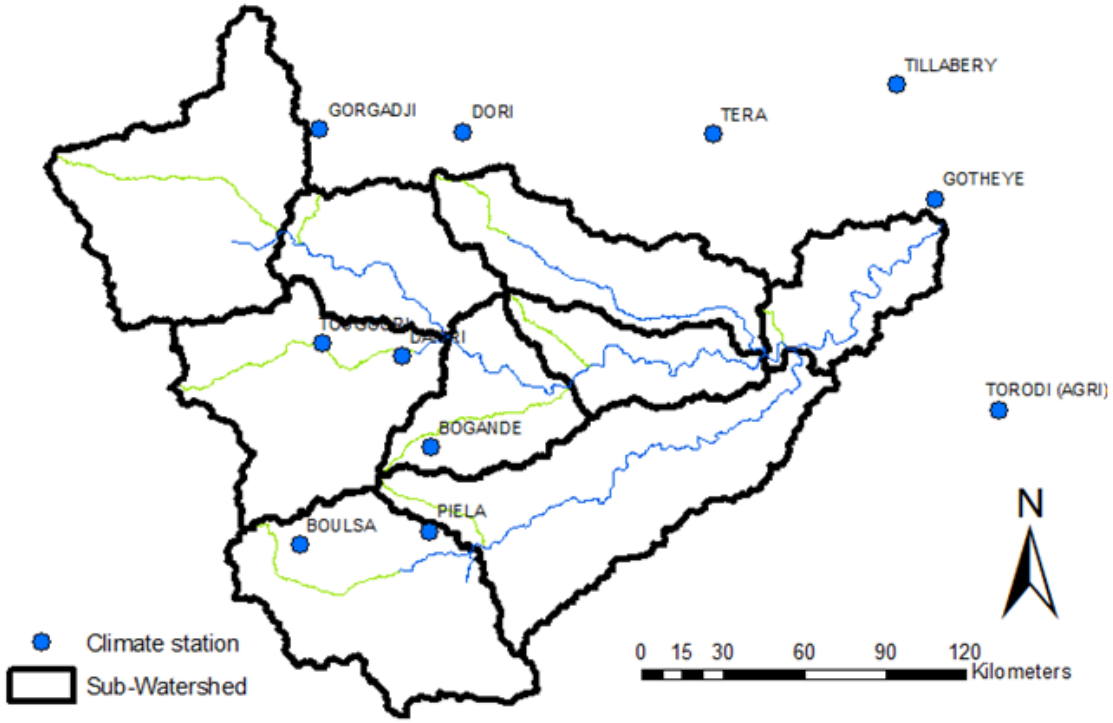

Figure 5.2: Climate stations in the Sirba basin

Table 5.1: Rain gage station details

Station number	**Station name**	**Longitude**	**Latitude**	**Country**
200024	Gorgagji	-0.52	14.03	Burkina Faso
200026	Dori	-0.03	14.03	Burkina Faso
200047	Tougouri	-0.5	13.32	Burkina Faso
200048	Dakiri	-0.23	13.28	Burkina Faso
200082	Boulsa	-0.57	12.65	Burkina Faso
200085	Bogande	-0.13	12.98	Burkina Faso
200086	Piela	-0.13	12.70	Burkina Faso
320002	Tera	0.82	14.03	Niger
320004	Tillabery	1.45	14.20	Niger
320005	Gotheye	1.58	13.82	Niger
320006	Torodi	1.80	13.12	Niger

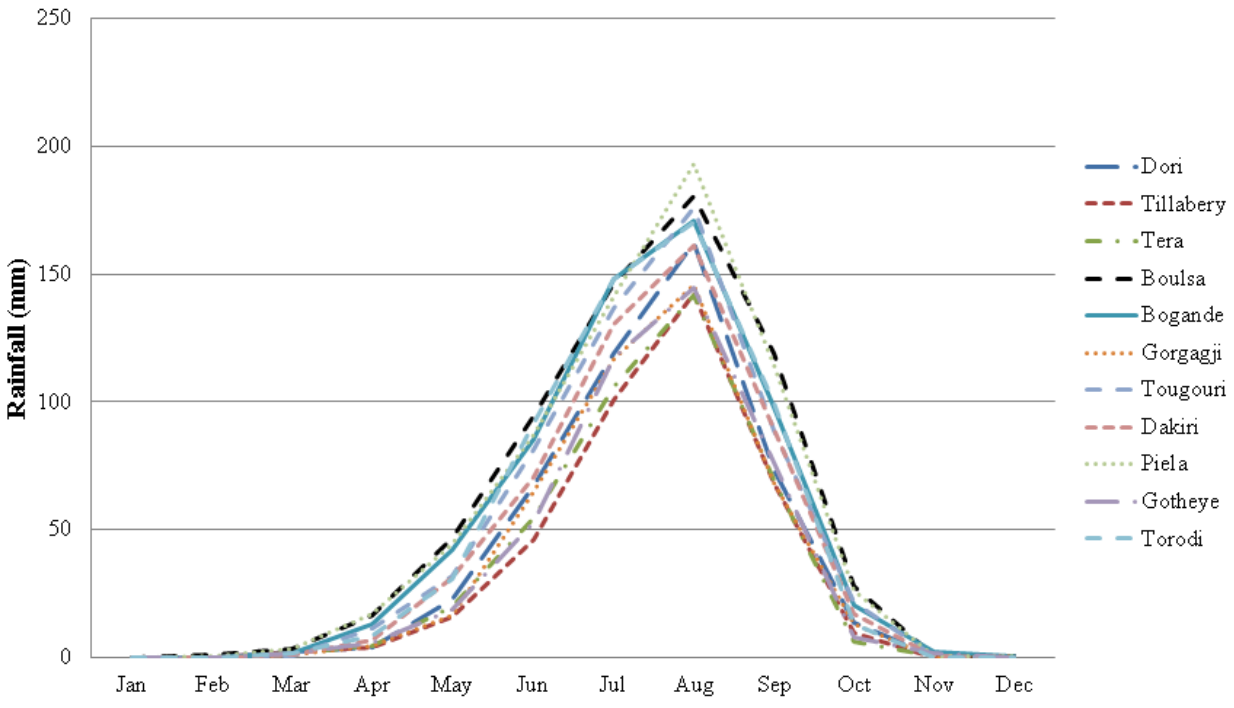

Figure 5.3: Rainfall climatology collected from 11 climate stations

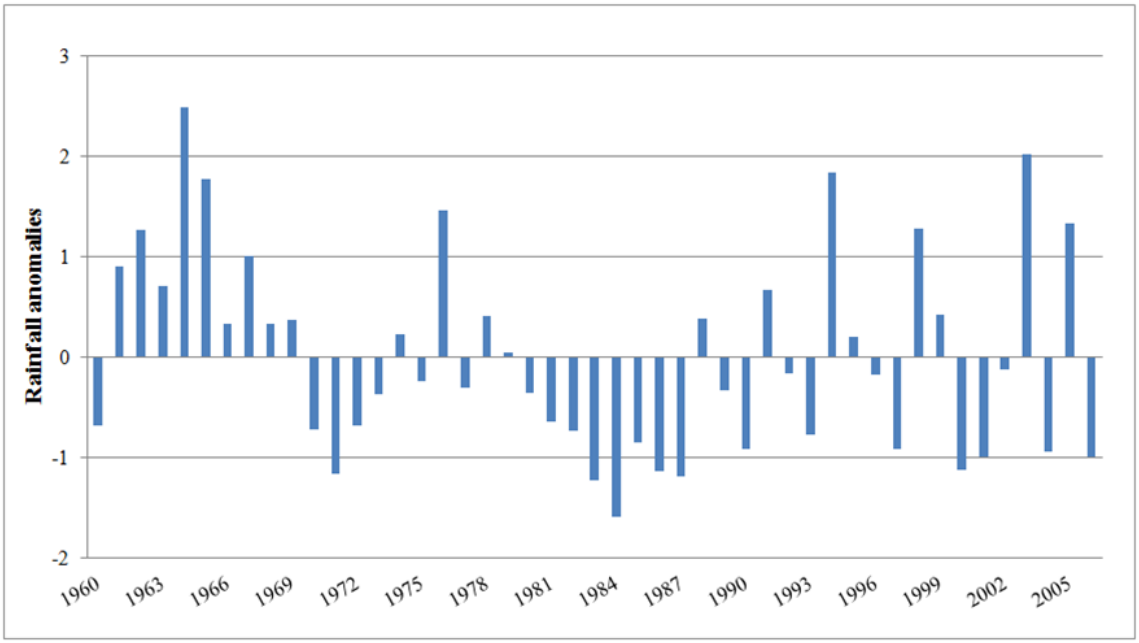

Figure 5.4: Annual rainfall anomalies from 1960 to 2006

5.2.2 Sea surface temperature

As discussed in Chapter 2, various studies have shown distinct relationships between sea surface temperature (SST) and rainfall, which was why SSTs were used as predictors in the statistical models in this study. Gridded SST data sets from the Pacific and Atlantic Oceans were used as initial pools of potential predictors for rainfall/streamflow forecasting in the Sirba watershed. New potential predictors were generated by aggregating the initial predictors over continuous periods of up to 18 months.

The tropical Pacific SST data ranges from 1970 to 2003, and is located within latitudes 29S to 29N and longitudes 124E to 70W, with a spatial resolution of 2x2 grid data (30 by 84 points) on the Celsius scale (Reynolds and Smith, 1994; Woodruff et al., 1993). The data was prepared by the Climate Prediction Center of the National Oceanic and Atmospheric Administration (NOAA) National Weather Service (US). The monthly time scale Atlantic SST data ranges from 1964 to 2010, and consists of 25 points on the y-axis (latitudes 19S to 29N) and 38 points on the x-axis (longitudes 59W to 15E). It was obtained from the Meteorology and Water Resource Center of Ceara State, Brazil. Both data sets were downloaded from the International Research Institute for Climate and

Society. Figure 5.5 indicates the locations of the two data sets.

Figure 5.6 illustrates monthly climatology data of the tropical Pacific and Atlantic SSTs, and clearly shows that the data sets are highly consistent. Surface temperature of both oceans increased gradually from January to April and decreased from May to August, then rose slightly to November and declined again in December. The maximum and minimum temperatures of the Pacific Ocean SST were 26.1C and 25.7C respectively, slightly higher than the Atlantic SST maximum and minimum of 25.8C and 25.2C respectively throughout the entire period. Figure 5.7(a) and (b) display the SST climatology of April (maximum) (a) and August (minimum) (b) over the two areas. For the Pacific Ocean, the high temperatures were near Indonesia, in the mid- ocean and on the east coast of Peru in April, then moved toward northern tropical region close to Japan in August. The high SST in Atlantic Ocean was around Guinea, Ghana and Nigeria in April, then shifted toward northern South America in August.

These two SST sets were introduced as input layers in all statistical models. Empirical equations of the relationship between each SST and either local rainfall or streamflow were established, and their forecasts were generated based on these relationships.

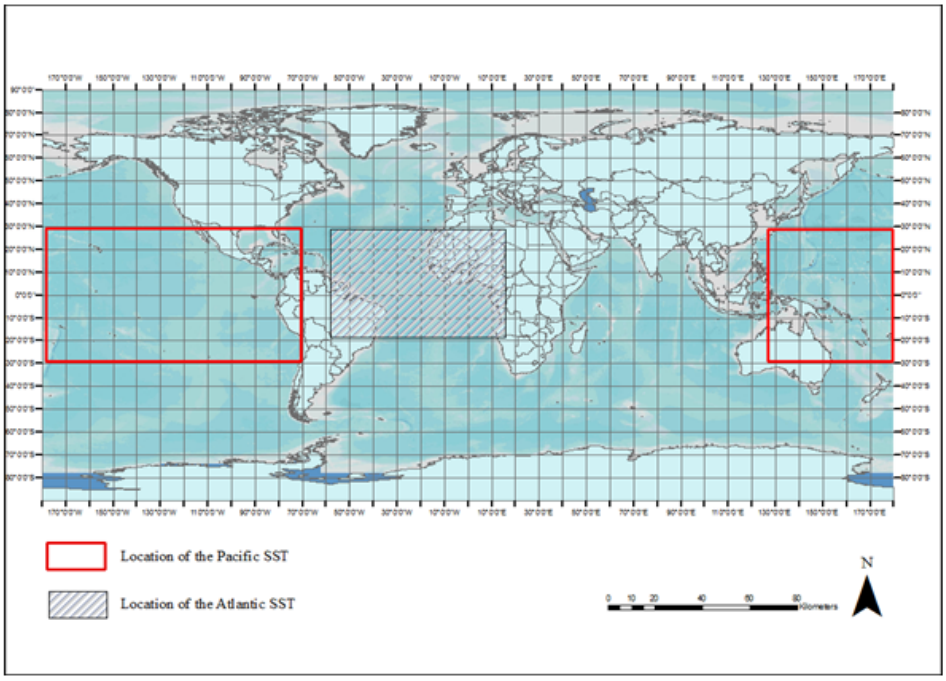

Figure 5.5: Locations of the Pacific and Atlantic SSTs

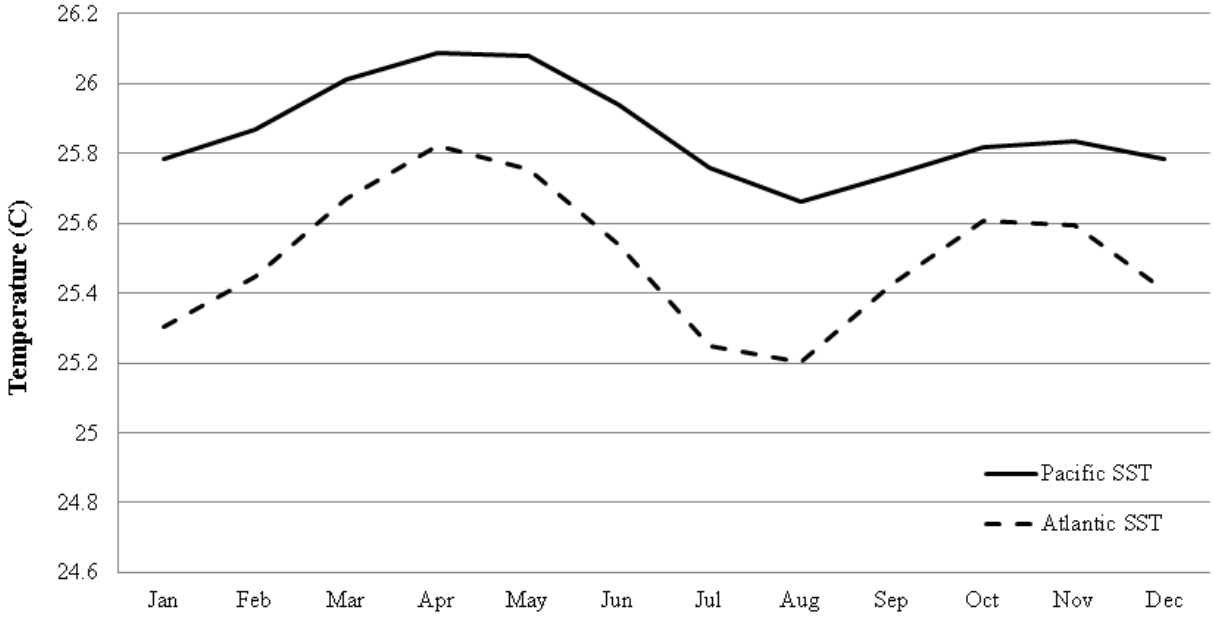

Figure 5.6: Pacific and Atlantic SST climatology

5.2.3 Streamflow observations

Streamflow data used in this study were collected at the GarbeKorou station (latitude 13.73, longitude 1.90) on a daily time scale, and prepared by Direction of Water Resources (Direction des Resources en Eau: DRE) of Niger. The data set covers from 1962 to 2002 (41 years) and has less than 10% missing data. The monthly time series of streamflow from this period were built as in Figure 5.8, and this pattern shows considerable agreement with the rainfall climatology illustrated in Figure 5.3. High flows typically occurred from July to October in the summer rainfall season, and low flows generally took place in the first five months of the year and approximately year end. The annual average flow was approximately 27 m^3/s and the standard deviation was 18 m3/s. If only the July to September discharge was considered, the annual mean flow increased to 86 m^3/s with a standard deviation of 56 m^3/s. The highest and lowest average annual flows for this period were 235 m^3/s in 1998 and 7 m^3/s in 1968 respectively.

Observed streamflow anomalies are presented in Figure 5.9. It shows the prolonged drought period from 1968 to 1987, as well as the serious flooding in the basin in 1988, 1991, 1994 and 1998 that corresponds to the positive rainfall anomalies in Figure 5.4.

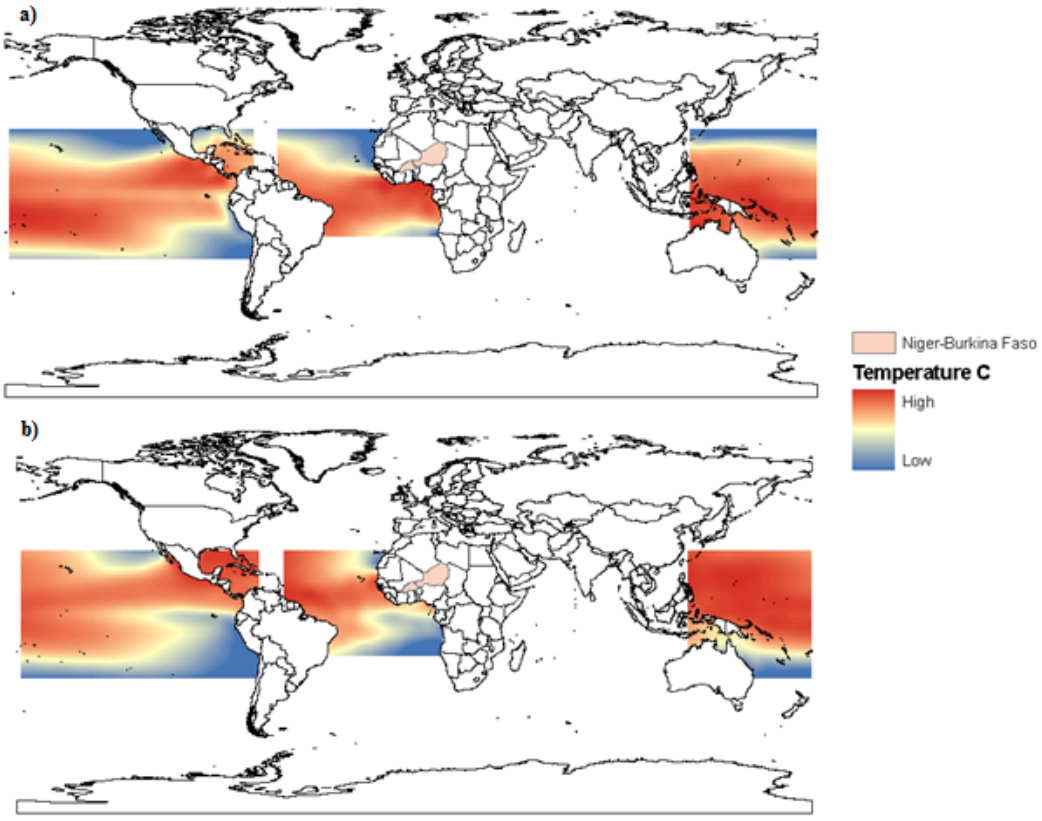

Figure 5.7: SST variability over the Pacific and Atlantic oceans in a) April (maximum temperature) and b) August (minimum temperature)

There are also opposing events when rainfalls and streamflows were inconsistent, such as in 1963, 1966 and 1968. These could be due to errors of measurements or the complexity of rainfall-runoff transformation processes.

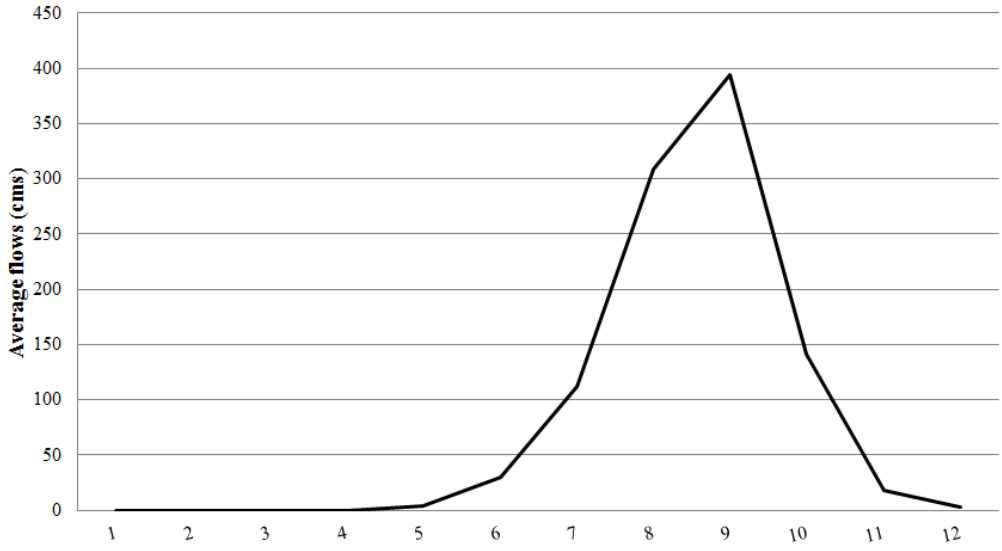

Figure 5.8: Monthly observed streamflow from 1962 to 2002

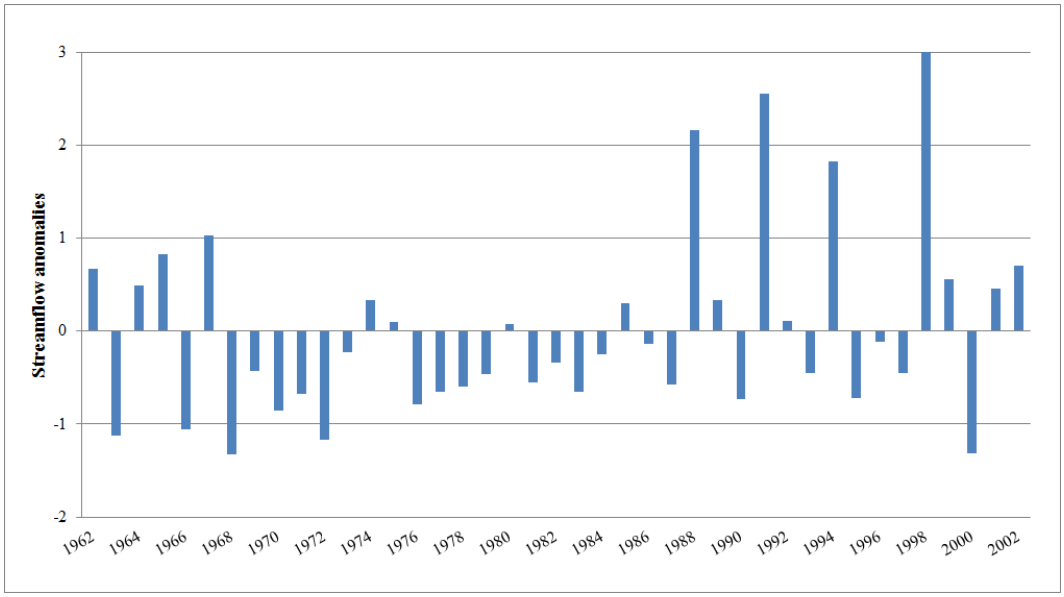

Figure 5.9: Streamflow anomalies from 1962 to 2002

5.2.4 Climate data

Climate data other than precipitation are described in this section. SWAT requires the data of four climate variables: temperature, relative humidity, solar radiation and wind speed. All the climate data used in this study were collected by National meteorological offices of Burkina Faso and Niger. The characteristics of the data sets follow.

a) Temperature: SWAT requires maximum and minimum air temperatures on either daily or sub-daily time scale. The variables are important due to their effect on evaporation, which is the major process that removes water from the watershed. Temperature data are necessary to accurately calculate the water balance in the basin, since they influence various physical, chemical and biological processes (Neitsch et al., 2011). Two time series were available for this research, the maximum and minimum daily temperatures from 1989 to 2002. The highest temperature was approximately 42 C in April, and the lowest about 17 C in January. During the July-September summer rainy season, the minimum and maximum temperatures were 24 C and 36 C respectively.

b) Relative humidity Relative humidity can be calculated at a given temperature from the ratio of actual vapor pressure to saturation vapor pressure. Daily relative humidity is used in SWAT to estimate potential evaporation in the basin (Neitsch et al., 2011). The data set was from 1980 to 1990, and SWAT used a weather generator to simulate the missing data. The average relative humidity in the area was 59% and the minimum and maximum were 15% and 100% respectively.

c) Solar radiation: SWAT requires solar radiation data since it is the main factor controlling water movement in the land phase of the hydrologic cycle, and has a significant influence on the rate of evaporation in the basin (Neitsch et al., 2011). Similar to relative humidity, there were 11 years of solar radiation data available, from 1980 to 1990. The weather generator acted the study period of 1989 to 2002, and the solar radiation data sets (average, maximum and minimum data) were applied for streamflow forecasting. The average of solar radiation during the observation period was $9Kw/m^2$. The minimum and maximum values were 0 and 12 Kw/m^2.

d) Windspeed Wind speed data are used to estimate potential evapotranspiration and transpiration (Neitsch et al., 2011). These were obtained from three climate stations over the period of 1980 to 1990, and the SWAT weather generator was applied

to complete missing data. The average daily wind speed over the basin was 2.4 m/s, with a high of 12 m/s and a low of 0 m/s.

5.2.5 Land use

Land use is an important factor for computing runoff in the basin. Neitsch et al. (2002) described land use as one of significant parameters used to produce an accurate estimation of evapotranspiration. The source of the land use data for the Sirba watershed was the USGS Global land Cover Characterization database, with a spatial resolution of one kilometer (map available at http://www.waterbase.org). As discussed in Chapter 4, this region is a rural area with most of the land use dedicated to agriculture and livestock. More than half of the total area of the basin (53%) is savanna grassland, with pasture and cropland making up about 23% each. The remaining area (1%) is sparsely vegetated, shrub land and water. The land use map for the Sirba basin is shown in Figure 5.10.

5.2.6 Soil data

Soil characteristics are basically used to calculate runoff and infiltration rates, which relate to water balance and are key factors for estimating the movement of water through a soil profile. The soil data used in this study was prepared by the Food and Agriculture Organization of the United Nations in 1995, with a spatial resolution of 10 kilometers (map available at http://www.waterbase.org). Details of soil properties were obtained from Reynolds et al. (1999). There is no variability in soil types as soil data is global and has a low spatial resolution. The entire basin is sandy-loam soil (60% sand, 30% silt and 10% clay).

5.2.7 Digital Elevation Map

A digital elevation map (DEM) displays the continuous elevation of a terrain, which is one of three criteria used to partition the basin into hydrological response units (HRUs). The African DEM is from Shuttle Radar Topography Mission data, processed by NASA and the United States Geological Survey. The CGIAR Consortium for Spatial Information (CGIAR-CSI) distributes this data set (Jarvis et al., 2008). This map can be used for sub-watershed delineation in the basin, where the elevation range is from 0 to 454 meters. Figure 5.10 shows the DEM of the Sirba watershed.

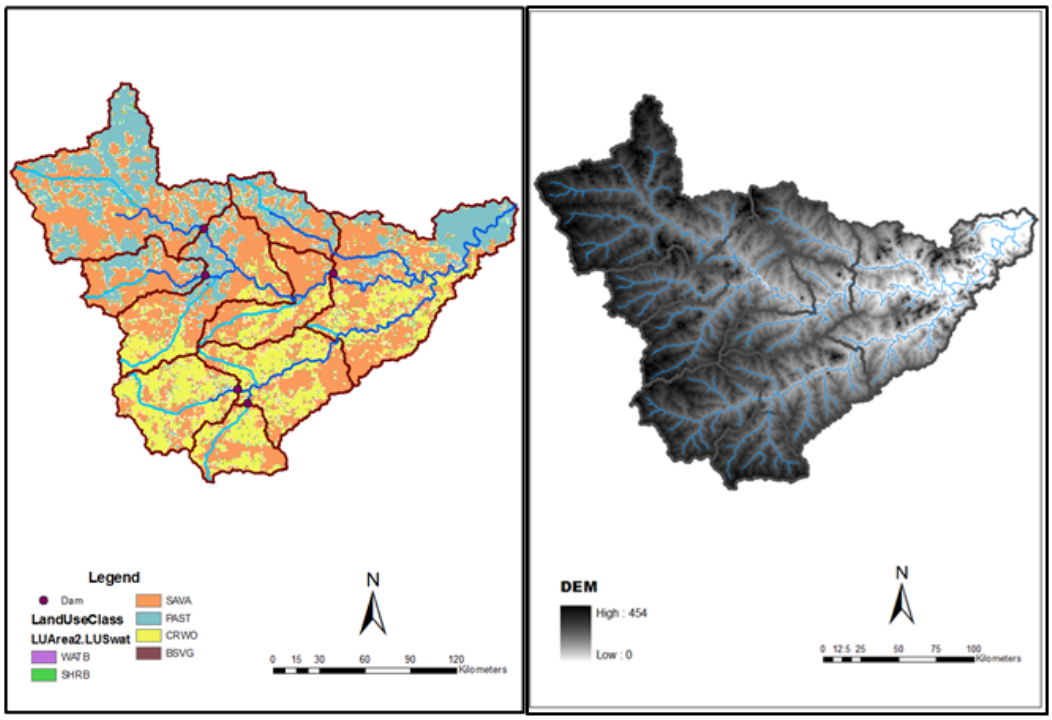

Figure 5.10: Land use and DEM maps for the Sirba watershed

5.3 Generated data

Forecasted data developed on various time scales are shown as green parallelograms in Figure 5.1. Rainfalls were primarily generated first using statistical models, then streamflows were constructed using both statistical and hydrological models.

5.3.1 Rainfall time series

Rainfalls were primarily forecasted on seasonal (JAS) time scales using statistical models driven by SSTs as predictors. The performance of each model forced by SST data sets for rainfall generation was estimated using the Nash-Sutcliffe coefficient (E_f), the coefficient of determination (R^2) and the hit score (H). The details of each indicator are discussed in Chapter 3. The seasonal rainfall forecasts were later disaggregated into daily time scales to allow them to be used as input data for SWAT. The accuracy of the rainfall forecasts before and after disaggregation are reported. The best time period of each SST suitable for rainfall forecasting is also indicated.

5.3.2 Streamflow time series

Streamflows were forecasted using the SWAT model forced by rainfall forecasts (the indirect method), and statistical models using SSTs as predictors (the direct method). The SWAT method generated monthly time series, while the other gave seasonal streamflow forecasts from July to September. In order to compare the performance of the two approaches, seasonal streamflow forecasts were disaggregated to monthly flows. The same criteria used to evaluate rainfall forecasting were applied to estimate the models' performance for streamflow forecasting.

5.4 Research activities

This section describes all the procedures used in this study. It first details the statistical models employed for both rainfall and streamflow forecasting, then explain the techniques applied to prepare aggregate SSTs forced to statistical models. Steps for streamflow forecasting using either SWAT (indirect) or only statistical (direct) models are then detailed. Finally, the uncertainty analysis approach and the cost/loss ratio method used for economic estimates of the forecasting systems are presented.

5.4.1 Statistical models development

Linear and non-linear regressions were applied for rainfall and streamflow forecasting in the Sirba basin. Additional steps were taken before using the regression approaches, in order to obtain high predictive SST grid points and produce more accurate forecasts. All combinations of statistical techniques were tested, and their forecasting performance are explained.

The Pacific and Atlantic SSTs were used as predictors in the models. The SST data sets had high dimensions of 2,460 for the Pacific and 950 for the Atlantic; thus, the data required filtering to obtain only grid points with high correlation to predictands (rainfall/streamflow). Principal component analysis (PCA) and canonical correlation analysis (CCA) were then applied to reduce the number of data sets, and overcome the multicollinearity of the SST data. A cross-validation method was applied to reduce over-fitting of outputs generated by the models. Either multiple linear regression polynomial regression of degree two to six was then applied to establish empirical equations for hydrological simulations of rainfall and streamflow.

1) Screening most important SST grid points: Two techniques, R^2 and E_f were tested to determine their capability to filter SST grid data. If R^2 was used, the model specifically selected the grids of SST with a relationship to the predictand P-value of less than 0.05. The remaining SST grid data were then ordered according to their R^2 value, and arbitrary assigned a number of the SST time series (N_{max}) from 10 to 200 with ten increments for use in PCA and CCA. For example, the first set of SST data contains ten SST grid points, and these ten time SST series were used as independent variables in PCA and CCA applications. Then 20 time SST series were used in the second run, and so on. The process was repeated with the different numbers of SST time series until 200 grid points were used as independent variables.

If E_f was performed in the screening step instead of R^2, a simulation was generated using each SST grid point at the first step. The E_f value was then computed using observations and forecasts, and the number of E_f depended on the amount of SST grid data. All E_f data were then ordered from high to low, and N_{max} was defined to specifically maintain powerful predictors to use in PCA and CCA. This process of changing N_{max} to obtain various SST time series was repeated until 200 SST grid points were applied in the models.

2) Predictor vector dimension reduction methods: After running the previous step, the SST grid data dimension ranged from 10 to 200 data points, with 10 increments. PCA and CCA were applied to reduce the number of grid data with the same statistical information as the original predictor data sets. PCA constructed a new variable data set with each data called a principal component (PC). How many principal components (PCs) were generated using PCA, based on the number of remaining SST grid points (N_{max}) obtained after the screening step. For example, if ten SST grid points are constrained to drive the statistical models, the number of generated PCs is also ten. Stepwise regression was then applied to retain the most effective PCs to build an empirical equation to use in the next step.

Similar to PCA, CCA has the ability to reduce the number of variables. The difference between the two methods is the number of initial data sets used to calculate new data. CCA considers intercorrelation between both predictors and predictands, whereas PCA calculates new data sets using only predictor data. CCA typically develops only one set of predictor. Thus, if CCA is used rather than PCA, it is not necessary to apply stepwise regression before regression analysis.

3) Empirical model generation: Both linear and non-linear regressions were tested to determine the best method for rainfall/streamflow forecasting. Simple and multiple linear regressions were performed after CCA and PCA applications. If only one predictor data set remained after a predictor reduction process, simple linear regression is used; otherwise multiple linear regression is applied instead. Polynomial regressions of degree two to six were used for the non-linear regression model. A one-year cross validation approach was performed to avoid overestimation bias; both the predictor data set of the pervious year and the predictand data set of the forecasts issue year were not involved in generating the empirical equation. The coefficients of the equation were used to simulate response variables (i.e. rainfall or streamflow) based on the SST of the year that was discarded at the first step. This process was repeated until variables of all years were simulated. More details of the processes used to manage data are described in the SST data preparation section.

The eight following statistical models were employed in this study. Model performances were evaluated using three criterions. Figure 5.11 shows the general steps of all statistical models.

- Model I: R^2-PCA-Simple/Multiple linear regression
- Model II: R^2-CCA-Simple/Multiple linear regression
- Model III: E_f-PCA-Simple/Multiple linear regression
- Model IV: E_f-CCA-Simple/Multiple linear regression
- Model V: R^2-PCA-Polynomial regression
- Model VI: R^2-CCA-Polynomial regression
- Model VII: E_f-PCA-Polynomial regression
- Model $VIII$: E_f-CCA-Polynomial regression

The steps used for statistical models as follows:

For each aggregated SST, the cross validation method was applied to generate forecasted rainfall/streamflow. Details of the steps for cross validation are explained below.

a) For each period the SST was aggregated, the cross validation method was applied as follows (Figure 5.12):

i For each year Y in the period for which the SST of year Y-1 prior to the forecasted month of year Y, and rainfall/streamflow in the Sirba watershed for year Y were available:

1. The SST of year Y-1 was removed from the SST grid.
2. The rainfall/streamflow of year Y was removed from the rainfall data set.
3. The dimension of the remaining SST data set was reduced using the methods described in Section 5.4.1 to obtain a smaller number of predictors.
4. A regression was fitted between the SST and rainfall/streamflow time series.
5. The fitted regression was used to simulate the rainfall/streamflow of year Y.

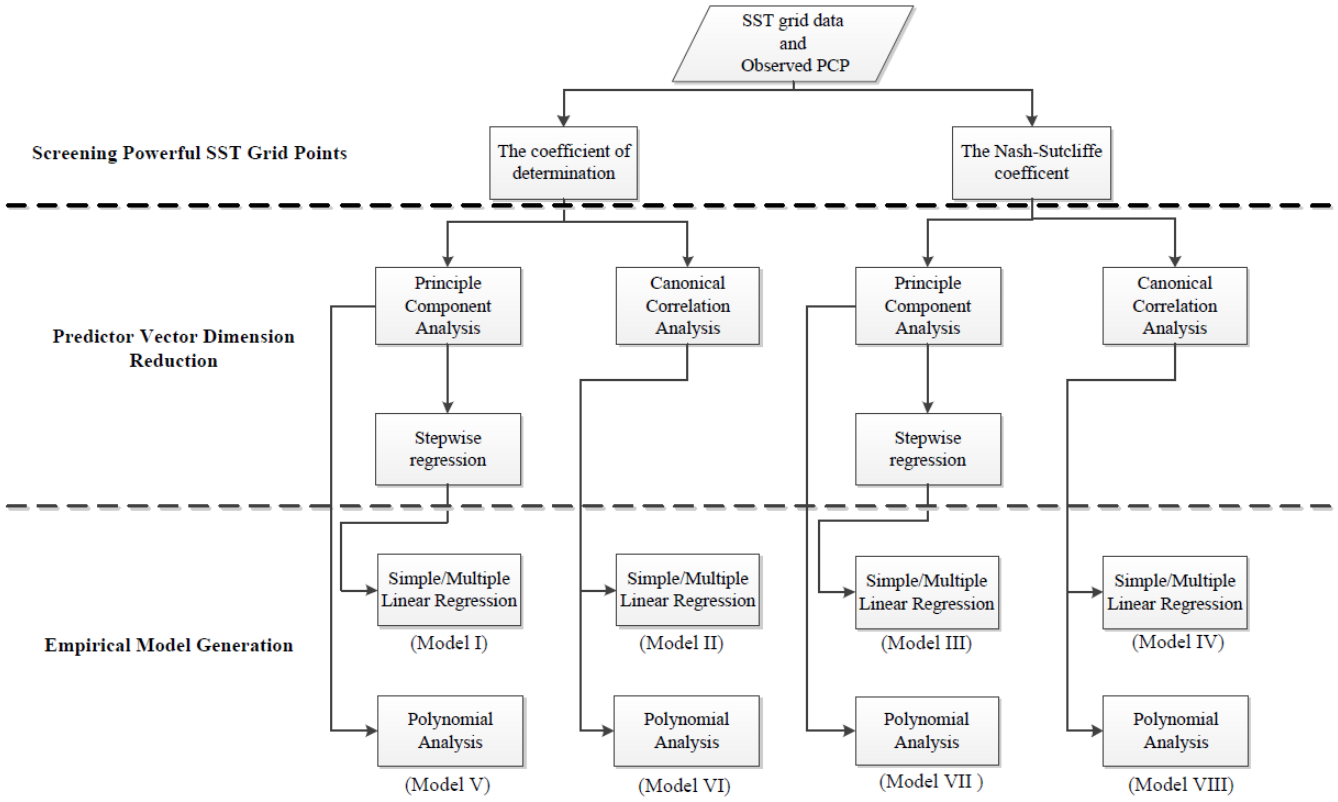

Figure 5.11: Statistical models

[If the SST and rainfall/streamflow were from the same year (year Y), only SST and rainfall/streamflow time series for year Y were removed in the first step, before applying in the statistical models]

ii When the forecasted rainfall/streamflow was available for each year in the historical period, the objective functions E_f, R^2 and H were calculated to estimate model performance.

b) For a given SST data set, the period that gave the best performance was presented.

The statistical models used in this research involved repetitive steps, in order to include all aggregate SST periods and N_{max} values in the process. Thus, the loops for programming in Figure 5.13 to 5.16 can help clarify all procedures used to develop forecasted outputs. Though the figures show the model practices for precipitation forecasting, streamflow forecasting also applied the same procedures. Figure 5.13 shows an overview of three procedural subprocesses of a) precipitation and SST data preparation, b) SST dimension reduction and c) forecast generation. Figure 5.14 presents the loop, and explains how aggregate SSTs are generated in a specific period corresponding to the seasonal precipitation to be forecasted. It also shows how to apply repetition for the next aggregate SST generation for all years of the study period. Figure 5.15 and 5.16 show the procedure used to decrease SST dimension and develop the forecasts respectively.

5.4.2 SST data preparation

SST data were available on a monthly time scale, but it is common practice to prepare SST averaged over longer periods, such as trimesters, before using them in seasonal forecasting models. The choice of the period when the SST is averaged (known as the SST averaging period) will affect the performance of the forecast. Since the best period was not known in advance, SST data sets were aggregated over various periods with different lengths and start dates. The periods started at the beginning of a calendar month, and finished at the end of a calendar month. The beginning of a period had to be later than or equal to January 1^{st} of the previous year (i.e Y-1, where Y is the year with the rainy season for which the forecast was issued). The end of the period had to be prior to or equal to June 30^{th} of year Y. Figure 5.17 demonstrates how all 171 periods corresponding to the above criteria were systematically arranged. The upper bar

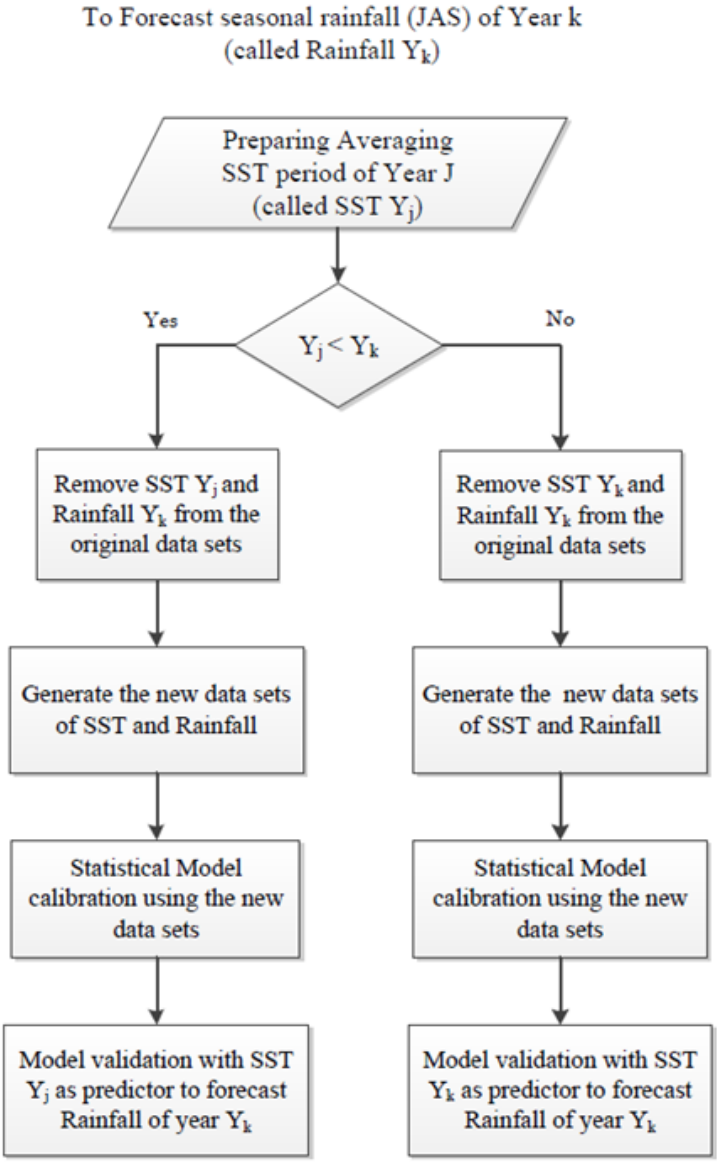

Figure 5.12: Cross validation process to generate forecasted rainfall/streamflow for each SST averaging period

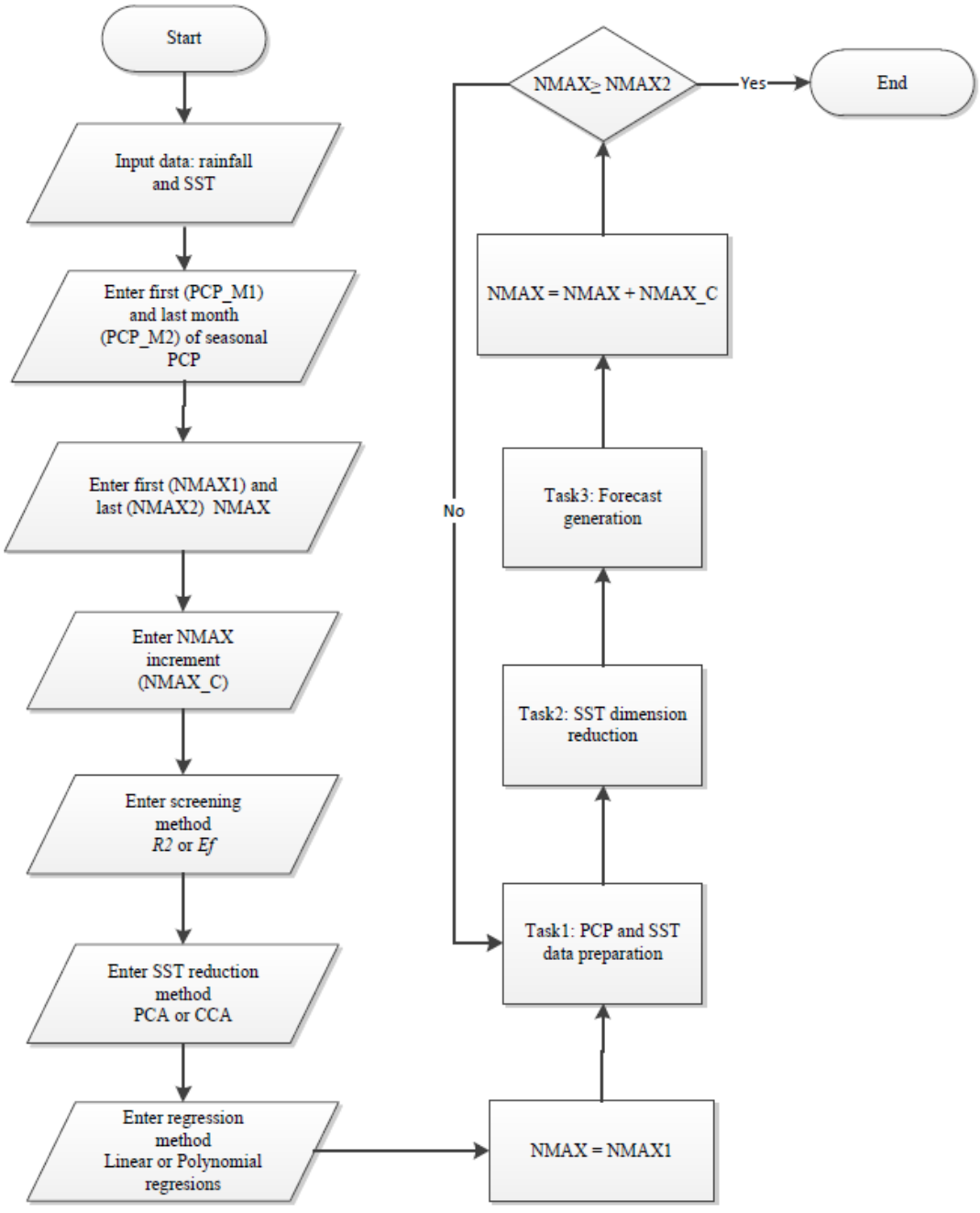

Figure 5.13: Overview of procedure in the statistical models

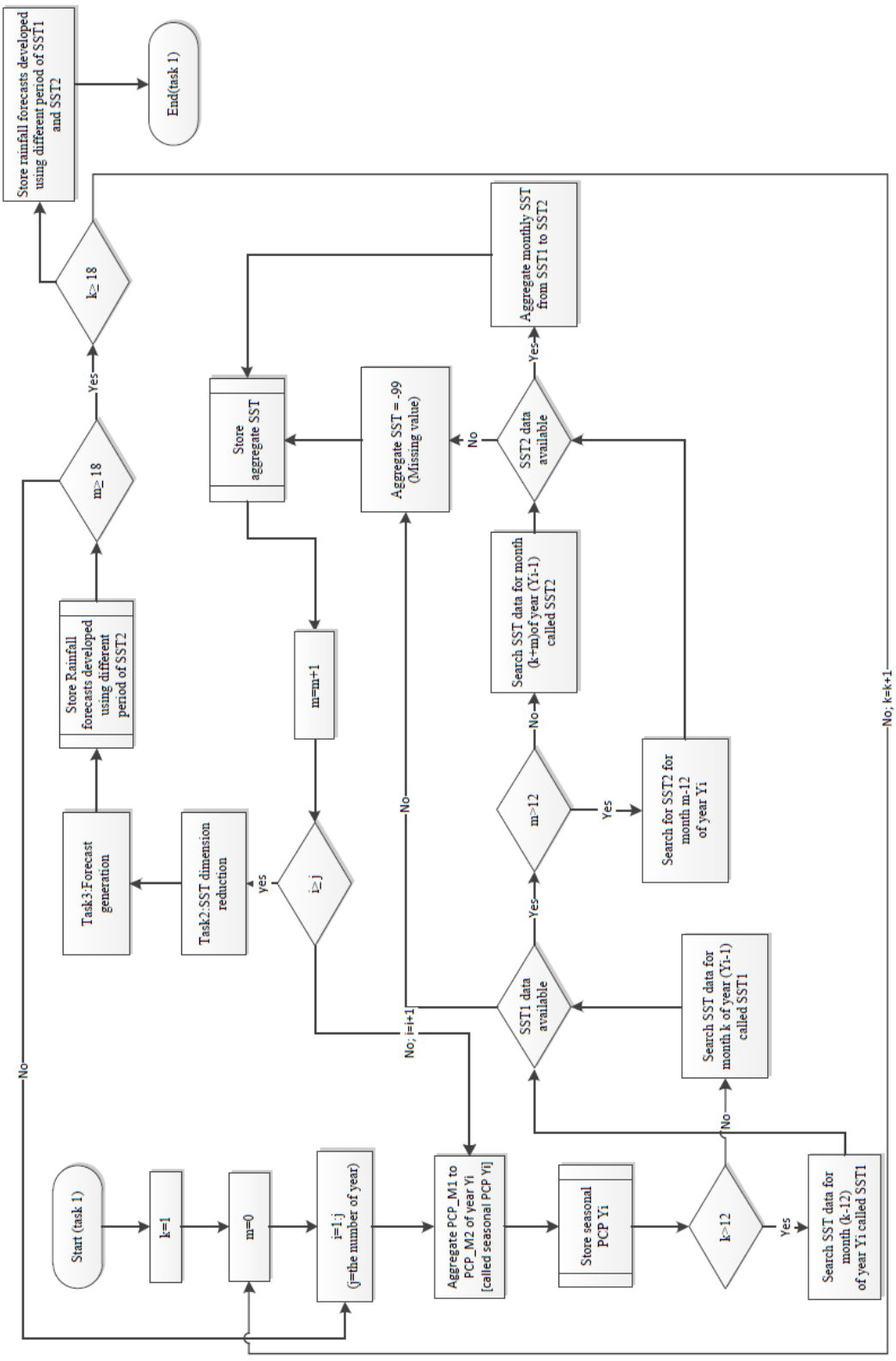

Figure 5.14: Aggregate SST and seasonal precipitation generation

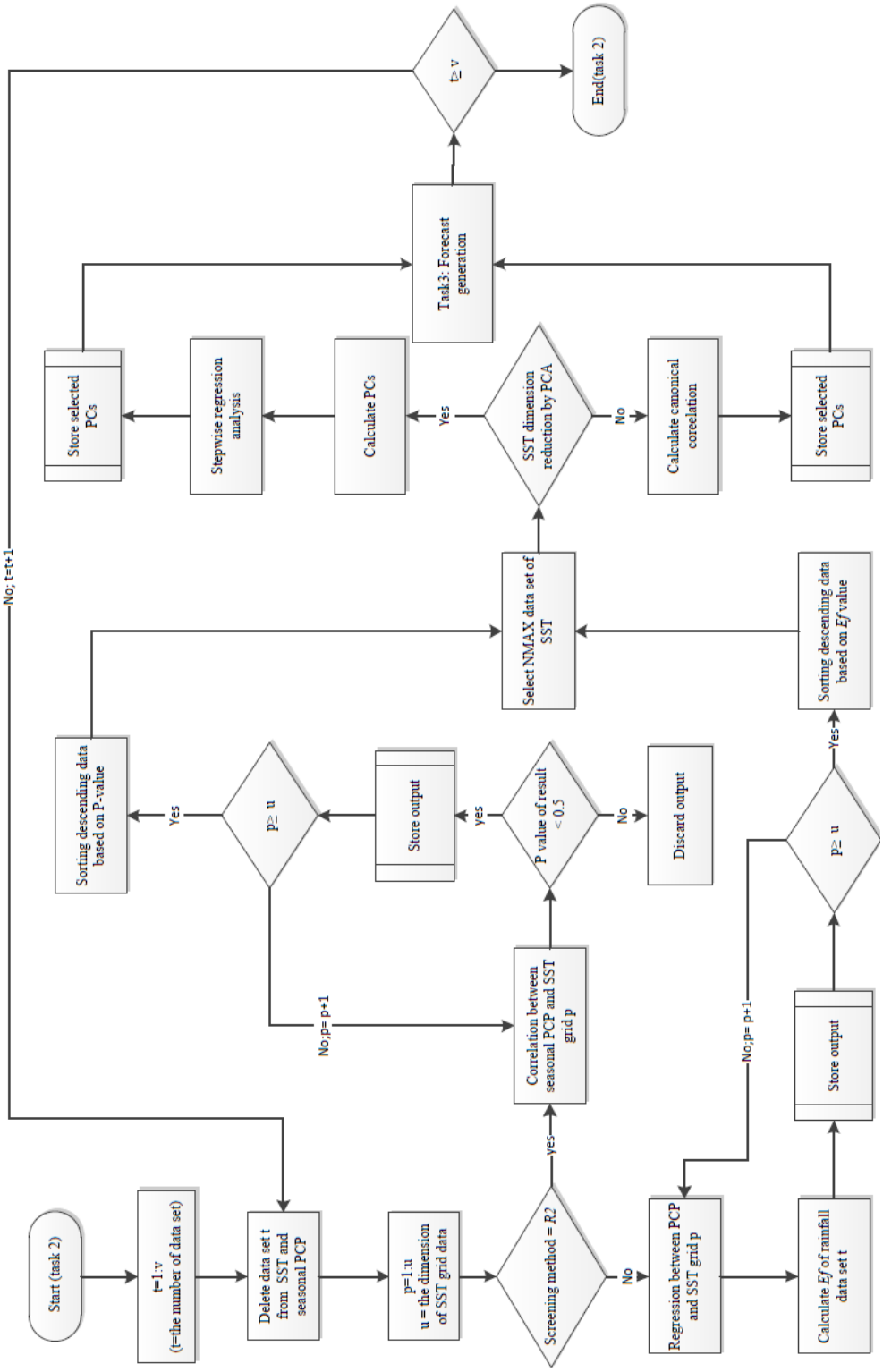

Figure 5.15: SST dimension reduction procedure

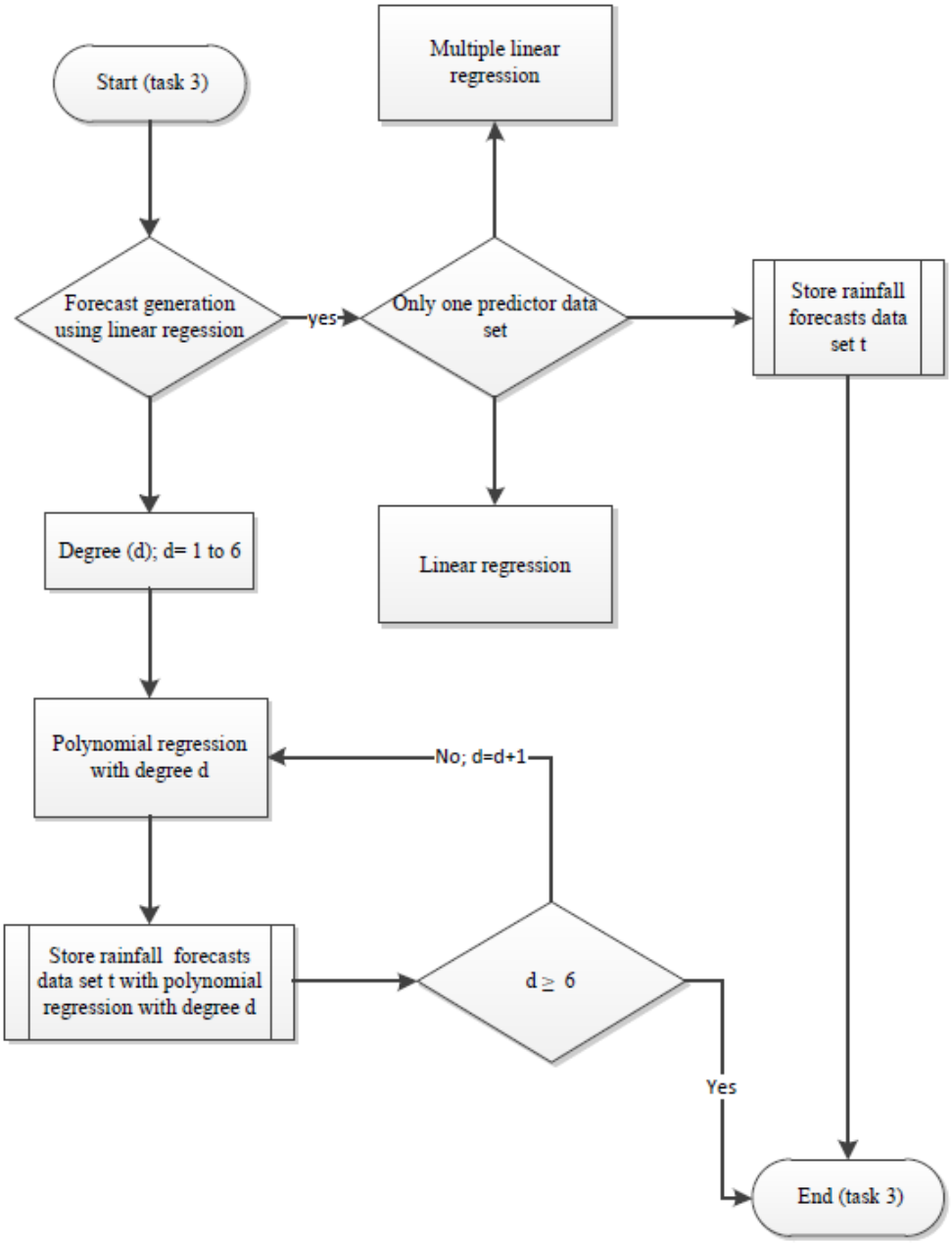

Figure 5.16: Forecast Generation

indicates all the months from January of the previous year (Y-1) to June of the year the forecast is issued (Y). For example, in the first run only the SST of January (Y-1) was selected a predictor. The SST average over January and February (Y-1) was used as a predictor in the second run. This process was repeated at one month increment until June (Y) was reached as the end of the period. Then, the SST of February (Y-1) was used as a predictor followed by the SST average over February and March (Y-1). The process was iterated until only the SST of June (Y) was used.

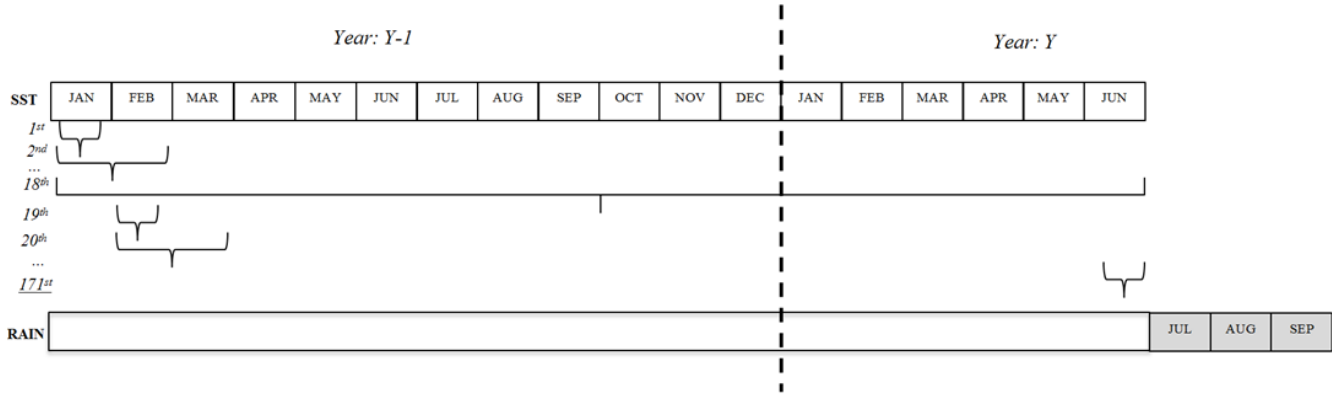

Figure 5.17: SST averaging periods

5.4.3 Streamflow forecasting using the indirect method

The section clarifies the methodology used to forecast streamflow with a physically based model. Three main steps used to develop streamflow forecasts by SWAT are discussed: 1) generation of rainfall forecasts, 2) temporal disaggregation technique and 3) SWAT model operation.

5.4.3.1 Generation of rainfall forecasts

This simulation employed daily local rainfall observations in the Sirba basin as predictands and monthly SSTs as predictors. Seasonal rainfalls during July to September (JAS) of the entire period (1960 to 2006) were considered for use in the statistical models. SST averaging periods to be used as predictors were prepared as described in Section 5.4.2, which meant there were 171 predictor data sets for each SST region, with different periods from January of the previous year until June of the year the forecasts were issued.

Consequently, 171 seasonal rainfall forecasts (JAS) were produced using each statistical model with only one N_{max}. As stated above, the N_{max} value was determined in order to define the number of SST grid data to be used to drive the model. A number of N_{max} from 10 to 200 with 10 increments were put in the model for each run. Thus, 3,420 seasonal rainfall forecasts were developed with each statistical model and SST region for all N_{max} values.

All 3,420 forecasted rainfall time series were evaluated to determine the most accurate rainfall forecast developed by assessing each SST region with three objective functions: E_f, R^2 and H. Though all three criteria were applied to measure model accuracy, E_f was the key function used to select the best simulation as it is specifically designed for estimating model performance with continuous variables and can indicate the difference in magnitude between observations and simulations. The four generated seasonal rainfall time series developed with either linear or non-linear regressions, and the Pacific or Atlantic SSTs that showed the highest E_f were processed in the next step.

5.4.3.2 Temporal disaggregation technique

SWAT uses only daily or sub-daily precipitation data for hydrologic simulation, so the seasonal forecasted rainfalls temporal resolution had to be increased to a daily scale. This was done using the fragment method, which is the simplest method for temporal disaggregation. A difficulty of this technique is selecting the proper fragment series to generate the most accurate daily rainfall. The fragment series was multiplied with seasonal rainfall forecasts, there by producing daily rainfalls for a given year. Three fragment series were generated using three different methods, and the best one for producing daily rainfall forecasts corresponding to observations was applied to prepare the data for the SWAT model in the next step.

a) Fragment series selection (F-I): This fragment series generation is based on the original fragment method proposed by Harms and Campbell (1967). First, the average daily rainfall observations over the Sirba basin were calculated using the Theissen polygon method, then the average daily rainfalls from July to September were aggregated to convert the time scale from daily to seasonal. With the exception of year i, the forecasted seasonal rainfall of all years ($SR_{sim,yi}, i = 1, 2...n$; n being the number of years in the study period) was compared to observed seasonal rainfalls. The year j ($j = 1, 2...n-1$) showing the amount of observed seasonal rainfall ($SR_{obs,yj}$) closest to $SR_{sim,yi}$ was selected to compute the fragment series,

which can be generated by dividing the observed daily rainfall of year j ($DR_{obs,yj}$) by$SR_{obs,yj}$. All fragment series were then multiplied with $SR_{sim,yi}$ and daily forecasted rainfalls of year i ($DR_{sim,yi}$) were simulated. These processes were repeated until all seasonal rainfall forecasts were changed to daily time scales. Since this method was based on areal average rainfall observations, only one rainfall time series was produced.

b) Fragment series selection II (F-II): This method did not apply the Theissen polygon in the first step, but daily rainfall observations from all stations were considered for the fragment series calculation. These daily rainfall observations from July to September were aggregated to a seasonal scale, and $SR_{sim,yi}$ was compared to the seasonal observed rainfalls of all years (except year i) and all stations. The seasonal observation of a given year and a given station ($SR_{obs,yj,stk}; j = 1, 2...n-1$ and $k = 1, 2...m$; m being the number of station) showing the closest rainfall amount to $SR_{sim,yi}$ was used to calculate the fragment series. The ratios of fragment series were computed by dividing the observed daily rainfall of year j station k ($DR_{obs,yj,stk}$) by $SR_{obs,yj,stk}$. Daily rainfall simulation of year i ($DR_{sim,yi}$) were then constructed by multiplying the forecasted seasonal rainfall with the fragment series. These processes were repeated until the time scales of the rainfall simulations of all years were increases to daily rainfall. Only one time series of daily rainfall was produce by this method.

c) Fragment series selection III (F-III): The Theissen polygon was applied to generate areal average daily rainfall observations in the basin, then seasonal rainfall observations (July to September) were computed. Similar to the method F-I, the differences in seasonal rainfall simulations of a given year ($SR_{sim,yi}$) and seasonal rainfall observations of the entire period except year i were calculated, and the year with the least difference between seasonal forecast and seasonal observation was selected for fragment series calculation. Then, daily rainfalls of all stations of the selected year were computed for the fragment series by dividing $DR_{obs,yj,stk}$ by the corresponding observed seasonal rainfall $SR_{obs,yj,stk}$. Daily rainfall forecasts of year i for all stations were generated by multiplying ($SR_{sim,yi}$) by the fragment series of all stations. These steps were repeated until the forecasted seasonal rainfalls of all years were calculated. Thus, the number of disaggregated daily rainfall series generated with this method depended on the number of stations in the basin.

One time series of seasonal rainfall forecast was tested using all the above selection methods. The fragment method producing the best disaggregated forecasts showing high agreement with daily observations was selected for all rainfall forecasts generated by either linear or non-linear regression and either the Pacific or Atlantic SSTs.

5.4.3.3 SWAT model application

This section provides the details related to streamflow generation using SWAT. The ArcSWAT, an ArcGIS-Arcview extension user input interface for SWAT, was primarily used to generate all relevant files. Similar to most rainfall-runoff models, SWAT requires an initial calibration process to determine the most suitable values of significant parameters for the basin. The steps of parameter generation for streamflow simulation using ArcSWAT are first described, followed by the calibration process using observed rainfalls as an input layer. Finally, the model with the optimal value of sensitive parameters was applied to forecast flows using the daily rainfall forecasts rather than observed rainfalls, and all outputs were compared. Figure 5.18 schematically displays the processes for generating the SWAT model for the Sirba watershed.

a) SWAT simulation This section explains the procedures used to generate the input/output files of the SWAT model for use in the Sirba basin, including the approaches for running the model and sensitivity analysis application for streamflow generation. Details of all processes used in ArcSWAT can be found in Winchell et al. (2007).

- **Watershed delineation:** This tool was used to automatically delineate sub-watersheds for the basin based on DEM data. Stream networks and outlets of sub- basins are generated using the watershed boundary and the spatial data of rivers in the basin. Then the outlet of the entire watershed is defined. The reservoirs in the basin are added manually. The information of study area identified five dams in the Sirba basin, and they were also added in this step. Ultimately, nine sub-basins were created by this process (Figure 5.2)
- **HRU analysis:** Hydrological response unit (HRU) is the combination of unique land use, soil and slope in the sub-basin which is a lumped land area. The HRU analysis function in ArcSWAT was used to overlay these three classifications in order to determine HRUs and their distributions for each sub-basin in the watershed. The hydrologic parameters for each HRU are

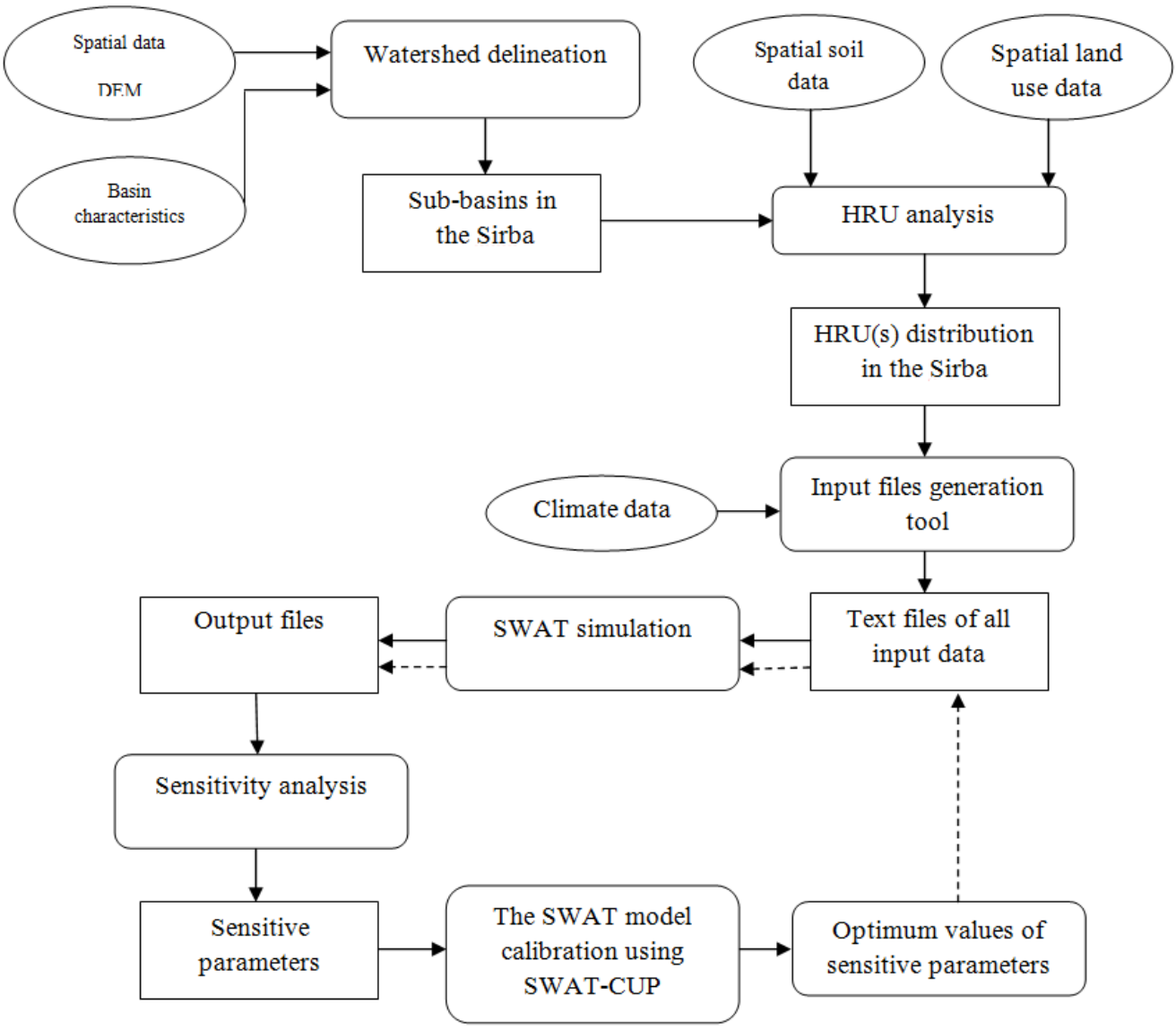

Figure 5.18: The SWAT model generation for the Sirba basin

different. The spatial maps of land use, soil and DEM of the Sirba basin from Section 5.2 were uploaded to ArcSWAT. 34 HRUs were generated for the nine sub-basins in the Sirba watershed (Figure 5.19)

- **Import weather data:** This tool was used to import five climate variables in the basin to the model (i.e. rainfall, temperature, relative humidity, radiation and wind speed). In the first step, the latitude and longitude of the weather stations were put into the model, then the weather data were introduced in ArcSWAT. A time scale of rainfall data needed to be defined. Since each climate variable had a different time period. All missing values in the climate data sets were replaced with the values generated using the weather generator. In the first simulation only observed data were forced to SWAT in order to prepare all required input files for continuous use in the calibration process.
- **Input file generation:** Database files containing all the information required for SWAT were first built, then 15 main groups of input files (below) were generated. The number of files in each group depends on how many sub-basins and HRUs are created in the basin; details of input files can be found in Neitsch et al. (2004). As the Sirba watershed had nine sub-basins and 34 HRUs, more than 200 input files were developed in this study.
  - Configuration file (.fig)
  - Soil data (.sol)
  - Weather generator data (.wgn)
  - Sub-basin general data (.sub)
  - HRU general data (.hru)
  - Main channel data (.rte)
  - Groundwater data (.gw)
  - Water use data (.wus)
  - Management data (.mgt)
  - Soil chemical data (.chm)
  - Pond data (.pnd)
  - Stream water quality data (.swq)
  - Watershed general data (.bsn)
  - Watershed water quality data (.wwq)
  - Master watershed file (.cio)

- **Running SWAT:** Output files can be generated using either the ArcSWAT interface or the SWAT model formatted in a command line tool. The period of simulation including the time scale of output needs to be defined. After successfully running the SWAT model, the following seven output files were constructed (see Neitsch et al. (2004)). All the input and output files were automatically saved in the TxtInOut folder, a key repository for the calibration process.
  - The input summary file (input.std)
  - The output summary file (output.std)
  - The HRU output file (output.hru)
  - The sub-basin output file (output.sub)
  - The main channel output file (output.rch)
  - The HRU impoundment output file (output.wtr)
  - The Reservoir output file (output.rsv)
- **Sensitivity analysis:** This function is available after creation of the TxtInOut. It consists of three groups of parameters, flow, sediment and water quality, that can be evaluated in the sensitivity analysis application. Since this study focused on the discharge in the Sirba watershed, only parameters relating to flow data were considered. The ten most sensitive parameters and their ranges are shown in Table 5.2. For example, the first parameter influencing flow generation was CN2, the moisture condition II curve number. It is used to calculate a retention parameter, which is continuously applied to the accumulated runoff in the basin. This parameter is significant only when the SCS curve number procedure is applied. All these sensitivity parameters were closely monitored in the calibration process discussed in the next section.

b) Calibration process To generate more accurate simulations with SWAT, the model needs to be calibrated to find the optimal values of parameters describing the Sirba basin behavior; to do this the SWAT Calibration and Uncertainty Program (the SWAT-CUP) was applied for this purpose. This model has been widely used to calibrate SWAT model (e.g. Masih et al., 2001, Jajarmizadeh et al., 2013, Wang et al., 2014).

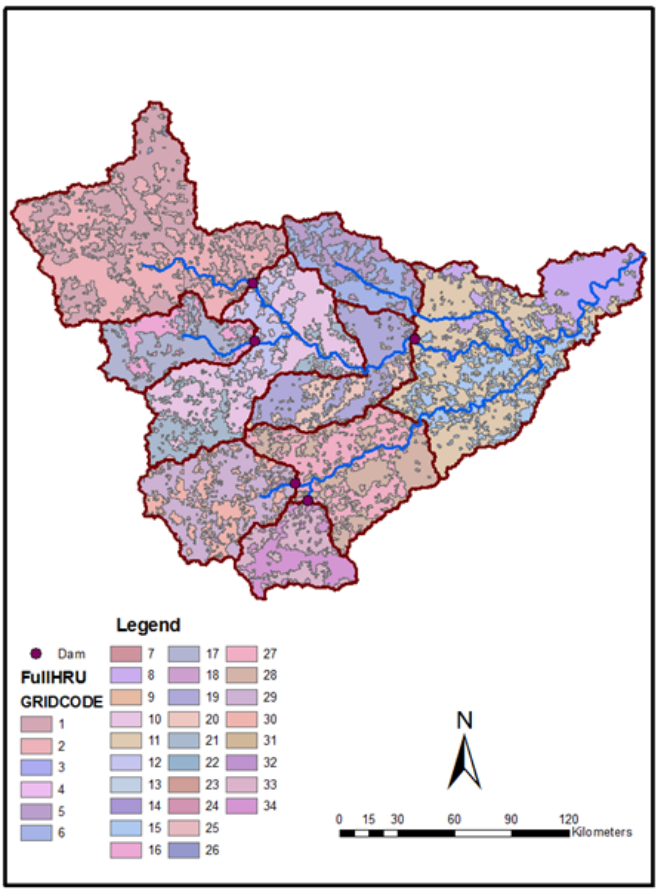

Figure 5.19: HRU classification in the Sirba basin

Table 5.2: Ten most sensitive parameters of the SWAT model for streamflow in the Sirba watershed

Parameter	**Variable name in SWAT**	**Range**
Moisture condition II curve number	CN2	20-90
Soil evaporation compensation coefficient	ESCO	0.01-1
Available water capacity of the soil layer	SOL_AWC	0-1
Depth from soil surface to bottom of layer (mm)	SOL_Z	0-3500
Threshold water level in shallow aquifer for base flow (mm H2O)	GWQMN	0-5000
Effective hydraulic conductivity (mm/hr)	CH_K2	0-150
Maximum canopy storage (mm)	CANMX	0-100
Threshold depth of water in the shallow aquifer for revap to occur (mm)	REVAPMN	0-500
Potential maximum leaf area index for the plant	BLAI	0-12
Surface runoff lag coefficient	SURLAG	1-24

As mentioned in the previous section, for this step SWAT-CUP requires the TexInOut folder containing the input/output files generated with ArcSWAT. Sequential Uncertainty Fitting (SUFI2) in the SWAT-CUP was performed for model calibration. This method considers all potential sources of model uncertainties including input data, conceptual models and parameters (Abbaspour, 2013). The value of the ten parameters shown in Table 5.2 were adjusted based on their ranges. The required information that must be specified for each run is as follows.

- Number of parameters
- Number of simulations
- SWAT output file name
- Number of interesting variables (Flow variable for this study)
- Total number of sub-basins
- The beginning/end years of simulation
- Observed data (Flow observation for this study)

The steps used to calibrate the model are briefly described below:

1. As an example, in the par_inf.txt the most sensitive parameter (CN2.mgt) was put in the model. The number of parameters and the number of simulations for the first run were 1 and 500 respectively.
2. In the SUFI2_swEdit.def, again the first and last simulation numbers were defined for example at 1 and 500 respectively.
3. In the Observed_rch.txt, the streamflow observations at the outlet of Sirba basin from 1989 to 2002 were determined. Missing values were deleted, and the final number of data was indicated.
4. In the SUFI2_extract_rch.def, a SWAT output file name was defined. For example, this study is focusing on the stramflow simulation which is in the output.rch file. The list of information required in the SUFI2_extract_rch.def is as follows:
   - The number of variables for the simulation.
   - The column number of the variables in the SWAT output file.
   - The total number of sub-basins.

- The number of sub-basins for the variables.
- The beginning and the end years of simulation.
- The time step of the simulation must be determined.

5. In the observed.txt, the streamflow observation has to be put in the model again. SWAT-CUP requires determination of objective function used to estimate simulations. This study used E_f as the criterion.
6. After carefully following the above steps, SUFI2_pre.bat was run. A Successful running message indicates that there are no errors in all relevant files. SUFI2_run.bat was applied in the next step for model calibration and then SUFI2_post.bat was performed.
7. Calibration outputs are presented in various files. Summary_Stat.txt shows statistics of the best simulation corresponding to the threshold and objective function selected in step (5). The best_Par.txt shows the values of specified parameters.

A number of simulations was arbitrarily set for each parameter and the optimum value was estimated using E_f, then the most favourable value of each parameter was assigned to the model. The best model had R^2 and E_f of 0.83 and Hit score (H) of 86%. Figure 5.20 illustrates outputs of model calibration comparing to observed streamflows from 1989-2002.

c) Forecasted streamflow generation: Streamflow forecasts were generated with daily rainfall forecasts driving the SWAT model, and the optimum values of parameters obtained from the calibration process were used in the model. Four sets of forecasted daily rainfall forecasts using either SST region or regression method were considered to force to the model. Other climate variables, including spatial data used in the first run, were retained for use as input variables. Consequently, the number of months in advance that river flow was forecasted depending on the lead time of corresponding forecasted rainfall. Finally, the reliability and accuracy of all simulations were estimated using E_f, R^2 and H, and the results were compared to the direct method discussed in the following section.

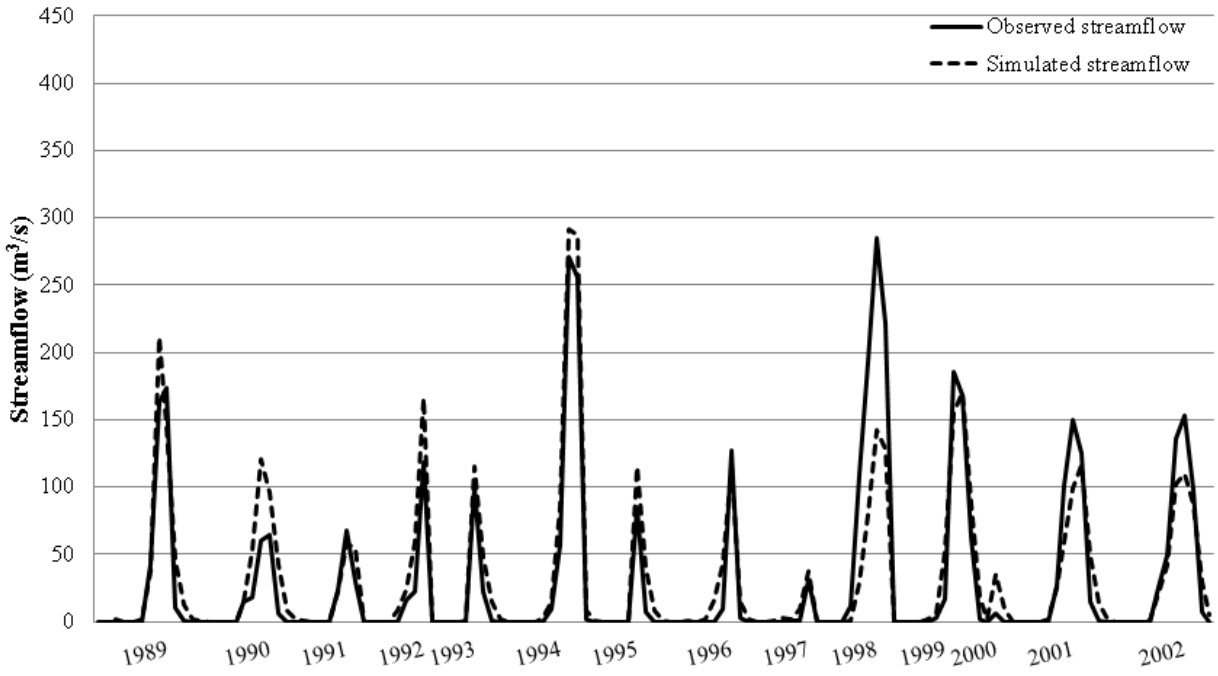

Figure 5.20: Hydrographs of forecasted streamflows developed by the calibration process compared to observations

5.4.4 Streamflow forecasting using the direct method

Though SWAT can manage the physical interactions between climate, land and river channels to generate streamflows in the basin, it requires significant amount of climate data and basin characteristics. As the high computational cost of calibration can constrain seasonal streamflow forecasting, statistical applications are another option to directly forecast river flows. In this study, the statistical models explained in the Section 5.4.1 were applied to predict streamflows, with SSTs of both regions (the Pacific and Atlantic Oceans) used as predictors and observed flows as predictands. Each SST data set driven the model was prepared using all steps in Section 5.4.2. Streamflows were directly modeled without taking the characteristics and physical processes of the basin into account. This application was similar to that described in Section 5.4.3 (Generation of rainfall forecasts) except for a difference in a predictand data set. The total number of forecasted streamflow time series was equal to the number of forecasted rainfall time series. Only the best outputs constructed with either linear or non-linear regressions from both predictors (Pacific and Atlantic SSTs) were used. They were then disaggregated from seasonal to monthly forecasted flows in order to compare their performance to the indirect method.

5.4.5 Uncertainty analysis

The accuracy and reliability of streamflow prediction depends on various factors, including, input data, model parameters and model structure, and model errors are largely due to the inherent uncertainties of these factors. Typically, a decision maker requires not only deterministic simulations but uncertainty estimates as well, which are represented by the model prediction interval (Shrestha and Solomatine, 2008). Integrating the simulations and uncertainty estimates can enhance the capability of simulated data for to act as a warning system, and contribute to water resource management policy in the future. In this study, the basic technique used to estimate the prediction interval base on the analysis of the model errors was applied. In addition, the performance of Bayesian model averaging (BMA) to decrease uncertainty due to model selection was also assessed.

5.4.5.1 Uncertainty analysis based on the analysis of model error

The framework discussed in this section was extended to provide information about uncertainty in the forecasted precipitation (for the indirect method) and streamflow (for the indirect and direct method). For the indirect method, it was assumed that the forecasted precipitation would follow a normal distribution with the mean being the estimate of the seasonal forecasting precipitation and the standard deviation being the standard deviation of the residuals. This assumption allowed the calculation of n equiprobable values of the total precipitation by taking n annual precipitation values with exceedance probability 1/2n, 3/2n, ..., (2n - 1)/2n, given the previously defined probability distribution of the forecasted annual rainfall. Each value was disaggregated and fed into the SWAT model of the Sirba watershed, resulting in n hydrographs representing the uncertainty in the hydrologic forecast. A histogram displaying the relative probability of various flow magnitudes can be plotted, and if n is large enough, the probability distribution of future flow could be also plotted. The same methodology was applied for the flow forecasts developed by the direct method. After the forecasted flow was successfully generated using the statistical models, n hydrographs were directly constructed. The uncertainty boundary was created, and model uncertainties could be evaluated by considering the observed flows in the range of these bands.

5.4.5.2 Bayesian model averaging

Forecasting model applications that employ regression analysis usually select optimal predictors and parameters by applying the maximum likelihood technique in a training period. However, other predictors should not be ignored as considering all predictors might lead to higher reliability forecasts, and give decision-makers higher confidence to use the forecasts for water resource management. The Bayesian model averaging (BMA) approach can overcome this issue, as it allows users to apply all predictors in the process. An important benefit of the BMA approach is the capability to produce predictive density of expected value and the standard error calculated from all models. It helps an end-user visualize the expected value compared to the observation, and get an indication of the range of the response variable. The level of uncertainty can be establish from the outputs. The posterior probability of each model is typically generated based on the prior and likelihood functions of the model; BMA combines all models to generate posterior model distribution. Each model is weighted by its posterior model probability, and the final outcome of BMA is a probabilistic forecast that can represent a forecasting uncertainty.

Feldkircher and Zeugner (2009) developed a BMA package called BMS, which is well used in statistical software known as R. Unlike regression statistics, BMA allows a user to develop forecasts from all models in the model space. Similar as using the statistical models, 171 aggregate periods were considered. Thus, the total number of independent variables for streamflow prediction were 2,520x171 and 950x171, which can be used to build models of $2^{(2{,}520x171)}$ and $2^{(950x171)}$ for the Pacific and Atlantic SSTs respectively. Due to the extremely large number of models, several preprocessing steps were taken to decrease them to an amount that is manageable using BMA. The overall process used to develop the BMA model is illustrated in Figure 5.21. In order to avoid overestimation, the cross-validation method was employed throughout the BMA process.

Let M1_1, M1_2, M1_3, ... , M18_18 denote aggregate SST period over January(Y-1), January(Y-1) to February(Y-1), January(Y-1) to March(Y-1) , ..., June(Y) respectively.

i Reduction of the predictor set by selecting grid points with high predictive power

For each period of SST:

(1) All variables, each corresponding to a grid point and an averaging period, were screened by assessing their linear relationships with observed streamflow. Only variables strongly corresponding to observations with P-value less than 0.05 were selected.

(2) PCA was applied to the remaining variables and PCs were generated. Only the first PC (PC1) that accounts for the highest variance of data was collected for use in the next step.

(3) These above two steps were repeated until all 171 periods were addressed. Finally, the number of predictor was decreased to 171 variables.

ii Due to the large number of predictor, there were 2^{171} models combinations in the model space. All data were collected into 18 groups with each group containing predictors obtained by averaging SST over a particular month. For example, M1 _1, M1_2, ..., M1_18 were in the first group (G1). M2_2, M2_3,..., M2_18 were in the second group (G2), and so on. G1 consisted of the highest volume of predictors with 18 data sets, while G18 had only one predictor (X18_18) Ultimately, 18 groups of predictors were prepared to be used in BMA.

iii For each group (G1 to G18):

(1) All variables were fed into BMA with a uniform prior probability condition to ensure even allocation of their initial credibility. Posterior model probability (PMP) was analytical for every variable in all models. All PMP values from all modes were totaled, an action known as the posterior inclusion probability (PIP). Higher PIP values highlight the predictors that are included in posterior models more often, and thus are more important than those with lower PIP values.

(2) To develop predictive density two types of BMA models (BMA1 and BMA2) were tested, based on the criteria for selecting final predictors:

- **BMA1:** The variable with the highest PIP was selected for developing the predictive density distribution.
- **BMA2 :** Since the top variables in some groups might have low PIP values, selecting only the highest PIP variables could lead to unintentionally discarding meaningful variables, or keeping those with low PIP values in the process. Thus, only variables with PIP above 0.6 were arbitrarily selected in order to keep only high potential predictors in the process.

(3) This process was repeated until all 18 groups were implemented.

BMA1 and BMA2 were applied with a uniform prior probability, and predictive density distributions were then developed. The expected value, variance and model size distribution, representing the average number of prior and posterior predictors, were generated.

5.4.6 Estimation of economic value of streamflow forecast

This section discusses the methodology used to assess the economic value of forecasts developed by indirect and direct methods. The basic cost/loss ratio method was employed with different situations. Before estimating the potential benefits of streamflow forecasts, specific thresholds need to be specified in order to measure the value of forecasts based on each adverse event. The basic concept used to calculate the frequency analysis for hydrology follows, then the steps used in the cost/loss ratio method are examined.

Frequency analysis is a technique used to estimate the probable frequency of occurrence of a given extreme event. In this study, the exceedance probabilities of streamflow were arbitrarily defined as 0.5, 0.2 and 0.1; corresponding to a 50%, 20% and 10%

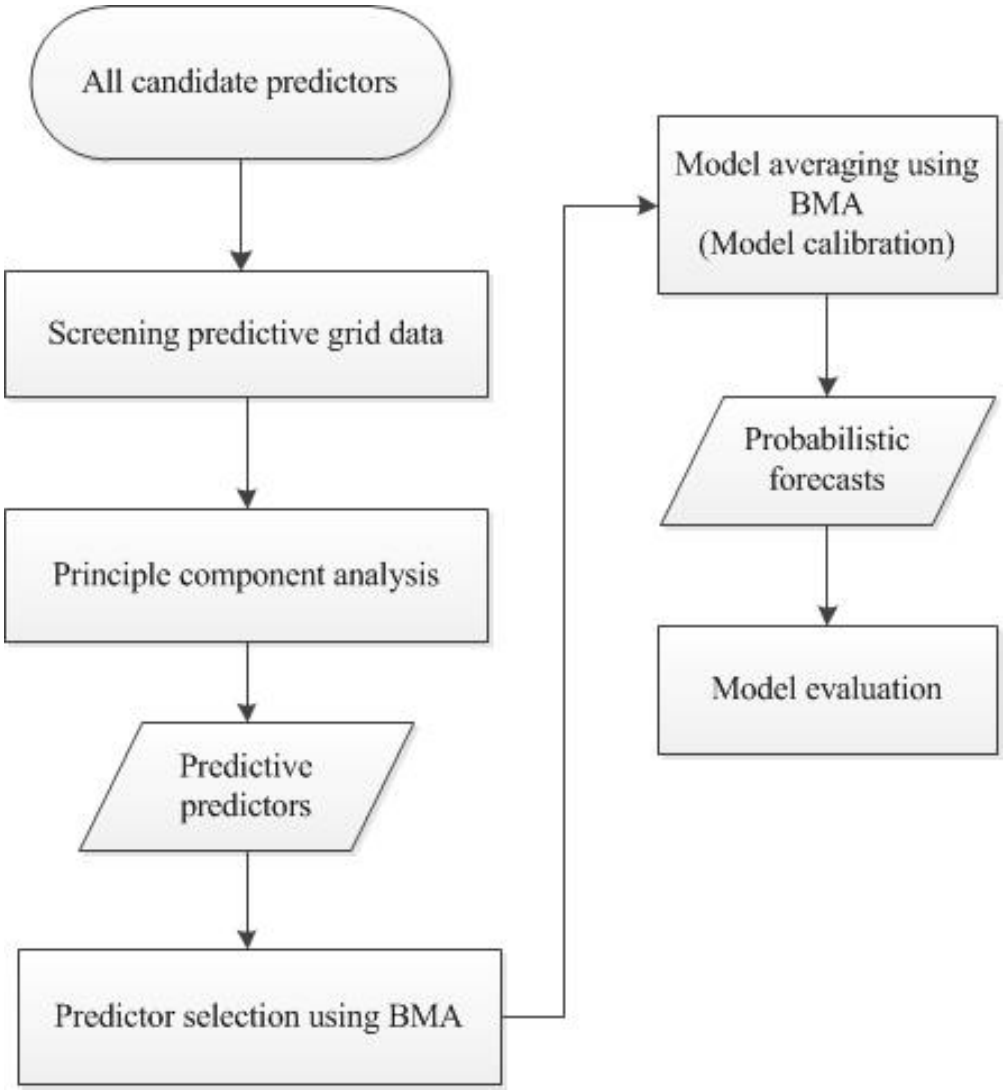

Figure 5.21: Forecast generation using BMA

chance of occurring in a given year. The recurrence intervals, also known as return periods, of these exceedance probabilities were 2, 5 and 10 year respectively. To estimate the streamflow value for each return period, the probability distribution must initially fit the observations. The most widely used distributions in hydrologic analysis are the log-normal, the log-Pearson Type III and the normal distribution (McCuen, 2005). However, in this study 11 distributions were tested in order to ensure the most fitting distribution for the Sirba streamflow. Table 5.3 shows the characteristics, parameters and probability density functions of 11 distributions. As suggested by Rao and Hamed (2000), a Chi-Square test was applied to estimate the flood frequency.

The Chi-Square test (χ^2) measures how well observed data and expected data generated from a specific theoretical distribution fall in the same class interval. The range of χ^2 is in between 0 to ∞ while $\chi^2 = 0$ indicating that observations and expected frequencies agree precisely. Equation 5.1 shows the method used to calculate χ^2. O_j and E_j are the observed and expected number of events in the class j and k is an arbitrary number of classes (Rao and Hamed, 2000).

$$\chi^2 = \sum_{j=1}^{k} \frac{(O_j - E_j)^2}{E_j} \tag{5.1}$$

After obtaining the specific distribution effectively described the sample streamflow, the specific flow values the 2, 5 and 10 year return periods can be defined.

Continuous forecast data were converted to categorical data based on the flows of the 2, 5 and 10 year return periods. Ten uncertainty data series based on normal distributions of forecast results were also calculated and added to the contingency table to account for forecast uncertainty. A number of data falling into each group were counted and used to calculate economic values.

The cost/loss ratio model was then used to calculate the economic values of the forecasts. Both those generated using the direct method and the SWAT model were evaluated for their economic benefits. Equation 5.2 is the formula used to compute a forecasting value.

$$V = (E_{climate} - E_{forecast})/(E_{climate} - E_{perfect}) \tag{5.2}$$

V is the economic value of forecast system and it can be defined as the ratio of the reduction in mean expense to the reduction of expense when perfect forecasts are accessible (Richardson, 2012). $E_{climate}$ can be obtained by considering the minimum of either cost of protective action (C) or the multiplication of the climatological base rate

Table 5.3: Characteristics, parameters and PDF of eleven probability distributions

Distribution	**Characteristics**	**Parameters**	**PDF**
Normal	Symmetric distributio	μ, σ	$f(x) = \frac{1}{\sigma\sqrt{2\pi}} exp[-\frac{1}{2}(\frac{x-\mu}{\sigma})^2]$
Log normal	Positively skewed; used when the logarithm of the data is normal	μ, σ	$f(x) = \frac{1}{x\sigma\sqrt{2\pi}} exp[-\frac{1}{2}(\frac{lnx-\mu}{\sigma})^2]$
Three parameters log normal	Positively skewed	a, b, c	$f(x) = \frac{1}{(x-a)c\sqrt{2\pi}} exp(\frac{-[ln(x-a)-b]^2}{2c^2})$
Exponential normal	Positively skewed	a	$f(x) = \{ae^{-ax}, x \geq 0 \text{ or } 0 \leq 0$
Pearson type III	Positively skewed	a, b, c	$f(x) = \frac{1}{a\Gamma(b)}(\frac{x-c}{a})^{b-1} exp(-\frac{x-c}{a})$
Gamma	Positively skewed	a, b	$f(x) = \frac{1}{b^a\Gamma(a)} x^{a-1} e^{\frac{-x}{b}}$
Logistic	Symmetric distribution	μ, σ	$f(x) = \frac{1}{\sigma} * \frac{e^{-(x-\mu)/\sigma}}{(1+e^{-(x-\mu)/\sigma})^2}$
Generalized logistic	Positively or negatively skewed relying on k	k,σ, μ	$f(x) = \frac{(1+k(\frac{x-\mu}{\sigma})^{-1}\frac{-1}{k})}{\sigma(1+(1+k(\frac{x-\mu}{\sigma})^{-1/k})^2)}$
Extreme value	Negative skewed	μ, σ	$f(x) = \sigma^{-1} exp(\frac{x-\mu}{\sigma}) exp(-exp(\frac{x-\mu}{\sigma}))$
Generalized Extreme value	Positively or negatively skewed relying on k	ξ,μ, σ	$f(x) = \frac{1}{\sigma}(1 + \xi z)^{\frac{-1}{\xi-1}} exp(-[1 + \xi(\frac{x-\mu}{\sigma})]^{\frac{-1}{\xi}})$
Generalized pareto	Positively skewed	k, σ, θ	$f(x) = (\frac{1}{\sigma})(1 + k\frac{(x-\theta)}{\sigma})^{-1-\frac{1}{k}}$

probability (s) and expense of loss (L) for each event [$E_{climate} = min(C, sL)$]. $E_{forecast}$ is the likelihood base rate probabilities [$E_{forecast} = F(1-s)C - Hs(L-C) + sL$]. $E_{perfect}$ is the mean expense of the action would be taken when the extreme event was going to occur [$E_{perfect} = sC$] (Richardson, 2012) . In this study, we varied the cost/loss ratio ranged from 0 to 1, since decision makers would not take a protective action if the cost was greater than the potential loss (Richardson, 2012). The economic values of both forecasts are discussed in the next section, and the ranges of cost/loss ratio referring to positive values of forecasting system were also clarified.

Chapter 6

Results

This chapter presents and discusses the results obtained from this research study. It is organized in five sections: 1) streamflow forecasting using the indirect method; 2) streamflow forecasting using the direct method; 3) a discussion of the advantages and disadvantages of both the indirect and direct approaches for streamflow forecasting; 4) quantification of the forecast uncertainty; and 5) estimation of the economic value of the forecasts. The main findings for each topic are summarized at the end of the related section.

6.1 Seasonal streamflow forecasting using the indirect method

The purpose of this section is to analyze the performance of the indirect approach, which consists of three steps:

1. Seasonal rainfall forecasting using statistical models.
2. Temporal disaggregation of the forecasted rainfall to the daily time step.
3. A rainfall-runoff transformation using the SWAT model.

The indirect method was applied using two different pools of predictors (the Atlantic or the Pacific SSTs), two different screening methods (using R^2 or E_f) to select a limited number of grid points), two different predictor dimension reduction techniques (CCA or PCA) and finally two type of relationships (simple/multiple linear regressions or polynomial regressions of degree two to six). All possible combinations of steps to generate

Table 6.1: Statistical models for seasonal streamflow forecasting using the indirect method

Model class	**Screening process**	**Predictor dimension reduction**	**Link between predictor and seasonal rainfall**	**Temporal diaggregation**	**Rainfall-runoff conversion**
I	R^2	PCA	Simple/multipl linear regression	The fragment method	The SWAT model
II	E_f	PCA	Simple/multiple linear regression	The fragment method	The SWAT model
III	R^2	CCA	Simple/multipl linear regression	The fragment method	The SWAT model
IV	E_f	CCA	Simple/multipl linear regression	The fragment method	The SWAT model
V	R^2	PCA	Polynomial regression	The fragment method	The SWAT model
VI	E_f	PCA	Polynomial regression	The fragment method	The SWAT model
VII	R^2	CCA	Polynomial regression	The fragment method	The SWAT model
$VIII$	E_f	CCA	Polynomial regression	The fragment method	The SWAT model

a forecast using the indirect method after the predictor pool was chosen are shown in Table 6.1. Each combination (referred herein as a model class) is given a number from I to $VIII$ and will be referred in the remainder of as model XXX where XXX is the number assigned in Table 6.1. Model XXX_p will refer to the best model of class XXX using the Pacific ocean as a predictor; model XXX_a will refer to the best model of class XXX using the Atlantic ocean as a predictor.

Because of the large number of individual models in each class (one model is build for each potential predictor: refer to Chapter 5, Section 5.4.2), only the best one (i.e the one that led to the best values of E_f, R^2 and H) for a model class is discussed. For a given pool of predictors (i.e the Atlantic or the Pacific SSTs), two forecasted rainfall time series (generated with the best linear model and the best polynomial model) were used to drive the SWAT model of the Sirba watershed.

6.1.1 Seasonal rainfall forecasting using linear models

This section focuses on the use of simple/multiple linear regression models for seasonal rainfall forecasting. Even though there is no conceptual reason to have a linear relationship between rainfall and SST, linear models are appealing because of their simplicity. Either simple or multiple linear regressions was used at the final step depending on whether one or several predictors were obtained after the screening and dimension reduction steps. Only the best model in each class and each pool of predictors (Atlantic or Pacific oceans) was examined.

a)Models using the Pacific SST as pool of predictor: The Pacific SST data set had 2,520 grid points. At each grid point, a time series of monthly SST from 1970 to 2003 was available. The time series at each grid point were aggregated over various time periods (as described in Chapter 5, Section 5.4.2). Screening and predictor dimension reduction steps (using values of N_{max} from 10 to 200 with increments of 10) were performed for each period to obtain the inputs for a model. The best rainfall forecasts which yield the best value of E_f was retained.

As it is clear in Table 6.2, models that use PCA for predictor dimension reduction (models I_p and II_p) perform significantly better than those models using CCA (models III_p and IV_p). A positive value of E_f was obtained whenever PCA was used; the use of CCA on the other hand always led to a negative value of E_f . The best rainfall forecast was obtained with model II_p using the average from March to June SST (Y-1) as predictor. This was achieved by using N_{max}=90 (i.e. a maximum

of 90 grid points were retained after the screening process). The performance of model II_p was $E_f = 0.39$, $R^2 = 0.46$ and $H = 67\%$. The first principal component (PC) that accounted for around 42 to 83% of the variance of the reduced predictor data set was always selected in stepwise regression analysis. The best performance achieved with model I_p was $E_f = 0.26$, $R^2 = 0.38$ and $H = 50\%$ using the average SST from February(Y) to March(Y).

The two statistical models that used CCA for predictor dimension reduction (models III_p and IV_p) yielded negative values of E_f (-3.91 for model III_p used SST averaging period of May (Y-1); -2.18 for model IV_p used SST averaging period of April (Y-1)) and therefore had no value for seasonal forecasting.

Figure 6.1 shows the time series of observed and forecasted rainfall on the Sirba watershed, with the upper and lower panels displaying forecasts generated using models that used PCA (models I_p and II_p) and CCA (models III_p and IV_p) as dimension reduction technique respectively. Figure 6.1 (a) shows that forecasts issued with model I_p were generally consistent with the observed precipitation, except for 1975, 1982 and 1988 when a discrepancy between observations and predictions was obvious, and 1994 when the forecast significantly underestimated the highest rainfall observation. The performance of model II_p was similar to that of model I_p, with the outputs largely agreeing with the observations for the entire period, except in 1994 when it could not capture the magnitude of the observed precipitation. Figure 6.1 (b) shows that the agreements between observations and simulations developed using models III_p and IV_p were clearly lower than those generated using models I_p and II_p. Model III_p systematically under-predicted precipitation on the Sirba watershed and model IV_p clearly showed large simulation errors.

b) Models using the Atlantic SST as pool of predictors: PCA was again found to be the best approach for predictor dimension reduction; model I_a outperformed models II_a, III_a and IV_a. Model I_a used the average Atlantic SST from September(Y-1) to December (Y-1) (six months lead time) and yielded a performance of E_f of 0.23, R^2 of 0.29 and H of 48% (Table 6.2) using a value of $N_{max} = 50$. The variance explained by the selected PCs was approximately 80%. Model II_a yielded the second best results (E_f=0.13; R^2=0.14; H =48%) at a lead time of 5 months (with the averaging period from July (Y-1) to January (Y)).

In contrast to the Pacific SST, a positive value of E_f was obtained with one model using CCA for predictor dimension reduction (model III_a) which was slightly better

than model II_a. Model III_a used March to June (Y-1) to forecast JAS rainfall (12 months lead time). The forecasting skills were however relatively low, with E_f, R^2, and H of 0.16, 0.16 and 40% respectively. The best performance achieved with model IV_a was E_f = -0.05, R^2=0.16 and H = 43%. It is therefore not a viable seasonal forecasting model. All model performances using the Atlantic SST can be found in Table 6.2.

Figure 6.2 displays forecasted rainfalls using the Atlantic SST as predictor. Figure 6.2 (a) shows predictions developed using model I_a and II_a. Overall, the rainfall simulations had relatively good agreement with observations. Both PCA models produced rainfall forecasts that somewhat agreed with observations, but they failed to match the high and low extreme rainfalls of some years, including 1984, 1994 and 2000. Model III_a yielded near constant rainfall forecasts for the entire study period, as showed in Figure 6.2 (b), so it could not be used to predict high and low rainfalls. Model IV_a led to a marked overestimation in 1990.

6.1.2 Seasonal rainfall forecasting using polynomial models

The relationships between rainfall and other large scale ocean and atmospheric circulation processes or hydrological variables (e.g. SST and streamflow) are inherently non-linear. An attempt to capture that nonlinearity was done here by replacing the linear relation in models I,II, III and IV by polynomial regressions of degree two to six (models V, VI, VII, $VIII$).

a) Models using the Pacific SST as pool of predictors: Models V_p to $VIII_p$ were developed using the same processes as the linear models (models I_p to IV_p respectively), excluding the last stage when polynomial regression was applied. It was found that using either R^2 or E_f in the first step to select grid points (the screening process) had no influence on the final set and on the final model performance . The same time series of rainfall forecasts were produced when either R^2 or E_f was used as criteria to filter predictors. The best forecasts were generated by models using PCA as predictor dimension reduction technique (models V_p and VI_p), with the polynomial regression of degree three at the last stage. The optimal period for aggregating SST for these models was January to February (Y) (4 months lead time); which yielded a performance of E_f of 0.18, R^2 of 0.22 and H of 50% (Table 6.2), using a value of N_{max} = 20. Increasing the degree of the polynomial equation did

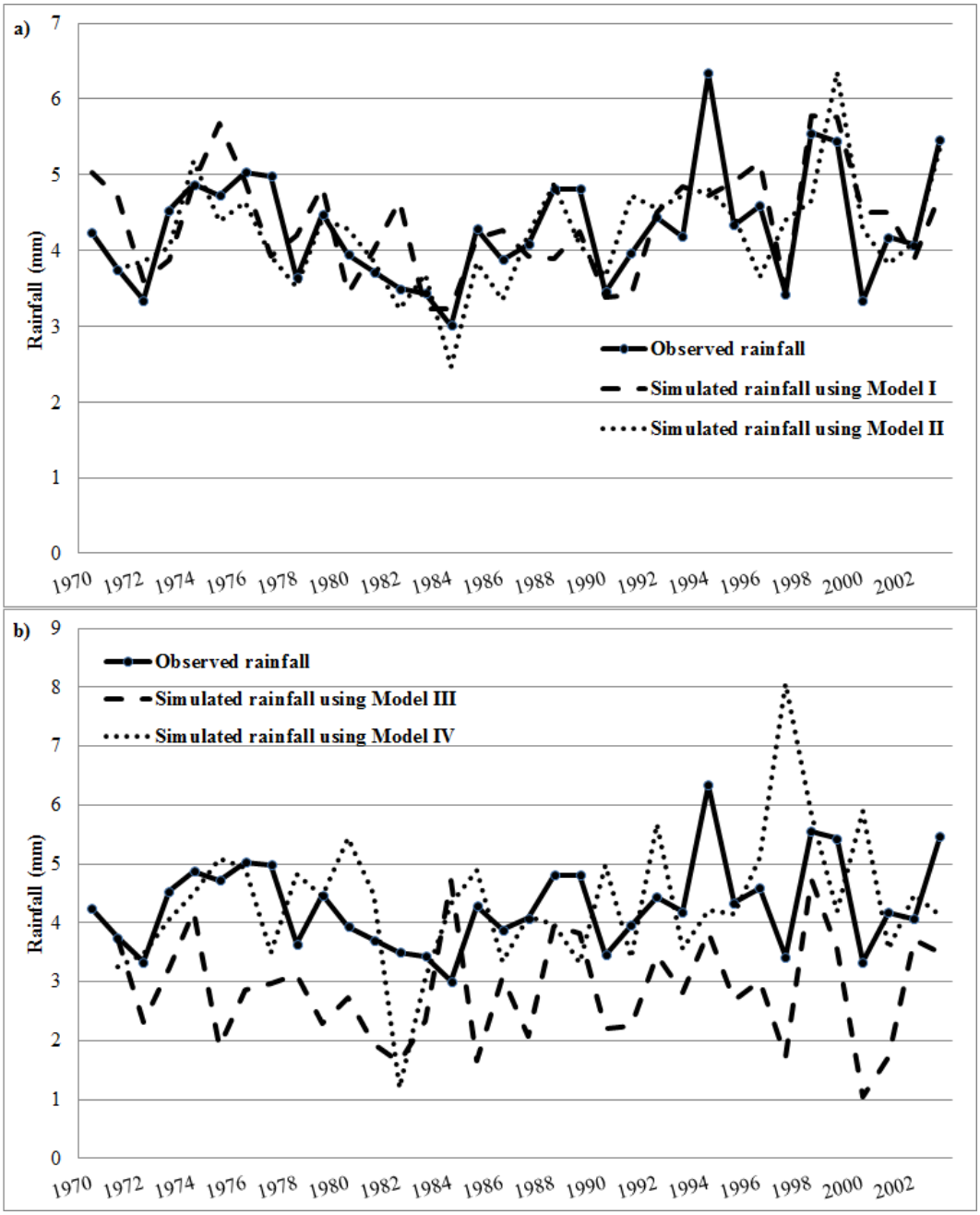

Figure 6.1: Observed and forecasted rainfall using the Pacific SST as predictor; a) models I_p and II_p and b) models III_p and IV_p

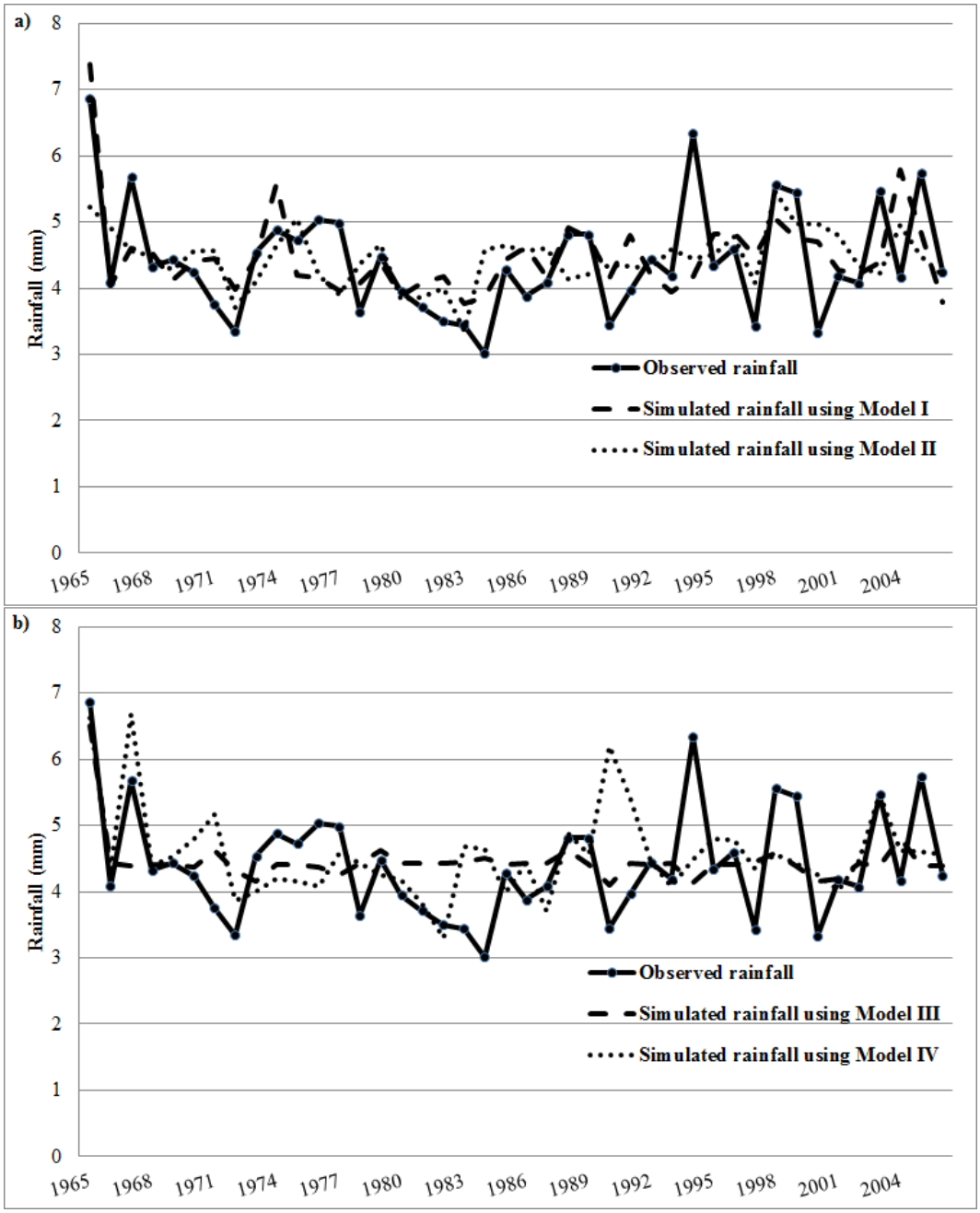

Figure 6.2: Observed and forecasted rainfall using the Atlantic SST; a) models I_a and II_a and b) models III_a and IV_a

Table 6.2: Model efficiencies for seasonal rainfall forecasting in the Sirba watershed

	Model	**Degree**	**Period**	**Lead time (month)**	E_f	R^2	H	**NMAX**
			Pacific SST					
Linear	I_p	-	Feb (Y) to Mar (Y)	3	0.26	0.38	50	20
	II_p	-	Mar (Y-1) to Jun (Y-1)	12	0.39	0.46	67	90
	III_p	-	May (Y-1)	13	-3.91	0.21	40	10
	IV_p	-	Apr (Y-1)	14	-2.18	0.002	42	20
Non-linear	V_p	3	Jan (Y) to Feb (Y)	4	0.18	0.22	50	20
	VI_p	3	Jan (Y) to Feb (Y)	4	0.18	0.22	50	20
	VII_p	6	Oct (Y-1)	8	-0.27	0.05	42	10
	VII_p	6	Oct (Y-1)	8	-0.27	0.05	42	10
			Atlantic SST					
Linear	I_a	-	Sep (Y-1) to Dec (Y)	6	0.23	0.29	48	50
	II_a	-	July (Y-1) to Jan (Y)	5	0.13	0.14	48	180
	III_a	-	Mar (Y-1) to Jun (Y-1)	12	0.16	0.16	40	10
	IV_a	-	Apr (Y-1) to Jun (Y-1)	12	-0.05	0.16	43	10
Non-linear	V_a	4	Jan (Y) to Feb (Y)	4	0.14	0.17	53	10
	VI_a	6	Sep (Y-1) to Jan (Y)	5	0.28	0.32	36	200
	VII_a	3	Feb (Y-1) to Sep (Y-1)	9	0.18	0.20	50	10
	VII_a	5	Oct (Y-1) to Dec (Y-1)	6	-0.32	0.009	40	10

not always improve forecasting performance. Models using polynomial regressions of degree two to three performed better than those using higher degree polynomials.

Similarly to what was found previously, a very low performance was achieved when CCA was used (E_f = -0.27 ; R^2 = 0.05 and H = 42%). Figure 6.3 shows the observed and forecasted rainfall time series using models V_p to $VIII_p$. As mentioned, there was no difference between models V_p and VI_p, nor between models VII_p and $VIII_p$; therefore only one time series of forecasts was shown in each chart. Figure 6.3 (a) clearly shows that the forecasts followed the trend of observations, except in 1980 and 1981. During dry periods, rainfall forecasts had high agreement with observed rainfall, but discrepancies can be observed during wet years such as 1994, 1997 and 2002. Models VII_p and $VIII_p$ in the second chart show opposite trends between observations and forecasts in various years, including 1980, 1988, 1993, 1997 and 2001. Forecasts generated using VII_p and $VIII_p$ were unable to capture high and low rainfalls.

b) Models using the Atlantic SST as pool of predictors: When the Atlantic SST was used in the non-linear models, the screening technique (R^2 or E_f) had an impact on the forecasts. As shown in Table 6.2, model VI_a yielded the best forecasting performance (E_f = 0.28, R^2 = 0.32 and H =36%). It used the average Atlantic SST from September (Y-1) to January (Y) as predictors, and linked it to the predictand using polynomial regression of degree three. Model V_a had a slightly lower performance than model VI_a (E_f, R^2 and H were 0.14, 0.17 and 53% respectively). The model used polynomial regression of degree four to link the predictor (the average SST from January (Y) to February (Y)) to the seasonal rainfall. Relatively decent performance was achieved by model VII_a (the one using CCA) which yielded a performance of E_f=0.18, R^2=0.20 and H = 50% (Table 6.2) when the average Atlantic SST from February (Y-1) to September (Y) was used. This was contrary to model $VIII_a$ which yielded a negative E_f and extremely low value of R^2.

Figure 6.4 shows observed and forecasted rainfalls generated using models V_a to $VIII_a$. Models V_a and VI_a produced acceptable forecasts as shown in Figure 6.4 (a). Their predictions were generally consistent with the trends of observations, with some exceptions, such as in 1982 and 1983. However, they were unable to predict rainfall during dry years (1984 and 2000) and wet years (1994). Figure 6.4 (b) shows the results generated by models VII_a and $VIII_a$. Model VII_a was almost constant in the mid-1979 to 1991 period, but it predicted high rainfall seasons in

1977 and 1994 better than model $VIII_a$. In addition, outputs developed by model $VIII_a$ often resulted in the opposite trends, such as in 1967, 1968, 1975 and 1983.

6.1.3 Seasonal rainfall forecasting: findings

Of all the rainfall forecasting models investigated in this thesis, model II_p (driven by the Pacific SST, using E_f for predictor screening, PCA for predictor dimension reduction, and finally a multiple linear relation between the retained predictors and the predictand) generated the best forecasts with up to 12 months lead time. The next best model was model VI_a with a lead time of 5 months. These results showed that the added effort of fitting a more complex model with more parameters (therefore more flexibility) to link SST to rainfall in the Sirba watershed did not pay out. These results are however only valid for the Sirba watershed and the time period under investigation. Different results could be achieved in other watersheds.

The performance of model II_p (R=0.68; R^2=0.46) compared favourably with that of seasonal forecasting models reported in Barnston et al. (1996), Garric et al. (2002) and Mo and Thiaw (2002). Barnston et al. (1996) used canonical correlation analysis with quasi-global SST as predictors to forecast rainfall in Africa, and the seasonal rainfall forecasting in the Sahel region obtained a correlation coefficient of 0.33 at one month lead time. Garric et al. (2002) used the Atlantic and Indian Oceans SST and the Nino-3 index over the April to June period as predictors to forecast the monsoon rainfall (JAS) over Central Sahel. They tested a simple regression for each predictor, and the best correlation coefficients using the Nino-3 index were 0.34 to 0.53 (R^2=0.12-0.29) at various lead times. Mo and Thiaw (2002) applied an ensemble canonical correlation prediction method to forecast JAS mean seasonal rainfall over the Sahel using the March to May mean global SST as one of various predictors. The simulation skill at each grid point of rainfall correlation gave a mean anomaly correlation of 0.34 (R^2=0.10). Folland et al. (1991) also attempted to forecast rainfall in the Sahel using SST as the predictor and obtained a correlation coefficient of 0.72 (R^2=0.52) at one month lead time.

The four best forecasted seasonal rainfalls generated with linear or non-linear regressions, and driven by the Pacific or Atlantic SSTs were adapted to a daily time scale. The daily rainfall data sets were introduced as an input layer in the SWAT model for monthly streamflow generation.

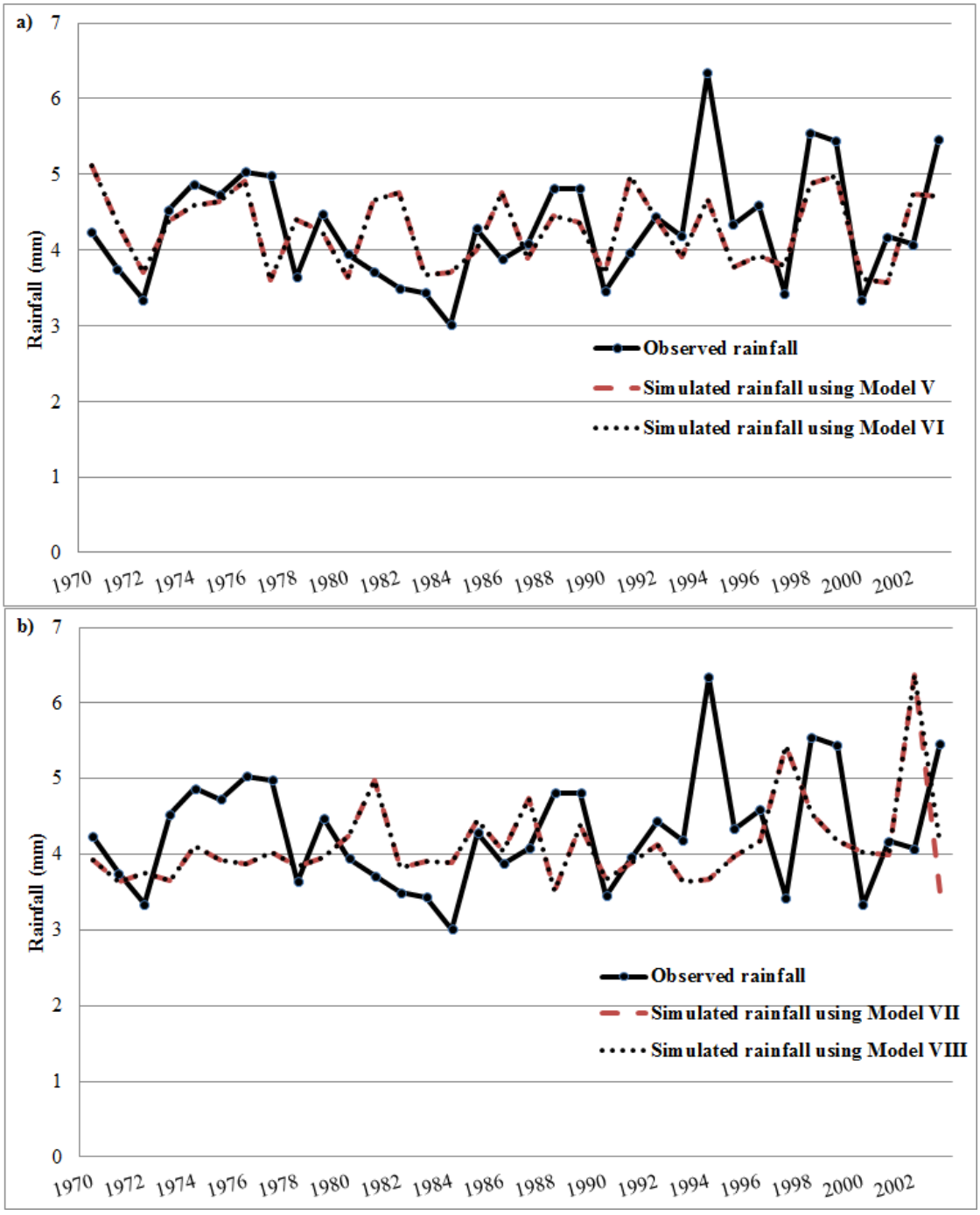

Figure 6.3: Observed and forecasted rainfall using the Pacific SST; a) models V and VI and b) models VII and $VIII$.

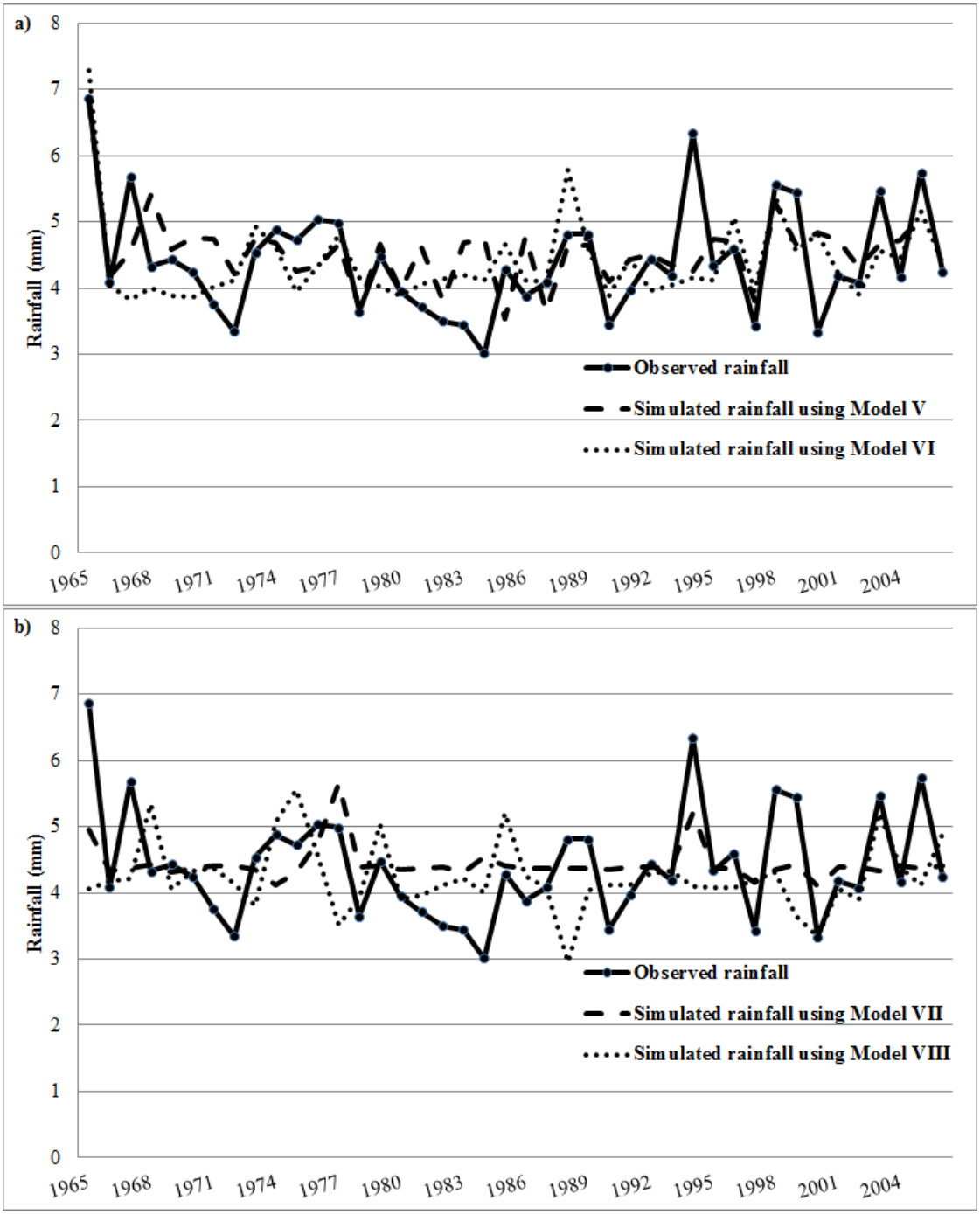

Figure 6.4: Observed and forecasted rainfall using the Atlantic SST; a) models V_a and VI_a; b) models VII_a and $VIII_a$

6.1.4 Performance of the fragment method for temporal disaggregation

The method of fragment was used to increase the temporal scale of the rainfall forecasts from annual to daily data. Temporal disaggregation is required before the rainfall forecasts can be converted to streamflow forecasts using the SWAT model, since SWAT uses daily time series for streamflow generation. The fragment method consists of developing a series of ratios (the fragments) that are later used to generate daily time series by multiplying the original forecast with the series of fragments. Three approaches used for building the fragment series (described in Section 5.4.3.) were tested, and the one with the most accurate daily data was selected to use in the remainder of the thesis.

The performance of the best model (model II_p) was reassessed after each of the fragment generation methods were used to disaggregate the forecasts. The performance of the forecasts were then recalculated using monthly time series instead of yearly time series and presented in Table 6.3. Results show that there were only slight differences in performance when one fragment method was replaced by another; E_f, R^2 and H were in ranges of 0.62 to 0.81, 0.68 to 0.81 and 78 to 84 respectively. There were insignificant differences in terms of the average and standard deviation between rainfall observations and disaggregated rainfalls. The original fragment method (Method F-I) gave the best performance, but by construction it generated only one time series for the whole watershed. Method F-III was capable of producing nine series of rainfall forecasts (one for each sub-watershed in the model), with sightly lower performance compared to Method F-I. Therefore, Method F-III was selected to use for disaggregation. Figure 6.5 illustrates disaggregated rainfall using fragment Method F-I and F-II, and Figure 6.6 shows an example of disaggregated rainfall forecast for station 200082 using Method F-III.

Four sets of daily seasonal rainfall forecasts (generated using models II_p,V_p,I_a,VI_a) were prepared for use in the SWAT model. Table 6.4 shows the performance of the four best forecasts after application of the fragment method. The values of the three performance criteria confirmed that the method proposed to select fragment series maintained the forecasting skills of the model to which it was applied. E_f, R^2 and H were in ranges between 0.78 to 0.83, 0.78 to 0.83, and 82 to 87% respectively. There were insignificant differences between disaggregated outputs from each model.

Figure 6.7 compares disaggregated forecasts with observations. It shows that the forecasts could frequently capture high amounts of rainfall, with some exception including

1989 to 1990 and 1994 to 1995 (upper panel), and 1989, 1991 and 1994 (lower panel). In summary, the results in this section show reasonable forecasts were achieved even after temporal disaggregation. The forecasts were forced to the SWAT model for streamflow forecasting. Since only precipitation is forecasted, the other inputs to SWAT (temperature, wind, solar radiation and relative humidity) were assumed perfectly known. This assumption should only have a minimal impact on the results as precipitation is by far the main driver of streamflow in the watershed.

Table 6.3: Performance of the four best forecasting models after application of the fragment method.

Method	E_f	R^2	H	Average		Standard deviation	
				Observation	Disaggregated rainfall	Observation	Disaggregated rainfall
F-I	0.81	0.81	84	1.47	1.44	1.97	1.93
F-II	0.62	0.68	78	1.47	1.46	1.97	2.09
F-III	0.79	0.80	82	1.47	1.33	1.97	1.83

Table 6.4: Abilities of the fragment method for rainfall forecasting disaggregation

Predictor	**Model**	E_f	R^2	H
Pacific SST	II_p	0.82	0.83	82
	V_p	0.83	0.83	82
Atlantic SST	I_a	0.78	0.78	87
	VI_a	0.80	0.81	82

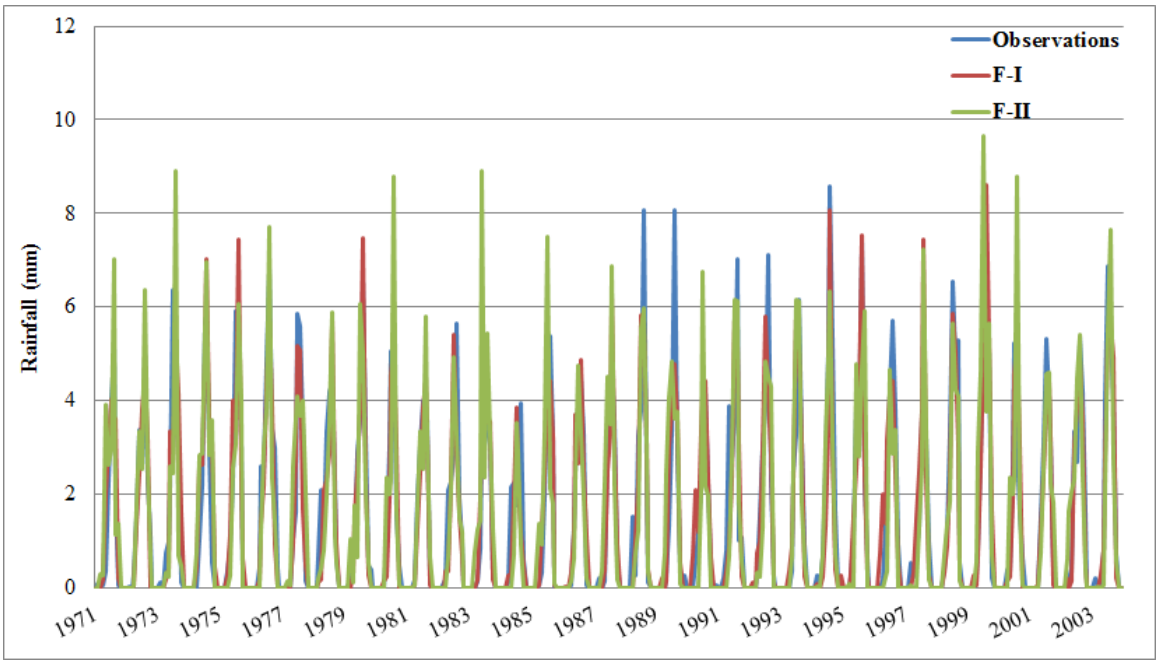

Figure 6.5: Disaggregated rainfall using fragment Method F-1 and F-II

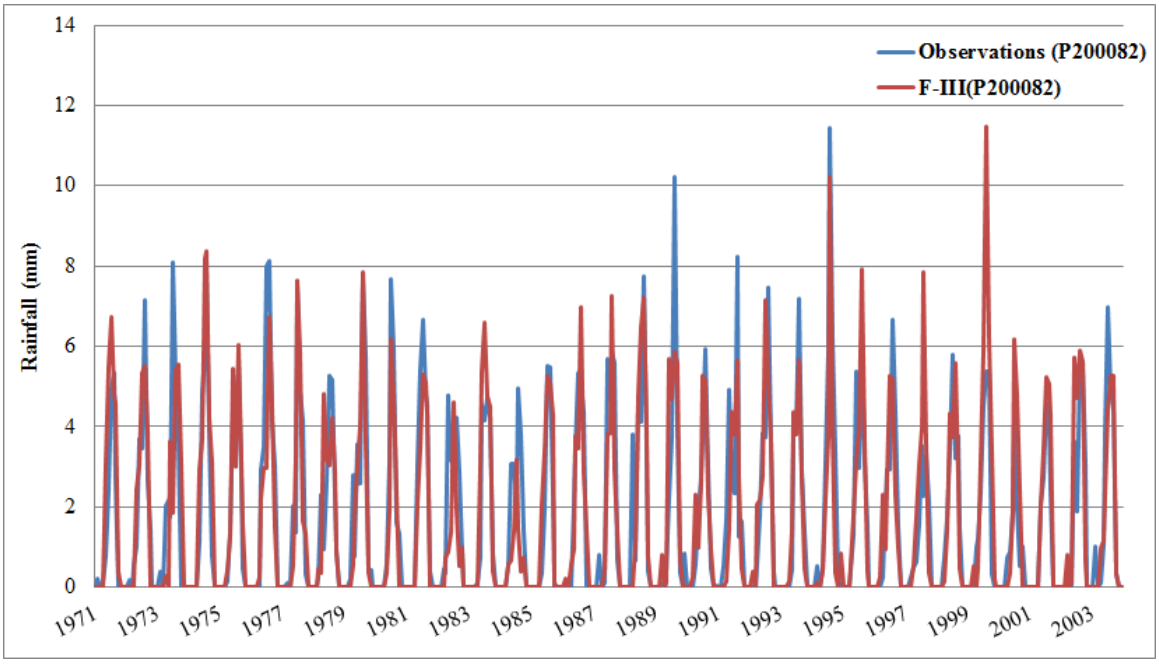

Figure 6.6: Disaggregated rainfall using fragment Method F-III, with station 200082 as an example

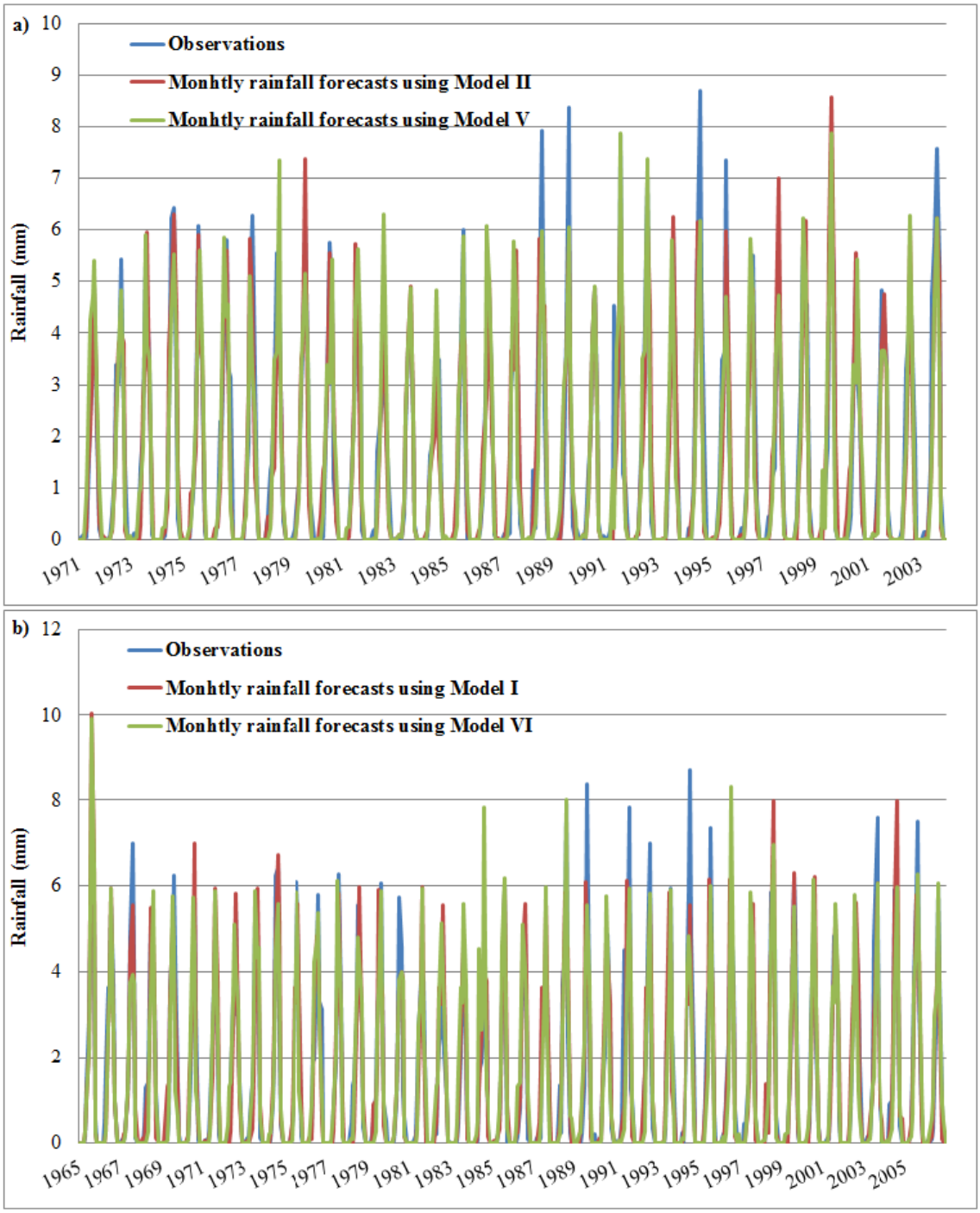

Figure 6.7: Disaggregating monthly rainfall forecasts using (a) the Pacific SST and (b) the Atlantic SST

6.1.5 Performance of streamflow forecasting using the indirect method

This section examines streamflow forecasts generated using the indirect method. The calibration process described in Chapter 5 was initially performed using the SWAT-CUP program with the Sequential Uncertainty Fitting (SUFI2). No validation was performed given the short span of the streamflow observations. The fit between forecasted streamflows and observed streamflow was excellent (E_f =0.83, R^2 = 0.83 and H = 86%). The calibrated model was used for streamflow forecasting with four different daily rainfall forecasts. The results are discussed below.

a) Models using the Pacific SST as pool of predictors: The streamflow forecasting skills of all four retained seasonal forecasting models are summarized in Table 6.5. Slight differences were found between model II_p and V_p. The one using a polynomial regression to predict rainfall (model V_p) performed slightly better in terms of E_f and R^2 than the one using linear regression (model II_p). Model V_p yielded values for both E_f and R^2 of 0.65, whereas with model II_p these values were of 0.58 and 0.59 respectively. Considering that they had lead times of 4 and 12 months, such a performance were deemed reasonable. Figure 6.8 (a) shows observed streamflow time series from 1989 to 2002, and two forecasted streamflow time series. It appears that flow simulations using rainfall forecasts from model V_p was generally consistent with observations in the year having average flow rates. However, the model was unable to capture extreme events in 1994 and 1998; there was also significant overestimations in 1992. Forecasts generated using model II_p often underestimated the upcoming flood, while overestimations were found in 1993 and 1999. Likewise results generated from daily rainfall model V_p showed that flow simulations also failed to reach peak flows in 1994 and 1998.

The most interesting result emerging from this exercise was the inversion of the ranking of models II_p and V_p depending of which variable is being forecasted. Model II_p was better than model V_p for rainfall forecasting, but streamflow forecasting was outperformed by model V_p. This apparent inversion in performance could have occurred because the objective functions used to estimate forecasting performances were unable to capture all the characteristics of the rainfall/streamflow time series. As well, the time scale of the forecasted results (seasonal versus monthly) could have affected estimation of the forecasting abilities of the models.

b) Model using the Atlantic SST as pool of predictors: Forecasted rainfall time series from model I_a were disaggregated and forced to the calibrated SWAT model. Model I_a generated streamflow forecasts at lead time of up to 6 months and exceptionally high skills ($E_f = 0.70$, $R^2 = 0.69$ and $H = 77\%$). Model VI_a had a lower but decent performance ($E_f = 0.59$, $R^2 = 0.59$ and $H = 82\%$). Figure 6.8 (b) illustrates streamflow time series of both observations and forecasts. Strong evidences of underestimation for both models were found during high flow seasons in 1994 and 1998. Model VI_a regularly over-predicted streamflows (e.g. in 1990, 1996 , 1997 and 2000) while model I_a performed generally well in average years.

Table 6.5: Performance of streamflow forecasting using the indirect method

Rainfall forecasting			**Performance**		
Predictor	Model	Lead time	E_f	R^2	H
Pacific SST	II_p	12	0.58	0.59	78
	V_p	4	0.65	0.65	75
Atlantic SST	I_a	6	0.69	0.70	77
	VI_a	5	0.59	0.59	82

6.1.6 Streamflow forecasting using indirect method: findings

Eight statistical models, linear (models I to IV) and polynomial regression of degree two to six (models V to $VIII$), were used to link the Sirba rainfall with the ocean temperatures in the Pacific and Atlantic regions. The finding suggested that the linear model (model II_p) outperformed the polynomial model for rainfall forecasting when the Pacific SST was used as pool of predictors. An opposite conclusion was reached when the Atlantic SST was used as pool of predictors. The best overall model was model II_p, but the reader should be aware that these models are data driven and therefore very sensitive to the period and area under investigation. The only conclusion that could be reached was that sometime simpler models was able to outperform more complex models, and the comparison should be done in each situation.

It was also found that excellent streamflow forecasts could be achieved at 6 months lead time using model I_a (using the Atlantic SST as a predictor). This results is a priori

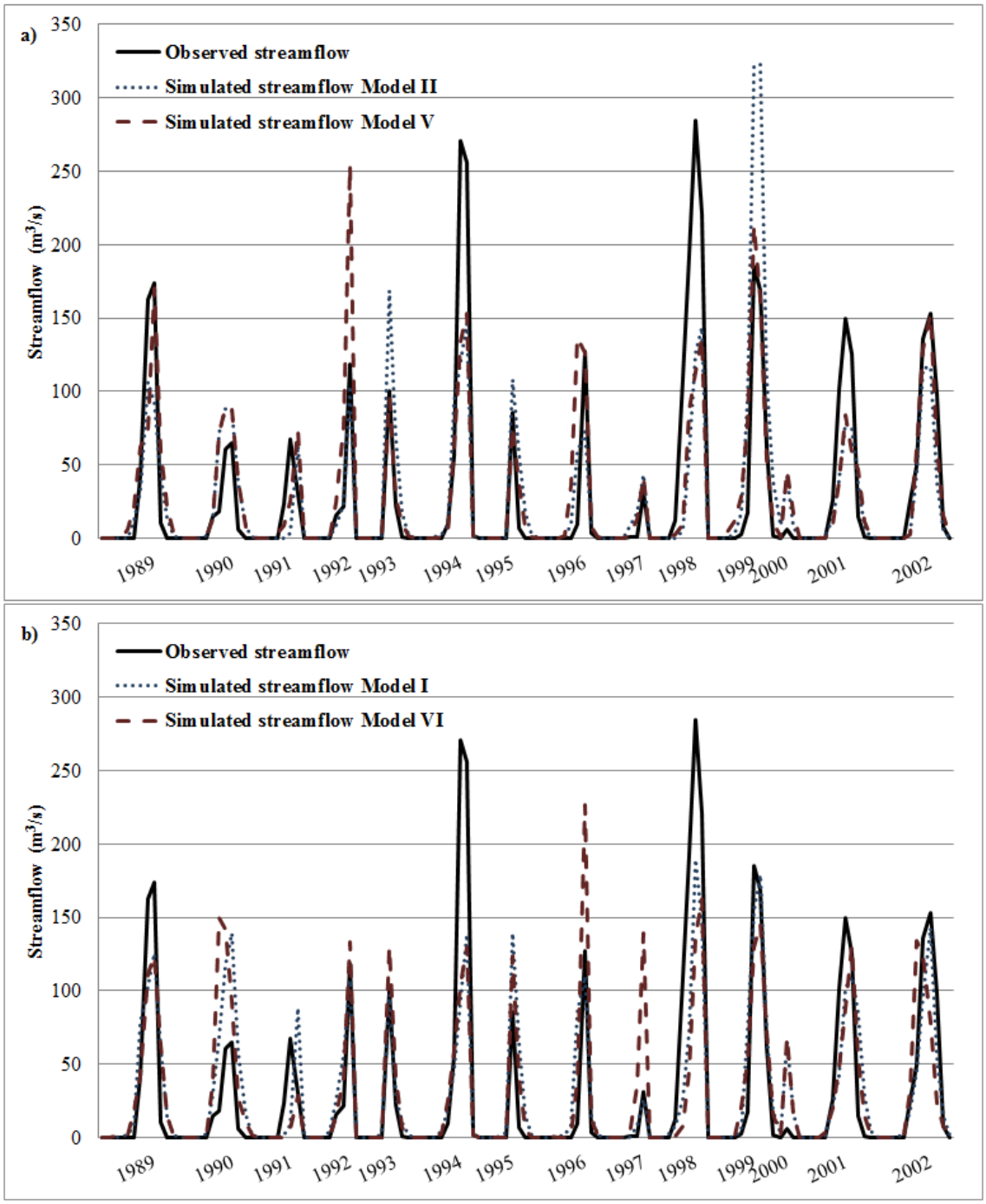

Figure 6.8: Comparison between observed and forecasted streamflows generated using the SWAT model driven by rainfall forecasts with a) the Pacific SST and b) the Atlantic SST

counter-intuitive as one would expect model II_p to be the best one for streamflow forecasting given that it outperformed its competitors in rainfall forecasting. As mentioned, this inversion in performance was due to the fact that the objective functions (E_f,R^2,H) were unable to capture all the characteristics of streamflow hydrographs. The inversion may also be affected by the technique chosen to perform the temporal disaggregation of the forecasted rainfall.

6.2 Seasonal streamflow forecasts using the direct method

Calibrating and running a rainfall-runoff model requires a large amount of data about catchment characteristics that are not always available, especially in Africa. Furthermore, the quality of the data should be high enough to allow a good calibration (e.g. minimal missing values and high temporal-spatial resolution). In study areas lacking climate stations and basin characteristic information, it is tempting to directly forecast streamflow using only statistical models. Models I to $VIII$ (refer to Chapter 5) were tested to determine their ability to directly forecast streamflow at the outlet for the Sirba basin using SSTs. The methodology was exactly the same as for rainfall forecasting except that the predictand was the average streamflow over the rainy season. The model development steps were therefore omitted and results were presented directly.

6.2.1 Streamflow forecasts using linear models

a) Models using the Pacific SST as pool of predictors: The performances of statistical models for seasonal streamflow forecasting are shown in Table 6.6. Results in Table 6.6 show that the screening step had no influence on the forecast when the Pacific SST was used as predictor. Models driven by the Pacific SST yielded the best forecasts (E_f=0.39, R^2=0.42 and H = 50%). They used the average SST from March (Y) to June (Y) as predictor, with 0 lead time (i.e the forecast was issued right at the beginning of the rainy season).

Once again, the use of CCA proved to be counter productive. Model III_p yielded E_f, R^2 and H values of only 0.08, 0.21 and 58% respectively using the average period of the Pacific SST from May (Y-1) to June (Y-1). Figure 6.9 (a) illustrates streamflow time series between observations and simulations using the Pacific SST

as predictor at an annual time scale. There was higher agreement between observations and forecasts developed using model I_p compared to the observed flows with simulations from model III_p. Both models seemed unable to capture the wet episodes, except in 1998 using model I_p.

b) Models using the Atlantic ocean SST as pool of predictors : Model II_a produced the best forecasts with E_f, R^2 and H values of 0.42, 0.43 and 43% respectively. This modest forecasting skill was attractive, since it was generated prior to the rainy season at 12 months lead time with the monthly Atlantic SST in June of the previous year. Model I_a generated forecasted flows with slightly less performance (E_f=0.33, R^2=0.38, H=36) , but the different criteria in the screening step seemed to influence the best simulations, and their outputs were only slightly different, as shown in Figure 6.9 (b). Once again, models using PCA still performed better than those using CCA. The best forecasts using model III_a and IV_a gave negative values of E_f (Table 6.6). Figure 6.9 (b) displays time series of both observations and forecasts and shows that underestimations often occurred during years with large flows. However, the trend of forecasted time series developed from model I_a and II_a agreed with the observations. Predictions of model III_a and IV_a were generally inconsistent with observations.

6.2.2 Streamflow forecasts using polynomial models

a) Models using the Pacific SST as pool of predictors: Once again, the screening step had no influence on the final result. Table 6.6 shows the performance of the best models in each class along with their corresponding degrees. The high performance of model V_p was apparent with E_f, R^2 and H values of 0.72, 0.79 and 79% respectively using the aggregate Pacific SST from November (Y-1) to January (Y). Model V_p driven by this predictor data set was the most effective application for streamflow forecasting of the eight models in this study, with the performance to predict streamflow in a rainy season with five months lead time.The models using CCA as predictor reduction technique were unable to develop skillful forecasts; an E_f of only 0.19 was obtained from models VII_p and $VIII_p$ with one month lead time. Figure 6.10 (a) displays the comparison between observations and simulations with the Pacific SST. The models using PCA to reduce SST grid points were able to develop simulations with high agreement to observed flows over the entire study period. They were capable of capturing dry episodes, and showed

only slightly underestimation during wet years. Models VII_p and $VIII_p$ (based on CCA) were unable to correctly predict streamflow at the beginning of the study period (1989 to 1993), and their forecasts could not capture peak flows efficiently.

a) Models using the Atlantic ocean SST as pool of predictors: The use of polynomial regression models driven by the Atlantic SST was less effective than using models driven by the Pacific SST. Introducing the aggregate monthly Atlantic SST from October to November of the previous year to model V_a and VI_a resulted in forecasted streamflow with an E_f of 0.47, R^2 of 0.49 and H of 57%. Models VII_a and $VIII_a$ again showed low efficiency to forecast streamflow with E_f, R^2 and H values of 0.03, 0.25 and 21% respectively. The peak flows in 1994 and 1998 were captured by models V_a and VI_a as shown in Figure 6.10 (b). Though models VII_a and $VIII_a$ also correctly forecasted the peak flow in 1998, they were generally unable to predict the streamflow time series corresponding to observations.

6.2.3 Seasonal streamflow forecasting using the direct method: findings

Tables 6.7 and 6.8 present the performance of the best direct methods at monthly and annual scales. The performances at monthly scale were obtained after the fragment method was used to disaggregate the forecasts at annual scale generated using the direct methods. Only the forecasts of four models (the linear and polynomial models that use the Atlantic or Pacific ocean SST) were disaggregated at the monthly time scale.

The following conclusions can be drawn from the results obtained with the direct methods:

1. The performance criteria used at the screening step (either R^2 or E_f) had almost no influence on the final result, except in a case when Atlantic SST was used as predictor with linear regression (models I_a and II_a).

2. Using a polynomial regression instead of a linear regression between the selected predictors and streamflow led to better forecasts, and lead times of five to seven months. Longer lead times (12 months) were obtained with the linear models, but with lower performances. Therefore, the choice of which model to use should take in consideration both model accuracy and lag times.

Table 6.6: Performance of statistical models for streamflow forecasting using the direct method at the annual time scale

	Model	**Degree**	**Period**	**Lead time**	E_f	R^2	H	**NMAX**
			Pacific SST					
Linear	I_p	-	Mar (Y) to Jun (Y)	0	0.39	0.42	50	70
	II_p	-	Mar (Y) to Jun (Y)	0	0.39	0.42	50	70
	III_p	-	May (Y-1) to June (Y-1)	12	0.08	0.21	58	10
	IV_p	-	May (Y-1) to June (Y-1)	12	0.08	0.21	58	10
Polynomial	V_p	5	Nov(Y-1) to Jan (Y)	5	0.72	0.79	79	10
	VI_p	5	Nov(Y-1) to Jan (Y)	5	0.72	0.79	79	10
	VII_p	2	Feb (Y-1) to May (Y)	1	0.19	0.26	57	10
	$VIII_p$	2	Feb (Y-1) to May (Y)	1	0.19	0.26	57	10
			Atlantic SST					
Linear	I_a	-	June (Y-1)	12	0.33	0.38	36	170
	II_a	-	June (Y-1)	12	0.34	0.35	43	170
	III_a	-	Jan (Y-1) to Feb (Y)	4	-0.26	0.05	43	10
	IV_a	-	Jan (Y-1) to Feb (Y)	4	-0.26	0.05	43	10
Polynomial	V_a	5	Oct (Y-1) to Nov (Y-1)	7	0.47	0.49	57	200
	VI_a	5	Oct (Y-1) to Nov (Y-1)	7	0.47	0.49	57	200
	VII_a	2	Oct (Y-1) to Apr (Y)	2	0.03	0.25	21	10
	$VIII_a$	2	Oct (Y-1) to Apr (Y)	2	0.03	0.25	21	10

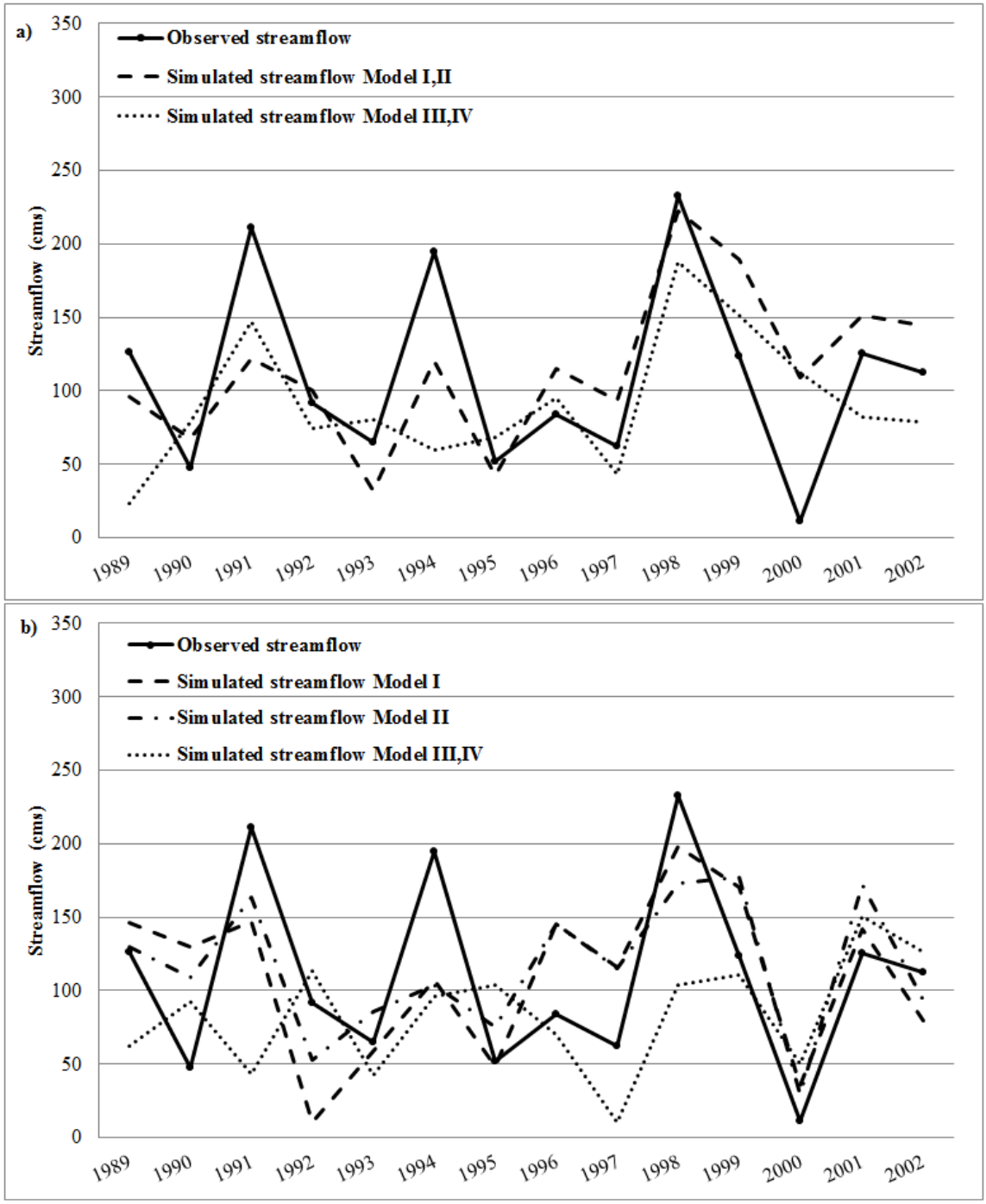

Figure 6.9: Comparison between annual observed and forecasted streamflows generated using linear regression models a) the Pacific SST and b) the Atlantic SST

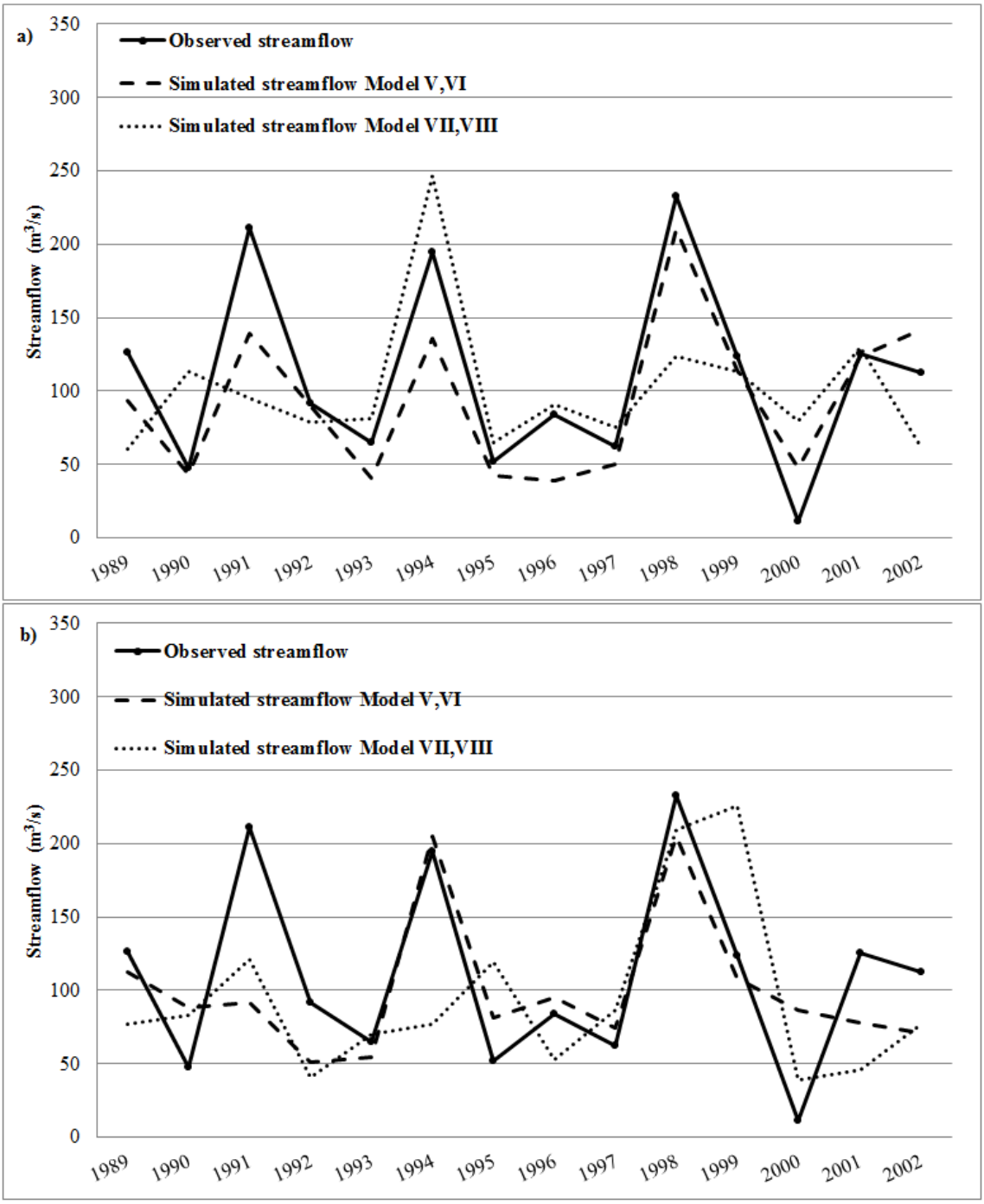

Figure 6.10: Comparison between annual observed and forecasted streamflows generated using polynomial regression models a) the Pacific SST and b) the Atlantic SST

3. The accuracy of forecasts in this study is equal to or higher than those published by others, when both performance criteria and lag time are taken into account. For instance, Kwon et al. (2009) used a hierarchical Bayesian approach to forecast seasonal and annual maximum flows in the Yangtze River basin in China with SST and upland snow cover as predictors. They used a one season lead time. Their model performed well and yielded a correlation coefficient (R) of 0.8 (average seasonal flow) and 0.73 (annual peak flow). Some other studies could not be compared to the ones in this thesis as they used different performance criteria (absolute relative errors) : Karamouz and Zahraie (2004) forecasted seasonal streamflows in the Salt River Basin in Arizona using autoregressive integrated moving average six to nine months in advance. Snow water equivalents were used as the main predictor, and the ENSO index was added to improve the forecasting skills. Absolute relative errors decreased from 29% to 24% and 43% to 40% in various seasons when ENSO was also used as a predictor. Piechota et al. (1998) used linear discriminant analysis as a tool to forecast seasonal streamflows in eastern Australia. They applied SST, the Southern Oscillation Index (SOI) and streamflows from previous seasons as predictors. These model performances were compared with the outputs of the climatology condition and showed better skills in most stations.

6.3 Comparison of the direct and indirect streamflow forecasting methods

The direct methods produced only one value (the average streamflow over the rainy season) while the indirect methods generated a hydrograph of monthly flows. In order to compared the two methods, the fragment method was used to disaggregate the forecasts of the direct method to the monthly scale. The forecasts issued with the indirect methods were also aggregated to the annual scales. The performances of the best four models are presented in Tables 6.7 (monthly scale) and 6.8 (annual scale). Overall the best model was a direct model using polynomial regression to link the predictor and predictand. Despite it's complexity, the indirect method is always outperformed by the direct method. The indirect method systematically fails at the annual scale with negative or extremely low values of E_f. Two possible reasons may be behind the counter-performance of the indirect method:

1. The quality of the data used to calibrate and validate the SWAT model. It is well known that data quality from climate and streamflow stations in Africa is low because of lack of funding and maintenance. Furthermore, the soil and land use data was obtained from global sources at a very coarse resolution.

2. The realism of the disaggregation technique used to disaggregate the projected rainfall to daily values. The fragment method was used here for its simplicity but it is based on the assumption that two years with similar precipitation amounts have the same temporal distribution of precipitation. Streamflow generation by rainfall-runoff models is extremely sensitive to the distribution of rainfall. The use of more sophisticated temporal disaggregation techniques may lead to better results.

The conclusion is that in the specific context of the Sirba watershed, the direct methods are preferable because they can achieve a decent performance and outperform the indirect method despite a lower cost of implementation. The indirect method may be considered in areas where higher quality data is available. The forecasting skills are lower at the annual scale compared to the monthly time scale because of the seasonal component in monthly time series. The indirect method outperform the direct method at the annual scale only when the Atlantic Ocean SST is used as predictor and when linear models are used.

6.4 Uncertainty analysis

The models presented in previous sections scored high in terms of E_f, R^2 and H. The performance criteria were calculated using a single value (the model output) without any consideration of the uncertainty around that value. It is well known that forecasts are unperfect and that the real outcome will be less or more far from the forecasted value. The risk which might occur when a decision maker takes by acting (or not acting) based on a forecast depending on the level of uncertainty associated with the forecast. Two approaches for calculating prediction uncertainty are explored in this thesis: a) the uncertainty due to (presumably) random model errors and the uncertainty due to our unperfect knowledge of the true model.

Table 6.7: Comparison of the performances of the indirect and direct methods for seasonal streamflow forecasting at the monthly time scale (1989-2002)

Predictor	**Method**	**Statistical model**	**Model**	**Lead time**	E_f	R^2	H
Pacific	Indirect	Linear	II_p	12	0.58	0.59	78
	Direct	Linear	II_p	0	0.66	0.71	82
	Indirect	Polynomial	V_p	4	0.65	0.65	75
	Direct	Polynomial	V_p	5	0.74	0.76	84
Atlantic	Indirect	Linear	I_a	6	0.70	0.69	77
	Direct	Linear	I_a	12	0.57	0.63	83
	Indirect	Polynomial	V_a	5	0.59	0.59	82
	Direct	Polynomial	V_a	7	0.74	0.75	85

Table 6.8: Comparison of the performances of the indirect and direct methods for seasonal streamflow forecasting at the annual time scale (1989-2002)

Predictor	**Method**	**Statistical model**	**Model**	**Lead time**	E_f	R^2	H
Pacific	Indirect	Linear	II_p	12	-0.38	0.02	35
	Direct	Linear	II_p	0	0.39	0.42	50
	Indirect	Polynomial	V_p	4	-0.17	0.01	29
	Direct	Polynomial	V_p	5	0.72	0.79	79
Atlantic	Indirect	Linear	I_a	6	0.04	0.01	43
	Direct	Linear	I_a	12	0.34	0.35	43
	Indirect	Polynomial	V_a	5	-0.14	0.007	50
	Direct	Polynomial	V_a	7	0.47	0.49	57

6.4.1 Uncertainty due to random model errors

The methodology described in Section 5.4.5.1 was applied to models V_p and I_a to generate ten equiprobable values of rainfall forecasts. They were then forced to the SWAT model and ten probabilistic streamflow forecasts were generated. Model V_p and V_a (direct method) were directly used to develop ten equiprobable streamflow hydrographs.Figure 6.11 a) and b) shows lowest and highest probabilistic rainfall forecasts generated with models V_p and I_a for the 1971-2003 and 1965-2006 periods respectively. The cloud of generated rainfall values is plotted along with the observed precipitation. The spread of the cloud is an indication of the uncertainty in the forecast; the uncertainty in the forecast is assumed to be well captured in the observation falls within the cloud most of the time.

Both graphs show that observed rainfalls mostly fell within their clouds except the wet year in 1995, and the dry years in 1983 for model V_p and 1999 and 2003 for model I_a. These ten equiprobable data sets were forced to the SWAT model for streamflow generation.

Figure 6.12 and 6.13 show the lowest and highest probabilistic streamflow forecast from the indirect and direct method respectively; again the cloud of generated monthly streamflow values is plotted against the observations. If the observations fall into the cloud, users aware of the forecast would have been protected as they would have taken measures so that no damage occur no matter which of the ten plausible flow happens. Accounting for the forecasts would therefore make the area resilient to climate variability. Figure 6.12 (a) and (b) illustrate the lowest and highest forecasts generated with the indirect method models V_p and I_a respectively. Most observed streamflows fell in the range of the highest and lowest forecasts of model V_p except in 1994, 1998, 2000 and 2001. Most observations also fell in the range of model I_a except in 1990 and 2000 with overestimations and underestimation in 1994.

Figure 6.13 presents the lowest and highest probabilistic forecast generated with (a) model V_p and (b) model V_a. Observed streamflow were in the range of forecasted streamflow from model V_p except a case of high overestimation in 1990, and a case of underestimation in 1994. High underestimation can be observed as well for model V_a in 1991 whereas overestimation occurred in 2000.

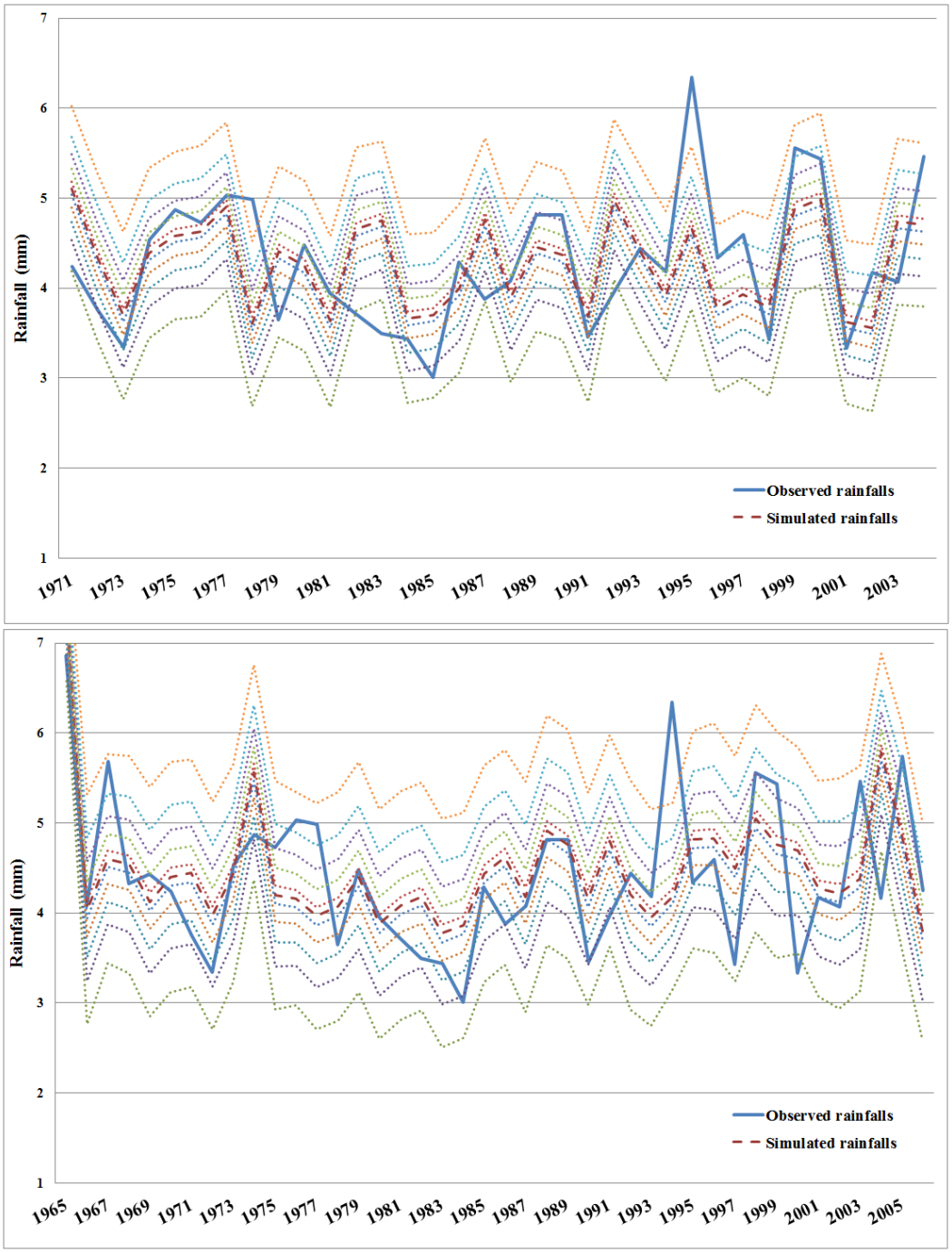

Figure 6.11: Cloud of ten equiprobable rainfall forecasts generated using a) model V_p forced by Pacific SST and b) model I_a forced by Atlantic SST

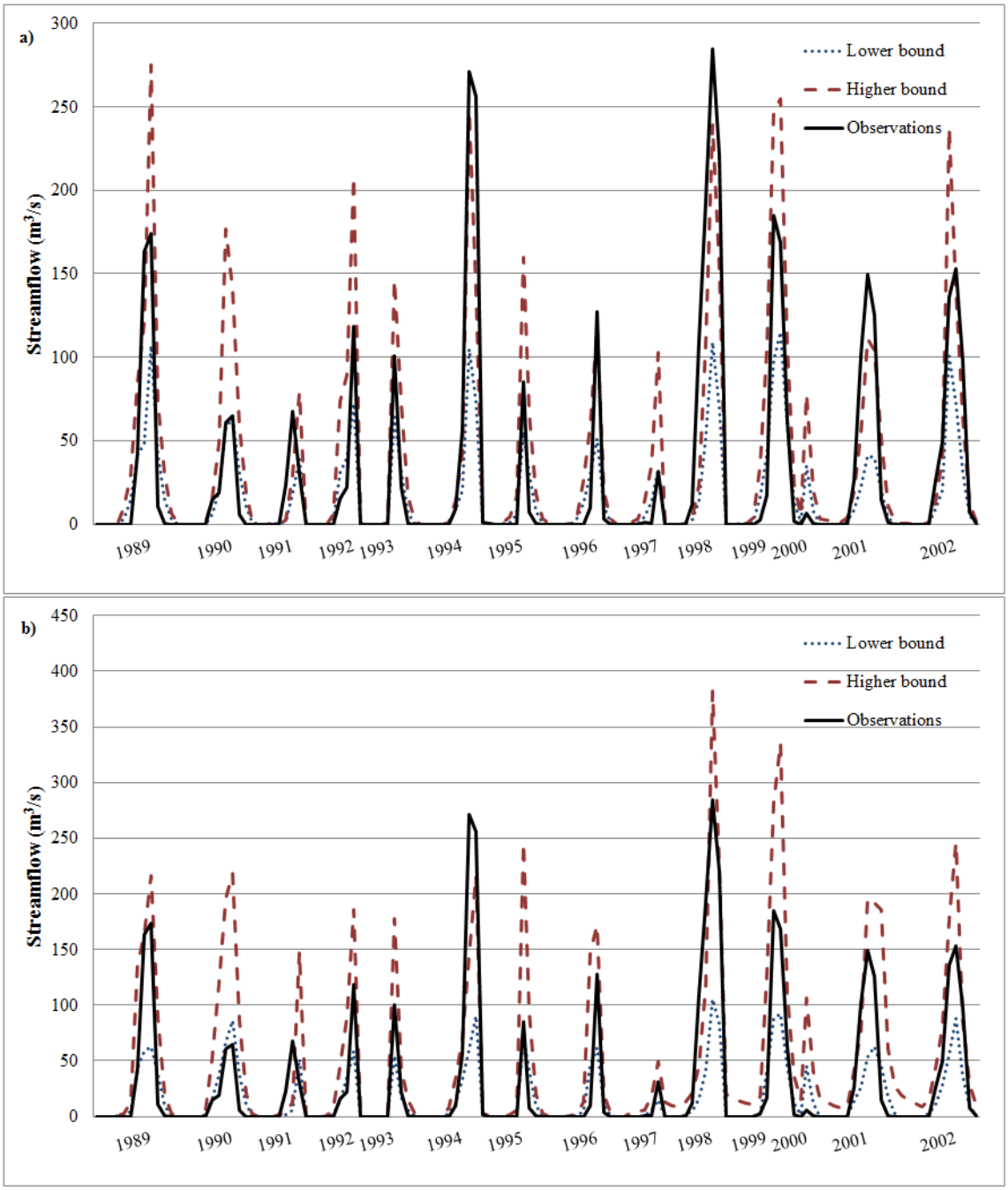

Figure 6.12: Highest and lowest probabilistic forecasts generated using the indirect method: a) Pacific and b) Atlantic SST

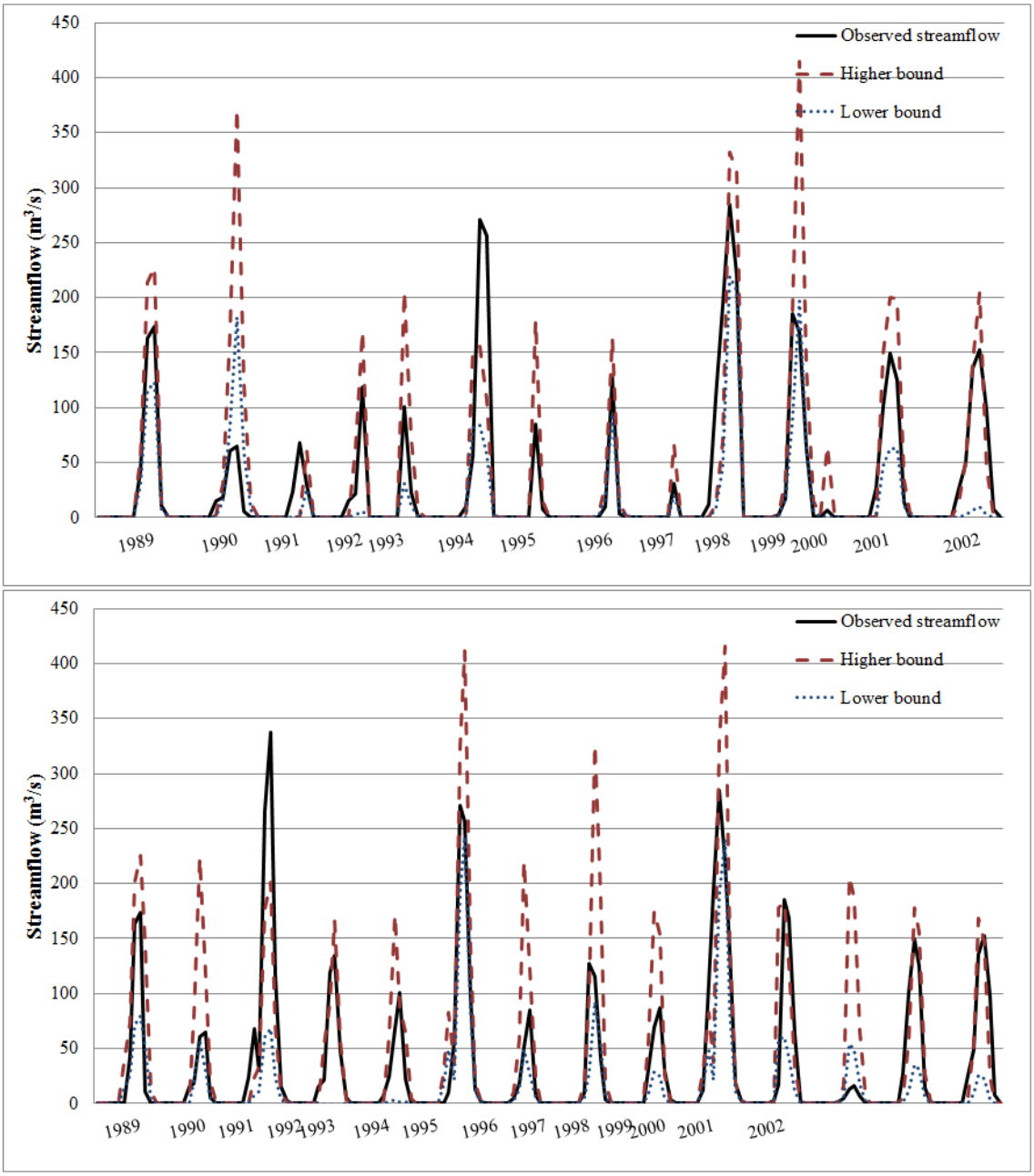

Figure 6.13: Highest and lowest probabilistic forecasts generated using the direct method: a) Pacific and b) Atlantic SST

6.4.2 Bayesian Model Averaging

This section describes the application to generate probabilistic forecasts at the outlet of the Sirba watershed. As it was done in the other statistical methods described in this thesis, the screening step to filter high predictive SST grid data was still applied, but as mentioned in the results of using the direct method clearly indicates, there was no difference between using R^2 with P-value less than 0.05 or E_f as a criterion. Therefore, only SST data showing correlation with streamflows with P-value less than 0.05 were kept in the process. PCA was then applied to the retained time series to obtain a series of principal components (PCs).

a) Predictor selection

As mentioned before, the filtering of SST grid points in the BMA approach was similar to that used for the statistical models. However, all retained grid points of each period were used as independent variables in PCA, and only the first principal component (PC1) was used in BMA. PC1 generally achieves the maximum percentage of explained variance. The average percentage of PC1 over all periods of the Pacific and Atlantic SSTs was 63% and 57% respectively, with highest values of 74% and 70%. Consequently, 171 PC1 of from the SST data sets were prepared for use in BMA.

All predictors in each group (Table 6.9) were forced into BMA individually, with a uniform prior probability condition evenly defining prior knowledge of the variables in each group. BMA accounted for all models in the model space, with a largest model space of 2^{18} for the group G1. Since the cross-validation method was used in this study, the final predictors for generating forecasts were different in each year, which is why the output of the last year (2002) was only an example. Table 6.9 shows the final predictors used to generate streamflow forecasts in 2002. Using the BMA1 technique of selecting predictors showing the highest PIP in each group produced 18 predictors for both the Pacific and Atlantic SSTs. BMA2 selected only predictors with PIP values higher than 0.6, which gave less predictors than BMA1. There were only eight and nine potential predictors remaining in the process for Pacific and Atlantic SSTs respectively. Thus, the top predictors in some groups, such as G5, G6 and G7, had a low probability (less than 0.6) of successfully developing the JAS streamflow in 2002.

Prior and posterior model size distributions from the BMA1 and BMA2 techniques are shown in Figure 6.14. The average prior model size of the Pacific SST using BMA1 and BMA2 was nine and four respectively, and for the Atlantic SST it was nine and

five. Since the BMA models were applied with uniform predictor distribution, the prior model size was a symmetric distribution around the number of predictors divided by two. After using BMA, the mean of the posterior model size of both SSTs was less than the prior model size: approximately seven and three for Pacific SSTs and five and three for Atlantic SSTs, using BMA1 and BMA2 respectively. This could indicate that less predictor combinations in the model leads to higher probability to successfully generate streamflows.

b) Streamflow simulation

The main advantage of BMA is its ability to generate the predictive density of forecasted results. Predictive density is a distribution curve generated by calculating average future predictions over the posterior densities for all unknown parameters. The density curve not only provides users with the expected value of forecasts, but the range of standard errors as well. The predictive densities of forecasted streamflows for all years were generated (again only the 2002 results are presented here). Figures 6.15(a) and (b) show the predictive densities of forecasted streamflows in 2002, generated with the Pacific SST and BMA1 and BMA2 respectively. They are normal distribution curves, with expected values of 117 and 149 m^3/s and standard deviations of 38 and 45 m^3/s respectively. As shown in Figures 6.15(c) and (d), the results with the Atlantic SST were similar, with bell curves and expected values of 83 and 98 m^3/s and standard deviations of 34 and 41 m^3/s, using BMA1 and BMA2 respectively. Standard errors and the distribution curve of predictive densities developed with BMA can help users quantify the uncertainty.

The performance of the two BMA approaches are shown in Table 6.10. BMA1 was slightly better at generating streamflows when the Pacific SST was used as predictor. Since BMA2 specifically employed predictors with PIP values higher than 0.6, models with lower prediction skills were left in the process, which could have led to lower forecasting skills. Monthly forecasts are compared to observations in Figure 6.16(a). BMA2 often overestimated in dry years such as 1990 and 2000, and also overestimated in wet years such as 1999, 2001 and 2002. Underestimations by BMA1 seemed random.

Significantly higher forecasting skills were achieved when the Atlantic SST was used with BMA2, compared to the linear regression and BMA1 models. This could be because using BMA1 with the Atlantic SST led to discarding models that could help improve the models ability to generate skillful forecasts.

Table 6.9: Example of group of 171 variables and selected variables developed using BMA for streamflow forecasting in 2002

Group	**Periods**	**Selected variables**			
		Pacific SST		**Atlantic SST**	
		BMA1	**BMA2**	**BMA1**	**BMA2**
G1	X1_1, X1_2, ..., X1_18	X1_1	X1_1	X1_2	
G2	X2_2, X2_3, ..., X2_18	X2_8	X2_8	X2_3	X2_3
G3	X3_3, X3_4, ..., X3_18	X3_3		X3_6	X3_6
G4	X4_4, X4_5, ..., X4_18	X4_6		X4_6	
G5	X5_5, X5_6, ..., X5_18	X5_5		X5_6	
G6	X6_6, X6_7, ..., X6_18	X6_6		X6_6	
G7	X7_7, X7_8, ..., X7_18	X7_9		X7_13	
G8	X8_8, X8_9, ..., X8_18	X8_9	X8_9,X8_18	X8_12	
G9	X9_9, X9_10, ..., X9_18	X9_9	X9_9	X9_12	
G10	X10_10, X10_11,..., X10_18	X10_18		X10_12	
G11	X11_11, X11_12,..., X11_18	X11_18		X11_12	
G12	X12_12, X12_13,..., X12_18	X12_18		X12_12	X12_12
G13	X13_13, X13_14,..., X13_18	X13_18		X13_13	X13_13
G14	X14_14, X14_15,..., X14_18	X14_18		X14_14	X14_14
G15	X15_15, X15_16,..., X15_18	X15_18		X15_15	X15_15
G16	X16_16, X16_17,X16_18	X16_18	X16_18	X16_16	X16_16
G17	X17_17, X17_18	X17_17	X17_17	X17_17	X17_17
G18	X18_18	X18_18	X18_18	X18_18	X18_18

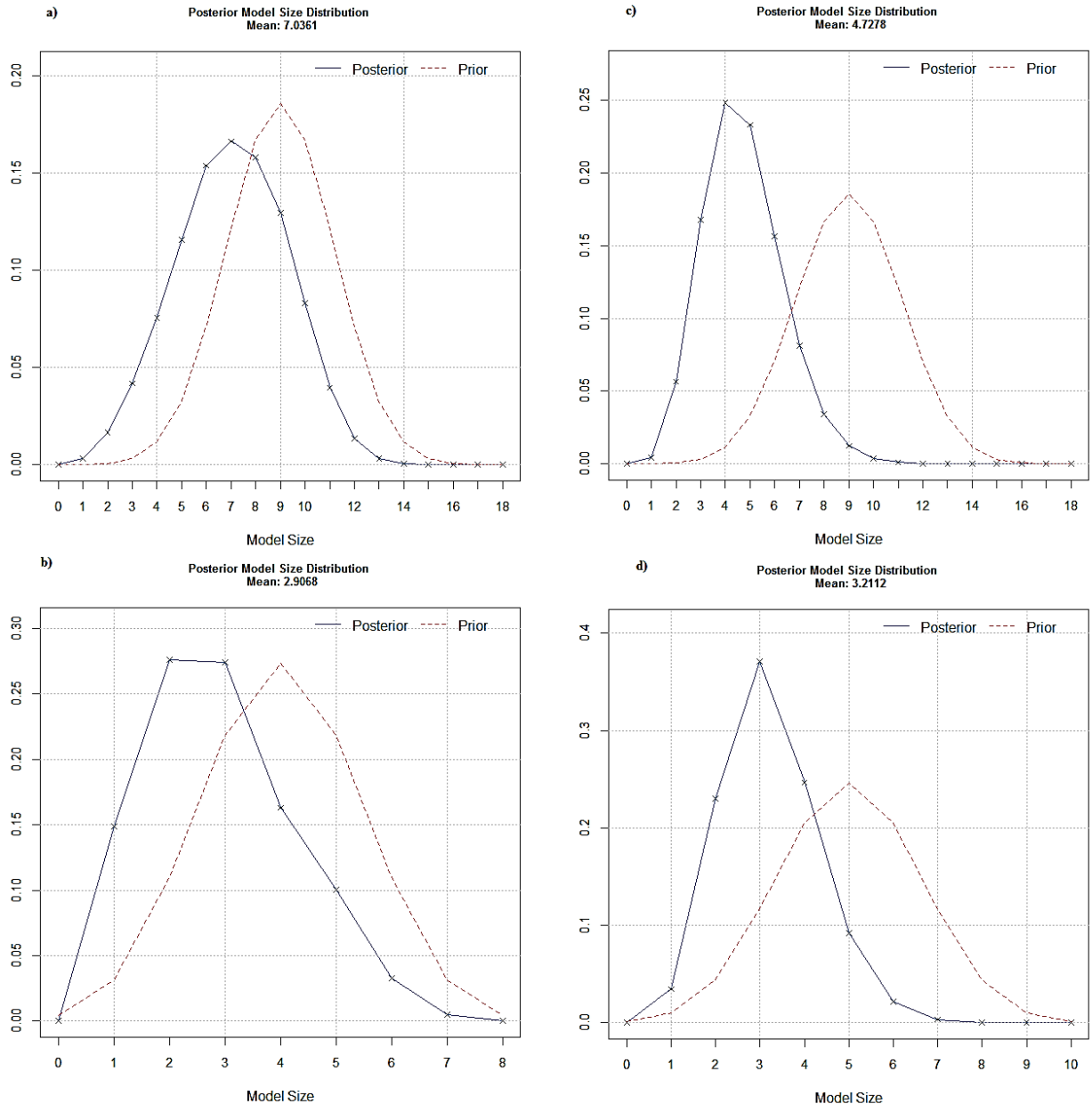

Figure 6.14: Prior and posterior model size distribution of Pacific SST using (a) BMA1 and (b) BMA2 and Atlantic SST (c) BMA1 and (d) BMA2 used for streamflow forecasting in 2002

Figure 6.17(a) compares observations and monthly July to September streamflow forecasts. Although overestimation was found for some years, including 1995, 1996 and 2000, the forecasts were able to capture the peak flows more often than when the Pacific SST was used as predictor.

c) Comparison between regression and Bayesian averaging models

Table 6.10 addresses the performance of BMA, linear and non-linear regression models to forecast streamflows. The polynomial regression model was the most successful method for streamflow forecasting using both the Pacific and Atlantic SSTs as predictors. It yielded an E_f of 0.74, R^2 of 0.75-0.76 and H of 84-85%, with lead times of 5 and 7 months for Pacific and Atlantic SSTs respectively. The performance of BMA and linear regression models was not significantly different. When the Pacific SST was used, linear regression gave slightly better forecasts than the BMA1 method. Figures 6.16(a) and (b) show hydrographs of forecasted and observed streamflows developed using the Pacific SST. Polynomial regression seemed to be the best model for capturing extreme events. The forecasts generated with BMA often showed high overestimation during dry periods and underestimation in wet periods.

The results when the Atlantic SST was used as predictor were quite the opposite, since BMA2 (E_f of 0.69, R^2 of 0.69 and H of 83%) performed better than linear regression.(E_f of 0.57, R^2 of 0.63 and H of 83%). This suggests that averaging various Atlantic SST periods can enhance model performance more effectively than using one period, as in linear regression. With the exception of 1991, polynomial regression with the Atlantic SST seemed to generate the best forecast fits to peak flows, and showed consistency with observations in dry periods, as seen in Figure 6.17.

Though BMA developed less streamflow forecasting skills than polynomial regression, and its performance was slightly better than that of linear regression when using with the Atlantic SST, the main advantage of BMA is the capability to generate predictive densities of forecasted outputs. Deterministic models like linear and polynomial regression only generate point data, with no information about the probability distribution of the forecast. Ignoring that forecast uncertainty could lead to sub-optimal decisions, when the forecasts are used for water resources management. Forecast distributions with BMA can help users obtain statistical information of forecasted streamflows, such as the type of distribution, standard deviation and expected value. BMA is also less sensitive to adding new predictors to the process than frequentist analysis.

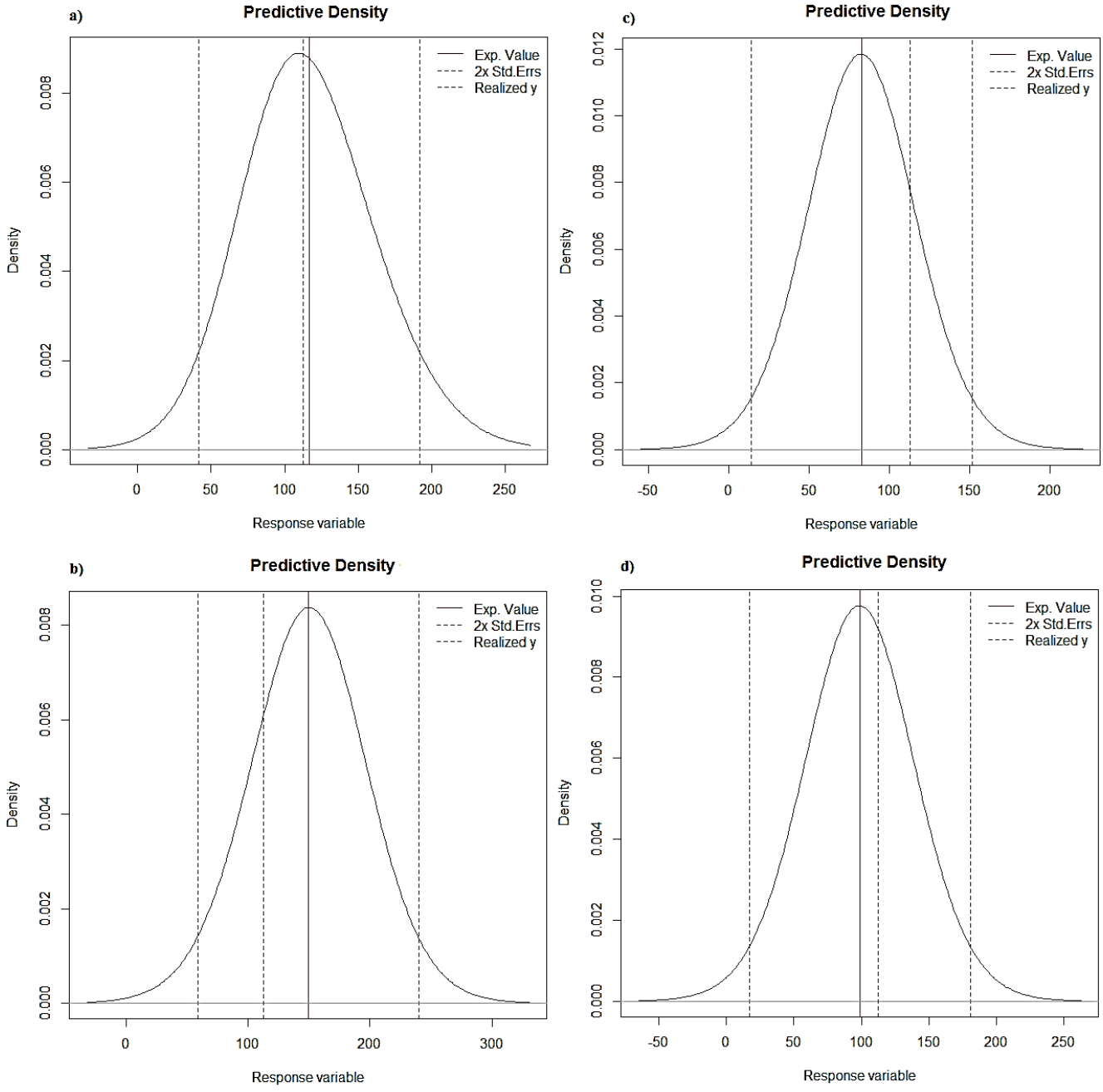

Figure 6.15: Predictive densities of streamflow forecasts in 2002 using Pacific SST with (a) BMA1 and (b) BMA2, and Atlantic SST with (c) BMA1 and (d) BMA2

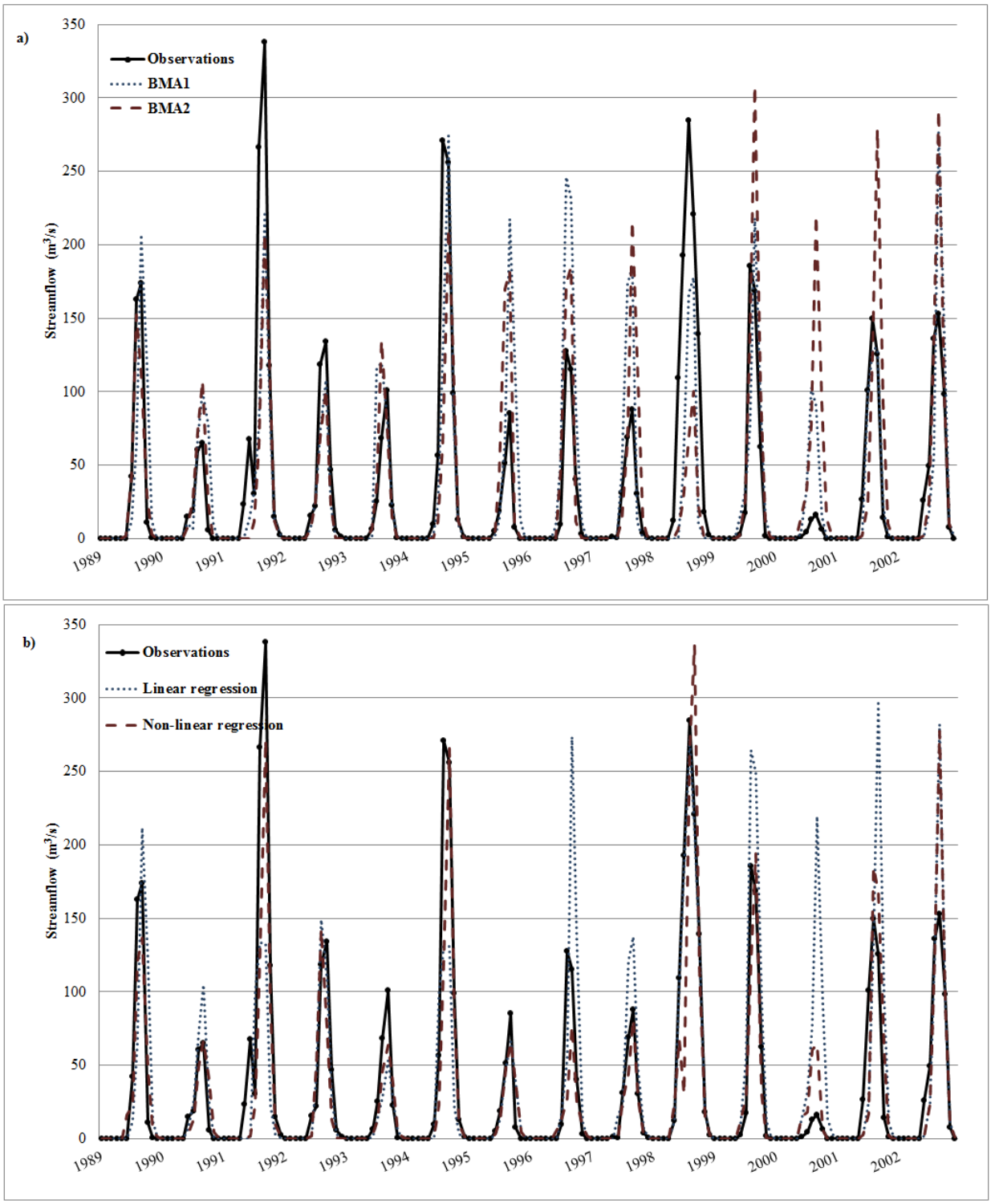

Figure 6.16: July-September monthly streamflow forecasts generated using Pacific SST with a) BMA and b) linear and non-linear regressions.

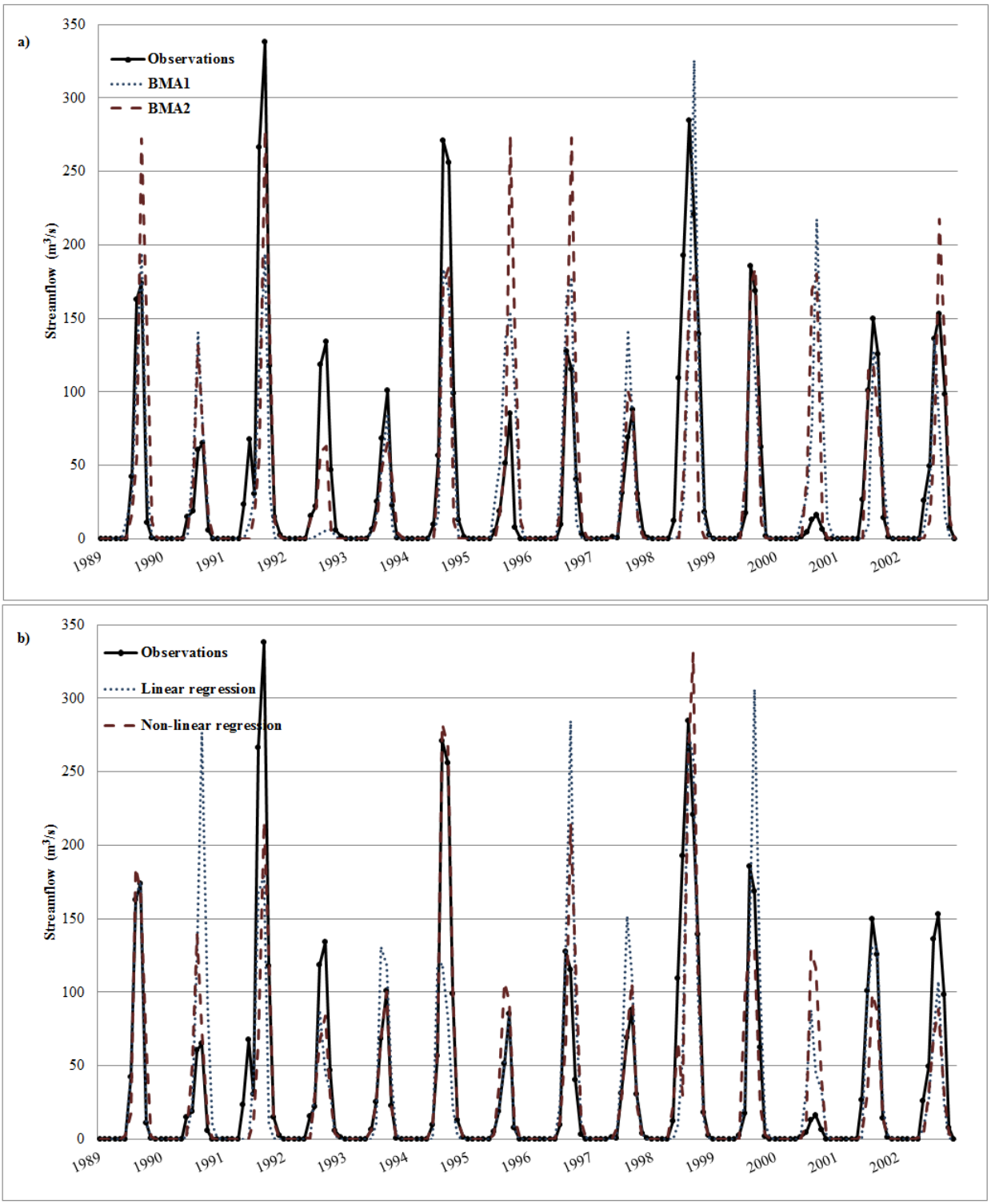

Figure 6.17: July-September monthly streamflow forecasts generated using Atlantic SST with a) BMA and b) linear and non-linear regressions.

Table 6.10: The performance of streamflow simulation using BMA and polynomial regression (1989-2002)

SST	**Model**	**Degree**	**Lead time**	E_f	R^2	H	**NMAX**
Pacific	BMA1	-	0	0.63	0.64	79	-
	BMA2		0	0.52	0.56	83	
	Linear regression		0	0.66	0.71	82	70
	Polynomial regression	5	5	0.74	0.76	84	10
Atlantic	BMA1	-	0	0.63	0.65	81	-
	BMA2		0	0.69	0.69	83	
	Linear regression		12	0.57	0.63	83	170
	Polynomial regression	5	7	0.74	0.75	85	200

6.5 Assessment of the economic value of the forecasts

The economic value of streamflow forecasts was estimated for three levels of extreme events (2, 5 and 10 year return periods). The streamflow values for these return periods were calculated by performing a frequency analysis on observed peak flows at the outlet of the Sirba watershed. For a given return period, once the corresponding discharge was calculated, forecasted streamflow values are used to build contingency tables and estimate the forecasts values for cost/loss rations ranging from 0 to 1.

6.5.1 Contingency tables for the 2, 5 and 10 year return period flow

The annual Sirba discharge from 1962 to 2002 were analysed to determine the best probability distribution among eleven candidate parent distributions using the flood frequency analysis software developed by Rao and Hamed (2000). The candidate distributions are the following:

1. Normal distribution
2. Log normal distribution
3. Three parameters log normal distribution
4. Exponential normal distribution
5. Pearson type III distribution
6. Gamma distribution
7. Logistic distribution
8. Generalized logistic distribution
9. Extreme value distribution
10. Generalized extreme value distribution
11. Generalized pareto distribution

The comparison between all eleven probability distributions and the observation data is shown in Figure 6.18 . It was found that the Pearson type III distribution was the best fit for the data, with χ^2 of 0.56 and P-value of 0.999. Using this distribution, the 2, 5 and 10 year return periods discharges were estimated as 116, 196 and 249 m^3/s, respectively. For each of these return period flows, the forecasted flows and observations were converted into two categories (above or below that particular flow value) and contingency tables were built. The contingency tables of streamflow observations and forecasts for each return period are shown in Tables 6.11 and 6.12.

6.5.2 Economic value of indirect and direct methods for streamflow forecasting

Figure 6.19 displays the economic value of the indirect and direct methods as a function of cost/loss ratio. The ratio ranged from zero to one since there is no need to consider situations with a protective cost that is higher than the loss. For a user who knows that the cost of a protective application is close to the potential loss (C/L ratio close to 1), taking an action only when there is high certainty of an extreme event occurring is most effective. If the cost for the protective action is significantly less than the potential loss

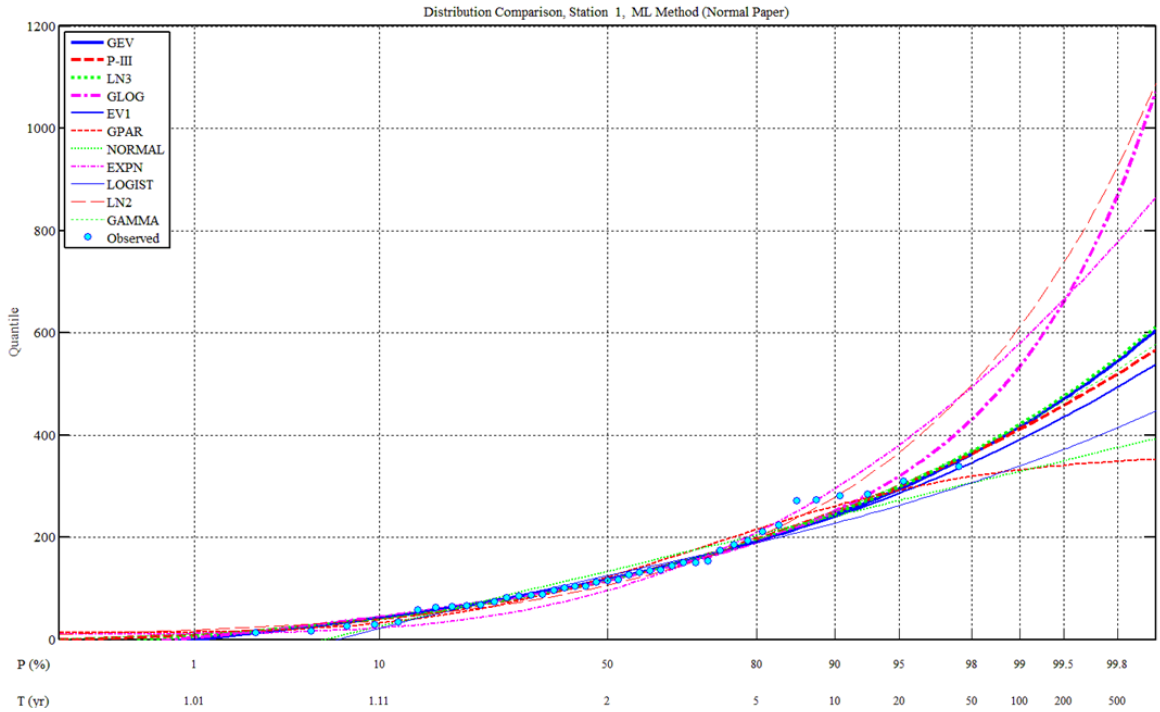

Figure 6.18: Goodness of fit tests for the distribution of observed streamflows at the outlet of the Sirba basin

Table 6.11: Contingency tables of streamflow forecasting using the indirect method based on 2, 5 and 10 year return periods

		2-year return period		
		Observation		
		< 116	≥ 116	
Forecast	< 116	1241	77	1318
	≥ 116	35	88	123
		1276	165	1441 months
		5-year return period		
		Observation		
		< 196	≥ 196	
Forecast	< 196	1384	37	1421
	≥ 196	13	7	20
		1397	44	1441 months
		10-year return period		
		Observation		
		< 249	≥ 249	
Forecast	< 249	1405	30	1435
	≥ 249	3	3	6
		1408	33	1441 months

Table 6.12: Contingency tables of streamflow forecasting using the direct method based on 2, 5 and 10 year return periods

		2-year return period		
		Observation		
		< 116	≥ 116	
Forecast	< 116	1269	49	1318
	≥ 116	7	116	123
		1276	165	1441 months
		5-year return period		
		Observation		
		< 196	≥ 196	
Forecast	< 196	1372	13	1385
	≥ 196	25	31	56
		1397	44	1441 months
		10-year return period		
		Observation		
		< 249	≥ 249	
Forecast	< 249	1387	19	1406
	≥ 249	21	14	35
		1408	33	1441 months

(C/L ratio close to 0), an action should be taken even if the probability of occurrence is low.

The economic value of model I_a and model V_p are shown in Figure 6.19. These two models were used because model I_a is the best direct method and model V_p is the best indirect method. Results show that the direct method has more economic value than the indirect method for almost all ranges of C/L values no matter the return period. It also shows that decision makers will get the most benefit with the 2-year return period of streamflow. The economic advantages of using the forecasts for water management gradually decreased when the return period increased. It is clear that the direct method for seasonal streamflow forecasting provided higher economic values than the indirect method. For the 2-year return period, the values of direct method were higher than zero along the entire range of the C/L ratio, and reached 0.7 when the C/L ratio was 0.8. The indirect method had no economic value when the C/L ratio was less than 0.3; it showed a highest value of 0.5 for a C/L ratio of 0.8.

For events of higher return periods (5 and 10 years), both the indirect and direct methods have an economic value above a certain value with cost/ loss ratio higher than 0.4 for the direct method, and 0.6 for the indirect method. The indirect method seemed to be of less interest than the direct method for economic estimation: it's highest value was approximately 0.1 while the direct method reaches values of 0.6 and 0.3 for the 5-year and 10-year return periods respectively.

In conclusion, increasing the peak flow apparently reduced the economic value of seasonal streamflow forecasts. Forecasts developed with the direct method were more valuable than those with the indirect method. This information can practical applications when the average expense of both protective cost and loss are available. In the case of the Sirba watershed, such information was not available.

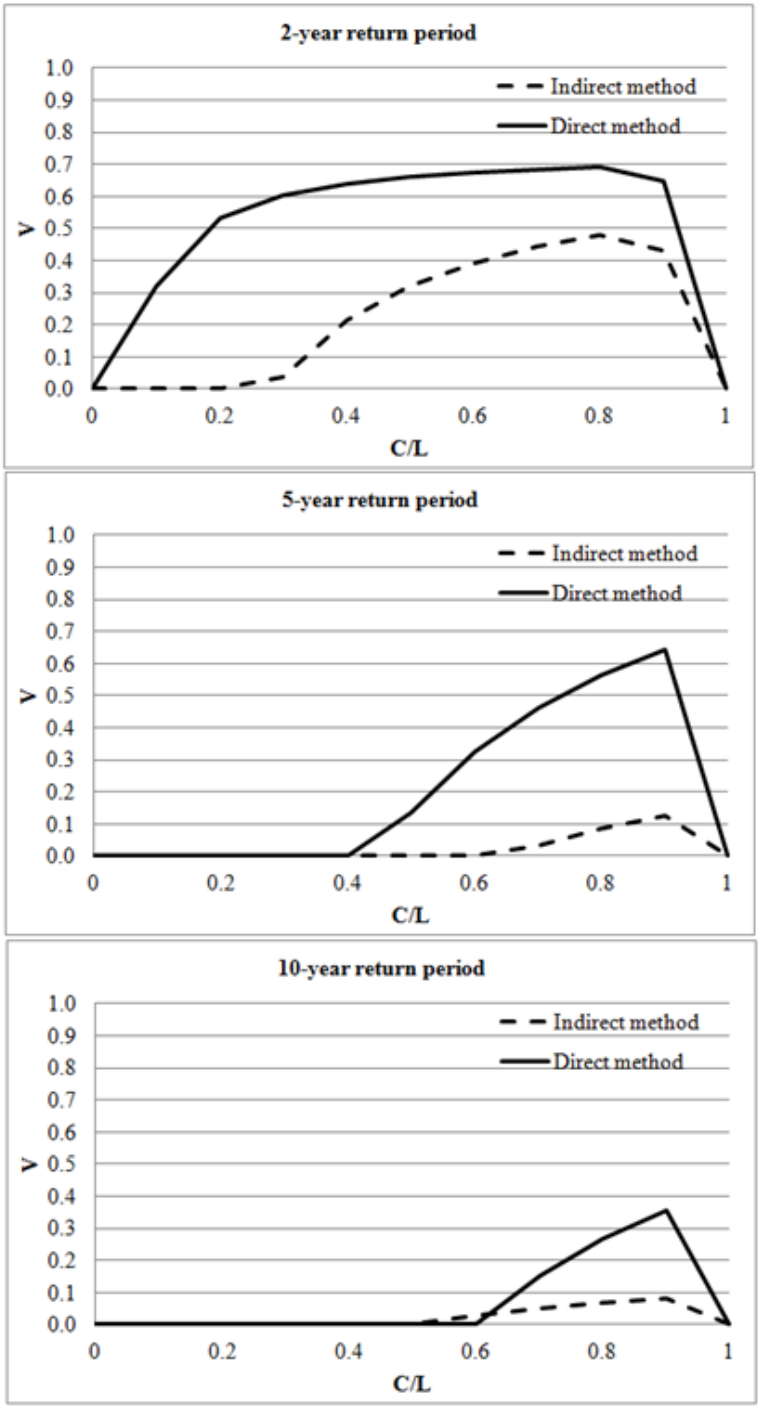

Figure 6.19: Economic value of forecasting systems of both the indirect and direct methods

Chapter 7

Seasonal Forecasting Software

In order to facilitate the dissemination of the methodologies developed in this thesis, a graphical user interface (GUI) for seasonal rainfall and streamflow forecasting was developped in MATLAB. The aim of the GUI is to help end-users implement the statistical models for seasonal forecasting almost effortlessly, and allow them to predict either rainfall or streamflow in nearby basins in the Sahel region. A limited GUI was developed for a decision maker who wants to use the Atlantic or Pacific SSTs as predictors for seasonal forecasting. However, the user can adjust the time period of the predictor and the model that will be used for prediction, which will effectively enhance the use of the statistical models. This chapter discusses all the data formats used in the interface and the interactive controls for users.

7.1 Data preparation

If users use the Pacific and Atlantic SSTs as a predictor, there is no requirement for users to prepare the predictor data for forecasting. However, if other predictors are applied, the format of the predictor needs to be well prepared for the development of interface. The predictor data file must be in the matlab file format (.mat), and contain four subfiles, namely a) latitude coordinate in decimal degree (Y), b) longitude coordinate in decimal degree (X), c) time period at a monthly scale in a serial date number (T) and d) variable data (e.g. SST). All the files except the variable data must be prepared in a vector format with only one column. The variable data file consists of three dimensions, Y, X and T.

If the observed precipitation used as the predictand was originally obtained from many stations, average precipitation data in the watershed should be determined before using the interface. The precipitation file must be in the matlab file format (.mat) and contain at least two sub-files: a) time period at daily scale in a serial date number (DATE) and precipitation data (VALUE). These two sub-files are in a vector format with one column. Similar to the precipitation data, if there is more than one data time series available, the spatial average of the streamflow data must be calculated. The file must be in the matlab format (.mat) at a monthly time scale, and contains only one sub–file. The data file has three columns; year, month and data respectively.

7.2 Using the graphical user interface

The graphical user interface proposes three main functions: a) input data and model selection, b) performance of the best output, and c) forecasting for the upcoming year. The user should carefully input all the relevant data to the same folder, to ensure that the GUI can access the data when used. Outputs developed using the interface will also be saved in one folder. Details of all outcomes are discussed in this chapter.

7.2.1 Input data and model selection

All predictands formatting should be done as described in the previous section, since users could encounter interface errors if there are mistakes in input data formatting. The type of forecasting, rainfall or streamflow, can be specified by selecting from the pop-up menu in the predictand information section. The file name must be put keyed into the interface correctly. This study focused the rainy season of the Sirba basin, approximately July to September, but users can change the aggregate period of interest by inputting the number of the first and last months of the period (e.g. July-September = 7-9).

Either the Pacific or Atlantic SST can be used as a predictor by choosing it from the pop-up menu in the predictor section. Since the interface was designed to apply all periods during the first and last month at one month increment, the user needs to define the first month, the end of the first month and the last month. The number of the month is formatted; for example January of the year before forecasts issued is 1, February of the year before forecasts issued is 2, and so on. January of the year forecasts issued is 13 and February of the same year is 14, etc. Users can look for a suitable predictor

period up to the month before the forecasts issued, and they can determine whether the data sets contain missing values, which are identified as -99. The interface will take less computational time to generate final results if there is no missing value in the predictor.

The next section is related to the model that will be used for forecasting. As described in Chapter 5, the number of predictor grid data is restricted by the N_{max} value. Thus, the user can specify how many grid data the model should apply in the predictor vector reduction step. The models were developed to receive the N_{max} with ten increments, and the first and last N_{max} are required in the interface. Increasing the number of N_{max} strongly impacts the computational time of the interface. The next step is for the user to specify the type of regression analysis. There are two applicable regression analysis approaches: linear regression and polynomial regression. Though, no additional information is needed for linear regression, the polynomial method requires the user to specify the first and last degrees. There is a limitation on the degrees that can be defined in the model: they must not be lower than two or higher than six. Next, the method to select only high predictive grid data must be determined, and this is done using the pop-up menu of the screening step. The interface allows the user to select either R^2 or E_f as the criterion for discarding predictor data with low predictive capability. Finally, new predictor data sets based on the original data are rearranged using either PCA or CCA. The user can select which predictor reduction step will be used in the method.

7.2.2 Performance of the best model

Since the interface was designed to generate and store all the simulations developed with all the predictor periods, N_{max} values and models with different degrees of polynomial regression. The number of simulations depends on the input information defined for the interface. All outcomes and input data are stored in the same folder of the interface (details of all data in the simulation folder are explained in the next section). Due to the large number of simulations, the interface displays only the best simulation in the result section, and reports the period of predictor, lead time, N_{max} and the degree (for polynomial regression) used to developed the best simulation. The three objective functions (R^2, E_f and H) used to estimate the best model performance are also presented as well as the time series of both the best result and observations at an annual time scale which highlights the inter-annual variability of both data sets.

7.2.3 Forecasting for the next year

If there is the predictor data available to forecast the year after the last year of the predictand period, the interface will use the best period and the most successful method applied in the best result section to predict the next year. The forecasting section will indicate the year forecast issued, the maximum and minimum daily data and the average seasonal and annual data. Forecasted output at a monthly time scale will also be shown in this section to allow users to consider the intra-seasonal variability for the next year.

7.3 Example of application

This section presents an example of how to use the interface for seasonal forecasting. Rainfall forecasting developed using the Pacific SST as a predictor with model II (E_f in the screening step, PCA in the vector dimension reduction approach and multiple linear regressions in the regression analysis) are performed as an example.

Figure 7.1 illustrates the graphical user interface for seasonal forecasting. Sections 1, 2 and 3 show the steps required to input all the required information. In the first section (predictand information), rainfall forecasting is selected in the pop-up menu in order to develop rainfall forecasts. The user can also choose streamflow forecasting instead to simulate streamflows. The predictand data file must be correctly named; the rainfall observation file used in this example is PCP_SIRBA. Then, the user can define a period of interest for forecasting, which for this study is a rainy season in the Sirba watershed. Thus, 7-9 (July to September) is input for the first and last month. The model will calculate the average data during this period, and annual rainfall for the wet season of each year will be generated.

The predictor information is then input to the interface. The Pacific SST was chosen as a predictor in this example. The user needs to specify the first month, the end of the first month and the last month to determine the aggregate period of interest that will be calculated at one month increment. The number of predictor depends on the duration time forced to the model. This example examined the predictive skills of the Pacific SST during March to June, thus, the number 3, 3 and 6 were input to the interface for the first month, the end of the first month and the last month respectively. Finally, four aggregate predictors (March, March to April, March to May and March to June) were applied to generate the forecasts. There is an active icon that indicates if there are missing values in the predictor. It saves running time if the predictor is complete, and

the user identifies it to the interface.

Next, the user indicates the specific statistical model that will be used to predict rainfall. The first and last N_{max} with ten increments specifically restricts the number of predictors forced to the dimension reduction approach. As shown in Figure 7.1, N_{max} is limited to starting from 80 to 90. The type of regression analysis is then defined (linear regression in the example). If polynomial regression is selected, the range of the degree of the regression is required. The boundaries of the polynomial regression in the interface are two to six degrees. The user must also specify the method to be applied in the screening step and the predictor reduction method. E_f and PCA were chosen in this example, as illustrated in Figure 7.1. Finally, the user actives the model by selecting the 'Run' button. A message box appears if the model completes the process successfully.

All outputs produced by the model are saved in the same location as input data. The lists of the files developed from each predictor and each N_{max} are described below;

- R_(the name of predictor)_(the screening method used)_(the vector reduction method used)_(the first month)_(the last month)_N_{max}.mat. This file contains sub-files with all the information used for forecasting (e.g. predictor, predictand, data after filtering), as well as the forecasted outcomes and performance criteria of the model.

- R_(the name of predictor)_(the screening method used)_(the vector reduction method used)_(the first month)_(the last month)_N_{max}.png. It is a figure file showing annual forecast of the specific season initially defined compared to observations for the entire study period.

- - R_(the name of predictor)_(the screening method used)_(the vector reduction method used)_N_{max}. This file tabulates output data only.

The interface was also designed to store all the objective functions that were estimated by the outputs developed using difference N_{max} in one file. This makes it convenient for the user to analyses all the outputs.

The best output is presented in the Result Section as illustrated in Figure 7.2. After clicking the 'Show the best output' button, a graph of rainfall time series (1971-2003) of both observations and simulations (hindcast simulations) appears, along with all information related to the best simulation. The example shows that the best predictor period was March to June of the previous year, with a lead time of 12 months and a suitable N_{max} number of 90. The objective functions used to estimate the goodness of fit between simulations and observations are also indicated.

Finally, the forecasts of the year after the last year of hindcast simulation was generated. Figure 7.3 illustrates the forecasting output for 2004, which was developed using the same model initially defined to the interface with the best period of predictor, the best N_{max}, and the most suitable degree if polynomial regression was selected. Monthly rainfall data of the next year is also presented, including extensive information related to minimum and maximum daily data, annual data for the specific season and annual data average over the entire year.

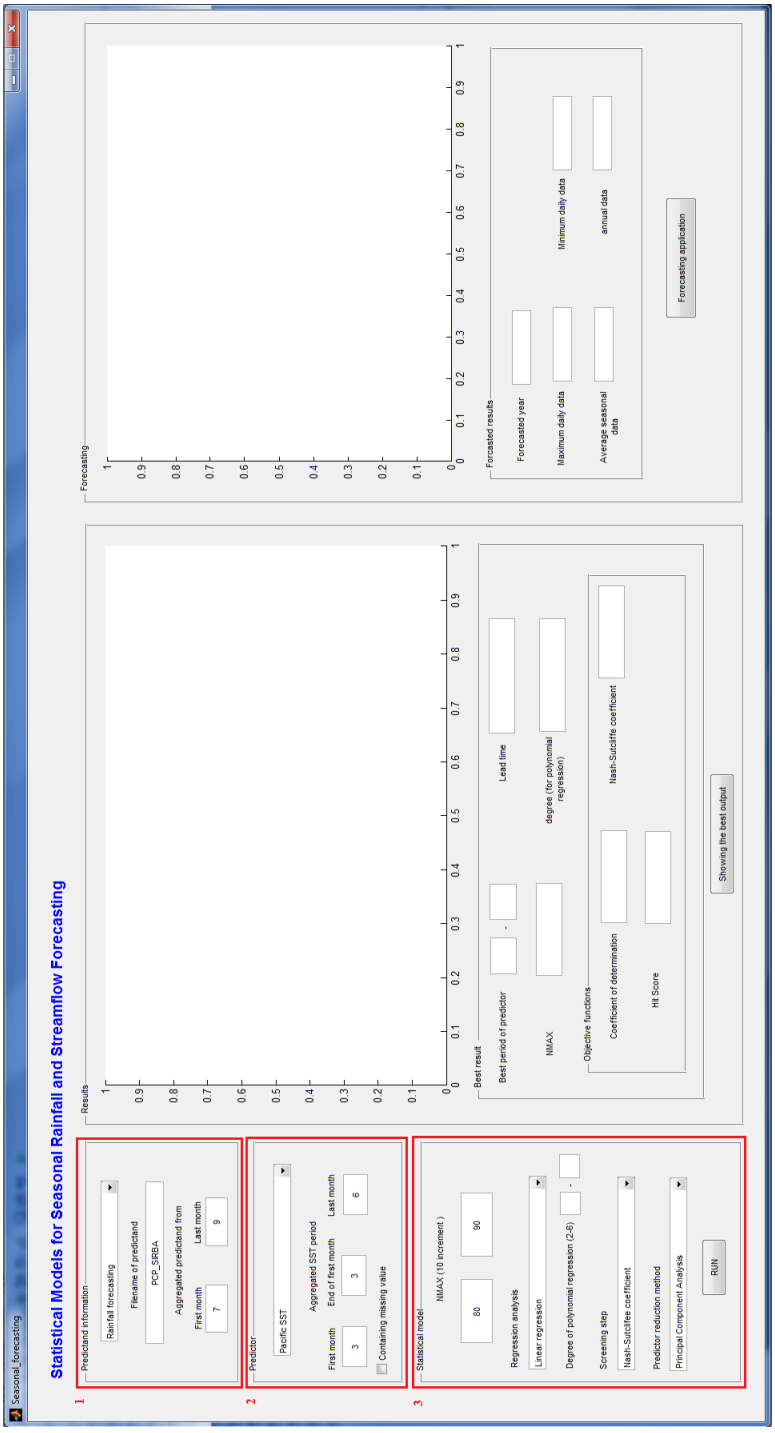

Figure 7.1: MATLAB seasonal forecasting package: input data section

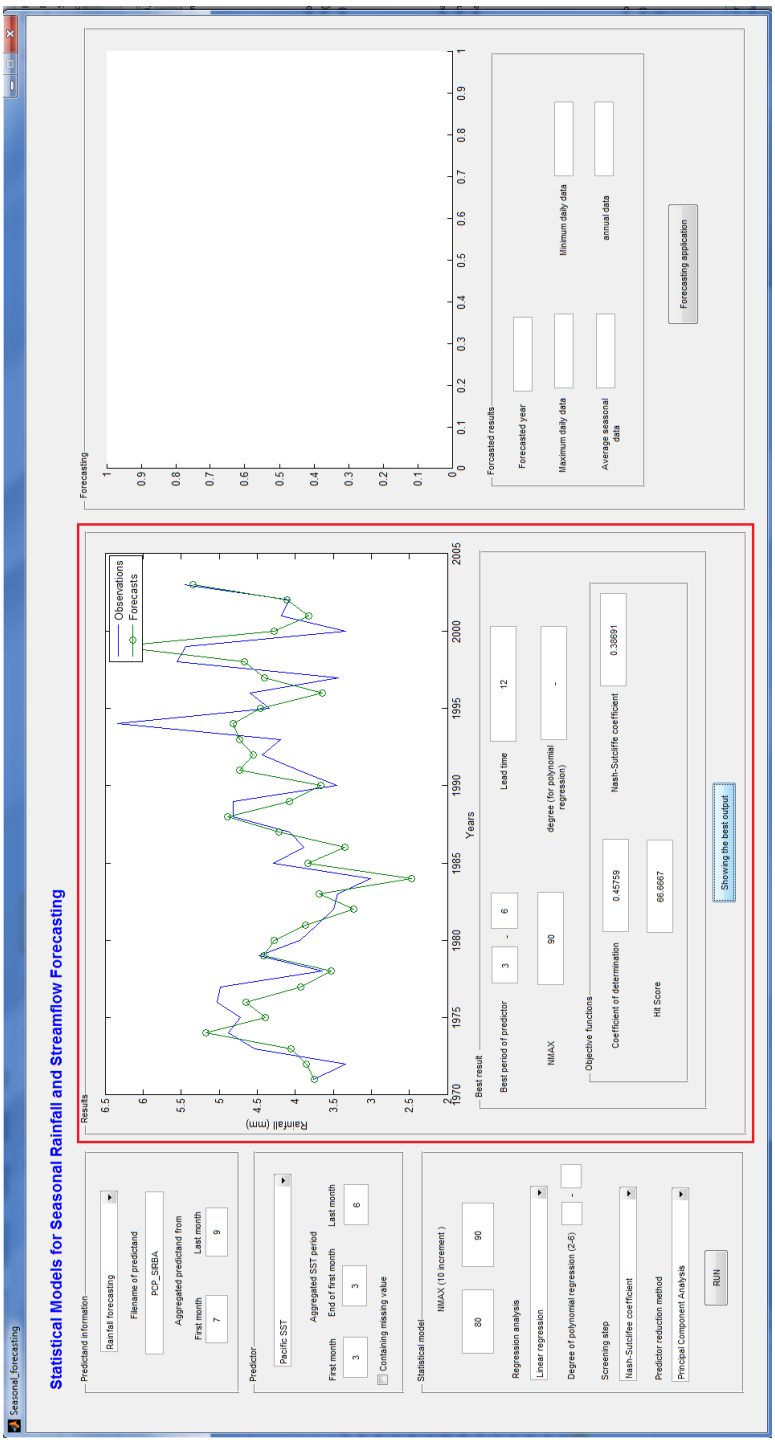

Figure 7.2: MATLAB seasonal forecasting package: best model performance

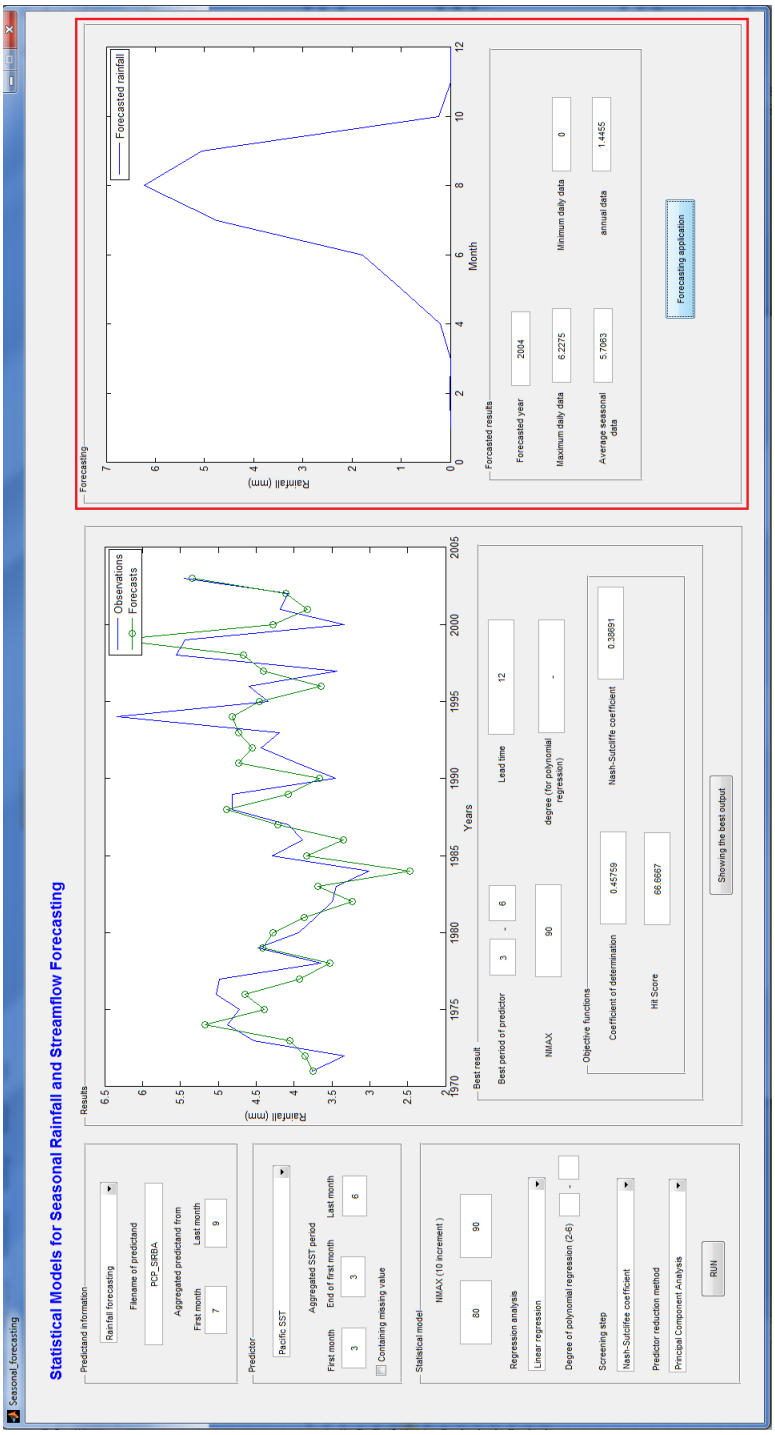

Figure 7.3: MATLAB seasonal forecasting package: forecasting for the upcoming season

Chapter 8

Conclusions

Seasonal streamflow forecasting is important for areas with high climate variability such as the Sahel region, where prolonged droughts and recurrent flooding events are devastating for the local population. The development of skillful seasonal rainfall and streamflow forecasting models will help government agencies to provide vital information for farmers, particulary, those who rely on rainfed agriculture and might need to switch crops. This research is intended to improve seasonal rainfall and streamflow forecasting skills using statistical models alone or in combination with rainfall-runoff models. While rainfall was forecasted using only statistical models, two approaches were considered for streamflow forecasting:

1. A two-steps stream forecasting approach (called as the indirect method) which first linked the average SST over a period prior to the date of forecast to seasonal rainfall amount in the upcoming rainy season, then linked the rainfall amount to streamflow using a rainfall-runoff model. In this approach, the forecasted rainfall was disaggregated at the daily time step before being fed into the rainfall-runoff model.

2. A one-step streamflow forecasting approach (called as the direct approach) which linked the average SST over a period prior to the date of forecast, to the average streamflow in the upcoming rainy season.

The tropical Pacific and Atlantic SSTs were used as predictors, but the developed methodologies can be applied with any other relevant predictor. The research went further than most seasonal forecasting studies by looking at the uncertainty in the prediction and estimating the economic value of the forecasts.

8.1 Rainfall/streamflow forecasting using statistical models alone

In this research, eight classes of statistical models for seasonal forecasting were developed. Each model was validated using a leave-one-out validation strategy (one year was discarded and the remainder of the data was used to build the predictive model). Once a year was discarded, the predictive model developed in four phases: a) screening of SST time series at grid points and retaining a limited numbers; b) predictor vector dimension reduction using principal components analysis (PCA) or canonical components analysis (CCA); c) the development of the forecasting model for each predictor and d) the selection of the best model. The first and second stages were required because most predictor data sets (e.g. large-scale atmospheric and oceanic indices) are generally collected on large grids. At the third step, either linear or polynomial regressions of degree two to six were used to link the predictors and predictand.

The following conclusions are reached about the performances of the statistical models for rainfall and streamflow forecasting:

Rainfall forecasting: The best model for rainfall forecasting in the study area was a linear model that used the average Pacific SST from March (Y-1) to June (Y-1) as a predictor (12 months lead time). The next best model used a polynomial regression of degree six to link seasonal precipitation on the Sirba watershed to the Atlantic SST averaged over September (Y-1) to January(Y) (5 months lead time). The rainfall forecasting skills were modest (E_f of 0.39 and 0.28 for the best and the second respectively), but compared well to results from other studies in terms of accuracy and lag time (e.g. Barnston et al. (1996); Garric et al. (2002) and Mo and Thiaw (2002)). Models consisting of PCA clearly performed better than those where CCA was used for predictor vector dimension reduction. While it is difficult to explain with certainty why this occurred, the fact that CCA provides a one-column predictor while PCA produces several potential predictors is a plausible explanation. Therefore, using PCA could increase the chance of a retained predictors having a significant link with the predictand. The results also indicated that arbitrarily choosing SST from a single month or trimester as predictors (as most authors do) might not lead to optimal forecasting.

Direct streamflow forecasting: Polynomial models performed better than linear models for streamflow forecasting with both Pacific and Atlantic SST. Unlike rainfall forecasting, the screening process did not influence the performance of the models used for streamflow forecasting. In addition, as it was the case for rainfall forecasting, models using PCA always had higher performance than those with CCA. Streamflow forecasting performance (R^2 of 0.7 with 7 months lead time) were reasonable compared to that obtained from other studies (e.g. Kwon et al. (2009) achieved predictive skills with R^2 of approximately 0.5 to 0.6 with one season prior). Since the lack of study about seasonal streamflow forecasting in the Sahel region and some other studies used different performance criteria, it made the comparison more difficult.

8.2 Streamflow forecasting using the indirect method

The indirect method consisted of using the eight classes of models to forecast seasonal rainfall, using the fragment method to disaggregate seasonal rainfall and then using the SWAT model to convert them into streamflow. The best model turned to be the SWAT model driven by rainfall forecasts developed using model I_a (with the average Atlantic SST over September (Y-1) to December (Y-1) as a predictor) at six months lead time. The next best model was the SWAT model forced by rainfall forecasts generated using model V_p (the average Pacific SST over January (Y) to February (Y)) at a four months lead time.

The comparison between the indirect and direct method showed that the direct method ultimately showed slightly higher performance than the indirect one driven by Pacific (using linear and polynomial regressions) and Atlantic SSTs (using polynomial regression), except when linear regression was used with the Atlantic SST the indirect method showed better performance. Models V_p and V_a (the direct method) were the best models when they were forced with the Pacific and Atlantic SST with five and seven months lead time respectively. There was insignificant difference in skill levels between these two SST data sets driven by the same model (model V). The indirect method showed higher forecasting skill only when it was forced by the rainfall forecasts developed by model I_a (linear regression model) with 6 months lead time.

When the monthly streamflow forecasts developed the indirect method were aggregate to annual time scale, they showed very low performance with negative values of E_f (accept the indirect method with linear regression and the Atlantic SST) and low R^2

and H values. Annual streamflow forecasts developed using the direct method were also lower than monthly time scale but significantly better than those developed using the indirect method. Interestingly, the direct method with polynomial regression (model V_p) forced by the Pacific SST was outstanding in both monthly and annual time scales.

Overall, the performance of the indirect and direct methods was not significantly different in terms of both forecasting accuracy and lead times. Each was capable of predicting rainfall and streamflow at a seasonal time scale with four - seven months in advance, and both showed moderate to high streamflow forecasting skills.

8.3 Limitations of the developed models

The benefit of using statistical models for seasonal forecasting are evident in this research. However, these models rely only on input data characteristics without concerning the physical mechanisms behind the correlations between independent and dependent variables. Therefore, statistical models are strongly sensitive to the input data. The use of the same type of predictor data sets with different methodologies could lead to different outputs in terms of forecast accuracy, lead time and model efficiency. Using statistical models also requires assuming that the stationary data indicating present or future trends will be behave as it has in the past; historical data patterns that are not similar to current or future events could cause forecast errors. Therefore, testing the statistical models to determine the optimum predictor periods when updated data are available before using them to forecast rainfalls or streamflows is strongly recommended. In addition, the quality of the data sets must be carefully monitored before using the statistical models. The performance of statistical models could also decrease when historical data of both the predictor and the predictand are not adequate to capture their relationships or if there are too many gaps in those data sets.

In the particular study, a good performance calibration with SWAT was obtained. However, the length of the streamflow time series did not permit a validation study. The main issue for using SWAT in the Africa is data availability. Incomplete input data sets or insufficient model calibration could lead to significant errors. The SWAT model requires relevant information about continental hydrology and climate data, and the quality of this data should be high enough to allow forecasting (e.g. minimal missing values, high temporal-spatial resolution). With these conditions, forecasting is very difficult in study areas lacking climate stations and basin characteristic information.

8.4 Uncertainty analysis

In this study a basic analysis of model error method was first used to measure the uncertainty level of the forecasts developed using the indirect and direct methods. Assuming a normal distribution for rainfall and streamflow forecasts, a set of forecasts were generated from which an empirical probability distribution could be derived. The mean value of the distribution was simply the forecasted value, and its standard deviation was assumed to be the standard deviation of the residuals. A cloud of monthly streamflow values was generated, and streamflow observations were mostly in the range of uncertainty, which tells users that the chances of unexpected event occurrences was low.

A disadvantage of using polynomial and linear regression for statistical seasonal forecasting is that only a few predictors from the pool of potential predictors are used in the final model. Using only certain predictors and discarding others could result in loss of potentially valuable information in those discarded. Using BMA can help address this problem, as it considers all predictors in the process. Though, there was no significant difference between using BMA and linear regression models for streamflow forecasting, the BMA is capable to produce the probability density of the forecast, and a standard error calculated from all the models. It is beneficial for users to be able to visualize the density of the expected values, and assess the level of uncertainty of the generated forecast. Higher uncertainty was expected to be found in the forecasts developed using BMA, since BMA accounts for two types of uncertainty: the model error and the model selection. Using the basic analysis of model error method investigates only an uncertainty of the model error.

A possible means of improving BMA performance would be to apply other types of priors, rather than using a uniform model prior that was defined in this study. Another option that could enhance forecasting skills is changing the predictors used in the models to other oceanic and atmospheric indices. The different factors usually affect different aspects of large-scale circulation, which could influence individual hydrological variables of interest.

8.5 Economic values of seasonal forecasts

The basic cost/loss ratio method was used to estimate the potential economic value of indirect and direct methods for streamflow forecasting. A protection action will have a specific cost and there will be a loss when an extreme event occurs without the protection. Since there is no benefit from a situation with a protection cost higher than the loss, only the cost/loss ratio range between 0 and 1 was considered. The economic impact of streamflow forecasts were evaluated events of 2, 5 and 10 year return periods. The frequency analysis was used to define the specific streamflow values based on the return periods. For more extreme events, the economic values of the forecasts developed using the indirect and direct methods decreased significantly, and the maximum benefit varied according to the event. The forecasts generated by the direct method were clearly more beneficial than those developed with the indirect method for all events and all cost/loss ratios. For the 5 and 10 year return periods, users with small cost/loss ratio (i.e. less than 0.4) would receive no economic benefits from the forecasts. However, all users could get economic benefits from the forecasts developed by the indirect method when the streamflows with 2 year return period occurred.

8.6 Recommendations and future work

This research study highlighted the benefits of systematically searching for the best period to aggregate SST when building predictors for seasonal precipitation or streamflow forecasting. An initial pool of potential predictors can be built by searching the relevant literature and/or by inference from known physical relationships between the potential predictors and predictands. Randomly selecting predictors without considering their physical relationships with predictands could lead to the failure of a forecast system.

The model efficiency estimation should be determined using a variety of criteria as only one estimator could be misleading; for example, a high value of R^2 only explains that the variance of observations is strongly described by the model. However, a plotted time series of both observations and forecasts could identify inconsistencies between their magnitudes. In addition, some criteria are sensitive to outliers, so it could be incorrect to assume the accuracy without examining them.

This study considered all observed data as stationary; their statistical properties were assumed to remain the same over the entire period and there was no abrupt change. However, abilities of detecting change points in the data series such as changing in mean,

variance or data trend might help improve seasonal forecasting skills. Those changes can occur from for example, changes in observation locations, measurement errors, substantial anthropogenic changes. There are various methods used for change point detections such as, standard normal homogeneity test, Nonparametric SNH test and the Bayesian approach for change point analysis. If there are abrupt changes detected in observed data, users might need to search for suitable methods to manage those data before directly using them. For example, the data might be divided into segments based on change points and analysed separately.

In this study, only the simple cost/loss ratio method used for estimating the economic values of forecasting systems was applied with the different cost/loss ratio situations. A specific case study containing the information of the practical cost and loss values with particular adverse events might be considered to estimate the value of forecasts. The other methods for economic estimation of forecasting system might be used such as, willingness-to-pay, minimax strategy, maximization of expected net returns. The appropriate methodology for a specific case is defined by the objectives of decision makers (Mjelde et al., 1989). Other characteristics of the forecasts such as lead time and time period of a given forecasts (specific month or seasonal) could be combined with the forecast accuracy to estimate the economic forecast values. A less accurate forecast but known earlier might lead to a higher economic value than the one developed with shorter lead time, and forecasts in a specific time period (particularly for an agricultural sector (e.g. a during growing season)) could give a higher value than those generated in other periods (Mjelde et al., 1989).

SSTs are not the only potentially useful predictors of rainfall and streamflow forecasting. Other atmospheric and oceanic patterns can also be applied to seasonal forecasting, including variables such as mean sea level pressure, ENSO index and wind velocity patterns. Thus, these model algorithms can be used with other predictors. In addition, the SWAT model of the Sirba watershed developed in this study can be applied to nearby basins in the Sahel region, since only small difference might be found. Other regression models are also strongly recommended, and can be implemented by following the guidelines in this study.

References

Abbaspour, K.C., 2012. SWAT-CUP 2012: SWAT calibration and uncertainty 7 programs. Eawag: Swiss Federal Institute of Aquatic Science and 8 Technology. Retrieved from http://www.neprashtechnology.ca.

Abedokun, J.A. (1979). Towards achieving an in-season forecasting of the West African precipitaton. *Archive for Meteorology, Geophysics and Bioclimatology Series A*, 28, 19-38.

Abudu, S., King, J.P. and Pagano, T.C. (2010). Application of partial least-square regression in seasonal streamflow forecasting. *Journal of Hydrologic Engineering*, 15, 612-623.

Akiner, M.E. and Akkoyunlu, A. (2012). Modeling and forecasting river flow rate from the Melen Watershed, Turkey. *Journal of Hydrology*, 456-457, 121-129.

Alansi, A.W., Amin, M.S.M., Abudul Halim, A., Shafri, H.Z.M. and Aimrun, W. (2009). Validation of SWAT model for streamflow simulation and forecasting in Upper Bernam humid tropical river basin, Malaysia. *Hydrology and Earth System Sciences Discussion*, 6, 7581-7609.

Amadou, A., Abdouramane, G.D., Ousmane, S., Ibrah, S.S. and Sittichok, K. (2014). *Changes to flow regime on the Niger River at Koulikoro under a changing climate. Hydrological Sciences Journal.* doi:10.1080/02626667.2014.916407

Anderson, I., Dione, O., Jarosewich-Holder, M. and Olivry, J.C. (2005). *The Niger river basin: a vision for sustainable management.* The International Bank for Reconstruction and Development / The World Bank. e-ISBN: 0-8213-6204-6.

Arnold, J.G., Moriasi, D.N., Gassman, P.W., Abbaspour, K.C., White, M.J., Srinivasan, R., Santhi, C., Harmel, R.D., Griensven, A.V., Van Liew, M.W., Kannan, N. and Jha, M.K. (2012). SWAT: model use, calibration, and validation. *American Society of Agriculture and Biological Engineers*, 55, 1491-1508.

Badr, H.S., Zaitchik, B.F. and Guikema, S.D. (2014). Application of statistical models to the prediction of seasonal rainfall anomalies over the Sahel. *Journal of Applied Metorology and Climatology*, 53, 614-636.

Baker, T.J. and Miller, S.N. (2013). Using the Soil and Water Assessment Tool (SWAT) to assess land use impact on water resources in an East African watershed. *Journal of Hydrology*, 486, 100-111.

Barnston, A.G., Thiao, W., and Kumar, V. (1996). Long-lead forecasts of seasonal precipitation in Africa using CCA, *Weather and Forecasting*, 11, 506-520.

Berri, G.J. and Flamenco, E.A. (1999). Seasonal volume forecast of the Diamante River, Argentina, based on El Nino observations and predictions. *Water Resources Research*, 35, 3803-3810.

Beven, K. (2012). Rainfall-runoff modelling: the primer, second edition. West Sussex:John Wiley & Sons, Ltd.

Brooks, N. (2004). *Drought in the African Sahel: long term perspectives and future prospects*. Tyndall Centre Woking Paper NO.61, Tyndall Centre for Climate Change Research, October 2004.

Biasutti, M., Battisti, D.S. and Sarachik, E.S. (2004). Mechanisms controlling the annual cycle of precipitation in the tropical Atlantic sector in an Atmospheric GCM. *Journal of Climate*, 17, 4708-4723.

Biasutti, M., Held, I.M., Sobel, A.H. and Giannini, A. (2008). SST forcing and Sahel rainfall variability in simulations of the twentieth and twenty-first centuries. *Journal of Climate*, 21, 3471-3486.

Biasutti, M. and Giannini, A. (2006). Robust Sahel drying in response to late 20th century forcings. *Geophysical Research Letters*, 33, 1-4.

Black, D., Wallbrink, P., Jordan, P., Waters, D., Carroll, C., Blackmore, J. (2011). *Guidelines for water management modelling: Towards best-practice model application*. eWater Cooperative Research Centre. ISBN 978-1-921543-46-3.

BMZ (Federal Ministry for Economic Cooperation and Development). (2010). Adaptation to climate change in the upper and middle Niger River Basin. Retrieved from $http://ccsl.iccip.net/niger_river_basin.pdf$

Bossa, A.Y., Diekkruger, B., Giertz, S., Steup, G., Sintondji, L.O., Agbossou, E.K. and Hiepe, C. (2012). Modeling the effects of crop patterns and management scenarios

on N and P loads to surface water and groundwater in a semi-humid catchment (West Africa). *Agricultural Water Managemen*t, 115, 20-37.

Busuioc, A., Tomozeiu, R., and Cacciamani, C. (2008). Statistical downscaling model based on canonical correlation analysis for winter extreme precipitation events in the Emilia-Romagna region. *International Journal of Climatology*, 28, 449-464.

Camberlin, P., Janicot, S. and Poccard, I. (2001). Seasonality and atmospheric dynamics of the teleconnection between African rainfall and tropical sea-surface temperature: Atlantic VS. ENSO. *International Journal of Climatology*, 21, 973-1005.

Caminade, C. and Terray, L. (2010). Twentieth century Sahel rainfall variability as simulated by the ARPEGE AGCM, and future changes. *Climate Dynamics*, 35, 75-94.

Casanova, S. and Ahrens, B. (2009). On the weighting of multimodel ensembles in seasonal and short-range weather forecasting. *Monthly Weather Review*, 137, 3811-3822.

Chambers, L.E. (2003). *South Australian rainfall variability and trends.* BMRC research report no.92, Bureau of meteorology Research Centre, Australia.

Chase, T.N., Pielke SR, R.A and Avissar, R. (2005). Teleconnections in the earth system. Encyclopedia of Hydrological Sciences, John Wiley & Sons, Ltd.
Retrieved from http://onlinelibrary.wiley.com/doi/10.1002/0470848944.hsa190/pdf

Chen, B. (2014). *General Linear Least-Squares and Nonlinear Regression.* Lecture note, Department of Computer Science & Information Engineering, National Taiwan Normal University.

Chiew, F.H.S. and McMahon, T.A. (2002). Global ENSO-streamflow teleconnection, streamflow forecasting and interannual variability. *Hydrological Sciences Journal*, 47, 505-522.

Chow, V.T., Maidment, D.R. and Mays, L.W. (1988). *Applied hydrology.* US: McGraw-Hill,inc.

Collins, D.C., Reason, C.J.C., and Tangang, F. (2004). Predictability of Indian Ocean sea surface temperature using canonical correlation analysis. *Climate Dynamics*, 22,481-497.

Conway, D., Persechino, A., Ardoin-Bardin, S., Hamandawana, H., Dieulin, C. and Mahe, G. (2009). Rainfall and water resources variability in sub-Saharan Africa during the twentieth century. *Journal of Hydrometeorology*, 10, 41-59.

Descroix, L., Mahe, G., Lebel, T., Favreau, G., Galle, S., Gautier, E., Olivry, J-C, Albergel, J., Amogu, O., Cappelaere, B., Dessouassi, R., Diedhiou, A., Breton, E.L., Mamadou, I. and Sighomnou, D. (2009). Spatio-temporal variability of hydrological regimes around the boundaries between Sahelian and Sudanian areas of West Africa: a synthesis. *Journal of Hydrology*, 375, 90-102.

Diro, G.T., Grimes, D.I.F. and Black, E. (2011). Teleconnections between Ethiopian summer rainfall and sea surface temperature: part I observation and modelling. *Climate Dynamics*, 37, 103-119.

Duan, Q., Sorooshian, S. and Gupta, V.K. (1994). Optimal use of the SCE-UA global optimization method for calibrating watershed models. *Journal of Hydrology*, 158, 265-284.

Duan, Q., Ajami, N.K., Gao, X., and Sorooshian, S. (2007). Multi-model ensemble hydrologic prediction using Bayesian model averaging. *Advances in Water Resources*, 30, 1371-1386.

Dzubakova, K. (2010). *Rainfall-runoff modelling: its development, classification and possible applications.* ACTA Geographica Universitatis Comenianae, 54, 173-181.

Eldaw, A.K., Salas, J.D. and Garcia, L.A. (2003). Long-range forecasting of the Nile River flows using climatic forecasting. *Journal of Applied Meteorology*, 42, 890-904.

FAO (1997). *Irrigation potential in Africa: A basin approach, Land and Water Bulletin 4.* Rome: Food and Agriculture Organization of the United Nations. Retrieved from http://www. fao.org/docrep/W4347E/w4347e00.htmContents.

Feldkircher, M. and Zeugner, S. (2009). *Benchmark priors revisited: on adaptive shrinkage and the supermodel effect in Bayesian model averaging.* IMF Working Paper 09-202.

Feyen, L., Vazquez, R., Christiaens, K., Sels, O. and Feyen, J. (2000). Application of a distributed physically-based hydrologically model to a medium size catchment. *Hydrology and Earth System Sciences*, 4, 47-63.

Fiseha, B.M., Setegn, S.G., Melesse, A.M., Volpi, E. and Fiori, A. (2013). Hydrological analysis of the Upper Tiber River Basin, central Italy: a watershed modelling approach. *Hydrological Processes*, 27, 2339-2351.

Folland, C.K., Palmer, T.N. and Parker, D.E. (1986). Sahel rainfall and worldwide sea temperatures, 1901-85. *Nature*, 320, 602-607.

Folland, C., Owen, J., Ward, M.N. and Colman, A. (1991). Prediction of seasonal rainfall in the Sahel region using empirical and dynamical models. *Journal of Forecasting*, 10, 21-56.

Fontaine, B. and Janicot, S. (1996). Sea surface temperature fields associated with West African rainfall anomaly types. *Journal of Climate Notes and correspondence*, 9, 2935-2940.

Fundel, F., Jorg-Hess, S. and Zappa, M. (2013). Monthly hydrometeorological ensemble prediction of streamflow droughts and corresponding drought indices. *Hydrology and Earth System Sciences*, 17, 395-407.

Garric, G., Douville, H., and Deque, M. (2002). Prospect for improved seasonal predictions of monsoon precipitation over Sahel. *International Journal of Climatology*, 22, 331-345.

Gassman, P.W., Reyes, M.R., Green, C.H. and Arnold, J.G. (2007). The Soil and Water Assessment Tool: historical development, applications and future research directions. *American Society of Agricultural and Biological Engineers,* 50, 1211-1250.

Giannini, A., Saravanan, R., and Chang, P. (2003). Oceanic forcing of Sahel rainfall on interannaul to interdecadal time scales. *Science*, 302, 1027-1030.

Gissila, T., Black, E., Grimes, D.I.F. and Slingo, J.M. (2004). Seasonal forecasting of the Ethiopian summer rains. *International Journal of Climatology*, 24, 1345-1358.

Goulden, M. and Few, R. (2011). *Climate change, water and conflict in the Niger river basin.* International Alert and University of East Anglia.

Guenni, L. and Bardossy, A. (2002). A two steps disaggregation method for highly seasonal monthly rainfall. *Stochastic Environmental Research and Risk Assessment*, 16, 188-206.

Gupta, H.V., Kling, H., Yilmaz, K.K. and Martinez, G.F. (2009). Decomposition of the mean squared error and NSE performance criteria: implications for improving hydrological modelling. *Journal of Hydrology*, 377, 80-91.

Haarsma, R.J., Selten, F.M., Weber, S.L. and Kliphuis, M. (2005). Sahel rainfall variability and response to greenhouse warming. *Geophysical Research Letters*, 32, 1-4.

Hamlet, A.F. and Lettenmaier, D.P. (1999). Columbia River streamflow forecasting based on ENSO and PDO climate signals. *Journal of Water Resources Planning and Management*, 125, 333-341.

Harms, A.A. and Campbell, T.H. (1967). An extension to the Thomas-Fiering model for the sequential generation of streamflow, *Water Resource Research*, 3, 653-661.

Hatzaki, M., Flocas, H.A., Asimakopoulos, D.N. and Maheras, P. (2007). The eastern Mediterranean teleconnection pattern: identification and definition. International *Journal of Climatology*, 27, 727-737.

Held, I.M., Delworth, T.L., Lu, J., Findell, K.L. and Knutson, T.R. (2005). Simulation of Sahel drought in the 20th and 21st centuries. *PNAS*, 102, 17891-17896.

Hissler, S. (2010). *Econometric study on the impact of rainfall variability on security in the Sahel region.* Security Implications of Climate Change in the Sahel Region, the OECD's Sahel and West Africa Club Secretariat.

Hooper, P. (2014). What is a P-value? Lecture note, the Department of mathematical and Statistical at the University of Alberta,
Retrieved from http://www.stat.ualberta.ca/ hooper/teaching/misc/Pvalue.pdf

Hotelling, H. (1936) Relations between two sets of variants. *Biometrika*, 28, 321-377.

Huggett, R.J. (1980). *Systems Analysis in Geography (Contemporary Problems in Geography).* Oxford: Oxford University Press.

Hunt, B.G. (2000). Natural climatic variability and Sahelian rainfall trends. *Global and Planetary Change*, 24, 107-131.

Ickowicz, A., Ancey, V., Corniaux, C., Duteurtre, G., Poccard-Chappuis, R., Toure, I., Vall, E. and Wane, A. (2012). *Crop-livestock production systems in the Sahel-increasing resilience for adaptation to climate change and preserving food security.* Building Resilience for Adaptation to Climate Change in the Agriculture Sector, Proceeding of a Joint FAO/OECD workshop 23-24 April 2012.

Ientilucci, E.J., (2014). Predicting atmospheric parameters using canonical correlation analysis. Retrieved from http://www.cis.rit.edu/ ejipci/Reports/CCA_paper.pdf

IRIN, 2013. WEST AFRICA: After the drought, floods - and harvest worries. *IRIN News.* September 23, 2013. Retrieved from http://www.irinnews.org/report/96313.

Jajarmizadeh, M., Harun, S., and Salarpour.(2013). An assessment on base and peak flows using a physically-based model. *Research Journal of Environmental and Earth Sciences*, 5, 49-57.

Jajarmizadeh, J. Lafdani, E., K., Harun, S. and Ahmadi, A. (2014). Application of SVM and SWAT models for monthly streamflow prediction, a case study in South of Iran. *KSCE Journal of Civil Engineering*, 1-13.

Janicot, S., Trzaska, S. and Poccard, I.(2001). Summer Sahel-Enso teleconnection and decadal time scale variations. *Climate Dynamics*, 18, 303-320.

Jarvis A, Reuter H I, Nelson A and Guevara E. (2008) Hole-Filled Seamless SRTM Data (online) V4. International Centre for Tropical Agriculture (CIAT). Retrieved from http://srtm.csi.cgiar.org.

Kandji, S.T., Verchot, L. and Mackensen, J. (2006). *Climate change and variability in the Sahel region: impacts and adaptation strategies in the agriculture sector*. World Agroforestry Centre and United Nations Environment Programme.

Karamouz M, Zahraie B. (2004). Seasonal streamflow forecasting using snow budget and El NinoSouthern Oscillation climate signals: application to the Salt River Basin in Arizona. *Journal of Hydrological Engineering,* 9, 523-533.

Keener, V.W., Feyereisen, G.W., Lall, U., Jones, J.W., Bosch, D.D. and Lowrance, R. (2010). El-Nino/Southern Oscillation (ENSO) influences on monthly NO3 load and concentration, stream flow and precipitation in the Little River Watershed, Tifton, Geogria (GA). *Journal of Hydrology*, 381, 352-363.

Ker, A.D.R., Moorse, M.W., Watts, E.R. and Gill, B.N. (1978). Agriculture in East Africa. Edward Arnold, London, UK.

Klonne, U. (2012). *Drought in the Sahel Global and Local Driving Forces and Their Impact on Vegetation in the* 20^{th} *and* 21^{st} *Century.* Bachelor degree thesis, Department of Physical Geography and Ecosystems Sciences, Lund University.

Knight, J.R., Folland, C.K. and Scaife, A.A. (2006). Climate impacts of the Atlantic Multidecadal Oscillation. *Geophysical Research Letter*s, 33, 1-4.

Konte, O. (2011). Verification des previsions climatiques saisonnieres sur les precipitationsen Afrique de I Ouest (PRESAO) sur la periode Juillet-Aout-Septembre (JAS) de 1998-2010, au Senegal. (draft)

Krause, P., Boyle, D.P. and Base, F. (2005). Comparison of different efficiency criteria for hydrological model assessment. *Advances in Geosciences*, 5, 89-97.

Krichak, S.O., Breitgand, J.S., Gualdi, S. and Feldstein, S.B. (2014). Teleconnection-extreme precipitation relationships over the Mediterranean region. *Theoretical and Applied Climatology*, 117, 679-692

Kruschke, J.K., Aguinis, H. and Joo, H. (2012). The time has come: Bayesian methods for data analysis in the organizational sciecne, *Organizational Research Methods*, 15, 722-752.

Kushwaha, A. and Jain, M.K. (2013). Hydrological simulation in a forest dominated watershed in Himalayan region using SWAT model. *Water Resources Management*, 27, 3005-3023.

Kwon, H.H., Brown, C., Xu, K., and Lall, U. (2009). Seasonal and annual maximum streamflow forecasting using climate information: application to the Three Gorges Dam in the Yangtze River basin, China. *Hydrological Science Journal*, 54, 582-595.

Landman, W.A., Mason, S.J., Tyson, P.D., and Tennant, W. J. (2001). Statistical downscaling of GCM simulations to streamflow. *Journal of Hydrology*, 252, 221-236.

Lee, K. and Lee, J. (2007). The economic value of weather forecasts for decision-making problems in the profit/loss situation. *Meteorological Applications*, 14, 455-463.

Lian, Y., Chan, I., Singh, J., Demissie, M., Knapp, V. and Xie, H. (2007). Coupling of hydrologic and hydraulic models for the Illinois River Basin. *Journal of Hydrology*, 344, 210-222.

Liang, Z., Wang, D., Guo, Y., Zhang, Y. and Dai, R. (2013). Application of Bayesian model averaging approach to multimodel ensemble hydrologic forecasting. *Journal of Hydrologic Engineering*, 18, 1426-1436.

Linderholm, H.W., Folland, C.K. and Walther, A. (2009). A multicentury perspective on the summer North Atlantic Oscillation (SNAO) and drought in the eastern Atlantic Region. *Journal of Quaternary Science*, 24(5), 415-425.

Liu, Z. and Alexander, M. (2007). Atmospheric bridge, oceanic tunnel, and global climatic teleconnections. *Reviews of Geographics*,45, 1-34.

Lopez-Bustins, J.-A., Martin-Vide, J. and Sanchez-Lorenzo, A. (2008). Iberia winter rainfall trends based upon changes in teleconnection and circulation patterns. *Global and Planetary Change*, 63, 171-176.

Lough, J.M. (1986). Tropical Atlantic sea surface temperatures and rainfall variations in sub-Saharan Africa. *Monthly Weather Review*, 114, 561-570.

Lu, J., and Delworth, T.L. (2005). Oceanic forcing of the late 20th century Sahel drought.*Geographic Research Letters*, 32, 1-5.

Lubini, A. and Adamowski, J. (2013). Assessing the potential impacts of four climate change scenarios on the discharges of the Simiyu River, Tanzania using the SWAT model. *International Journal of Water Sciences*, 2, 1-12.

Luo, L., Wood, E.F., and Pan, M. (2007). Bayesian merging of multiple climate model forecasts for seasonal hydrological predictions. *Journal of Geophysical Research*, 112, D10102.

Luo, P., Takara, K., He, B., Cao, W., Yamashiki, Y. and Nover, D. (2011). Calibration and uncertainty analysis of SWAT model in a Japanese river catchment. *Annual Journal of Hydraulic Engineering*, 55, 61-66.

Ma, X., Lu, X.X., Noordwijk, M.v., Li, J.T. and Xu, J.C. (2014). Attribution of climate change, vegetation restoration, and engineering measures to the reduction

of suspended sediment in the Keji catchment, southwest China. *Hydrology and Earth System Sciences*, 18, 1979-1994.

Madigan, D. and Raftery, A.E. (1994). Model selection and accounting for model uncertainty in graphical models using Occams Window. *Journal of the American Statistical Association*, 89, 1535-1546.

Maheepala, S. and Perera, B.J.C. (1996). Monthly hydrologic data generation by disaggregation. Journal of Hydrology, *Journal of Hydrology*, 178, 277-291.

Maity, R. and Kumar, D. N. (2007). Hydroclimatic teleconnection between global sea surface temperature and rainfall over India at subdivision monthly scale. *Hydrological Processes*, 21, 1802-1813.

Mamo, K.H.M. and Jain, M.K. (2013). Runoff and sediment modeling using SWAT in Gumera catchment, Ethiopia. *Open Journal of Modern Hydrology*, 3, 196-205.

Mango, L.M., Melesse, A.M., McClain, M.E., Gann, D. and Setegn, S.G. (2011). Land use and climate change impacts on the hydrology of the upper Mara River basin, Kenya: results of a modeling study to support better resource management. *Hydrology and Earth System Sciences*, 15, 2245-2258.

Marengo, J.A., Cavalcanti, I.F.A., Satyamurty, P., Trosnikov, I., Nobre, C.A., Bonatti, J.P., Camargo, H., Sampaio, G., Sanches, M.B., Manzi, A.O.,Castro, C.A.C., DAlmeida, C., Pezzi, L.P. and Candido, L. (2003). Assessment of regional seasonal rainfall predictability using the CPTEC/COLA atmospheric GCM. *Climate Dynamics*, 21, 459-475.

Masih, I., Maskey, S., Uhlenbrook, S., and V. Smakhtin. (2001). Assessing the impact of areal precipitation input on streamflow simulations using the SWAT model. *Journal of the American Water Resources Association*, 47, 179-195.

Mason, S.J. (1998). Seasonal Forecasting of South African rainfall using a non-linear discriminant analysis model. *International Journal of Climatology*, 18, 147-164.

Maurer, E.P. and Lettenmaier, D.P. (2003). Predictability of seasonal runoff in the Mississippi River basin. *Journal of Geographic Research*, 108, 2-1 to 2-13.

McCuen, R.H., Rawls, W.J. and Whaley, B.L. (1979). Comparative evaluation of statistical methods for water supply forecasting. *Water Resources Bulletin American Water Resources Association*, 15, 935-947.

McCuen, R.H. (2005). Hydrologic Analysis and Design. 3rd edition. New Jersy: Pearson Education, Inc.

Mcmahon, T.A. and Mein, R.G. (1986). *River and Reservoir Yield.* Water Resources Publications, Fort Collins, CO.

Messager, C., Gallee, H., Brasseur, O., Cappelaere, B., Peugeot, C., Seguis, L., Vauclin, M., Ramel, R., Grasseau, G., Leger, L. and Girou, D. (2006). Influence of observed and RCM-simulated precipitation on the water discharge over the Sirba basin, Burkina Faso/Niger. *Climate Dynamics*, 27, 199-214.

Meza, F.J., Hansen, J.W. and Osgood, D. (2008). Economic value of seasonal climate forecasts for agriculture: review of ex-ante assessments and recommendations for future research. *Journal of Applied Meteorology and Climatology*, 47, 1269-1286.

Mirsa, V. (2003). The influence of Pacific SST variability on the precipitation over Southern Africa. *Journal of Climate*, 16, 2408-2418.

Mjelde, J.W., Sonka, S.T. and Peel, D.S. (1989). The socioeconomic value of climate and weather forecasting: a review. Research report 89-01, Midwestern Climate Center, Climate & Meteorology Section Illinois State Water Survey.

Mo, K. C. and Thiaw, W.M. (2002). Ensemble canonical correlation prediction of precipitation over the Sahel. *Geophysical Research Letters*, 29, 11-1 to 11-4.

Mohamed-Saleem M A. (1984). Crop forage interactions. Paper presented at the *ILCA/NAPRI symposium on livestock production* in the subhumid zone of Nigeria, Lugard Hall, Kaduna, Nigeria 30 Oct - 2 Nov 1984.

Mohino, E., Janicot, S. and Bader, J. (2011). Sahel rainfall and decadal to multi-decadal sea surface temperature variability. *Climate Dynamic*, 37: 419-440.

Moradkhani, H. and Sorooshian, S. (2009). General review of rainfall-runoff modeling: model calibration, data assimilation, and uncertainty analysis. *Hydrological Modelling and the Water Cycle*, 1-24.

Moriasi,D.N., Arnold, J.G., Van Liew, M.W., Bingner,R.L., Harmel, R.D., and Veith, T.L. (2007). Model evaluation guidelines for systematic quantification of accuracy in watershed simulations. *American Society of Agricultural and Biological Engineers*, 50, 885-900.

Mulungu, D.M.M. and Munishi, S.E. (2007). Simiyu River catchment parameterization using SWAT model. *Physics and Chemistry of the Earth*, 32, 1032-1039.

Murphy, A.H. (1976). Decision-making models in the cost-loss ratio situation and measures of the value of probability forecasts. *Monthly Weather Review*, 104, 1058-1065.

Murphy, A.H. (1977). The value of climatological, categorical and probabilistic forecasts in the cost-loss ratio situation. Monthly Weather Review, 105, 803-816.

Mutai, C.C., Ward, M.N. and Colman, A.W. (1998). Towards the prediction of the east Africa short rains based on sea-surface temperature-atmosphere coupling. *International Journal of Climatology*, 18, 975-997.

Mylne, K.R. (2002). Decision-making from probability forecasts based on forecast value. *Meteorological Applications*, 9, 307-315.

Nash, J.E. and Sutcliffe, J.V. (1970). River flow forecasting through conceptual models part I - a discussion of principles. *Journal of Hydrology*, 10, 282-290.

Neitsch, S.L., Arnold, J.G., Kiniry, J.R., Srinivasan, R., Williams, J.R.(2002). *Soil and Water Assessment Tool. Users Manual.* Version 2005. GSWRL Report 02-02, BRC Report 2-06, Temple, Texas, USA

Neitsch, S. L., J. G. Arnold, J. R. Kiniry, R. Srinivasan, and J. R. Williams. (2004). *Soil and Water Assessment Tool Input/Output File Documentation. Version 2005.* Retrieved from http://ftp.brc.tamus.edu/pub/outgoing/sammons/swat2005.

Neitsch, S.L., Arnold, J.G., Kiniry, J.R. and Williams, J.R. (2011). *Soil and Water Assessment Tool Theoretical Documentation version 2009.* Texas Water Resources Institute Technical Report No. 406. Texas A&M University System, College Station, Texas.

Ndiaye, O., Goddard, L. and Ward, M.N. (2009). Using regional wind fields to improve general circulation model forecasts of July-September Sahel rainfall. International *Journal of Climatology*, 29, 1262-1275.

Ndiaye, O., Ward, M.N. and Thiaw, W.M. (2011). Predictability of seasonal Sahel rainfall using GCMs and lead-time improvements through the use of a coupled model. *Journal of Climate*, 24, 1931-1949.

Nichoson, S.E. (1995). Sahel, West Africa. *Encyclopedia of Environmental Biology*, 3, 261-275.

Nichoson, S.E. and Grist, J.P. (2001). A conceptual model for understanding rainfall variability in the West African Sahel on interannual and interdecadal timescales. *International Journal of Climatology*, 21, 1733-1757.

Nicholson, S.E. and Palao, I.M. (1993). A re-evaluation of rainfall variability in the Sahel part I. characteristics of rainfall fluctuations. *International Journal of Climatology,* 13, 371-389.

Nkonge, L.K., Sang, J.K., Gathenya, J.M. and Home, P.G. (2014). Comparison of two calibration-uncertainty methods for Soil and Water Assessment Tool in stream flow modeling. *Journal of Sustainable Research in Engineering*, 2, 40-44.

Palmer, T.N. (1986). Influence of the Atlantic, Pacific and Indian Oceans on Sahel rainfall. *Nature*, 322, 251-253.

Palmer, T.N. (2002). The economic value of ensemble forecasts as a tool for risk assessment: from days to decades. Quarterly Journal of the Royal Meteorological Society, 128, 747-774.

Picouet, C. (1999). *Geodynamique dun hydrosisteme tropical peu anthropise. Le Bassin superieur du Niger et son delta interieur.* Ph.D. thesis, Montpellier II Univ.

Pereira, A.R. (2004). The Priestley-Taylor parameter and the decoupling factor for estimating reference evapotranspiration. *Agriculture and Forest Meteorology*, 125, 305-313.

Piechota, T.C., Chiew, F.H.S., Dracup J.A. and McMahon, T.A. (1998). Seasonal streamflow forecasting in eastern Australia and the El Nino-Southern Oscillation. *Water Resources Research*, 34, 3035-3044.

Piechota, T.C. and Dracup, J.A. (1999). Long-range streamflow forecasting using El Nino-Southern Oscillation indicators. *Journal of Hydrologic Engineering*, 4, 144-151.

Pokhrel, P., Wang, Q.J. and Robertson, D.E. (2013). The value of model averaging and dynamical climate model predictions for improving statistical seasonal streamflow forecasts over Australia. *Water Resources Research,* 49, 6671-6687.

Porter, J.W. and Pink, B.J. 1991. A method of synthetic fragments for disaggregation in stochastic data generation. *International Hydrology and Water Resources Symposium, Perth, Australia*: 781-786.

Potts, M., Zulu, E., Wehner, M., Castillo, F. and Henderson, C. (2013). Crisis in the Sahel: Possible Solutions and the Consequences of Inaction. *OASIS conference* hosted by the University of California, Berkeley and Africa Institute for Development Policy in Berkeley on September 21, 2012.

Pui, A., Sharma, A. and Mehrotra, R. (2009). A comparison of alternatives for daily to sub-daily rainfall disaggregation. *18th World IMACS/MODSIM Congress*, Cairns, Australia 13-17 July 2009.

Raftery, A.E., Gneiting, T., Balabdaoui, F. and Polakowski, M. (2005). Using Bayesian model averaging to calibrate forecast ensembles. *Monthly Weather Review,* 133, 1155-1174.

Raicich, F., Pinardi, N. and Navarra, A. (2003). Teleconnections between Indian monsoon and Sahel rainfall and the Mediterranean, *International Journal of Climatology*, 23, 173-186.

Raje, D. and Mujumdar, P.P. (2011). A comparison of three methods for downscaling daily precipitation in the Punjab region. *Hydrological Process*, 25, 3575-3589.

Rajeevan, M., Pai, D.S. and Kumar, R.A. (2005). *New statistical models for long range forecasting of South West monsoon rainfall.* NCC research report, National Climate Center, India Meteorological Department, India.

Rao, A. R. and Hamed, K. H. (2000). Flood Frequency Analysis. Florida: CRC Press.

Refaeilzadeh, P., Tang, L. and Liu, H. (2008). Cross-validation. *Encyclopedia of Database Systems*, Springer, US.

Regonda, S., Demargne, J. and Seo, D.J. (2006). Hydrologic forecast verification. *RFC Short-Term Ensemble Workshop*, November 30, 2006.

Reynolds, J., R. Virginia, P. Kemp, A. de Soyza, and D. Tremmel. (1999). Impact of drought on desert shrubs: effects of seasonality and degree of resource island development. *Ecological Monographs,* 69,69-106.

Reynolds, R.W. and Smith, T.M. (1994). Improved global sea surface temperature analyses using optimum interpolation. *Journal of Climate*, 7, 929-948.

Richardson, D.S. (2001). Measures of skill and value of ensemble prediction systems, their interrelationship and the effect of ensemble size. *Quarterly Journal of the Royal Meteorological Society*, 127, 2473-2489.

Richardson, D.S. (2012). Economic value and skill. Forecast Verification: A Practitiioner's Guide in Atmospheric Science, Second Edition. John Wiley Sons, Ltd. ISBN: 978-0-470-66071-3.

Ridwansyah, I., Pawitan, H., Sinukaban, N. and Hidayat, Y. (2014). Watershed modeling with ArcSWAT and SUFI2 in Cisadane catchment area: calibration and validation to prediction of river flow. *International Journal of Science and Engineering*, 6, 12-21.

Robertson, D.E. and Wang, Q.J. (2012). A Bayesian approach to predictor selection for seasonal streamflow forecasting. *Journal of Hydrometeorology*, 13, 155-171.

Robertson, D.E., Pokhrel, P. and Wang, Q.J. (2013). Improving statistical forecasts of seasonal streamflows using hydrological model output. *Hydrology and earth System Sciences*, 17, 579-593.

Rodionov, S. and Assel, R. (2000). Atmospheric teleconnection patterns and severity of winters in the laurentian Great Lake basin. *Atmospheric Ocean*, 38, 601-635.

Rodriguez-Fonseca, B., Janicot, S., Mohino, E., Losada, T., Bader, J., Caminade, C., Chauvin, F., Fontaine, B., Garcia-Serrano, J., Gervois,S., Joly, M., Polo, L., Ruti, P., Roucou, P. and Voldoire, A. (2011). Interannual and decadal SST-forced responses of the West African monsoon. *Atmospheric Science Letters*,12, 67-74.

Rosen, L. (2013). Climate change and its impact on our world's rivers-Africa-part three. World Future Society. Retrieved from http://www.wfs.org/blogs/len-rosen/climate-change-and-its-impact-our-worlds-rivers-africa-part-three.

Roulin, E. (2007). Skill and relative economic value of medium-range hydrologica ensemble predictions. *Hydrology and Earth System Sciences*, 11, 725-737.

Rowell, D.P., Folland, C.K., Maskell, K., Owen, J.A. and Ward, M.N. (1992). Modelling the influence of global sea surface temperatures on the variability and predictability of seasonal Sahel rainfall. *Geophysical Research Letters*, 19, 905-908.

Rowell, D.P. (2001) Teleconnections between the tropical Pacific and the Sahel. *Quarterly Journal of the Royal Meteorological Society*, 127, 1683-1706.

Rowell, D.P. (2003). The impact of Mediterranean SSTs on the Sahelian rainfall season. *Journal of Climate*, 16, 849-862.

Saha, P.P, Zeleke, K and Hafeez, M. (2014). Streamflow modeling in a fluctuant climate using SWAT: Yass River catchment in south eastern Australia. *Environmental Earth Sciences*,71, 5241-5254.

Sahel and West Africa club. (2015). Livelihood system in the Sahel. Retrieved from http://www.oecd.org/swac/ourwork/siccs.htm.

Santhi, C., Arnold, J.G., Williams, J.R., Hauck, L.M. and Dugas, W.A. (2001). Application of a watershed model to evaluate management effects on point and nonpoint source pollution, *Transaction of the ASAE,* 44, 1559-1570.

Samimi, C., Fink, A.H. and Paeth, H. (2012). The 2007 flood in the Sahel: causes, characteristics and its presentation in the media and FEWS NET. *Natural Hazards and Earth System Sciences*, 12: 313-325.

Sankarasubramanian, A., Lall, U. and Espinueva, S. (2008). Role of retrospective forecast of GCMs foreced with persisted SST anomalies in operational streamflow forecasts development. *Journal of Hydrometeorology*, 9, 212-227.

Schepen A., Wang Q.J., and Robertson D.E. (2012). Combining the strengths of statistical and dynamical modeling approaches for forecasting Australian seasonal rainfall. *Journal of Geophysical Research,* 117, 1-9.

Schuol, J. and Abbaspour, K.C. (2006). Calibration and uncertainty issues of a hydrological model (SWAT) applied to West Africa. *Advances in Geosciences,* 9, 137-143.

Seibert, J., 1999. *Conceptual runoff models - fiction or representation of reality*? Acta Univ. Ups., Comprehensive Summaries of Uppsala Dissertations from the Faculty of Science and Technology 436. 52 pp. Uppsala. ISBN 91-554-4402-4.

Setegn, S.G., Srinivasan, R. and Dargahi, B. (2008). Hydrological modelling in the lake Tana Basin, Ethiopia using SWAT model. *The Open Hydrology Journal*, 2, 49-62.

Setegn, S.G., Melesse, A.M., Haiduk, A., Webber, D., Wang, X. and McClain, M.E. (2014). Modeling hydrological variability of fresh water resources in the Rio Cobre watershed, Jamica. *Catena*, 120, 81-90.

Shaman, J. and Tziperman, E. (2011). An atmospheric teleconnection linking ENSO and southwestern European precipitation. *Journal of Climate,* 24, 124-139.

Sheridan, S. and Lee, C.C. (2012). Synoptic climatology and the analysis of atmospheric teleconnections. *Progress in Physical Geography,* 36, 548-557

Shrestha, D. L., and D. P. Solomatine (2008), Data-driven approaches for estimating uncertainty in rainfall runoff modelling, *International Journal of River Basin Management*, 6, 109-122.

Shukla, S. and Lettenmaier, D.P. (2011). Seasonal hydrologic prediction in the United States: understanding the role of initial hydrologic conditions and seasonal climate forecast skill. *Hydrology and Earth System Science,*15, 3529-3538

Singh, O.P. (2001). Cause-effect relationships between sea surface temperature, precipitation and sea level along the Bangladesh coast. *Theoretical and Applied Climatology*, 68, 233-243

Sood, A., Muthuwatta, L. and McCartney, M. (2013). A SWAT evaluation of the effect of climate change on the hydrology of the Volta River basin. *Water International*, 38, 297-311.

Souza Filho, F.A. and Lall, U. (2003). Seasonal to interannual ensemble streamflow forecasts for Ceara, Brazil: Applications of a multivariate, semiparametric algorithm. *Water Resources Research,* 39, 1-13.

Srikanthan, R. and McMahon, T.A. (2001). Stochastic generation of annual, monthly and daily climate data: a review. *Hydrology and Earth System Sciences,* 5, 653-670.

Srikanthan, R., McMahon, T.A. and Sharma, A. (2002). S*tochastic generation of monthly rainfall data.* Technical report 02/8 Cooperative Research Centre for Catchment Hydrology.

Srivastava, A.K., Rajeevan, M. and Kulkarni, R. (2002). Teleconnection of OLR and SST anomalies over Atlantic Ocean with Indian summer monsoon. *Geophysical Research Letters*, 29, 125-1 to 125-4.

Taweye A., (1995). Contribution ltude hydrologique du bassin versant de la Sirba Garb-Kourou. Mmoire de fin dtudes, Agrhymet, Niamey, Niger, 98 p.

Thiaw, W.M. and Mo, K.C. (2005). Impact of sea surface temperature and soil moisture on seasonal rainfall prediction over the Sahel. *Journal of Climate*, 18, 5330-5343.

Thompson, J.C. (1952). On the operational deficiencies in categorical weather forecasts. *Bulletin of the American Meteorological Society*, 33, 223-226.

Tootle, G,.A., Singh, A.K., Piechota, T.C. and Farnham, I. (2007). Long lead time forecasting of U.S. streamflow using partial leas squared regression. *Journal of Hydrologic Engineering*, 12, 442-451.

Trambauer, P. Maskey, S. Winsemius, H. Werner, M. and Uhlenbrook, S. (2013). A review of continental scale hydrological models and their suitability for drought forecasting in (sub-Saharan) Africa. *Physics and Chemistry of the Earth*, 66, 16-26.

Tuteja, N.K, Shin D., Laugesen, R., Khan, U., Shao, Q., Wang, E., Li, M., Zheng, H., Kuczera, G., Kavetski, D., Evin, G., Thyer, M., MacDonald, A., Chia, T. and Le, B. (2011). *Experiment evaluation of the dynamic seasonal streamflow forecasting approach.* Technical Report, Bureau of Meteorology, Melbourne.

Udall, B. and Hoerling, M. (2005). S*easonal forecasting: skill in the intermountain west?* Feature Article from Intermountain West Climate Summary, May 2005. A joint project of University of Colorado and NOAA Climate Diagnostics Center.

UNEP. (2011). *Livelihood security climate change, migration and conflict in the Sahel. Climate Change, Conflict and Migration in the Sahel.* ISBN: 978-92-807-3198-9.

UNEP. (2012).*Sahel Atlas of Changing Landscapes: Tracing trends and variations in vegetation cover and soil condition.* United Nations Environment Programme, Nairobi. ISBN: 978-92-807-3300-6.

Vaze, J., Jordan, P., Beecham, P., Frost, R. and Summerell, G. (2012). *Guidelines for Rainfall - Runoff Modelling: Towards Best Practice Model Application.* eWater Cooperative Research Center. ISBN 978-1-921543-51-7.

Wainwright, J. and Mulligan, M. (2004). *Environmental Modelling Finding Simplicity in Complexity.* Chichester :John Wiley & Sons Ltd.

Wang, Q.J. Roberston, D.E. and Chiew, F.H.S. (2009). A Bayesian joint probability modelling approach for seasonal forecasting of streamflows at multiple sites. *Water Resource Research*, 45, 1-18.

Wang,E., Zhang, Y., Luo, J., Chie, F.H.S. and Wang, Q.J. (2011). Monthly and seasonal streamflow forecasts using rainfall-runoff modeling and historical weather data, *Water Resources Research*, 47, 1-13.

Wang, Q.J., Schepen, A. and Robertson, D.E. (2012). Merging seasonal rainfall forecasts from multiple statistical models through Bayesian model averaging. *Journal of Climate,* 25, 5524-5537.

Wang, G., Yang, H., Wang, L., Xu, Z. and Xue, B. (2014). Using the SWAT model to assess impacts of land use changes on runoff generation in headwaters. *Hydrological Processes*, 28, 1032-1042.

Ward, M.N. (1992). Provisionally corrected surface wind data, worldwide ocean-atmospheric surface fields, and Sahelian rainfall variability. *Journal of Climate*, 5, 454-475.

Ward, M.N. and Folland, C.K. (1991). Prediction of seasonal rainfall in the North Nordeste of Brazil using eigenvectors of sea-surface temperature. *International Journal of Climatology,* 11, 711-743.

Wetterhall, F., He, Y., Cloke, H., and Pappenberger, F. (2011). Effects of temporal resolution of input precipitation on the performance of hydrological forecasting. *Advances in Geosciences,* 29, 21-25.

Wey, K.M. (2006). *Temporal disaggregation of daily precipitation data in a changing climate.* A thesis of Master Applied Science in Civil Engineering, the University of Waterloo.

White, E.D., Easton, Z.M., Fuka, D.R., Collick, A.S., Adgo, E., McCartney, M., Awulachew, S.B., Selassie, Y.G. and Steenhuis, T.S. (2011). Development and application of a physically based landscape water balance in the SWAT model. *Hydrological Processes*, 25, 915-925.

Whyte, J.M., Plumridge, A. and Metcalfe, A.V. (2011). Comparison of predictions of rainfall-runoff models for changes in rainfall in the Murray-Darling Basin. *Hydrology and Earth System Sciences Discussions*, 8, 917-955.

Wilby, R. (2008). *A review of recent trends and projected climate changes for Niger, West Africa: Information climate change adaptation and water resources management policies.* A Technical Brief for Tearfund.

Wilks, D.S. (1995). *Statistical Methods in the Atmospheric Sciences: an Introduction, first edition*, Academic Press. California: A Division of Harcourt Brace & Company.

Wilks, D.S. (2011). *Statistical Methods in the Atmospheric Sciences, third edition.* Oxford: Elsevier Inc.

Winchell, M., Srinivasan, R., Di Luzio, M., Arnold, J. (2007). *ArcSWAT Interface for SWAT2005 Users Guide.* Texas Agricultural Experiment Station and United States Department of Agriculture, Temple, TX.

Wojcik, R. and Buishand, T.A. (2003). Simulation of 6-hourly rainfall and temperature by two resampling schemes. *Journal of Hydrology*, 273, 69-80.

Wolter, K. (1989). Modes of tropical circulation, southern oscillation, and Sahel rainfall anomalies. *Journal of Climate*, 2, 149-172.

Woodruff, S.D., Lubker, S.J., Wolter, K., Worley, S.J., and Elms, J.D. (1993). Comprehensive ocean-atmosphere data set (COADS). *Earth System Monitor,* 4, 1-8.

World Bank. (2013). *Transforming Agriculture in the Sahel: What Would It Take?.* African Region Sustainable Development.

Wyss, G.D. and Jorgensen, K.H. (1998). *A users guide to LHS: Sandias Latin Hypercube Sampling Software, Risk Assessment and Systems Modeling Departmen*t, Sandia National Laboratories. Retrieved from http://prod.sandia.gov/techlib/access-control.cgi/1998/980210.pdf

Xue, Y. and Shukla, J. (1998). Model simulation of the influence of global SST anomalies on Sahel rainfall. *Monthly Weather Review*, 126, 2782-2792.

Yang, J., Reichert, P., Abbaspour, K.C., Xia, J. and Yang, H. (2008). Comparing uncertainty analysis techniques for a SWAT application to the Chaohe Basin in China. *Journal of Hydrology*, 358, 1-23.

Ye, W., Bates, B.C., Viney, N.R., Sivapalan, M. and Jakeman, A.J. (1997). Performance of conceptual rainfall-runoff models in low-yielding ephemeral catchments. *Water Resources Research*, 33, 153-166.

Yossef, N. C., Winsemius, H., Weerts, A., Beek, R.V. and Bierkens, F.P.(2013). Skill of global seasonal streamflow forecasting system, relative roles of initial conditions and meteorological forcing. *Water Resources Research,* 49, 4687-4699.

Zheng, X., Eltahir, E.A.B. and Emanuel, K.A. (1999). A mechanism relating tropical Atlantic spring sea surface temperature and west Africa rainfall. *Quarterly Journal of the Royal Meteorological Society*, 125, 1129-1163.